

厚生労働科学研究費補助金
難治性疾患等政策研究事業
(難治性疾患政策研究事業)

胎児・新生児骨系統疾患の診断と
予後に関する研究

平成26年度 総括・分担研究報告書

研究代表者 澤井英明

平成27(2015)年3月

663-8501 西宮市武庫川町 1 - 1

兵庫医科大学 産科婦人科学 澤井英明

Phone 0798-45-6481 Fax 0798-46-4163 e-mail sawai-hyg@umin.ac.jp

目 次

I. 総括研究報告

- 胎児・新生児骨系統疾患の診断と予後に関する研究・・・・・・・・・・ 3
研究代表者 澤井英明

II. 分担研究報告

1. 症例の収集と診断の支援システム構築・・・・・・・・・・ 11
研究分担者 室月 淳、澤井英明、山田崇弘、堤 誠司
篠塚憲男、高橋雄一郎、鬼頭浩史、佐世正勝
宮寄 治、渡邊 淳、芳賀信彦、大藪恵一
2. 胎児CTの被曝線量の全国調査・・・・・・・・・・ 13
研究分担者 宮寄 治、山田崇弘
3. 骨形成不全症患者の歯科的所見に関する全国調査・・・・・・・・ 19
研究分担者 大藪恵一
4. 骨系統疾患 発症疫学コホート研究・・・・・・・・・・ 23
研究分担者 高橋雄一郎、山田崇弘、澤井英明、室月 淳、
堤 誠司、佐世正勝
5. タナトフォリック骨異形成症の発育調査・・・・・・・・・・ 27
研究代表者 澤井英明

III. 研究成果の刊行に関する一覧表

・・・・・・・・・・・・・・・・・・・・・・・・ 33

IV. 研究成果の刊行物・別冊

・・・・・・・・・・・・・・・・・・・・・・・・ 39

タナトフォリック骨異形成症1型・2型の診断基準と重症度分類（案）

I . 総括研究報告

厚生労働科学研究費補助金（難治性疾患等政策研究事業）

総括研究報告書

胎児・新生児骨系統疾患の診断と予後に関する研究

研究代表者 澤井英明 兵庫医科大学 産科婦人科 教授

研究要旨

本研究は胎児・新生児の骨系統疾患に遭遇した医師が適切な診断を早期に行い、医療・療育につなげることを目的とする。本研究班は産科・放射線科・小児科・整形外科・分子遺伝学の領域で、胎児や新生児の骨系統疾患を専門とする第一級の専門家で構成している。また本研究は代表者（澤井英明）が「胎児骨系統疾患フォーラム」という産科医中心の診断支援グループを中心に H22～24 年度まで厚生労働科学研究・致死性骨異形成症の診断と予後に関する研究班（代表者・澤井英明）で行った、致死性骨異形成症（現在の疾患名タナトフォリック骨異形成症：以下 TD と略）に対する取り組みをすべての胎児・新生児の骨系統疾患 456 疾患に拡大させ、疾患頻度を調べるコホート調査や確定診断指針作成など新たな課題に取り組んだ。

骨系統疾患は骨や軟骨などの組織形成の障害により、全身的な骨格が障害される疾患で、2010 年の国際分類では 456 疾患が存在する。個々の疾患の頻度は 2 万人に 1 人程度と低いが、疾患が多数あるため、全体の罹患頻度は多いが明確ではない。重症な疾患では胎児期から骨格異常を指摘され、代表的な疾患は、TD や軟骨無形成症、骨形成不全症、低フォスファターゼ症、軟骨無発生症などである。診断は X 線診断と一部は遺伝子診断によるが、治療は対症療法がほとんどで、標準的で有効な診断・治療法がない難治性疾患であり、研究の推進が必要である。

具体的には、1) 症例の診断確定と治療方針決定の支援と定期的な研修会等の開催（H26～28 年度）、2) 全国を一定の地域に分け、地域の医師に適切な診断と助言を行い、妊婦や患者家族に適切な診療ができる施設を全国（すべての都道府県）に整備（同期間）、3) ホームページ等を用いた一般の医師や妊婦、患者、家族が情報を得るシステムを構築（同期間）、4) 疾患頻度を明らかにするため、特定地域を対象としたコホート調査（同期間）、5) 骨格異常を有する胎児を診断し適切な妊娠管理を行うため、胎児超音波検査や胎児 CT、遺伝子検査による各診断方法の情報収集（H26～27 年度）、6) 胎児期および出生時点での確定診断指針（X 線診断や超音波検査、遺伝子検査等）を確立（H28 年度）、7) TD の長期生存患者の発育状況について詳細な聞きとり調査を実施（H26～27 年度）。8) 2014 年度予定の骨系統疾患国際分類の改定に対応した疾患整理（H27～28 年度）等である。

研究分担者氏名 所属機関名及び所属機関における職名

室月 淳 宮城県立こども病院産科・部長

山田崇弘 北海道大学病院産科・特任講師

堤 誠司 山形大学医学部産科婦人科・講師

高橋雄一郎 独立行政法人国立病院機構長良医療センター産科・医長

佐世正勝 山口県立総合医療センター総合周産期母子医療センター・センター長

篠塚憲男 胎児医学研究所臨床研究・代表

宮寄 治 国立成育医療研究センター放射線診療部・医長

芳賀信彦 東京大学医学部附属病院リハビリテーション科・教授

鬼頭浩史 名古屋大学医学部附属病院整形外科・准教授

渡邊 淳 日本医科大学付属病院 遺伝診療科・准教授

大藪恵一 大阪大学大学院 小児科・骨代謝学・教授

への対応方法を示し、患児の予後の改善と家族の支援を行うことが本研究の全体の目的である。

研究全体の目的としては1)症例の診断確定と治療方針決定の支援と定期的な研修会等の開催(H26～28年度)、2)全国を一定の地域に分け、地域の医師に適切な診断と助言を行い、妊婦や患者家族に適切な診療ができる施設を整備(同期間)、3)ホームページ等を用いた一般の医師や妊婦、患者、家族が情報を得るシステムを構築(同期間)である。そしてこの目的を達成するために、4)疾患頻度を明らかにするため、特定地域を対象としたコホート調査(同期間)、5)骨格異常を有する胎児を診断し適切な妊娠管理を行うために、胎児超音波検査や胎児CT、遺伝子検査による各診断方法の情報収集(H26～27年度)、6)胎児期および出生時点での確定診断指針(X線診断や超音波検査、遺伝子検査等)を確立(H28年度)、7)TDの長期生存患者の発育状況について詳細な聞きとり調査を実施(H26～27年度)。8)2014年度予定の骨系統疾患国際分類の改定に対応した疾患整理(H27～28年度)、等を実施する。

TDについては、本研究の代表者(澤井)や多くの分担者が加わった「致死性骨異形成症の診断と予後に関する研究班」(代表者・澤井)において、上記の一部を実施して、致死性骨異形成症の疾患名の変更の提案も含めて、大きな成果をあげている(日整会誌 vol17, 2013)。この成果をすべての胎児・新生児骨系統疾患に拡大する。

A. 研究目的

骨系統疾患は重症例では出生後早期に死亡し、整形外科的治療の対象とならない疾患もあり、産科医や小児科医が関わることが多い。各疾患の頻度は少なく、一般医師が多数の症例を経験しにくい一方で、疾患数は456疾患もあり、遭遇する機会は少なくない。骨系統疾患に詳しい医師は極めて少なく、疾患に遭遇しても診断や治療方針、予後の推定などが困難な状態である。この状況を克服する必要から、産科医や小児科医の骨系統疾患

B. 研究方法

本研究の全体計画は、以下の(1)～(3)で、これに至る個別の(4)～(8)の研究計画を策定した。

(1) 専門家チームによる骨系統疾患の診断支援(net support) (H26～28年度)：全国の医療機関で胎児や新生児の骨系統疾患疑い症例に遭遇した担当医師が本研究班にアクセスし、胎児の超音波検査の写真や胎児CTの画像を本研究班と「胎児

骨系統疾患フォーラム」の専門家チームのネット上の討議によって解析し、精度の高い診断を行って担当医師に呈示する。その後担当医師はその意見を参考にして、妊娠管理を行い、追跡データを還元する。症例の経過と画像の解析をもとに最終診断の妥当性を検討し、妊娠中の胎児の骨系統疾患の診断基準、少なくとも疾患絞り込みや予後の診断手法を確立する（代表者・澤井と分担者・室月を中心に分担者全員が関与。協力者・西村）。

（２）全国各地域に診断拠点施設を整備し、実際の診療を支援（real support）（H26～28年度）：全国の各地域で胎児や新生児の骨系統疾患を実際に診療できる施設を選定し、研究班と連携しつつ診療レベルの向上を目指す（代表者・澤井、分担者・大藪、室月）。（１）と（２）は密接に関連しており、診断の確定などの重要な点は研究班で討議し、実際の診療は各拠点施設で行い、その経過やデータを研究班とやりとりしつつ最適な疾患管理を行う。

（３）ホームページ等を用いた一般の医師や妊婦、患者、家族が情報を得るシステムを構築（H26～28年度）：医師は診断の参考になる検査法やその所見などを得ることができ、妊婦、患者、家族は近くに診療が可能な施設や個々の疾患の情報などを検索できるようにする（代表者・澤井）。

（４）疾患頻度を調査するため特定地域を対象としたコホート調査（H26～28年度）：地方には専門性の高い医療機関が少なく、ほぼ全例の骨系統疾患症例が単一の施設に集まる地域がある。北海道、と宮城県、山形県、岐阜県、兵庫県、山口県を拠点とし全症例把握を目標に実施する。（代表者・澤井、分担者・室月、山田、堤、高橋、佐世）。なお、少なくとも全国各県に症例を集めるような拠点を整備する。（代表者・澤井）

（５）骨系統疾患疑い胎児を診断し適切な妊娠管理を行うための、胎児超音波検査や胎児CT、遺伝子検査による診断方法の確立（H26～27年度）：超音波検査は日本人の標準値がない胸郭等のデータ収集を行い、確定診断指針につなげる（分担者・

篠塚）。胎児CTについては、被曝量の調査や診断に有用な画像処理法や撮影部位などを検討し、確定診断指針につなげる（分担者・宮寄）。遺伝子検査についても、実施可能ラボの情報を収集して、実施できる体制を作り、遺伝カウンセリングを含めた確定診断指針につなげる（分担者・渡邊、山田、協力者・池川）。

（６）胎児期および出生時点での確定診断指針（H28年度）：（５）で得られた胎児CTやX線診断や超音波検査、遺伝子検査等を総合的に組み合わせ、確定診断指針を作成する。胎児期については、確定診断が困難でも、疾患を絞り込み、予後を推定する手法も検討する（分担者・室月、篠塚、宮寄、山田、芳賀、鬼頭を中心に全員が関与）

（７）TDの長期生存患者の発育状況調査（H26～27年度）：長期生存例の人数や発育状況などの聞き取り調査を行い、発育状況を調査する（代表者・澤井）。

（８）骨系統疾患国際分類の改定に対応（H27～28年度）：2014年に予定されている改定に対応した疾患概念や分類を整理して周知する。（分担者・芳賀）

なお、骨系統疾患は456疾患もあるが、主な疾患と研究者の担当は、TD（澤井）、軟骨無形成症（大藪）、Ⅱ型コラーゲン異常症（室月）、低フォスファターゼ症（渡邊）、骨形成不全症（山田）、短肋骨異形成症（山田）、彎曲骨異形成症（堤）、変容性骨異形成症（澤井）、点状軟骨異形成症（佐世）、捻曲性骨異形成症（澤井）とし他の頻度の少ないものは適宜、経験のある医師が担当する。なお代表者（澤井）、分担者（室月、山田）は日本産科婦人科学会周産期委員会であり学会との連携を行う。

（倫理面への配慮）

本研究は、新たに介入する臨床研究ではなく、診療として実施されている症例の解析と登録、そして診断支援のネットワーク構築と維持である。従って研究自体への大きな倫理的な課題はないと

考える。

ただし、胎児 CT においては被曝の問題があるため、倫理的な配慮が必要であり、臨床検査であっても安易に実施してはならず、必要不可欠な場合に限り実施するように、研究期間中もその旨を各医療機関に周知する。また実施の際は夫婦に胎児被曝のリスクとそれによって得られる確定診断に近づくこととの有益性を説明し、インフォームド・コンセントを得て、実施するように依頼する。また、得られた超音波や CT の画像を研究班で分析する際には、臨床情報の提供は不可欠であるが、同時に個人情報の保護のために、必ず画像と臨床情報は匿名化する。またこれらの胎児や新生児の臨床情報の提供については夫婦の同意を得る。

胎児 CT の安全性をより確かなものとするために、安全性の確立を第一の目的として、被ばく線量軽減化のために、母体・胎児ファントムを用いた被ばく線量推定と軽減化プロトコルの作成を行う。

なお各個別の研究とは別に研究全体について、研究代表者の所属機関である兵庫医科大学において、倫理審査を受ける。

本研究は生命倫理の観点から議論の多い、出生前診断に関係する領域であるが、本研究の目的は成果を妊娠や分娩を適正に管理し、良い状態で児を出生させることにある。

C. 研究結果

(1) 専門家チームによる骨系統疾患の診断支援 (net support) :

胎児骨系統疾患フォーラムのメンバーの中で、全国の症例を集めて 4000 通以上のメールで症例検討を行ってきた。胎児骨系統疾患として診断されたのは、軟骨無形成症 (achondroplasia: ACH)、軟骨低形成症 (hypochondroplasia: HCH)、タナトフォリック骨異形成症 (thanatophoric dysplasia: TD)、低フォスファターゼ症 (hypophosphatasia: HP)、点状軟骨異形成症

(chondrodysplasia punctata)、軟骨無発生症 (achondrogenesis: ACG)、軟骨低発生症 (hypochondrogenesis: HCG)、先天性骨幹端異形成症 (spondyloepiphyseal dysplasia congenita: SEDC)、分節異常骨異形成症 (dyssegmental dysplasia)、屈曲肢異形成症 (campomelic dysplasia: CD)、骨形成不全症 (osteogenesis imperfect: OI)、短肋骨症候群 (多指 (趾) を伴うもの、伴わないもの) 等の疾患を診断した。

(2) 全国各地域に診断拠点施設を整備し、実際の診療を支援 (real support) :

拠点となる診断施設を北海道 (北海道大学)、宮城県 (宮城県立こども病院)、山形県 (山形大学)、岐阜県 (長良医療センター)、兵庫県 (兵庫医科大学)、山口県 (山口県立総合医療センター) を拠点として指定した。

(3) ホームページ等を用いた一般の医師や妊婦、患者、家族が情報を得るシステムを構築 :

致死性骨異形成症の診断と予後に関する研究班のホームページを www.thanatophoric.com 改編して、すべての骨系統疾患に対応した本研究班のホームページとして情報提供している。

(4) 疾患頻度を調査するため特定地域を対象としたコホート調査 :

上記の (2) の拠点診断施設の県内において、全骨系統疾患症例の把握による疾患出生頻度の把握を目的として、全数把握コホート調査を開始した。平成 26 年度中に北海道 (北海道大学)、宮城県 (宮城県立こども病院)、山形県 (山形大学)、岐阜県 (長良医療センター)、兵庫県 (兵庫医科大学)、山口県 (山口県立総合医療センター) のすべての施設において倫理審査を終了して、研究を開始している。

(5) 骨系統疾患疑い胎児を診断し適切な妊娠管理を行うための、胎児超音波検査や胎児 CT、遺伝子検査による診断方法の確立 :

胎児超音波検査の児頭大横径、上腕骨、脛骨、腓骨、大腿骨、橈骨、腓骨、腹囲、胸囲等の正常デー

タの統計解析を行った。

胎児CTの被曝量を調査するために全国の胎児CT実施施設に対して、過去3年間に実施した胎児CTの撮影条件を調査した。またより正確な被曝線量を調べるために、妊婦・胎児模型(ファントム)を作製した。

遺伝子診断については、全国の臨床検査会社や研究所に対して調査を行い、骨系統疾患の遺伝子検査実施可能リストを作成した。

(6) 胎児期および出生時点での確定診断指針:

難病の制度改定に合わせて、タナトフォリック骨異形成症の診断指針を作成した。

(7) TDの長期生存患者の発育状況調査:

13例の1年以上の長期生存症例を全国から集め、実際に訪問して主治医や家族から発育状況の聞き取り調査を行った。

(8) 骨系統疾患国際分類の改定に対応:

新規の国際分類の改定は論文化されなかったもので、翻訳作業は実施しなかった。

D. 考察

(1) 胎児骨系統疾患フォーラムとして実施しているため、引き続き全国の施設に参加を呼びかけて、全国レベルでの診断支援を行う。

(2) 日本産科婦人科学会周産期委員会の遺伝学的疾患評価のあり方に関する小委員会と協力して、引き続き拠点施設の整備を進めていく。

(3) ホームページに骨系統疾患の胎児を妊娠した場合や出産した児が骨系統疾患であった場合の問い合わせ窓口として活用できるように引き続き内容の充実に努める。

(4) 各県内の骨系統疾患の発症を可能な限り全例把握するために、それぞれの県内でプロジェクトの周知を行って、疾患の漏れを少なくするように努める必要がある。

(5) 超音波のデータについては各超音波機器メーカーのプログラムに組み込んでもらうことを要望していく予定である。胎児CTについては各施設

の標準的な照射線量についてのデータが揃ったため、今後は胎児CTの標準的な撮影条件の提示を行うと同時に、今後は撮影条件だけではなく、どのような疾患が疑われる場合やどのような週数で実施するかを含めたガイドラインを作成したい。遺伝子診断については全国規模の遺伝子検査解析ラボ一覧を積極的に活用していきたい。

(6) タナトフォリック骨異形成症以外に難病指定の対象となり、かつ適正な診断基準がない疾患については診断基準を作成する。

(7) 長期生存例は昨年京都大学iPS細胞研究所から報告されたスタチンがFGFR3遺伝子変異疾患に治療効果があるとの報告がされており、これらの患者については、臨床試験の対象となる可能性があるため、継続的に情報交換を続ける。

(8) 国際分類の改訂がなされた時点で検討する。

E. 結論

日本で初めて胎児・新生児骨系統疾患を総体的に取り扱う本研究を継続的に発展させていく必要がある。

F. 健康危険情報

特になし

G. 研究発表

1. 論文発表

Okada M, Ikegawa S, Morioka M, Yamashita A, Saito A, Sawai H, Murotsuki J, Ohashi H, Okamoto T, Nishimura G, Imaizumi K, Tsumaki N. Modeling type II collagenopathy skeletal dysplasia by directed conversion and induced pluripotent stem cells. *Hum Mol Genet.* 2015 Jan 15;24(2):299-313.

Nishiyama M, Yan J, Yotsumoto J, Sawai H, Sekizawa A, Kamei Y, Sago H. Chromosome abnormalities diagnosed in utero: a Japanese

study of 28 983 amniotic fluid specimens なし
collected before 22 weeks gestations. J Hum
Genet. 2015 Jan 8.

Morii-Kashima M, Tsubamoto H, Sato C, Ushioda
M, Tomita N, Miyoshi Y, Hashimoto-Tamaoki T,
Tamura K, Sawai H, Shibahara H. Development
of an integrated support system for
hereditary cancer and its impact on
gynecologic services. Int J Clin Oncol. 2014
Dec;19(6):1043-51.

Sago H, Sekizawa A; Japan NIPT consortium.
Nationwide demonstration project of next-
generation sequencing of cell-free DNA in
maternal plasma in Japan: 1-year experience.
Prenat Diagn. 2014 Nov 19.

Yamashita A, Morioka M, Kishi H, Kimura T,
Yahara Y, Okada M, Fujita K, Sawai H, Ikegawa
S, Tsumaki N. Statin treatment rescues FGFR3
skeletal dysplasia phenotypes. Nature. 2014
Sep 25;513(7519):507-11.

Miyazaki O, Sawai H, Murotsuki J, Nishimura
G, Horiuchi T. Nationwide radiation dose
survey of computed tomography for fetal
skeletal dysplasias. Pediatr Radiol. 2014
Aug;44(8):971-9.

2. 学会発表

H. 知的所有権の取得状況

1. 特許取得

なし

2. 実用新案登録

なし

3. その他

II. 分担研究報告

症例の収集と診断の支援システム構築

研究分担者	室月 淳	宮城県立こども病院 部長
	澤井英明	兵庫医科大学 准教授
	山田崇弘	北海道大学 特任講師
	堤 誠司	山形大学 講師
	篠塚憲男	胎児医学研究所 代表
	高橋雄一郎	長良医療センター 医長
	佐世正勝	山口県立総合医療センター センター長
	鬼頭浩史	名古屋大学 准教授
	宮崎 治	国立成育医療研究センター 医長
	渡邊 淳	日本医科大学 准教授
	芳賀信彦	東京大学 教授
	大藺恵一	大阪大学 教授
研究協力者	西村 玄	東京都立小児総合医療センター 部長

研究要旨 本研究は出生前に超音波検査で指摘された骨系統疾患疑いの胎児に対してどのように診断をアプローチし、その後の妊娠管理をどのように行い、分娩方式はどのようにして決定し、新生児管理に結びつけるかについて広範な専門集団が支援するシステムを構築するものである。具体的には1) インターネット利用による胎児の骨系統疾患を診断支援するための症例検討システムの構築、2) セキュリティの充実したウェブ閲覧型システムを構築して臨床医の診断の支援、3) 過去の症例検討のとりまとめ、4) 地域ごとの診断支援システムの構築、5) 臨床医への情報提供、6) 一般の妊婦や罹患児を持つ家族への情報提供といったシステム化されたフローを構築することである。

A. 研究目的

本研究は出生前に超音波検査で指摘された骨系統疾患疑いの胎児に対してどのように診断をアプローチし、その後の妊娠管理をどのように行い、分娩方式はどのようにして決定し、新生児管理に結びつけるかについて広範な専門集団が支援するシステムを構築するものである。

B. 研究方法

1) インターネット利用による胎児の骨系統疾患を診断支援するための症例検討システムの構築は、システムを兵庫医科大学の協力により同大学にサーバーを設置して、運営する。また専門システム開発業者とともにシステムの設計を行う。

2) 上記システムを用いて、実際に臨床医から問合せのあった症例の検討を行う。

3) 過去の症例検討のとりまとめは、上記のウェブ上のシステム構築までの段階で全国の症例を検討した4,000通以上のメールの内容の解析と症例の分析を行う。

4) 地域ごとに胎児骨系統疾患に詳しい産科の専門家を配置し、地域の医療機関からの相談に乗る体制を構築する。

5) 胎児骨系統疾患フォーラムと共同で臨床医への情報提供を目的に、講演会を開催し、またホームページでの情報提供を行う。

6) 一般の妊婦や罹患児を持つ家族への情報提供をホームページの作成により行う。

C. 研究結果

1) システムの構築をすでに完了しており、後述の「疾患頻度を調査するため特定地域を対象としたコホート調査（H26～28年度）」にWeb上の症例登録システムを用いている。

2) メーリングリストによる症例検討を継続している。

3) 研究班の研究分担者の属する施設を中心に、北海道、東北、東京、神奈川、東海、近畿、中国、四国、九州においてセンター施設を選定した。

4) 12月14日（日）に本研究班が主催で胎児骨系統疾患フォーラムが共催して、胎児・新生児骨系統疾患を診療する医師を対象に骨系統疾患X線診断講習会を開催し、胎児骨系統疾患のX線診断について集中的な講習と討議を行った。

また、本研究班で致死性骨異形成症のホームページ www.thanatophoric.com を作成し骨系統疾患の情報を提供し、診断や治療に取り組む産科医や小児科医などからの問い合わせを受け付ける体制を作った。地域の病院（産科）や患者家族から問い合わせがあり、上記の地域診断支援システムに紹

介して対応した。

5) ホームページにおいて情報発信を行っている。

D. 考察

本研究においては今年度で個別に体制はほぼ完成した。引き続き情報を更新して行きたいと考えている。従来のメーリングリストによる診療支援と、「疾患頻度を調査するため特定地域を対象としたコホート調査（H26～28年度）」のWeb上の症例登録システムの2本立てで今後の対応に当たることはこれまでよりも充実したシステムを提供できると考える。

E. 結論

出生前に超音波検査で指摘された骨系統疾患疑いの胎児に対してどのように診断をアプローチし、その後の妊娠管理をどのように行い、分娩方式はどのようにして決定し、新生児管理に結びつけるかについて広範な専門集団が支援するシステムを構築した。また患者家族が情報を得ることができウェブサイトも構築した。

F. 健康危険情報

なし

G. 研究発表

なし

H. 知的財産権の出願・登録状況

（予定を含む。）なし

胎児CTの被曝線量の全国調査

研究分担者

宮崎 治 国立成育医療研究センター 医長

山田崇弘 北海道大学 特任講師

研究協力者

佐々木 清昭 技師長（宮城県立こども病院 放射線部 診療放射線技師長）

笹木 工（北海道大学病院 診療支援部 診療放射線技師）

今井 瑠美（国立成育医療研究センター 放射線診療部 診療放射線技師）

堀内 哲也（国立成育医療研究センター 放射線診療部 臨床研究員）

名定 敏也（兵庫医科大学病院 放射線技術部 診療放射線技師）

木口 雅夫（広島大学病院 診療支援部高次医用画像部門 診療放射線技師）

研究要旨 胎児骨格 CTはここ数年行われるようになった新しい診断方法であるが、昨今 CT の X 線被ばくに対する問題意識が高まっている。そこで 2011 年に当研究班の前身である「致死性骨異形成症の診断と予後に関する研究班」では、胎児 CT 検査に関する被曝量の調査を施行した。胎児骨格 CT について、その施行頻度、適応、撮影方法、胎児被ばく線量などを調査し、本邦での胎児 CT の動向を知る必要があり、またその結果から胎児 CT 撮影方法の標準化が設定できることを目指した。今回は 2011 年の調査の後で、各施設でどのように被曝量の低減化が図られているかを調査した。前回 2011 年に調査を行った施設を基本に新たな施設を含み、対象施設 22 施設とした。胎児骨格系疾患フォーラムから参加を呼びかけ、フォーラムメンバーへコンサルトがあった施設を推薦し、また過去の国内学会発表、論文投稿があった施設を抽出して施設を決定した。また全国の主要施設の診療放射線技師らと連携 8 名のサブグループを結成し、ワークシートを検討・作成した。また主要メーカー 4 社（東芝、GE、SIEMENS、Philips）の技術系とコンタクト、ワークシートを完成させて調査を行った。第 2 回胎児 CT 線量 全国追跡調査を行った。その結果、胎児 CT の被ばく線量はこの 4 年間で有意に減少し DRL は 32% になった（68% 減）、減少の理由は前回 DRL の利用、逐次近似法の普及 kV の低下が考えられる。今回の調査結果、新たな DRL は CTDI vol = 4 mGy、DLP = 128mGycm となった。次の調査まで胎児 CT の DRL として普及が望まれる。

A. 研究目的

胎児 CT の実施は得られる情報が多い反

面、被曝の問題が避けられない。今後胎児 CT が適正に実施されるために、現状の調

査を行い、分析する。近年胎児 CT は胎児骨系統疾患の診断方法として新たに臨床に導入されたが、その被ばく線量については調査がされていない。現在、低線量被ばくが問題視（小児 CT 被ばく）され、胎児期の被ばくは将来発がんのリスクがゼロではない（LNT 仮説）とされている。胎児は他の X 線検査以上に、“正当化と最適化”が必須（ALARA 原則；As low as reasonably achievable）であることから現状を把握することは重要である。

致死性骨異形成症の診断と予後に関する研究班で実施した 2011 年の調査に引き続き、今回もアンケート調査により胎児 3D-CT が行われている本邦の CTDIvol DLP の現状を把握する。その結果から国内の診断参考レベルを設定することを目的とした。

B. 研究方法

胎児 CT サブグループの長期的目的は 2 つあり、まず胎児 CT 撮影の後方視調査（平成 22 年）を行い、胎児 CT 撮影ガイドライン作成（平成 26 年度に日本産科婦人科学会と日本医学放射線学会の合同 WG を設置）を行い、Diagnostic Reference Level (DRL) 設定と胎児 CT の指針の策定を行う。短期計画としては本年度に後方視サーベイ調査票を作成し、全国調査を実施する、回収、集計、解析を今年度中に行うこととした。

調査の対象医療機関は、前回の調査で協力を得られた施設に加えて、胎児骨系統疾患フォーラムと学会発表等から抽出した施設のうち調査協力を承諾が得られた 25 施設に対してアンケートを送付した。このうち 3 施設では前回調査後に胎児 CT を実施していないとのことで、最終的には 22 施設から回答を得た。

調査内容は 3 つのカテゴリーに分け、1) 産科的総論：2) CT 撮影・3D プロトコル

技術と分担した。

アンケートの内容は前半部に CT 撮影プロトコル以外の産科的質問などを設定した。

今回は被ばくのパラメーターである CTDIvol、DLP、管電圧、撮影範囲につき検討した。

C. 研究結果

22 施設、139 例のサンプルが得られた。同施設内の複数のプロトコルや、異なる 2 台の CT 使用は別のプロトコルとした。

図 1 に各施設（図 2）からの報告数を示す。施設によって実施件数には大きな差があることがわかる。また実施週数については、妊娠 28 週以降に実施されている施設が多いが、個別にはさらに早期に実施している施設もある。一部では妊娠 21 週未満で実施している施設もあった。

図 3. に前回調査と今回調査の CTDIvol の変化と図 4. に DLP の変化を示した。CTDIvol の 75% 参照値 (DRL) は $11.3 \Rightarrow 3.6 \text{ mGy}$ と 68% も低下しほぼ $1/3$ に低下している。また同様に DLP も $383 \Rightarrow 128 \text{ mGy} \cdot \text{cm}$ へ低下している。

図 5. に逐次近似法 (Iterative Reconstruction; IR) の有無による CTDIvol の比較を示した。逐次近似法を用いている施設では明らかに CTDIvol が低下していた。

D. 考察

この 4 年間に CTDI、DLP ともに有意に被ばく線量が低下した。その理由は 1) 前回調査結果が DRL として機能したこと（全体の 30% は前回調査報告を参考に、その後プロトコル変更を行っている）、2) 逐次近似法の普及したこと、前回調査：16 施設中、1 施設のみ（8%）今回調査：20 施設中、

14 施設 (70%)、3) CTDI 比較 ; 逐次近似 (IR)あり群くなし群であり、IR を使用しているほうが線量が有意に低い ($p < 0.01$)。4) 管電圧 (kV)設定も下がった。5) 放射線業界でさらに ALARA 概念が普及。6) 各施設が低線量でも撮影できることを経験。

今回、真の逐次近似法である、GE 社 Veo を 2 施設で使用していた。この 2 施設の CTDIvol は 1 mGy を下回り、0.5 mGy となり、胎児 CT の線量が単純撮影 (Guthman, Martius など) より低くなる時代が近づいている。

E. 結論

第 2 回胎児 CT 線量全国追跡調査を行った。胎児 CT の被ばく線量はこの 4 年間で有意に減少し、DRL は 32%になった (68%減)。減少の理由は前回 DRL の利用、逐次近似法の普及、kV の低下などである。今回の調査結果、新たな DRL は CTDI vol = 4 mGy、DLP = 128mGycm で、次の調査まで胎児 CT の DRL として普及が望まれる。CTDIvol と DLP が DRL を超過している施設は画質を維持しつつ斬減することが望まれる。

F. 健康危険情報

なし

G. 研究発表

Miyazaki O, Sawai H, Murotsuki J, Nishimura G, Horiuchi T. Nationwide radiation dose survey of computed tomography for fetal skeletal dysplasias. *Pediatr Radiol.* 2014 Aug;44 (8):971-9.

H. 知的財産権の出願・登録状況

(予定を含む。)

1. 特許取得

なし

2. 実用新案登録

なし

3. その他

なし

図1. 各施設から報告のあった症例数

過去3年9か月間に何件の胎児CTを行いましたか？
それらは妊娠何週に行いましたか？

施設	例数	何週から (w)	何週まで (w)	平均何週 (w)
1	12	28	36	32.5
2	3	無記入	無記入	無記入
3	16	28	36	無記入
4	3	30	34	31
5	5	29	36	31
6	1	30	30	30
7	3	30	33	31
8	24	21	36	30
9	3	29	33	31
10	4	20	24	21
11	8	24	36	32
12	19	17	35	28
13	8	24	36	30
14	9	29	33	31
15	未着	未着	未着	未着
16	1	32	32	32
17	3	28	38	33
18	2	28	28	28
19	未着	未着	未着	未着
20	10	19	34	24
21	1	34	34	34
22	4	30	34	32

集計
合計: 139症例
期間: 17~36週
平均: 30.1±3.1週

図2. 調査協力施設

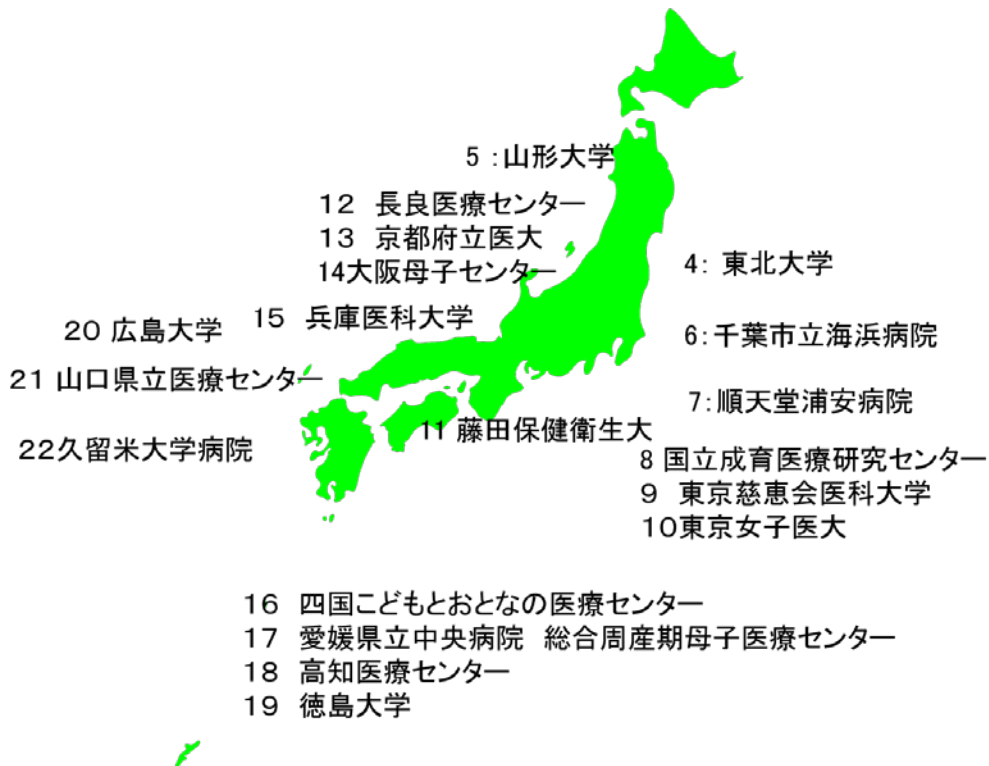


図 3. 各施設の CTDIvol の値の変化

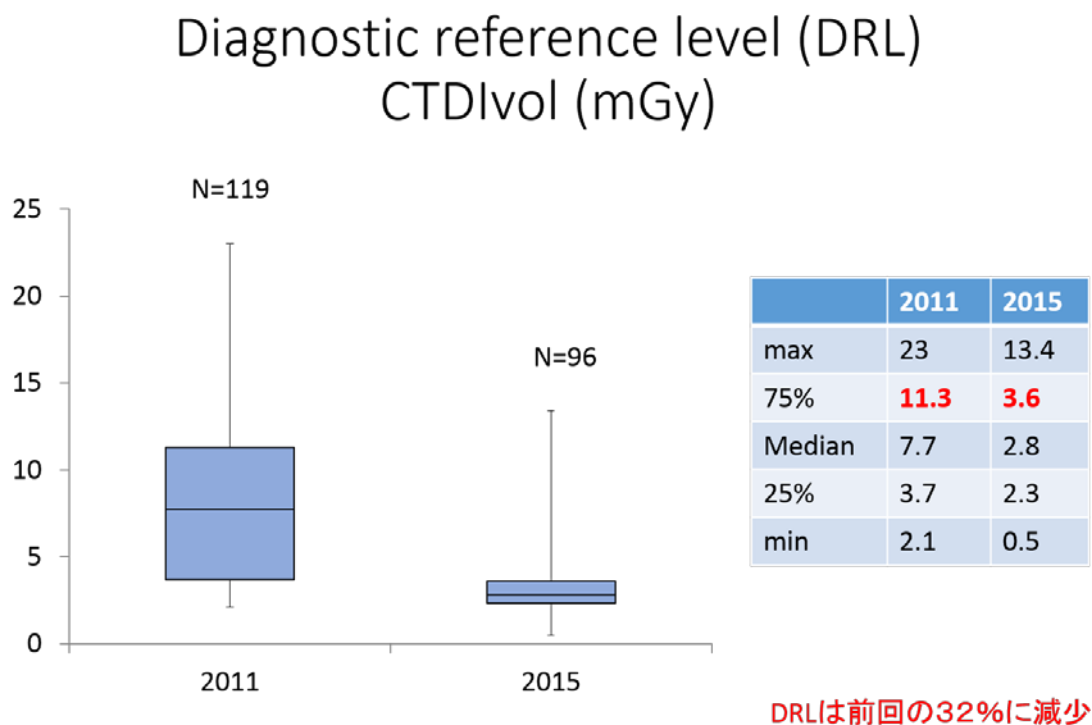


図 4. 各施設の DLP の値の変化

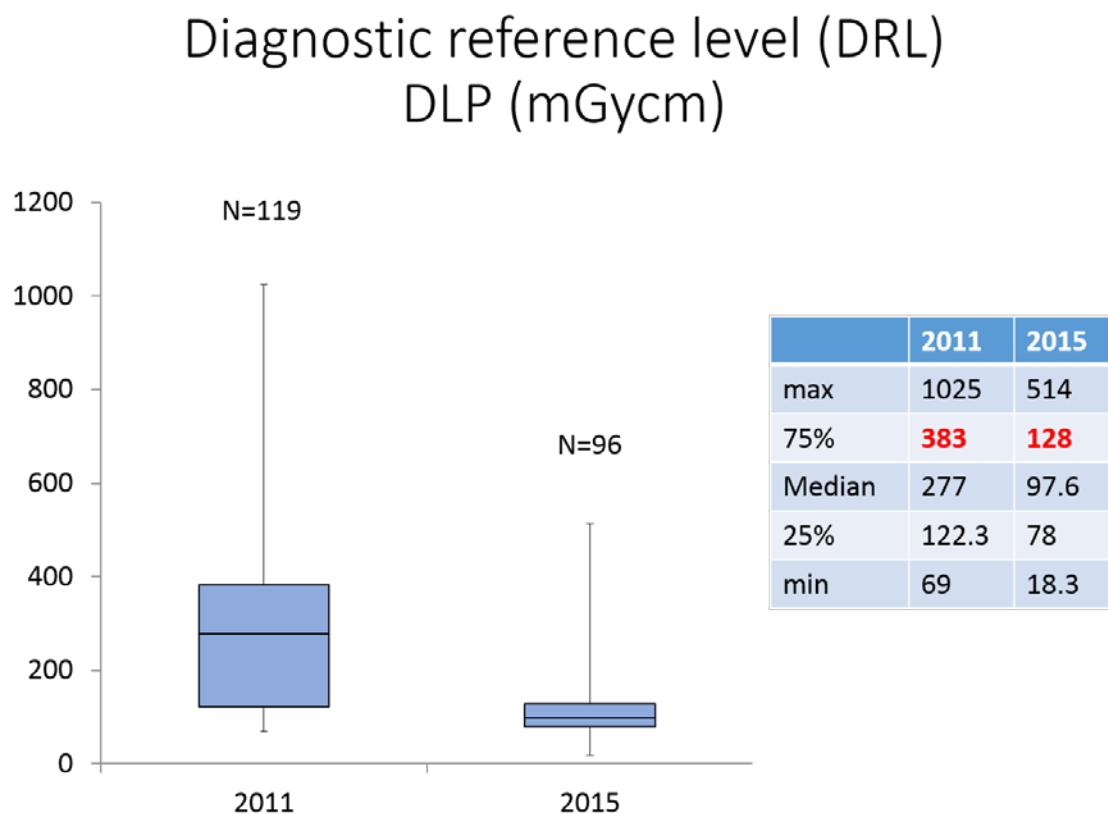
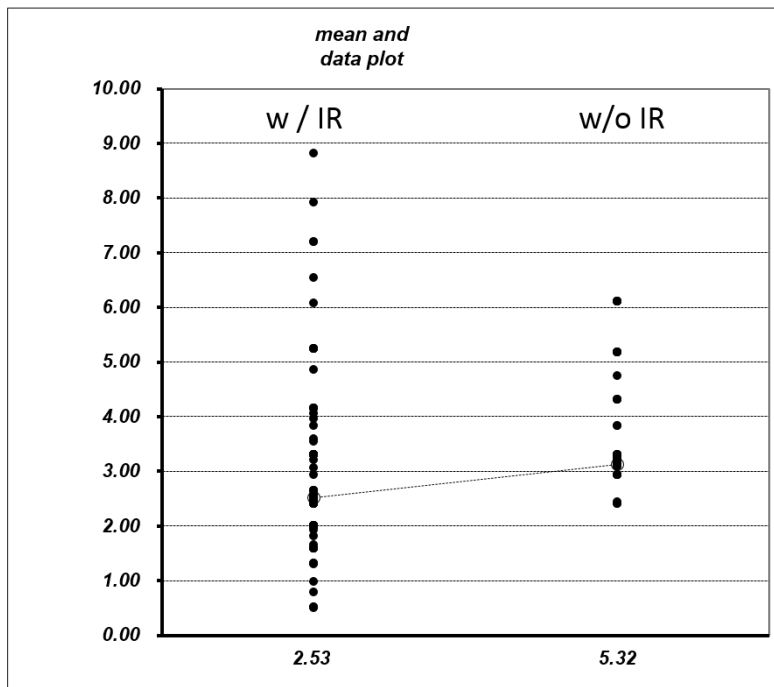


図5. 逐次近似法の有無とCTDIvolの関係について

逐次近似法 (Iterative Reconstruction; IR) 有無によるCTDIvolの比較



有意にIRありのほうが
CTDIが低かった
 $p < 0.01$ ($p=0.001$)

骨形成不全症患者の歯科的所見に関する全国調査

分担研究者 大藪恵一

所属 大阪大学大学院医学系研究科小児科学 職位 教授

研究協力者 仲野和彦

所属 大阪大学大学院歯学部研究科小児歯科学教室 職位 教授

研究協力者 大川玲奈

所属 大阪大学歯学部附属病院小児歯科 職位 助教

研究要旨

以前の班研究「重症骨系統疾患の予後改善に向けての集学的研究」で作成したホームページを維持し、診断基準等の情報を提供した。骨系統疾患の診断、治療の向上を目的として、講演、出版を行った。軟骨無形成症を含む8例のFGFR3異常症の遺伝子診断を行った。また、骨形成不全症患者の歯科的所見に対する全国における実態調査を行った。骨形成不全症の歯科的特徴である象牙質形成不全症、咬合異常が多く症例で認められた。また、ビスフォスフォネート製剤を服用している症例が多かったが、乳歯の抜歯においては特に異常が認められなかったため、ビスフォスフォネート製剤を服用していても交換期の乳歯抜歯に対しては、問題ない可能性が考えられた。

A. 研究目的

骨系統疾患、特に軟骨無形成症に対する診断と治療の向上にむけて、それらに対する啓蒙活動を行う。

骨形成不全症の患者においては、象牙質形成不全に代表される歯科的症状が認められることが多いものの、頻度が少なく重症度も様々であることから、一般的に歯科的対応が困難である。今回、全国の小児歯科専門施設及び口腔外科施設に対して骨形成不全症に関するアンケート調査を行い、骨形成不全症の歯科的所見について分析を行うことにした。

B. 研究方法

平成 24-26 年度に行った厚労省の班研究「重症骨系統疾患の予後改善に向けての集学的研究」で作成した疾患概要などを引き続き、ホームページで掲示する。軟骨無形成症、軟骨低形成症疑いの患者に対して、線維芽細胞増殖因子受容体3型(FGFR3)遺伝子の変異の有無を検討する。

全国の小児歯科関連 69 施設および口腔外科関連 465 施設を対象とし、骨形成不全症に罹患した症例の有無を問い合わせ、症例の内容について情報提供を依頼した。

具体的な項目としては、来院のきっかけ、医科からの紹介の有無、性別、初診時年齢及び最終来院年齢、Sillence の分類、視診とエックス線所見をもとにした乳歯と永久歯における象牙質形成不全症の有無、歯列咬合状態、ビスフォスフォネート製剤服用の有無、歯科処置内容について尋ねた。調査を行った施設のうち、小児歯科関連 42 施設および口腔外科関連 180 施設から回答があり、それらの分析を行った。

(倫理面への配慮)

遺伝子検査に関しては、大阪大学大学院医学系研究科倫理委員会の承認後、informed consent を得て行った。歯科的研究は大阪大学大学院歯学研究科倫理委員会の承認を得てから開始した。

C. 研究結果

「重症骨系統疾患の予後改善に向けての集学的研究」で作成した疾患概要などを引き続き、ホームページで掲示した (<http://www.bone.med.osaka-u.ac.jp/skeleton/>)。

FGFR3 遺伝子の解析を行った。軟骨無形成症例 2 例中 2 例、タナトフォリック骨異形成症 1 例中 1 例、軟骨低形成症 5 例中 3 例に変異を認めた。

回答のあった小児歯科関連 42 施設のうち、骨形成不全症の症例に遭遇していたのは 14 施設であり、遭遇したことがないのが 28 施設であった。一方で、口腔外科関連 180 施設では、骨形成不全症の症例に遭遇していたのは 25 施設であり、遭遇したことがないのが 155 施設であった。小児歯科関連施設および口腔外科関連施設

あわせて 82 症例 (男性 43 名、女性 37 名、無回答 2 名) の情報提供があり、そのうち医科からの紹介があったのは、48 症例であった。

来院のきっかけは、全顎的な精査・予防処置が 26 症例と最も多く、う蝕治療が 19 症例、矯正治療・咬合問題が 13 症例、抜歯依頼が 7 症例、象牙質形成不全が 5 症例、外傷が 4 症例と続き、13 症例がその他・不明であった。

Sillence の分類については、I 型が 22 症例、II 型が 4 症例、III 型が 11 症例、IV 型が 10 症例、V 型が 1 症例であり、不明または無回答が 34 症例であった。このうち、I 型では 11 症例、II 型では 3 症例、III 型が 8 症例、IV 型では 10 症例、V 型では 1 症例、不明または無回答では 9 症例において象牙質形成不全を認めた。

乳歯における象牙質形成不全に関しては、視診で認められたのが 33 症例であり、その中でエックス線所見でも認められた症例は 27 症例であった。一方、永久歯の象牙質形成不全症は視診で認められた症例が 30 症例であり、その中でエックス線所見が認められたのは 27 症例、未萌出などの理由により視診では未確認だがエックス線所見で認められたのが 3 症例であった。歯列咬合の異常としては、反対咬合・下顎前突が最も多く 19 症例であり、次いで開咬が 12 症例、叢生が 7 症例であった。

歯科治療としては、抜歯が 30 症例 (永久歯 5 症例、乳歯 25 症例) と最も多く、う蝕治療が 16 症例 (レジン充填 9 症例・小窩裂孔填塞処置 5 症例・歯髄処置 2 症例)、補綴処置が 9 症例 (乳歯冠 6 症例・

義歯 2 症例・鑄造冠 1 症例)、歯周治療が 7 症例、矯正治療が 5 症例 (咬合誘導 2 症例・外科矯正 3 症例)、外科処置が 3 症例と続いた。

ビスフォスフォネート製剤は 50 症例で服用されており、そのうち 18 症例で乳歯抜歯の経験があったが、全ての症例において抜歯時に異常は認められなかった。

D. 考察

軟骨無形成症治療の候補薬としてスタチンが報告される等、新規情報があり、軟骨無形成症の診断、診療に関する知識を広めていく必要がある。軟骨低形成症は、遺伝子変異が見つかる率が低く、診断基準の見直しが必要である。

歯科の調査から、骨形成不全症の歯科的特徴である象牙質形成不全症が多くの症例において認められた。ビスフォスフォネート製剤を服用している症例が多かったが、乳歯の抜歯においては特に異常が認められなかったため、ビスフォスフォネート製剤を服用していても交換期の乳歯抜歯に対しては、問題ない可能性が考えられる。また、咬合異常が多くの症例で認められたため、それぞれを追跡調査していく必要性が考えられた。

E. 結論

骨形成不全症の歯科的症状、重症度は個々の症例で様々であることから、低年齢時からの医科と連携した歯科的管理が重要である。今後さらに症例を蓄積し、骨形成不全症の実態を明らかにするとともに、よりよい臨床的アプローチについて考えていきたい。

F. 健康危険情報

なし

G. 研究発表

1. 論文発表

(1) Miura K, Kim OH, Lee HR, Namba N, Michigami T, Yoo WJ, Choi H, Ozono K, Cho TJ. Overgrowth syndrome associated with a gain-of-function mutation of the natriuretic peptide receptor 2 (NPR2) gene. *Am J Med Genet A*, 164A:156-163, 2014

(2) Kitaoka T, Miyoshi Y, Namba N, Miura K, Kubota T, Ohata Y, Fujiwara M, Takagi M, Hasegawa T, Jüppner H, Ozono K. Two Japanese familial cases of Caffey disease with and without the common COL1A1 mutation and normal bone density, and review of the literature. *Eur J Pediatr*, 173(6):799-804, 2014 Jun

(3) Kuroyanagi Y, Kawasaki H, Noda Y, Ohmachi T, Sekiya S, Yoshimura K, Ohe C, Michigami T, Ozono K, Kaneko K. A fatal case of infantile malignant osteopetrosis complicated by pulmonary arterial hypertension after hematopoietic stem cell transplantation. *Tohoku J Exp Med*. 2014;234(4):309-12.

(4) 大藪恵一 軟骨無形成症 小児科診療, 77 増刊号 : 613-615, 2014.

(5) 大藪恵一 骨格徴候を伴う, 過成長症候群 成長代謝 Review, 5, No.1, 2014.

2. 学会発表

(1) 佐賀佳奈衣、大川玲奈、野村良太、中野和彦 骨形成不全症患者に認められた象牙質形成不全症を呈した歯の予後に関する分析 第 52 回日本小児歯科学会大会、2014.5.17、東京

(2) Okawa R, Saga K, Nakano K. Dentinogenesis imperfecta in patients with osteogenesis imperfecta. 92nd International Association of Dental Research Meeting, 2014.6.27, Cape Town, South Africa.

(3) Okawa R, Saga K, Nakano K. Three cases of hypophosphatasia diagnosed from dental examination findings. The 9th Biennial Conference of the Pediatric Dentistry Association of Asia, 2014.8.24, Singapore.

(4) Okawa R, Saga K, Nakano K. Prevalence of dentinogenesis imperfecta in Japanese classified by osteogenesis imperfecta subtypes. The 9th International Dental Collaboration of the Mekong River Region Congress, 2014.12.4, Bali, Indonesia.

(5) Saga K, Okawa R, Nakano K. Importance of radiography for identification of dentinogenesis imperfecta in patient with osteogenesis imperfecta. The 9th International Dental Collaboration of the Mekong River Region Congress, 2014.12.4, Bali, Indonesia.

講演】

1) 大藪恵一：軟骨無形成症治療の現在と未来, nordiscience Ach worlshop プログラム, 札幌, 14. 10. 4, 岡山, 14. 10. 18.

【学会】

1) Ueyama K, Namba N, Kitaoka T, Yamamoto K, Fujiwara M, Ohata Y, Miura K, Kubota T, Ozono K : Endocrinological Evaluation in a Patient With Acrodysostosis. Pediatric Academic Societies and Asian Society For Pediatric Research JOINT MEETING ,

Vancouver, 14. 05. 03-06.

2) Kubota K, Miura K, Wang W, Yamamoto K, Fujiwara M, Ohata Y, Tachibana M, Kitaoka T, Miyoshi Y, Namba N, Ozono K : Serum Levels of Amino-terminal Propeptide of C-type Natriuretic Peptide may Predict Growth Response to Growth Hormone Treatment in Patients with Achondroplasia /Hypochondroplasia. ASBMR2014, Houston, 14. 9. 12-15.

3) Kubota T, Miura K, Wang W, Namba N, Kitaoka T, Ohata Y, Fujiwara M, Yamamoto K, Tachibana M, Miyoshi Y, Ozono K : Serum NT-proCNP levels in patients with achondroplasia/hypoplasia may predict response to therapy with growth hormone. 2nd Joint Meeting of the International Bone and Mineral Society and The Japanese Society for Bone and Mineral Research, 神戸, 13. 05. 28-06. 01.

4) 山本景子, 北岡太一, 藤原 誠, 大幡泰久, 三浦弘司, 窪田拓生, 難波範行, 大藪恵一：未熟児で出生し、高血圧を合併した軟骨無形成症の1例, 第47回日本小児内分泌学会学術集会, 東京, 13. 10. 10-12.

H. 知的財産権の出願・登録状況
(予定を含む。)

1. 特許取得
なし
2. 実用新案登録
なし
3. その他
なし

骨系統疾患 発症疫学コホート研究

研究分担者

高橋雄一郎(長良医療センター 産科医長)

山田崇弘(北海道大学大学院 特任講師)

堤 誠司(山形大学産婦人科 講師)

室月淳(東北大学大学院 教授)

澤井英明(兵庫医科大学産婦人科 教授)

佐世正勝(山口県立総合医療センター センター長)

骨系統疾患は国際分類では 456 種類も存在し、近年では新生児期の新しい治療方法の臨床応用への道が開発されつつある。しかし多くの疾患では、難治性で予後不良な経過をたどる事が多いのは事実である。診断および治療戦略を開発していくにあたっては、その発症疫学の正確な情報は不可欠である。しかし本邦におけるコホート研究はなく、流産症例に至ってはまったく把握されていない。しかし流産も含めた正確な前方視コホート研究は、日本全体で行うことは規模が大きすぎて、事実上不可能である。そのため、骨系統疾患の診断経験の多い地域を選択し、部分的な発症疫学研究を行う事で、より精度の高い情報が得られる可能性が考えられる。その発症疫学から日本全体での発症率を推計できれば、今後の治療戦略の一助となる。

本研究計画は各県内の医療機関で胎児の骨系統疾患が疑われる妊娠症例があった場合には、妊婦の同意を得て診断支援の一環として、その超音波検査や胎児 CT、出生後の X 線画像等を各拠点施設にて解析し、診断を行った症例を登録して、疾患頻度を調査することである。妊婦の協力が得られた場合には、各県の拠点施設で診断を確定し、確定しない場合は骨系統疾患診断チームにて検討して診断し、これを症例登録して発症頻度などを調査する。また本研究は疫学研究に関する倫理指針と臨床研究に関する倫理指針を遵守して実施される。

A. 研究目的

疾患頻度を明らかにするため、特定地域を対象としたコホート調査（同期間）を行う。

骨系統疾患は約 460 もの診断が存在すると言われている。近年では新生児期の新しい治療法の臨床応用への道が開発されるなど、疾患によっては有効な戦略がたてられる可能性がでてきている。しかし未だほとんどの多くの疾患では、難治性で予後不良な経過をたどる事が多い。診断および治療戦略を開発していくにあたっては、その発症疫学の正確な情報は不可欠である。しかし本邦におけるコホート研究はなく、流産症例がどれほど存在しているのかすら不明な状況である。

流産も含めた正確な前方視コホート研究は、これだけの医療機関が存在する現状では日本全体で行うことは事実上不可能である。そのため、骨系統疾患の診断経験の多い地域を選択し、部分的な発症疫学研究を行う事で、より精度の高い情報が得られる可能性が考えられる。その発症疫学から日本全体での発症率を推計できれば、今後の治療戦略の一助となる。

B. 研究方法

1道5県における population based の前方視的コホート疫学研究である。対象施設；北海道 山形県、宮城県、岐阜県、兵庫県、山口県、で出産、流産を取り扱う全産婦人科施設 注) この地域で合計約 148502 出生(平成 24 年、人口動態調査) / 1037231(全国)。約 14.3%の出生割合地域で

のコホートとなる。

各県 100%の施設参加を前提とする注；参加できない施設がある場合には、全体からその施設の同期間の分娩数を差し引いて分母を調整して計算する

患者対象

成人妊婦のうち以下の(1)、(2)に該当する患者で、出生を各指定地域でおこなった症例とする。

(1) 各県で妊娠中絶した症例において、胎児骨系統疾患が疑われる場合

(2) 各県での妊娠 22 週以降の出生児において骨系統疾患が疑われる場合

期間

2015 年 3 月 1 日から 2018 年 12 月 31 日までの 3 年間。ただし、2015 年 3 月からの 2 年間は症例登録期間とし、2017 年 3 月からの 1 年間はデータ解析、論文作成などの研究期間とする。

情報収集

収集するものは生後の児のレントゲンもしくは CT 画像で通常の臨床で用いているものとし、本研究の為に新たに撮像することとはしない。流産の場合には同意を得て撮像した症例とする。(生後の確定が得られなかった場合には胎児情報をもって判断する。)

周産期情報、画像情報はデジタル化したものを匿名で回収し、第三者機関(仮称；骨系統疾患 診断チーム；下記)において診断が確定した場合に発症と認定する。

分娩が発生した時点で、所定の用紙に無記名で情報を記載していただく。

(連結可能匿名化)

事務局；(各県にそれぞれ事務局を設置) 岐阜県の場合は「岐阜県胎児骨系統疾患 発症疫学研究 事務局」宛 長良医療センター産科；Fax 058 (295) 0077

情報解析 一年間の登録期間の後、班会議研究者において解析を行う。

Primary endpoint) 骨系統疾患の流産も含めた発症疫学を計算
Secondary endpoints) 疾患別の大まかな発症疫学を検討 生後の画像診断による確定診断部門(仮称;骨系統疾患 診断チーム)

<診断部門>西村玄(都立小児総合医療センター)、宮寄 治(国立成育医療研究センター) 澤井英明(兵庫医科大学) 室月淳(宮城こども病院)

<症例提示>山田崇弘(北海道大学)、佐藤秀平(青森労災病院)、堤誠司(山形大学)、室月淳(宮城こども病院)、高橋雄一郎(長良医療センター)、澤井英明(兵庫医科大学)、佐世正勝(山口県総合医療センター)

倫理指針の遵守

前方視コホート研究に関しては平成 14 年度 文部省、厚労省の「疫学研究に関する倫理指針」を遵守して本研究プロトコールを作成した。

インフォームド・コンセントのための手続

患者研究説明を用いて、患者情報の fax 前にて、文書にて同意をえる。

研究に参加することにより期待される利益及び起こりうる危険並びに必然的に伴う不快な状態 の明記済み。

各産婦人科施設への研究説明書

本研究書および「研究協力していただく医療機関の主治医の先生へ」を用いて事前に各施設に研究説明を行い研究参加の意思の確認を行う。

倫理委員会

岐阜県では事務局を設置する長良医療センターにおいて倫理委員会の承認を得る。各県の研究分担者の施設においても同様。

個人情報保護の方法

情報を収集する事務局においては、データ解析を行わず班会議分担研究者以外はデータベースを使用しない。

研究機関の名称 および 研究者等の氏名
岐阜県

岐阜大学医学部産科婦人科

森重健一郎 (教授)

国立病院機構長良医療センター 産科医長

高橋 雄一郎 (事務局)

<全体診断部門>

西村玄(都立小児総合医療センター 診療放射線科部長)

宮寄 治(国立成育医療研究センター放射線科医長)

山田崇弘(北海道大学大学院 特任講師)

佐藤秀平(青森労災病院)

堤誠司（山形大学産婦人科 講師）

室月淳（東北大学大学院 教授）

高橋雄一郎（長良医療センター 産科医長）

澤井英明（兵庫医科大学産婦人科 准教授）

佐世正勝（山口県立総合医療センター センター長）

C. 結果

D. 考察

E. 結論

平成 27 年度に継続しているので、現段階ではこれらは記載せず。

厚生労働科学研究費補助金（難治性疾患政策研究事業）

研究分担報告書

タナトフォリック骨異形成症の発育調査

研究代表者 澤井英明 兵庫医科大学 教授

研究協力者 潮田まり子 兵庫医科大学 大学院生

研究要旨

タナトフォリック骨異形成症（致死性骨異形成症）の1年以上の生存例を把握し、どのような発育状態であるのかを調査した。タナトフォリック骨異形成症は胎児期より重度の四肢短縮を示す重症の先天性骨系統疾患である。その多くは出生直後より呼吸不全をみとめ周産期致死性の疾患とされている。しかしながら近年、出生直後からの呼吸管理により長期生存が可能である症例がしばしば報告されている。当研究班の2010年の全国調査（1次調査）では、出生した51名のうち1年以上の生存例は16名にのぼっている。長期生存例はしばしば報告されているが、長期生存児の状況を集約した情報はない。今回、生後1年以上生存している児の調査を行い、病歴や生活歴などを主治医および患者家族から得て、それらの情報をまとめて報告する事を目的に二次調査を開始した。医療の進歩に伴い、長期生存例が多く見られるようになってきている。呼吸器管理は必須であった。気管切開の多くは生後1年未満に行われていた。半数は在宅管理が可能であった。変異遺伝子はArg248Cysが最も多かった。精神発達は症例により差はあるものの、3か月程度から1～1歳6ヶ月程度までの発達で、全例に精神発達遅滞を認めた。運動発達は定額はみとめなかった。ほとんどの症例で四肢と頭部がわずかに動く程度であった。発達の良好なものは体幹を使った運動が可能であった。言語発達は呼吸器管理が行われており評価不能であったが、嫌な時や誰かを呼ぶときは発語している様子は見られた。加齢とともに皮膚病変の増加を認めた。しかしながら、呼吸器管理は必須であり、全例において運動精神発達遅滞を認めた。

A. 研究目的

タナトフォリック骨異形成症は胎児期より重度の四肢短縮を示す重症の先天性骨系統疾患である。その多くは出生直後より呼吸不全をみとめ周産期致死性の疾患とされている。しかし厚生労働科学研究費補助金・難治性疾患克服研究事業・致死性骨異形成症の診断と予後に関する研究班の全国調査で、タナトフォリック骨異形成症はその名称とは異なり、周産期致死性とは必ずしも言えないことが明らかとなった。出生直後からの呼吸管理により長期生存が可能である症例がしばしば報告されている。当研究班の2010年の全国調査(1次調査)では、出生した51名のうち1年以上の生存例は16名にのぼっている。長期生存例はしばしば報告されているが、長期生存児の状況を集約した情報はない。今回、生後1年以上生存している児の調査を行い、病歴や生活歴やなどを主治医および患者家族から得て、それらの情報をまとめて報告する事を目的に二次調査を行うこととした。

B. 研究方法

1年以上生存している長期生存例の調査を実施した。全国のNICUまたは小児科施設に協力を求める依頼を行い、新たに数例の可能性のあるケースを把握した。本調査は施設内倫理委員会の承認を得て2012年から2014年の間に研究班のHPの掲載や全国の小児科研修施設137施設への調査協力依頼を行い、主治医および患者家族から同意を得られたものを調査対象とした。

現在までに16症例の登録を行い、患者本人や主治医、患者家族等と面会により情報を得た。主に出生時の経過、呼吸器管理法、

精神発達、運動発達などについて調査を行った。

(倫理面への配慮)

タナトフォリック骨異形成症の発育調査については、兵庫医科大学倫理委員会において承認を得て調査を実施した。

C. 研究結果

次ページに記載

D. 考察

タナトフォリック骨異形成症の長期生存例の実際の発育・発達状況:現在まだ研究を継続しているので、結論は出ていないが、概要では、タナトフォリック骨異形成症で長期生存しているケースでは呼吸管理が不可欠であり、呼吸管理をしていない例はほとんどが周産期死亡となっている。そしてその後の発達・発育には低酸素状態にあったかどうかが大きく発育に影響すると思われるので、低酸素状態が推測される場合にはすみやかな人工換気が必要と思われる。呼吸器管理は必須であった。気管切開の多くは生後1年未満に行われていた。半数は在宅管理が可能であった。変異遺伝子はArg248Cysが最も多かった。精神発達は症例により差はあるものの、3か月程度から1~1歳6ヶ月程度までの発達で、全例に精神発達遅滞を認めた。運動発達は定額はみとめなかった。ほとんどの症例で四肢と頭部がわずかに動く程度であった。発達の良好なものは体幹を使った運動が可能であった。言語発達は呼吸器管理が行われており評価不能であったが、嫌な時や誰かを呼ぶときは発語している様子は見られた。加齢とともに皮膚病変の増加を認めた。

E. 結論

医療の進歩に伴い、長期生存例が多

く見られるようになってきている。しかしながら、呼吸器管理は必須であり、全例において運動精神発達遅滞を認めた。

患者背景

症例	性別	管理場所	調査時年齢	症例	性別	管理場所	調査時年齢
1	男	入院	22歳4か月	9	男	在宅	5歳0か月
2	女	在宅	7歳7か月	10	女	在宅	10歳0か月
3	男	在宅	8歳7か月	11	女	入院	6歳4か月
4	男	入院	2歳0か月	12	女	入院	5歳7か月
5	男	在宅	1歳5か月	13	男	入院	13歳11か月
6	男	在宅	3歳2か月	14	男	在宅	6歳8か月
7	女	入院	3歳3か月	15	女	在宅	9歳5か月
8	男	入院	3歳2か月	16	女	入院	27歳10か月

男:女=9:7

家族背景および遺伝検査

症例	父年齢	母年齢	家族歴	変異遺伝子
1	31	29	なし	Arg248Cys
2	35	34	なし	未実施
3	34	31	なし	未実施
4	37	37	なし	Arg248Cys
5	不明	不明	なし	Arg248Cys
6	30	29	なし	未実施
7	29	28	なし	未実施
8	38	37	なし	Tyr373Cys
9	35	31	なし	未実施
10	40	38	なし	Arg248Cys
11	35	35	なし	Tyr373Cys
12	36	35	なし	Arg248Cys
13	31	32	なし	あり(詳細不明)
14			なし	
15	49	36	なし	Arg248Cys
16	30	30	なし	Arg248Cys

置換部位	Kitoh の報告 (1998)	Xueら の報告 (2014)
TD1		
Arg248Cys	57	115
Ser249Cys	9	11
Gly370Cys	1	4
Tyr373Cys	21	41
Lys650Met	2	2
Stop codon mutation	7	14
TD2		
Lys650Glu	23	31
Total	120	218

出生時情報

症例	出生時週数	AS	分娩方法	出生前診断	産生風量	小児科医の立会
1	36週5日	4/6	帝王切開	あり(US)	あり	あり
2	40週3日	4/6	経陰分娩	あり	あり	あり
3	35週2日	1/2	帝王切開(胎児適応)	あり(US)	あり	あり
4	37週5日	6/8	帝王切開(胎児適応)	あり(CT)	あり	あり
5	38週2日	2/6	経陰分娩	なし	あり	なし
6	38週0日	8/9	経陰分娩	あり(US,CT)	あり	あり
7	39週0日	4/6	帝王切開(骨盤位)	あり(US)	あり	あり
8	33週5日	3/8	帝王切開(早割)	あり(3DCT)	あり	あり
9	37週3日	6/9	帝王切開	あり(US)	あり	あり
10	38週1日	5/5	帝王切開(分娩停止)	あり(羊水遺伝子)	あり	あり
11	36週4日	8/8	経陰分娩	あり(US)	あり	あり
12	37週2日	8/9	帝王切開(胎児適応)	あり(US,CT)	あり	あり
13	36週3日	4/6	帝王切開(CPD)	あり(US)	あり	あり
14	30週1日	5/6	経陰分娩(母体適応)	あり	あり	あり
15	39週3日	3/5	帝王切開(胎児心拍異常)	あり(MRI)	あり	あり
16	36週3日	6/8	経陰分娩	あり(US)	あり	あり

出生直後の対応

・積極的に管理 14例

⇒ 出生前診断が行われており、可能な限りの医療介入を希望。

・対症療法のみ 1例

⇒ 看取り予定で酸素投与のみであったが、24時間経過後も自発呼吸があり生存したため、その後積極的な医療介入となる。

・小児科医不在 1例

⇒ 出生前診断が行われていなかったため、個人入院で分娩となる。分娩後酸素投与にて新生児科搬送となる。

出生時の体格

症例	往胎週数	体重(g)	身長(cm)	頭圍(cm)	胸圍(cm)
1	36週5日	2798 (+0.45D)	不明	不明	不明
2	40週3日	2978	38 (-5.95D)	38 (+3.65D)	不明
3	35週2日	2783 (+1.65D)	35 (-3.55D)	32.3 (+0.55D)	27.9
4	37週5日	2800	39 (-3.65D)	37.5 (+3.65D)	28.5
5	38週2日	2528	37 (-4.65D)	37 (+3.05D)	26
6	38週0日	2362 (-1.75D)	40 (-3.45D)	36 (+2.35D)	26
7	39週0日	2606 (-0.85D)	32 (-6.85D)	38.2 (+3.95D)	27(day2)
8	33週5日	1720	35 (-3.25D)	32 (+0.95D)	不明
9	37週3日	2744	34 (-4.75D)	38.2 (+4.15D)	不明
10	38週1日	3686 (+2.85D)	41.4 (-3.05D)	37.8 (+3.75D)	不明
11	36週4日	2538	40 (-2.65D)	35 (+1.95D)	不明
12	37週2日	2754 (+0.25D)	38 (-3.75D)	36.8 (+3.15D)	26.8
13	36週3日	2464	36 (-3.65D)	37.5 (+3.85D)	27.5
14	30週1日	不明	不明	不明	不明
15	39週3日	3026 (+0.35D)	37 (-5.65D)	不明	29
16	36週3日	2904 (+1.15D)	39 (-2.85D)	35 (+1.65D)	30.2

頭圍
平均+2.85D
身長
平均-4.15D

※症例7は日齢2の数値
※標準偏差は「在胎期間別出生時体格標準値2011年」より算出

呼吸器管理

本疾患は呼吸器管理からの離脱は困難であり、早期から気管切開を導入している症例が多くみられる。

全例人工呼吸器管理

気管切開実施例 12例

気管切開非実施例 4例

症例	気管切開施行時期
1	8d月
2	51日
3	131日
4	97日
5	38日
6	187日
9	3歳
10	1106月
12	8d月
13	3歳
14	あり
15	65日

・気管頭頸動脈瘻のリスクが高い
・手術の際の体位確保が困難
・特に頸部が短く太く術野の確保が困難

生後1年未満が9例
在宅呼吸器管理 8例

栄養管理

栄養方法	N
経管栄養	11
経管栄養+経口摂取	2
経口摂取	3

経鼻チューブ 10例
胃ろう造設 1例

必要な栄養素・水分を両方の摂取形態で補いながら行っている。
症例A: メインは経管栄養
離乳食は嫌がるが、おやつ(赤ちゃんせんべい)は自分の手で把持して食べる。
症例B: 調子の良いときは離乳食で8割摂取する。

症例2: 通常小児食
症例4: 離乳食
症例15: ミキサー食

精神運動発達

発達評価方法

客観的な評価: 発達評価スケールでの回答は気管切開が行われ発語がないなどの理由より評価困難であり、調査回答を得られなかった。

運動、社会性、言語それぞれに対して、可能な限りの聞き取り調査を行ったので、個々の症例について紹介する。

精神発達	症例	調査時年齢	精神発達状況	おおよその発達年齢
	1	22歳4か月	寝たきり(重度脳障害)	評価できず
	2	7歳7か月	笑う 簡単な指示やルールを理解する 音楽に合わせてタンバリンをならす 空襲警など「あーあー」し声に出し伝える 人の区別をする	1歳以上
	3	8歳7か月	あやすと笑う、顔をしかめる 人の区別はしている印象	6ヶ月
	4	2歳0か月	笑う 自分の気持ちやジェスチャーで伝える 人見知りあり	
	5	1歳5か月	追視、音のする方向を見る 笑う、泣く、顔をしかめる 人見知りをする 人を呼ぶときに顔をならす	1歳
	6	3歳2か月	あやすと笑う、顔をしかめる 人を呼ぶジェスチャーをする 兄弟がそばで遊んでいると、自分も体を動かし踊る 寝たなると顔にガーゼをのせる癖がある	1歳
	7	3歳3か月	寝たきり 生後3ヶ月で重度脳障害を起すまではあやすと笑う、追視あり	評価できず
	8	3歳2か月	あやすと笑う、泣く、顔をしかめる、追視	3ヶ月

精神発達	症例	調査時年齢	精神発達状況	おおよその発達年齢
	9	5歳0か月	あやすと笑う、泣く、顔をしかめる、追視 音のする方を見る 人の区別はなし	3ヶ月
	10	10歳0か月	笑う、泣く、顔をしかめる 絵本の絵を音で追う 呼び鈴が鳴るとドアの方を見る 歯ブラシを見せると口をあける	1歳以上
	11	6歳4か月	笑う、泣く、顔をしかめる、追視 音に対する反応あり	1歳
	12	5歳7か月	笑う、泣く、顔をしかめる、追視、音に対する反応 わざと呼吸器チューブをはずし人を呼ぶ	6ヶ月~1歳
	13	13歳11か月	看護師がいなくなると声を出して呼ぶ 口を開けてというと、口を開ける いやな時は音を出す 知らない人が笑ると反応が低下する(人見知り?)	1歳以上
	14	6歳8か月	追視なし、音に対する反応なし(聴覚、聴力が低い?) 手をさわると、目を向けて反応する。	評価できず
	15	9歳5か月	手首に鈴のおもちゃをつけると、ふって遊ぶ 自分の名前を呼ばれると、その方向を向く ジュースを見せると口を開ける	1歳以上
	16	27歳10か月	笑う、泣く、顔をしかめる、追視なし	3ヶ月

精神発達

・全例呼吸器管理を行っており、運動能力も低いいため、発達評価は困難であった。

・精神発達は寝たきり、3ヶ月程度~1歳以上とばらつきがあった。

・脳障害がなければ、あやすと笑う・泣く・顔をしかめる・追視と3ヶ月程度の発達は認める。

・精神発達が1歳以上と比較的発達の良いものは栄養管理も経口摂取ができていたものが多い。

運動発達	症例	調査時年齢	運動発達
	1	22歳4か月	寝たきり
	2	7歳7か月	3歳ころから活発になる。 手足をよく動かし、背中ですりばいして移動する。
	3	8歳7か月	四肢をわずかに動かす。
	4	2歳0か月	介助をすとお菓子を手全体でつかみ、口元にもっていく。 手足を動かす。
	5	1歳5か月	四肢の動きあり、手ではらいのける。
	6	3歳2か月	四肢の動きあり。そばにあるガーゼを顔にかける。 寝返りあり 姉が踊る姿を見て、同じ様に体を左右に動かす。 足を拳上した状態で保持する事ができる。
	7	3歳3か月	寝たきり
	8	3歳2か月	四肢の動きは認めず。 顔をわずかに左右に動かすのみ。
	9	5歳0ヶ月	四肢をわずかに動かす。 顔を左右に動かす。

運動発達	症例	調査時年齢	運動発達
	10	10歳0か月	四肢の動きはほとんど認めず。
	11	6歳4か月	上肢の動きあり。下肢は動きなし。 手は頬まであがり、頬をかくこともある。
	12	5歳7か月	右上肢は耳まで動く。 左上肢・下肢はわずかに動く程度。 物を顔の上のせるとはらいのける。
	13	13歳11か月	四肢がわずかに動く程度。
	14	6歳8か月	四肢がわずかに動く程度。
	15	9歳5か月	手を口元にもっていき、指しゃぶりする。 手首につけたおもちゃを振る。 側臥位の位置まで動かす事ができる。
	16	27歳10か月	四肢、体幹の動きは認めず。

運動発達

- 運動発達には症例によって差が見られた。
- 多くの症例が、わずかに四肢を動かす事は可能である。
- 運動発達の良い症例では、体幹を使って体を移動させたり、側臥位や寝返りをうてる症例があった。
- せんべいを指で挟むという対立運動ができる症例があった。

皮膚病変

- 黒色表皮腫 acanthosis nigricans
加齢とともに皮膚の褐色化を認める。
特に額・頸部・腋窩に著明に認める。
- 脂漏性角化症 seborrheic keratosis



皮膚病変の経時的変化

※症例が違うので、一概には言えませんが・・・



3歳2ヶ月



3歳3ヶ月



5歳0ヶ月



7歳7ヶ月



8歳7ヶ月



22歳4ヶ月

その他

- 便秘症
- 体温調節障害
- 水頭症
- 大後頭孔狭窄
- 痙攣
- てんかん(脳波異常)
- 膀胱機能障害
- 嚥下障害
- 歯芽発育あり

Ⅲ. 研究成果の刊行に関する一覧表

書籍

無し

著者氏名	論文タイトル名	書籍全体の 編集者名	書籍名	出版社名	出版地	出版年	ページ

雑誌

発表者氏名	論文タイトル名	発表誌名	巻号	ページ	出版年
Yamashita A, Morioka M, Kishi H, Kimura T, Yahara Y, Okada M, Fujita K, Sawai H, Ikegawa S, Tsumaki N.	Statin treatment rescues FGFR3 skeletal dysplasia phenotypes.	Nature.	513(7 519):	507-11.	2014
Miyazaki O, Sawai H, Murotsuki J, Nishimura G, Horiuchi T.	Nationwide radiation dose survey of computed tomography for fetal skeletal dysplasias.	Pediatr Radiol.	44(8):	971-9.	2014
Okada M, Ikegawa S, Morioka M, Yamashita A, Saito A, Sawai H, Murotsuki J, Ohashi H, Okamoto T, Nishimura G, Imaizumi K, Tsumaki N.	Modeling type II collagenopathy skeletal dysplasia by directed conversion and induced pluripotent stem cells.	Hum Mol Genet. 2015	24(2):	299-313.	2014
高田雅代, 渡邊淳, 澤井英明, 丸山秀彦, 塚原紗耶, 渋谷昇平, 片山典子, 立石洋子, 熊澤一真, 中西美恵, 多田克彦, 森茂弘, 森田啓督, 山邊陽子, 中村信, 影山操.	出生前に超音波検査により疑われ, 出生後の遺伝子解析で確定診断した周産期型低フォスファターゼ症の1例.	日本周産期・新生児医学会雑誌	50:	362 - 367.	2014

Kaga A, Murotsuki J, Kamimura M, Kimura M, Saito-Hakoda A, Kanno J, Hoshi K, Kure S, Fujiwara I.	Association of achondroplasia with Down syndrome: difficulty in prenatal diagnosis by sonographic and 3-D helical computed tomographic analyses.	Congenit Anom (Kyoto)	epub	epub	2014
Imai R, Miyazaki O, Horiuchi T, Kurosawa H, Nosaka S.	Local diagnostic reference level (DRL) based on size-specific dose estimates (SSDE): Assessment of pediatric abdominal/pelvic computed tomography (CT) at a Japanese national children's hospital	Pediatr Radiol	Epub	Epub	2014
Nagata E, Kano H, Kato F, Yamaguchi R, Nakashima S, Takayama S, Kosaki R, Tonoki H, Mizuno S, Watanabe S, Yoshiura K, Kosho T, Hasegawa T, Kimizuka M, Suzuki A, Shimizu K, Ohashi H, Haga N, Numabe H, Horii E, Nagai T, Yoshihashi H, Nishimura G, Toda T, Takada S, Yokoyama S, Asahara H, Sano S, Fukami M, Ikegawa S, Ogata T	Japanese founder duplications/triplications involving BHLHA9 are associated with split-hand/foot malformation with or without long bone deficiency and Gollop-Wolfgang complex.,	Orphanet J Rare Dis	9	125	2014
Mishima K, Kitoh H, Haga N, Nakashima Y, Kamizono J, Katagiri T, Susami T, Matsushita M, Ishiguro N:	Radiographic characteristics of the hand and cervical spine in fibrodysplasia ossificans progressiva.	Intractable Rare Dis Res	3	46-51	2014,

Matsushita M, Hasegawa S, Kitoh H, Mori K, Ohkawara B, Yasoda A, Masuda A, Ishiguro N, Ohno K.	Meclozine promotes longitudinal skeletal growth in transgenic mice with achondroplasia carrying a gain-of-function mutation in the FGFR3 gene.	Endocrinology	Epub	Epub	2014
Olney RC, Prickett TCR, Espiner EA, Mackenzie WG, Duker A, Ditro C, Zabel B, Hasegawa T, Kitoh H, Aylsworth AS, Bober MB.	C-type natriuretic peptide (CNP) plasma levels are elevated in subjects with achondroplasia, hypochondroplasia, and thanatophoric dysplasia.	J Clin Endocrinol Metab	Epub	Epub	2014
Matsushita M, Kitoh H, Subasioglu A, Colak FK, Dundar M, Mishima K, Nishida Y, Ishiguro N.	A glutamine repeat variant of the RUNX2 gene causes cleidocranial dysplasia.	Mol Syndromol	in press	in press	
Kitoh H, Kaneko H, Mishima K, Matsushita M, Kadono I, Nishida Y, Ishiguro N.	Early and late fracture following extensive limb lengthening in achondroplasia and hypochondroplasia	Bone Joint J	96-B:	1269-1273	2014
Hoover-Fong J, Sobreira N, Jurgens J, Modaff P, Blout C, Moser A, Kim OH, Cho TJ, Cho SY, Kim SJ, Jin DK, Kitoh H, Park WY, Ling H, Hetrick KN, Doheny KF, Valle D, Pauli RM.	Mutations in PCYT1A, encoding a key regulator of phosphatidylcholine metabolism, cause spondylometaphyseal dysplasia with cone-rod dystrophy	Am J Hum Genet	94	105-112	2014
Matsushita M, Kitoh H, Kaneko H, Mishima K, Itoh Y, Tokita Y, Ishiguro N.	A novel in-frame deletion of the RUNX2 gene causes a classic form of cleidocranial dysplasia	J Bone Miner Metab	32	96-99	2014

Matsushita M, Kitoh H, Michigami T, Tachikawa K, Kaneko H, Mishima K, Ishiguro N.	Benign prenatal hypophosphatasia: a treatable disease not to be missed.	Ped Radiol	44	340-343	2014
Watanabe A*, Satoh S, Fujita A, Naing BT, Orimo H, Shimada T.	Perinatal hypophosphatasia caused by uniparental isodisomy.	Bone.	60	93-97	2014
Miyagawa K, Yamazaki M, Kawai M, Nishino J, Koshimizu T, Ohata Y, Tachikawa K, Mikuni-Takagaki Y, Kogo M, Ozono K, Michigami T.	Dysregulated gene expression in primary osteoblasts and osteocytes isolated from hypophosphatemic Hyp mice.	PLoS ONE	9(4)	e93840	2014
Kawai M, Kinoshita S, Shimba S, Ozono K, Michigami T.	Sympathetic activation induces skeletal Fgf23 expression in a circadian rhythm-dependent manner	J Biol Chem,	289:	1457-1466	2014
Yamazaki M, Kawai M, Miyagawa K, Ohata Y, Tachikawa K, Kinoshita S, Nishino J, Ozono K, Michigami T.	Interleukin-1-induced acute bone resorption facilitates the secretion of fibroblast growth factor 23 into the circulation.	J Bone Miner Metab	Epub	Epub	2014
Takeyari S, Yamamoto T, Kinoshita Y, Fukumoto S, Glorieux FH, Michigami T, Hasegawa K, Kitaoka T, Kubota T, Imanishi Y, Shimotsuji T, Ozono K	.Hypophosphatemic osteomalacia and bone sclerosis caused by a novel homozygous mutation of the FAM20C gene in an elderly man with a mild variant of Raine syndrome., ,	Bone	67C:	56-62	2014
Kubota T, Kitaoka T, Miura K, Fujiwara M, Ohata Y, Miyoshi Y, Yamamoto K, Takeyari S, Yamamoto T, Namba N, Ozono K.	Serum fibroblast growth factor 23 is a useful marker to distinguish vitamin D-deficient rickets from hypophosphatemic rickets.	Horm Res Paediatr	81(4)	251-7	2014

Ozono K, Hasegawa Y, Minagawa M, Adachi M, Namba N, Kazukawa I, Kitaoka T, Asakura Y, Shimura A, Naito Y.	Therapeutic use of oral sodium phosphate (phosribbon® combination granules) in hereditary hypophosphatemic rickets.	Clin Pediatr Endocrinol,	23(1)	9-15	2014
Kitaoka T, Miyoshi Y, Namba N, Miura K, Kubota T, Ohata Y, Fujiwara M, Takagi M, Hasegawa T, Jüppner H, Ozono K.	Two Japanese familial cases of Caffey disease with and without the common COL1A1 mutation and normal bone density, and review of the literature	Eur J Pediatr,	173(6)	799-804	2014
Matsushita M, Hasegawa S, Kitoh H, Mori K, Ohkawara B, Yasoda A, Masuda A, Ishiguro N, Ohno K.	Meclozine promotes longitudinal skeletal growth in transgenic mice with achondroplasia carrying a gain-of-function mutation in the FGFR3 gene.	Endocrinology.	156(2)	548-54	2015
Matsushita M, Kitoh H, Mishima K, Nishida Y, Ishiguro N.	A case of severe proximal focal femoral deficiency with overlapping phenotypes of Al-Awadi-Raas-Rothschild syndrome and Fuhrmann syndrome.	Pediatr Radiol	44(12)	1617-9	2014
Miura K, Kim OH, Lee HR, Namba N, Michigami T, Yoo WJ, Choi IH, Ozono K, Cho TJ	Overgrowth syndrome associated with a gain-of-function mutation of the natriuretic peptide receptor 2 (NPR2) gene	Am J Med Genet A.	164A(1)	156-63	2014
Kuroyanagi Y, Kawasaki H, Noda Y, Ohmachi T, Sekiya S, Yoshimura K, Ohe C, Michigami T, Ozono K, Kaneko K.	A fatal case of infantile malignant osteopetrosis complicated by pulmonary arterial hypertension after hematopoietic stem cell transplantation.	Tohoku J Exp Med.	234(4)	309-12.	2014

大藪恵一	骨格徴候を伴う、過成長症候群	PAS/ASPR Joint Meeting Report		8	2014
大藪恵一	軟骨無形成症	小児科診療	77	613- 615	2014

IV. 研究成果の刊行物・別冊

A Glutamine Repeat Variant of the *RUNX2* Gene Causes Cleidocranial Dysplasia

Masaki Mastushita^a Hiroshi Kitoh^a Asli Subasioglu^b Fatma Kurt Colak^c
Munis Dundar^c Kenichi Mishima^a Yoshihiro Nishida^a Naoki Ishiguro^a

^aDepartment of Orthopedic Surgery, Nagoya University Graduate School of Medicine, Nagoya, Japan;

^bDepartment of Medical Genetics, Izmir Katip Celebi University Atatürk Training and Research Hospital, Izmir, and

^cDepartment of Medical Genetics, Erciyes University, Kayseri, Turkey

Key Words

Cleidocranial dysplasia · Glutamine repeat variant · Q/A domain · *RUNX2*

Abstract

Cleidocranial dysplasia (CCD), an autosomal dominant skeletal dysplasia characterized by hypoplastic clavicles and delayed closure of the cranial sutures, is caused by mutations of the runt-related transcription factor 2 (*RUNX2*) gene. The *RUNX2* gene consists of a glutamine and alanine repeat domain (Q/A domain, 23Q/17A), a DNA-binding Runt domain and a proline/serine/threonine-rich domain. We report on a familial case of CCD with a novel mutation within the Q/A domain of the *RUNX2* gene, which is an insertion in exon 1 (p.Q71_E72insQQQQ) representing the Q-repeat variant (27Q/17A). Functional analysis of the 27Q variant revealed abolished transactivation capacity of the mutated *RUNX2* protein. This is the first case report that demonstrated a glutamine repeat variant of the *RUNX2* gene causes CCD.

© 2015 S. Karger AG, Basel

Cleidocranial dysplasia (CCD) is an autosomal dominant skeletal dysplasia characterized by hypoplastic or aplastic clavicles, delayed closure of the fontanelles and cranial sutures, delayed ossification of the pelvis, dental abnormalities such as late eruption of permanent teeth and multiple supernumerary teeth, and moderately short stature [Cooper et al., 2001]. CCD is caused by hypomorphic or haploinsufficiency of the runt-related transcription factor 2 (*RUNX2*) gene [Lee et al., 1997; Mundlos et al., 1997].

To date, the mutations occur throughout the *RUNX2* gene, but are clustered in the Runt domain in CCD. Most of the mutations within the Runt domain are missense mutations. On the other hand, nonsense mutations, insertions or deletions are predominant within the Q/A domain or the proline/serine/threonine-rich domain [Kim et al., 2006]. The Q/A domain has the capacity to mutate via strand slippage during DNA replication [Yoshida et al., 2002]. Glutamine repeat sequence expansion has been the cause of some diseases that show genetic anticipation, where severity increases in subsequent generations as the repeat length increases due to errors in replication [McMurray, 2010]. Wild-type human *RUNX2* contains a

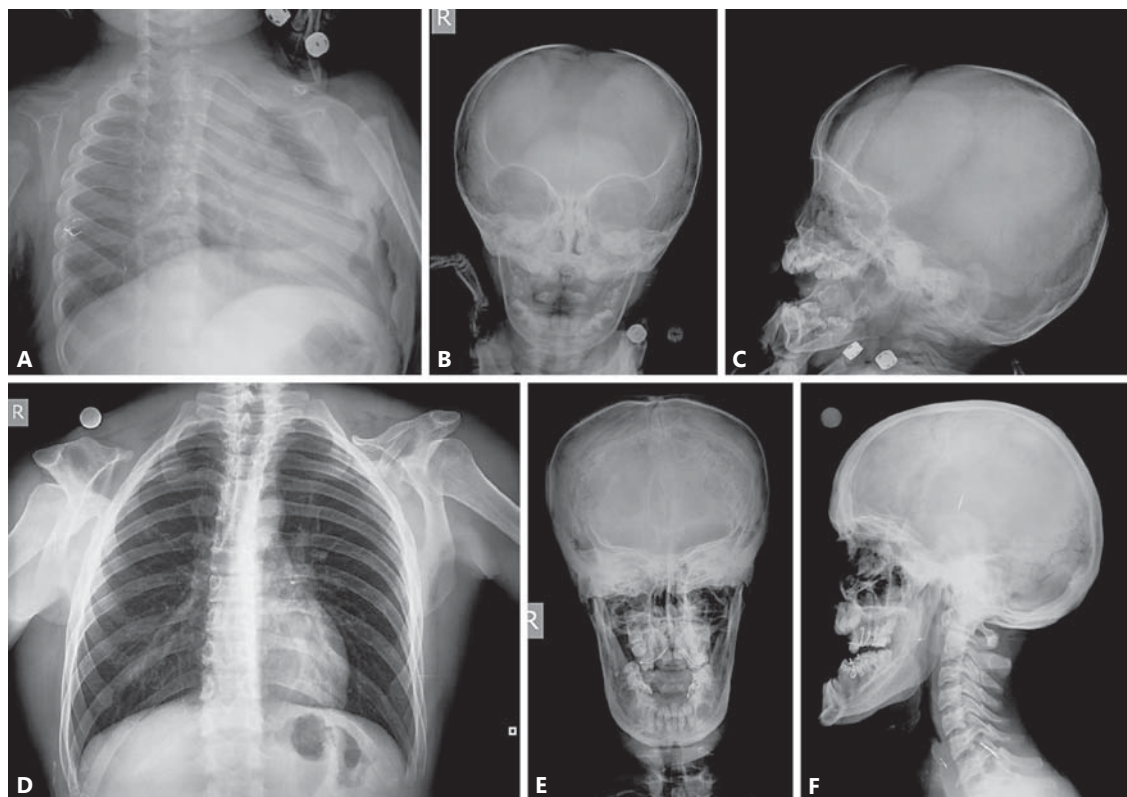


Fig. 1. Radiographs of the proband's chest and skull demonstrating the complete absence of bilateral clavicles, open large fontanelles, multiple wormian bones, supernumerary teeth, and mandibular protrusion (A–C). Anteroposterior radiograph of the father's chest demonstrating bilateral absence of clavicles (D) and radiographs of his skull demonstrating multiple wormian bones, a relatively thick skull and prognathism (E, F).

23Q/17A repeat: 23 consecutive glutamine residues followed by 17 alanine residues. An insertion of the polyalanine tract (23Q/27A) was previously observed in only one CCD patient [Mundlos et al., 1997].

Here, we describe a familial case of CCD with a novel mutation within the Q/A domain, which is an insertion of the polyglutamine tract (27Q/17A). In vitro functional analysis was performed to assay the transactivation capacity of the mutant RUNX2 protein.

Case Report

A family with the clinical diagnosis of CCD from the Erciyes University, Turkey, was examined in this study. The proband, a 2-year-old boy, is the only child of an affected father (27 years old) and a healthy mother (23 years old). Radiographs of the proband showed a large defect of the parietal and occipital bones, supernumerary teeth, sclerosis of the cranial base, multiple wormian bones, and bilateral absence of clavicles (fig. 1A–C). The last 2 radio-

graphic manifestations (multiple wormian bones and absent clavicles) were also observed in the boy's father (fig. 1D, E), although he had a relatively thick skull and prognathism (fig. 1F). The craniofacial manifestations, including frontal bossing, midface hypoplasia and a small face, were shared in both the proband and his father.

Methods

After informed consent was obtained from all family members, genomic DNA was extracted from peripheral blood leukocytes. The exons (0–7) and their flanking intronic regions of the *RUNX2* gene were amplified by PCR using sets of primers. Direct sequence analysis of the affected patients' DNA from this family demonstrated a novel heterozygous mutation within the Q/A domain, c.213_214insCAGCAGCAGCAG (p.Q71_E72insQQQQ).

For in vitro functional studies of the mutant RUNX2 protein identified in this family, the entire cDNA of p.Q71_E72insQQQQ (27Q) was constructed as follows. We confirmed that the mutation was located between 2 PstI sites (181 bp) in exon 1 and obtained the oligonucleotide duplex containing the mutation (Integrated

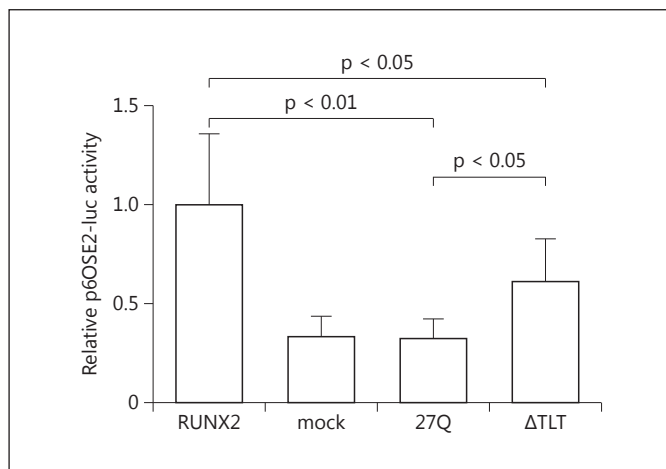


Fig. 2. Transactivation ability of the wild-type and mutant RUNX2 proteins. COS7 cells were transfected with p6OSE2-luc as a reporter plasmid, full-length, wild-type or mutant RUNX2 as effector plasmids, and phRL-TK as an internal control of transfection efficiency. Data are presented as fold activation relative to the activity obtained with wild-type RUNX2 vector plasmid. Bars represent the average ratios of luciferase to Renilla activity. Standard deviations are represented by error bars. Both the 27Q variant and Δ TLT198_200 mutants showed significantly reduced transactivation ability compared to the wild type. Moreover, transactivation of the 27Q variant was significantly lower than that of the Δ TLT198_200 mutant.

DNA Technologies MBL, Japan). PCR fragments of the oligonucleotide duplex were double-digested with PstI. This insert was cloned into the human full-length RUNX2 cDNA (Ori-Gene Technologies, Rockville, Md., USA) at the PstI sites. On the other hand, p.T198_T200del (Δ TLT), which was previously identified in a patient with CCD, was constructed by using the QuikChange site-directed mutagenesis kit (Stratagene, La Jolla, Calif., USA) [Matsushita et al., 2014]. Transient transfection experiments in COS7 cells were performed using FuGENE 6 (Roche, Indianapolis, Ind., USA). Aliquots of 400 ng expression plasmid containing either wild-type or mutagenized RUNX2 were cotransfected with 400 ng of a reporter plasmid p6OSE2-luc (kindly provided by T. Komori, Nagasaki University, Japan) [Harada et al., 1999]. All transfection experiments were done 8 times. The transactivation study showed that the 27Q variant and Δ TLT mutants had significantly lower transcription activities (32 and 61% of the wild type, respectively) (fig. 2).

Discussion

Clinical and radiographic manifestations of the present cases seemed to be typical for CCD, including complete absence of bilateral clavicles, multiple wormian bones and supernumerary teeth. Mutation analysis of this

family showed a Q-repeat variant within the Q/A domain, which resulted in a significant reduction of transactivation of the RUNX2 protein.

Q-repeat variants within the RUNX2 gene were identified in an Australian fracture cohort (15Q, 16Q, 24Q, and 30Q) [Vaughan et al., 2002], a randomly selected population from Aberdeen (16Q) [Vaughan et al., 2004], and a Spanish population study (16Q, 18Q and 30Q) [Pineda et al., 2010]. A 30Q variant of the RUNX2 gene has never been reported to be associated with CCD phenotypes. On the other hand, a novel 27Q variant caused CCD by downregulating the transactivation activity of the RUNX2 protein. Generally, triplet repeat expansion disorders accelerate their phenotypes according to the repeat length. Huntington's disease, for example, is one of the polyQ-repeat disorders, and its severity is usually associated with the length of the polyQ tracts. It has been suggested that aggregation of the polyQ fibers is pathogenic of the disease. Perutz [1996] reported that Huntington's disease has not been observed in individuals with <37 repeats, and absence of disease has never been found in those with >41 repeats. This indicated that polyQ expansion beyond the pathological threshold of 36–40 repeats leads to a clinical manifestation. According to the model of Perutz et al. [2002], polyQ fibers are composed of nanotubes with 20 residues per turn, and a minimum of 2 turns (40 repeats) is necessary for pathogenic polyQ aggregates. It is possible that the 27Q variant is pathogenic, while the 30Q variant is benign, since the repeat length is not necessarily related to the severity of the disease when it is <40 repeats.

Sears et al. [2007] showed that Q/A tandem repeat ratio correlated to RUNX2 transcriptional activity. Morrison et al. [2012] demonstrated that transactivation activity was reduced by the RUNX2 Q-repeat variants, but rescued by PEBP2 β , which is the partner subunit for heterodimerization with the Runt domain. In a study on dogs, Fondon and Garner [2004] demonstrated that the length of the Q repeat is significantly associated with midface length and nose curvature. We previously reported a CCD patient with the in-frame deletion (Δ TLT) who showed a milder phenotype than the present cases, including mild short stature (–1.75 SD), delayed fontanelle, midface hypoplasia, pseudoarthrosis of the right clavicle, and hypoplasia of the left clavicle [Matsushita et al., 2014]. Δ TLT mutation decreased the transactivation activity of the RUNX2 protein by abolishing the heterodimerization of the RUNX2 protein with the PEBP2 β . Significantly lower transactivation activity of the 27Q variant than that of the Δ TLT mutant may reflect the phenotypic severity of the disease.

References

- Cooper SC, Flaitz CM, Johnston DA, Lee B, Hecht JT: A natural history of cleidocranial dysplasia. *Am J Med Genet* 104:1–6 (2001).
- Fondon JW 3rd, Garner HR: Molecular origins of rapid and continuous morphological evolution. *Proc Natl Acad Sci USA* 101:18058–18063 (2004).
- Harada H, Tagashira S, Fujiwara M, Ogawa S, Katsumata T, et al: *Cbfa1* isoforms exert functional differences in osteoblast differentiation. *J Biol Chem* 274:6972–6978 (1999).
- Kim HJ, Nam SH, Kim HJ, Park HS, Ryoo HM, et al: Four novel *RUNX2* mutations including a splice donor site result in the cleidocranial dysplasia phenotype. *J Cell Physiol* 207:114–122 (2006).
- Lee B, Thirunavukkarasu K, Zhou L, Pastore L, Baldini A, et al: Missense mutations abolishing DNA binding of the osteoblast-specific transcription factor OSF2/CBFA1 in cleidocranial dysplasia. *Nat Genet* 16:307–310 (1997).
- Matsushita M, Kitoh H, Kaneko H, Mishima K, Itoh Y, et al: A novel in-frame deletion of the *RUNX2* gene causes a classic form of cleidocranial dysplasia. *J Bone Miner Metab* 32:96–99 (2014).
- McMurray CT: Mechanisms of trinucleotide repeat instability during human development. *Nat Rev Genet* 11:786–799 (2010).
- Morrison NA, Stephens AA, Osato M, Polly P, Tan TC, et al: Glutamine repeat variants in human *RUNX2* associated with decreased femoral neck BMD, broadband ultrasound attenuation and target gene transactivation. *PLoS One* 7:e42617 (2012).
- Mundlos S, Otto F, Mundlos C, Mulliken JB, Aylsworth AS, et al: Mutations involving the transcription factor CBFA1 cause cleidocranial dysplasia. *Cell* 89:773–779 (1997).
- Perutz MF: Glutamine repeats and inherited neurodegenerative diseases: molecular aspects. *Curr Opin Struct Biol* 6:848–858 (1996).
- Perutz MF, Finch JT, Berriman J, Lesk A: Amyloid fibers are water-filled nanotubes. *Proc Natl Acad Sci USA* 99:5591–5595 (2002).
- Pineda B, Hermenegildo C, Laporta P, Tarín JJ, Cano A, García-Pérez MÁ: Common polymorphisms rather than rare genetic variants of the *Runx2* gene are associated with femoral neck BMD in Spanish women. *J Bone Miner Metab* 28:696–705 (2010).
- Sears KE, Goswami A, Flynn JJ, Niswander LA: The correlated evolution of *Runx2* tandem repeats, transcriptional activity, and facial length in carnivora. *Evol Dev* 9:555–565 (2007).
- Vaughan T, Pasco JA, Kotowicz MA, Nicholson GC, Morrison NA: Alleles of *RUNX2/CBFA1* gene are associated with differences in bone mineral density and risk of fracture. *J Bone Miner Res* 17:1527–1534 (2002).
- Vaughan T, Reid DM, Morrison NA, Ralston SH: *RUNX2* alleles associated with BMD in Scottish women; interaction of *RUNX2* alleles with menopausal status and body mass index. *Bone* 34:1029–1036 (2004).
- Yoshida CA, Furuichi T, Fujita T, Fukuyama R, Kanatani N, et al: Core-binding factor beta interacts with *Runx2* and is required for skeletal development. *Nat Genet* 32:633–638 (2002).

C-type natriuretic peptide (CNP) plasma levels are elevated in subjects with achondroplasia, hypochondroplasia, and thanatophoric dysplasia

Robert C. Olney,¹ Timothy C.R. Prickett,² Eric A. Espiner,² William G. Mackenzie,³ Angela L. Duker,³ Colleen Ditro,³ Bernhard Zabel,⁴ Tomonobu Hasegawa,⁵ Hiroshi Kitoh,⁶ Arthur S. Aylsworth,⁷ Michael B. Bober³

¹Nemours Children's Clinic, Jacksonville, FL; ²University of Otago, Christchurch, New Zealand; ³Nemours/Alfred I. duPont Hospital for Children, Wilmington, DE ⁴University Hospital Freiburg, Freiburg, Germany; ⁵Keio University School of Medicine, Tokyo, Japan; ⁶Nagoya University School of Medicine, Nagoya, Japan; ⁷University of N Carolina, Chapel Hill, NC

Context: C-type natriuretic peptide (CNP) is a crucial regulator of endochondral bone growth. In a previous report of a child with acromesomelic dysplasia, Maroteaux type (AMDM), due to loss-of-function of the CNP receptor (NPR-B), plasma levels of CNP were elevated. In vitro studies have shown that activation of the MEK/ERK MAP kinase pathway causes functional inhibition of NPR-B. Achondroplasia, hypochondroplasia, and thanatophoric dysplasia are syndromes of short-limbed dwarfism caused by activating mutations of fibroblast growth factor receptor-3, which result in over-activation of the MEK/ERK MAP kinase pathway.

Objective: To determine if these syndromes exhibit evidence of CNP resistance as reflected by increases of plasma CNP and its amino terminal propeptide (NTproCNP).

Design: This was a prospective, observational study.

Subjects: Participants were 63 children and 20 adults with achondroplasia, 6 children with hypochondroplasia, 2 children with thanatophoric dysplasia, and 4 children and 1 adult with AMDM.

Results: Plasma levels of CNP and NTproCNP were higher in children with achondroplasia with CNP SD scores (SDS) of 1.0 (0.3–1.4) [median (intraquartile range)] and NTproCNP SDS of 1.4 (0.4–1.8) ($p < 0.0005$). NTproCNP levels correlated with height velocity. Levels were also elevated in adults with achondroplasia, CNP SDS 1.5 (0.7–2.1) and NTproCNP SDS 0.5 (0.1–1.0), $p < 0.005$. In children with hypochondroplasia, CNP SDS were 1.3 (0.7–1.5) ($p = 0.08$) and NTproCNP SDS were 1.9 (1.8–2.3) ($p < 0.05$). In children with AMDM, CNP SDS were 1.6 (1.4–3.3) and NTproCNP SDS were 4.2 (2.7–6.2) ($p < 0.01$).

Conclusions: In these skeletal dysplasias, elevated plasma levels of proCNP products suggest the presence of tissue resistance to CNP.

C-type natriuretic peptide (CNP) is a member of the natriuretic peptide family that includes atrial natriuretic peptide and B-type natriuretic peptide. The cognate receptor for CNP is natriuretic peptide receptor-B (NPR-B, gene NPR2), a membrane receptor that generates cyclic GMP as the second messenger. C-type natriuretic

peptide is produced in the growth plate and is a potent positive regulator of linear growth (reviewed in 1). Homozygous or biallelic inactivating mutations of NPR2 cause acromesomelic dysplasia, Maroteaux type (MIM 602 875, AMDM), a form of short-limbed dwarfism (2).

C-type natriuretic peptide levels can be measured in

ISSN Print 0021-972X ISSN Online 1945-7197

Printed in U.S.A.

Copyright © 2014 by the Endocrine Society

Received July 1, 2014. Accepted November 6, 2014.

Abbreviations:

plasma, although specific clearance pathways result in low levels. Biosynthetic processing of CNP generates an amino-terminal propeptide (NTproCNP) that is released from the cell in an equimolar ratio to CNP. This propeptide is not subject to specific clearance pathways. As a result, plasma NTproCNP levels reflect CNP production more accurately than levels of the active peptide (3). In a previous report, we documented greatly elevated plasma concentrations of CNP and NTproCNP in a child with AMDM (1), suggesting that reduced intracellular CNP pathway activity may increase CNP production.

Achondroplasia (MIM 100 800) is the most common skeletal dysplasia with incidence estimates ranging from 1 in 15 000 to 1 in 26 000 births (4). Achondroplasia is caused by a mutation in the fibroblast growth factor receptor-3 gene (FGFR3) (5). A single mutation (G380R) accounts for greater than 98% of all reported cases of achondroplasia and is a gain-of-function mutation. Hypochondroplasia (MIM 146 000) is a related, but milder skeletal dysplasia. Thanatophoric dysplasia (MIM 187 600) is a rarer syndrome of skeletal dysplasia, with phenotypic features more severe than in achondroplasia and is often lethal in the neonatal period. Both hypochondroplasia and thanatophoric dysplasia are also caused by gain-of-function mutations in FGFR3 (6, 7).

In the growth plate, FGFR-3 activates a number of signaling cascades, the most important of which appear to be the signal transducers and activators of transcription (STAT1) pathway, which inhibits chondrocyte proliferation, and the MEK/ERK mitogen-activated protein kinase (MAP kinase) pathway, which inhibits chondrocytic differentiation and increases matrix degradation. The net result is poor bone growth (reviewed in 8). The MEK/ERK MAP kinase pathway and the CNP intracellular signaling pathway interact and are mutually inhibitory (9). Evidence of functional inhibition of NPR-B by FGFR-3 overactivity, and our finding of raised plasma CNP peptides in a patient with a homozygous loss-of-function mutation in NPR2, lead us to postulate that plasma levels will also be raised in disorders associated with constitutive activation of FGFR-3.

Materials and Methods

Subjects

Subjects were healthy people with the clinical diagnosis of achondroplasia (63 children, 20 adults), hypochondroplasia (6 children), thanatophoric dysplasia (2 children), or AMDM (4 children and 1 adult). This study was approved by the Nemours Florida Institutional Review Board. All children had written parental permission obtained. All adult subjects had written informed consent obtained.

Study procedures

With the exception of AMDM, this was a prospective study. All subjects with achondroplasia, hypochondroplasia, or thanatophoric dysplasia were seen in the Skeletal Dysplasia Clinic at Nemours/Alfred I. duPont Hospital for Children in Wilmington, DE. Anthropometrics were done, including standing height by wall-mounted tape measure or recumbent length by measuring table and weight by electronic scale. If the subject was an established patient, heights from previous visits were obtained from the medical record for determination of annualized height velocity.

Subjects with AMDM were seen by a variety of geneticists around the world. Blood was drawn locally and plasma was frozen and shipped for analysis.

Assays

Blood was drawn into EDTA tubes and stored at 4 C until processed. Blood was centrifuged at 4 C and plasma aliquoted and frozen at -80 C until assayed.

The radioimmunoassays used for CNP and NTproCNP were as previously described (10, 11).

Statistical analysis

Standard deviation scores (SDS) were calculated using the LMS method (12). Height SDS were calculated using Center for Disease Control 2000 data (13). For the subjects with AMDM residing outside the US, country specific height data were used. Standard deviation scores for CNP, NTproCNP, and CNP-to-NTproCNP ratio were calculated using reference data from our previous studies of healthy children (10) and adults (11). Achondroplasia-specific height SDS were calculated using estimates of age-specific mean and SD from height charts reported by Horton, et al (14).

Data are summarized as median and interquartile range (25th - 75th percentiles). For height SDS data, one sample Student's t-tests were used to compare groups to the general population. For the peptide assay data, because of the widely differing ranges of variance in the sample groups, nonparametric tests were used. For the children, comparison between the reference population, and subjects with achondroplasia, hypochondroplasia, or AMDM were made using Kruskal-Wallis tests, with Holm-adjusted Mann-Whitney rank sum tests for post hoc pairwise comparisons. For the adults, comparison of SDS data were made using Mann-Whitney rank sum tests. Correlation between NTproCNP level and height velocity were done by fitting a line by least squares and performing linear regression analysis. Pearson product-moment correlation coefficients (r) are reported. Statistics were calculated using Primer of Biostatistics software (version 7; The McGraw-Hill Companies, Inc., New York, NY). Significance was assumed for p values less than 0.05.

Results

Achondroplasia

The characteristics of the subjects with achondroplasia are shown in Table 1. In children with achondroplasia, plasma concentration of both CNP and NTproCNP (Figure 1) were higher than in the reference population ($P <$

Table 1. Subjects with Achondroplasia or Hypochondroplasia

	Achondroplasia		Hypochondroplasia
	children	adults	children
number	63	20	6
sex (F:M)	31:32	11:9	3:3
age (y)	4.7 (2.9–7.5)	41 (36–45)	8.6 (6.6–10.9)
height _{SD} score ^a	−4.8 (−5.6– −4.2)**	ND	−3.1 (−3.7– −2.2)* [†]
height _{SD} score ^b	−0.1 (−0.8–0.5)	ND	1.9 (1.3–3.0) [†]
CNP (pM)	2.1 (1.7–2.4)	0.9 (0.7–1.1)	2.3 (1.9–2.5)
CNP _{SD} score	1.0 (0.3–1.4)**	1.5 (0.7–2.1)*	1.3 (0.7–1.5)*
NTproCNP (pM)	53.0 (47.3–63.0)	17.0 (16.0–19.3)	55.2 (52.1–58.7)
NTproCNP _{SD} score	1.4 (0.4–1.8)**	0.5 (0.1–1.0)*	1.9 (1.8–2.3)*
NTproCNP:CNP ratio	26 (31–22)	21 (16–36)	23 (25–22)
NTproCNP:CNP _{SD} score	−0.1 (−0.7–0.4)	−0.9 (−1.6–0.4)	0.2 (−0.4–0.2)

Data are median (intraquartile range)

ND, not determined

^aUsing general population reference standards

^bUsing achondroplasia-specific reference standards

* $P < 0.01$ compared to the reference population

** $P < 0.0005$ compared to the reference population

[†] $P < 0.01$, compared to subjects with achondroplasia

.0005 for both), despite markedly reduced height. Similarly, adults with achondroplasia also had higher levels of CNP and NTproCNP ($P < .005$ for both)(Table 1). The NTproCNP-to-CNP ratio is a measure of CNP clearance and did not differ from the reference population (Table 1).

Linear regression analysis showed that in children with achondroplasia, NTproCNP level had a significant positive correlation with height velocity ($n = 62$, $r^2 = 0.42$, $P < .0005$)(Figure 1, panel C). A similar relationship was found in the reference population ($n = 139$, $r^2 = 0.51$, $P < .0005$) (10). The regression line for children with achondroplasia differed from that of the reference population both for slope (1.76 ± 0.27 vs. 2.41 ± 0.20 pM/cm/y respectively, mean \pm SE, $P < .05$) and for intercept (46.7 ± 2.3 vs. 24.1 ± 1.3 pM, $P < .0005$).

Hypochondroplasia

Table 1 shows the characteristics of the subjects with hypochondroplasia, all of whom were children. Compared to the reference population, these subjects had elevated plasma CNP and NTproCNP levels (Figure 1)($P < .05$ for both). Compared to subjects with achondroplasia, the CNP and NTproCNP SDS were not different (Figure 1).

Thanatophoric dysplasia

We studied two young children with thanatophoric dysplasia. One subject was a 2.3 year old boy with a height SDS of −11.5. His plasma CNP level was 3.0 pM (SDS of 3.0) and his NTproCNP level was 67.3 (SDS of 1.1). The second subject was a 2.7 year old boy with a height SDS of

−11.1. His plasma CNP level was 1.0 pM (SDS of 0.0) and his NTproCNP level was 72.2 (SDS of 1.8).

Acromesomelic dysplasia, Maroteaux type

Table 2 shows the characteristics of subjects with AMDM. In the children, CNP SDS ($n = 3$, $P < .01$) and NTproCNP SDS ($n = 4$, $P < .005$) were significantly higher than in the reference population and were also higher than values in achondroplasia (CNP SDS, $P < .05$; NTproCNP SDS, $P < .005$, Figure 1). In the adult with AMDM, both plasma CNP and NTproCNP were markedly elevated.

Discussion

The finding that CNP products in plasma were greatly elevated in a subject with profound short stature due to a disruption of the CNP receptor (NPR-B) and reports from others that activation of the MEK/ERK MAP kinase pathway inhibits NPR-B signaling, lead us to postulate that plasma levels would also be elevated in people with FGFR-3-related skeletal dysplasias such as achondroplasia. The current findings clearly show that circulating products of proCNP are raised not only in children and adults with achondroplasia, but also in children with related conditions of FGFR-3 overactivity.

People with AMDM have absent or disrupted CNP receptors. Since CNP is a growth promoting factor and people with AMDM have profound growth failure, this is a classic instance of hormone resistance. We have shown

Table 2. Subjects with Acromesomelic Dysplasia, Maroteaux Type

Age (y)	Genotype	Sex	height SDS	CNP (pM)	CNP SDS	NTproCNP (pM)	NTproCNP SDS	NT:CNP	NT:CNP SDS
2.5	G413E/G413E	M	-5.1	2.7	1.6	86.3	2.8	32.0	-0.5
4.9	del/del	M	-5.3	ND	ND	110.2	5.6		
7.5	R668stop/R218C	F	-2.3	2.1	1.1	58.0	2.4	27.6	-0.6
7.9	I364fs/I364fs	F	-8.5	7.6	5.0	172.0	7.9	22.6	0.1
30	Q853stop/R989 liter	M	-8.6	7.8	46.6	144.0	8.0	18.5	-1.7

ND, not determined

here that CNP and NTproCNP levels are markedly elevated in people with AMDM, suggesting that CNP, as in virtually all other hormone axes, is regulated by a negative feedback loop. Supporting this conclusion are two reports

of subjects with activating mutations of NPR-B causing skeletal overgrowth (15, 16), in whom plasma NTproCNP concentrations were profoundly reduced. Little is known about the factors that regulate CNP expression and translation; the details of this feedback loop require further study.

The interaction between the MEK/ERK MAP kinase and CNP/cGMP pathways has been defined in vitro in chondrogenic cell systems and in organ culture. Phosphorylated MEK1/2 and/or ERK1/2 directly or indirectly inhibit cGMP generation by NPR-B (9). Meanwhile, NPR-B-generated cGMP, in a pathway that involves cGMP-dependent protein kinase II (PRKG2) and the MKK/p38 MAP kinase pathway, inhibits MEK/ERK activation by inhibiting RAF1 (17, 9, 18, 19). Hence in vitro data describe a potential mechanism in which overactivation of the MEK/ERK MAP kinase pathway can result in resistance to CNP.

In this study, we observed a clear increase in CNP and NTproCNP levels in subjects with achondroplasia and hypochondroplasia. We also provide evidence for increased levels in two children with thanatophoric dysplasia, although the sample size was too small for statistical confirmation. Assuming the presence of CNP regulatory feedback loop as suggested by the data from subjects with AMDM, the finding of elevated CNP levels in a population with severe short stature suggests that these individuals may also have resistance to CNP. This is further demonstrated by Figure 1 (panel C), which shows that the slope of the regression line linking NTproCNP and height velocity is significantly reduced in children with achondroplasia compared to the reference population.

There are other potential explanations for our findings. It may be that another branch of the FGFR-3 signaling cascade up-regulates CNP expression and that the MAP kinase inhibition of NPR-B signaling is not occurring or is not relevant in vivo. Another possibility is that the elevated blood levels of CNP are arising from other tissues and not the growth plate and hence not relevant to the growth failure. Now that the observation has been made, further definition is needed to provide clarity. Of interest, products of proCNP in plasma are also elevated in adults with

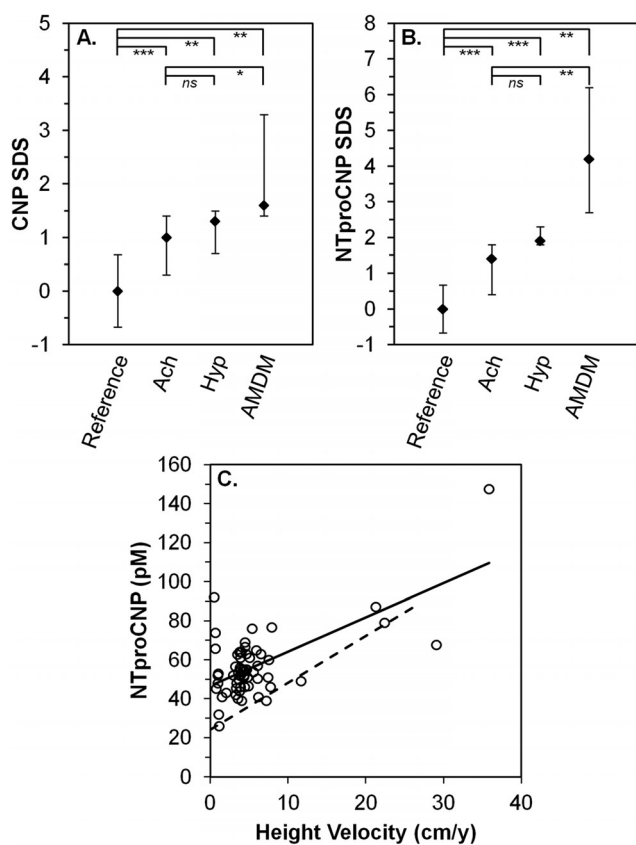


Figure 1. C-type natriuretic peptide and NTproCNP levels in children. Panels A & B, comparison between different skeletal dysplasias. Standard deviation scores are shown for CNP (Panel A) and NTproCNP (Panel B) for children from the reference population (n = 318), children with achondroplasia (n = 63, Ach), hypochondroplasia (n = 6, Hyp), and acromesomelic dysplasia, Maroteaux-type (n = 4, AMDM). Diamonds show the median for each group and error bars the 25th and 75th percentile. ns, difference is not significant. *P < .05; **P < .01; ***P < .0005. Panel C shows the correlation between height velocity and NTproCNP levels in children with achondroplasia. Annualized height velocity was determined using the height at a previous clinic visit and the height from the study visit. Solid line, least mean squares linear regression line. The correlation is significant (n = 62, r² = 0.416, P < .0005). Dashed line, previously published regression line from children from the general population (n = 139, r = 0.711, P < .0005) (10). The two regression lines differ both in intercept (P < .05) and in slope (P < .0005).

achondroplasia or AMDM. The tissues that contribute to plasma levels of CNP and NTproCNP after growth plates have closed have not been clearly defined, but are likely to include skeletal, vascular, and cardiac (11, 20) tissue. C-type natriuretic peptide, NPR-B, and FGFR-3 are all expressed in these tissues. The finding of elevated plasma levels of CNP in adults with achondroplasia suggests that alteration of the CNP pathway by activating FGFR3 mutations is not limited to the growth plate.

Acknowledgments

The authors would like to thank the subjects and their families for participating in this project.

Address all correspondence and requests for reprints to: Robert C. Olney, MD, Nemours Children's Clinic, Jacksonville, FL 32207, (904) 697-3674 fax: (904) 697-3948, rolney@nemours.org.

Disclosure summary: T.C.R.P. and E.A.E. have a patent filed entitled "Assessment of skeletal growth using measurements of NT-CNP peptides"

Clinical Trial Registration Number: NCT01541306

Reprint requests: to corresponding author

This work was supported by Support: developmental funds from Nemours.

References

- Olney RC. C-type natriuretic peptide in growth: a new paradigm. *Growth Horm IGF Res.* 2006;16 Suppl A:S6-14.
- Bartels CF, Bukulmez H, Padayatti P, Rhee DK, Ravenswaaij-Arts C, Pauli RM, Mundlos S, Chitayat D, Shih LY, Al Gazali LI, Kant S, Cole T, Morton J, Cormier-Daire V, Faivre L, Lees M, Kirk J, Mortier GR, Leroy J, Zabel B, Kim CA, Crow Y, Braverman NE, van den Akker F, Warman ML. Mutations in the Transmembrane Natriuretic Peptide Receptor NPR-B Impair Skeletal Growth and Cause Acromesomelic Dysplasia, *Type Maroteaux.* *Am J Hum Genet.* 2004;75:27-34.
- Prickett TCR, Espiner EA. 2012 C-type natriuretic peptide (CNP) and postnatal linear growth. 2789-2810.
- Hunter AG, Bankier A, Rogers JG, Sillence D, Scott CI, Jr. Medical complications of achondroplasia: a multicentre patient review. *J Med Genet.* 1998;35:705-712.
- Shiang R, Thompson LM, Zhu YZ, Church DM, Fielder TJ, Bocian M, Winokur ST, Wasmuth JJ. Mutations in the transmembrane domain of FGFR3 cause the most common genetic form of dwarfism, achondroplasia. *Cell.* 1994;78:335-342.
- Bellus GA, McIntosh I, Smith EA, Aylsworth AS, Kaitila I, Horton WA, Greenhaw GA, Hecht JT, Francomano CA. A recurrent mutation in the tyrosine kinase domain of fibroblast growth factor receptor 3 causes hypochondroplasia. *Nat Genet.* 1995;10:357-359.
- Tavormina PL, Shiang R, Thompson LM, Zhu YZ, Wilkin DJ, Lachman RS, Wilcox WR, Rimoin DL, Cohn DH, Wasmuth JJ. Thanatophoric dysplasia (types I and II) caused by distinct mutations in fibroblast growth factor receptor 3. *Nat Genet.* 1995;9:321-328.
- Foldynova-Trantirkova S, Wilcox WR, Krejci P. Sixteen years and counting: the current understanding of fibroblast growth factor receptor 3 (FGFR3) signaling in skeletal dysplasias. *Hum Mutat.* 2012;33:29-41.
- Ozasa A, Komatsu Y, Yasoda A, Miura M, Sakuma Y, Nakatsuru Y, Arai H, Itoh N, Nakao K. Complementary antagonistic actions between C-type natriuretic peptide and the MAPK pathway through FGFR-3 in ATDC5 cells. *Bone.* 2005;36:1056-1064.
- Olney RC, Permuy JW, Prickett TC, Han JC, Espiner EA. Amino-terminal propeptide of C-type natriuretic peptide (NTproCNP) predicts height velocity in healthy children. *Clin Endocrinol (Oxf).* 2012;77:416-422.
- Prickett TC, Olney RC, Cameron VA, Ellis MJ, Richards AM, Espiner EA. Impact of age, phenotype and cardio-renal function on plasma C-type and B-type natriuretic peptide forms in an adult population. *Clin Endocrinol (Oxf).* 2013;78:783-789.
- Cole TJ. The LMS method for constructing normalized growth standards. *Eur J Clin Nutr.* 1990;44:45-60.
- National Center for Health Statistics 2002 2000 CDC Growth Charts for the United States: Methods and Development. *Vital and Health Statistics* 11:1-203.
- Horton WA, Rotter JI, Rimoin DL, Scott CI, Hall JG. Standard growth curves for achondroplasia. *J Pediatr.* 1978;93:435-438.
- Miura K, Namba N, Fujiwara M, Ohata Y, Ishida H, Kitaoka T, Kubota T, Hirai H, Higuchi C, Tsumaki N, Yoshikawa H, Sakai N, Michigami T, Ozono K. An Overgrowth Disorder Associated with Excessive Production of cGMP Due to a Gain-of-Function Mutation of the Natriuretic Peptide Receptor 2 Gene. *PLoS One.* 2012;7:e42180.
- Hannema SE, van Duyvenvoorde HA, Prensler T, Yang RB, Mueller TD, Gassner B, Oberwinkler H, Roelfsema F, Santen GW, Prickett T, Kant SG, Verkerk AJ, Uitterlinden AG, Espiner E, Ruivenkamp CA, Oostdijk W, Pereira AM, Losekoot M, Kuhn M, Wit JM. An activating mutation in the kinase homology domain of the natriuretic peptide receptor-2 causes extremely tall stature without skeletal deformities. *J Clin Endocrinol Metab.* 2013;98:E1988-E1998.
- Yasoda A, Komatsu Y, Chusho H, Miyazawa T, Ozasa A, Miura M, Kurihara T, Rogi T, Tanaka S, Suda M, Tamura N, Ogawa Y, Nakao K. Overexpression of CNP in chondrocytes rescues achondroplasia through a MAPK-dependent pathway. *Nat Med.* 2004;10:80-86.
- Krejci P, Masri B, Fontaine V, Mekikian PB, Weis M, Prats H, Wilcox WR. Interaction of fibroblast growth factor and C-natriuretic peptide signaling in regulation of chondrocyte proliferation and extracellular matrix homeostasis. *J Cell Sci.* 2005;118:5089-5100.
- Hutchison MR. BDNF alters ERK/p38 MAPK activity ratios to promote differentiation in growth plate chondrocytes. *Mol Endocrinol.* 2012;26:1406-1416.
- Palmer SC, Prickett TC, Espiner EA, Yandle TG, Richards AM. Regional release and clearance of C-type natriuretic peptides in the human circulation and relation to cardiac function. *Hypertension.* 2009;54:612-618.

Radiographic characteristics of the hand and cervical spine in fibrodysplasia ossificans progressiva

Kenichi Mishima¹, Hiroshi Kitoh^{1,2,*}, Nobuhiko Haga², Yasuharu Nakashima², Junji Kamizono², Takenobu Katagiri², Takafumi Susami², Masaki Matsushita¹, Naoki Ishiguro¹

¹Department of Orthopaedic Surgery, Nagoya University Graduate School of Medicine, Nagoya, Aichi, Japan;

²The Research Committee on Fibrodysplasia Ossificans Progressiva, Tokyo, Japan.

Summary

Fibrodysplasia ossificans progressiva (FOP) is a disabling heritable disorder of connective tissue characterized by progressive heterotopic ossification in various extraskelatal sites. Early correct diagnosis of FOP is important to prevent additional iatrogenic harm or trauma. Congenital malformation of the great toes is a well-known diagnostic clue, but some patients show normal-appearing great toes. The thumb shortening and cervical spine abnormalities are other skeletal features often observed in FOP. This study aimed to address the quantitative assessment of these features in a cohort of patients with FOP, which potentially helps early diagnosis of FOP. Radiographs of the hand and cervical spine were retrospectively analyzed from a total of 18 FOP patients (9 males and 9 females) with an average age of 13.9 years (range 0.7-39.3 years). The elevated ratio of the second metacarpal bone to the distal phalanx of the thumb ($> +1SD$) was a consistent finding irrespective of the patient's age and gender. Infant FOP patients, in addition, exhibited an extremely high ratio of the second metacarpal bone to the first metacarpal bone ($> +3SD$). The height/depth ratio of the C5 vertebra increased in patients over 4 years of age ($> +2SD$). Additionally, the ratio of (height+depth) of the C5 spinous process to the C5 vertebral depth was markedly elevated in young patients ($> +2SD$). We quantitatively demonstrated the hand and cervical spine characteristics of FOP. These findings, which can be seen from early infancy, could be useful for early diagnosis of FOP even in patients without great toe abnormalities.

Keywords: Fibrodysplasia ossificans progressiva, early diagnosis, radiographic characteristics

1. Introduction

Fibrodysplasia ossificans progressiva (FOP) is a severely disabling genetic disorder of connective tissues characterized by congenital malformations of the great toes and progressive heterotopic ossification (HO) in various extraskelatal sites including muscles, tendons, ligaments, fascias, and aponeuroses. FOP is caused by a recurrent activating mutation (c.617G > A, p.R206H) in the gene encoding activin receptor IA/activin-like kinase 2 (ACVR1/ALK2), a bone morphogenetic protein (BMP) type I receptor (1). HO typically begins

to form during the first decade of life preceded by painful soft tissue swelling and inflammation (flare-ups), which are sometimes mistaken for aggressive fibromatosis or musculoskeletal tumors. Surgical resection of HO leads to explosive new bone formation (2). Since there is no definitive treatment to prevent progressive HO in FOP to date (3), early correct diagnosis is necessary to maintain their mobility by preventing additional iatrogenic harm (4).

Malformations of the great toes, such as hallux valgus, deformed proximal phalanges and shortened first metatarsal bones, are well-known pre-osseous features of FOP (5). A reported incidence of these deformities is 95%, suggesting that there exists rare FOP cases without the great toe abnormalities (6). We demonstrated additional early radiographic signs of FOP including shortening of the first metacarpal bones and hypertrophy of the posterior element of the cervical

*Address correspondence to:

Dr. Hiroshi Kitoh, Department of Orthopaedic Surgery, Nagoya University Graduate School of Medicine, 65 Tsurumai, Showa-ku, Nagoya, Aichi, 466-8550, Japan.
E-mail: hkitoh@med.nagoya-u.ac.jp

spine (7). Clinical awareness of these deformities can aid clinicians in making early diagnosis of FOP, but quantitative assessment of these deformities has not yet been determined.

In this study, we retrospectively examined radiographs of the hand and cervical spine in FOP patients and demonstrated various abnormal radiographic parameters helpful for early diagnosis of this specific disorder.

2. Materials and Methods

2.1. Demographics

This study represents a retrospective case-control study consisting of Japanese FOP patients followed up at health care facilities where members of the Research Committee on Japanese Fibrodysplasia Ossificans Progressiva practiced. After approval from the Institutional Review Board of the Nagoya University Hospital, we collected the hand and/or cervical spine radiographs from 18 FOP patients (9 males and 9 females) with an average age of 13.9 years (range 0.7-39.3 years) at the time of this study. The patients were diagnosed clinically and radiographically based on various characteristic findings of FOP including deformities of the great toes, extraskeletal HO, joint contractures, cervical fusions, broad femoral necks, and osteochondroma-like lesions. Molecular testing was performed on fourteen patients. Thirteen showed the common *ACVR1/ALK2* mutation within the glycine/serine-rich regulatory (GS) domain (c.617G > A, p.R206H), and one patient had an atypical mutation within the protein kinase domain (c.774G > T, p.R258S). Molecular studies were not conducted for the remaining 4 patients who showed characteristic skeletal features of FOP. We examined anteroposterior (AP) radiographs of the hands and lateral radiographs of the cervical spine in each individual. The earliest hands and cervical spine films were analyzed using image processing and analysis software ImageJ®.

2.2. Radiographic assessment of the hand

According to the measurement method by Poznanski *et al.* (8), the length of each phalanx and metacarpal bone was measured. In brief, the tangent lines were drawn at both ends of each bone, which were perpendicular to the bone axis, and a bone length was defined as the distance between these two lines (Figure 1). We measured a length of the distal (D1) and proximal (P1) phalanges of the thumb as well as that of the first and second metacarpal bones (MET1 and MET2), and calculated the following bone length ratios, MET2/MET1, MET2/P1, MET2/D1, MET1/P1, MET1/D1, and P1/D1. Radiographs of both hands from one patient were separately analyzed to obtain the average value of the measurements. Reference ranges of these

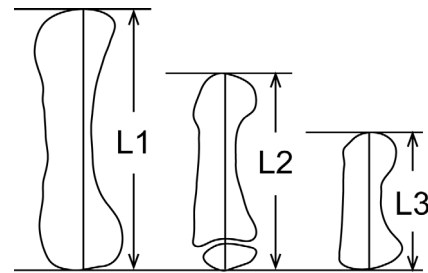


Figure 1. A schematic diagram illustrating the measurement method of bone length in the hand. Bone length was defined as the distance between the tangents drawn to each end of the bone, which were perpendicular to the bone axis. The entire bone length was measured for adults (L1), children (L2), and infants (L3).

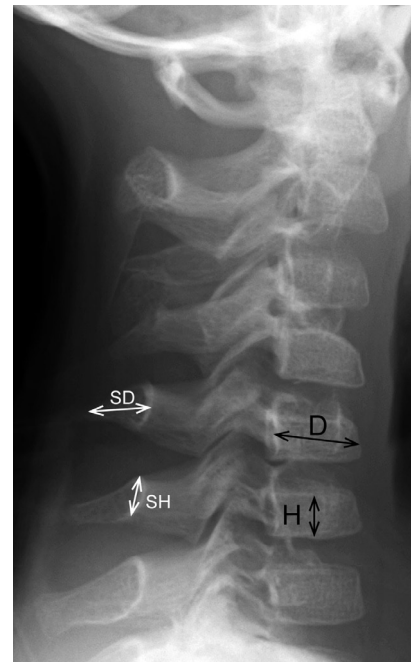


Figure 2. A radiograph depicting the measurements of the bone length in the cervical spine. The height (H) and depth (D) of the C5 vertebral body was measured at the midpoint of the body. The height of the C5 spinous process (SH) was defined as the distance from the cranial to the caudal rim at the juxta-laminar zone. The depth of the spinous process (SD) was measured from the midpoint of the anterior wall to that of the posterior rim.

measurements in different ages and genders were used based on the literature from Poznanski *et al.* (8). The control data of these measurements in infant ($n = 21$) were determined by the radiographic database in Nagoya University Hospital.

2.3. Radiographic assessment of the cervical spine

According to the measurement method proposed by Remes *et al.* (9), the height and depth of the C5 vertebral body were measured. Briefly, vertebral body height (H) was measured at the midpoint of the vertebra, perpendicular to the lower end plate. The vertebral body depth (D) was measured at the midpoint of the body from the anterior wall to the posterior wall (Figure 2). The H/D ratios of the C5 vertebra were then calculated

Table 1. Characteristics and quantitative indices for the study population

Patient	Sex	ALK2 mutation	Age at X-ray (yrs)		Deviation of the bone length ratios (SD)			
			Hand/Cervical spine		MET2/D1	MET2/D1	H/D	(SH+SD)/D
1	M	R206H	0/0		1.0	1.0	0.6	0.1
2	M	R206H	0/0		2.4	2.4	0.6	7.1
3	M	R206H	1/3		3.1	3.1	0.9	2.8
4	F	R206H	5/6		2.8	2.8	3.3	8.3
5	M	R206H	8/7		6.2	6.2	2.8	3.7
6	M	R206H	12/18		4.1	4.1	1.9	1.5
7	F	R206H	17/17		4.0	4.0	4.1	NA
8	F	R206H	20/NA		2.2	2.2	NA	NA
9	M	R206H	29/NA		2.7	2.7	NA	NA
10	M	R206H	34/NA		3.5	3.5	NA	NA
11	F	R206H	36/NA		1.0	1.0	NA	NA
12	M	R206H	39/16		1.9	1.9	3.0	1.8
13	F	R206H	NA/18		NA	NA	0.6	2.4
14	F	R258S	14/14		1.7	1.7	4.9	NA
15	M	ND	NA/4		NA	NA	3.2	8.8
16	F	ND	NA/8		NA	NA	9.2	7.9
17	F	ND	NA/16		NA	NA	4.4	NA
18	F	ND	5/5		5.3	5.3	5.3	5.4

M denotes male; F, female; ND, not determined; NA, not applicable; SD, standard deviation.

and compared to normal reference values established by Remes *et al.* in different age and gender groups (9). In addition, we measured the height and depth of the C5 spinous process. The height of the spinous process (SH) was defined as the distance from the cranial to caudal margin at the junction of the spinous process and lamina. The depth of spinous process (SD) was measured from the midportion of the anterior wall to that of the posterior rim demarcating a thick cortex shadow (Figure 2). The sum of SH and SD measurements was used for the evaluation of spinous process size, then the (SH + SD)/D ratio of the C5 vertebra was calculated. Reference values of the (SH + SD)/D ratio were established from the radiographic database of normal controls in Nagoya University Hospital.

3. Results

3.1. Characteristics of the study cohort

Patients' characteristics and quantitative indices of the measurements are shown in Table 1. Deviation of the bone length ratios in the hand and cervical spine was calculated based on age-matched reference values.

3.2. Radiographic characteristics of the hand

Mean and standard deviation of the MET2/D1 and MET2/MET1 ratio in control infants ($n = 21$) are 2.9 ± 0.29 and 1.64 ± 0.08 , respectively. Twenty-six hand radiographs from 14 patients (8 males and 6 females) were available. Regardless of age and gender, all FOP patients showed a MET2/D1 ratio larger than +1SD of normal controls (Figure 3A and 3B). In infant patients without an epiphyseal ossification center of the first metacarpal bone, the MET2/MET1 ratio was extremely

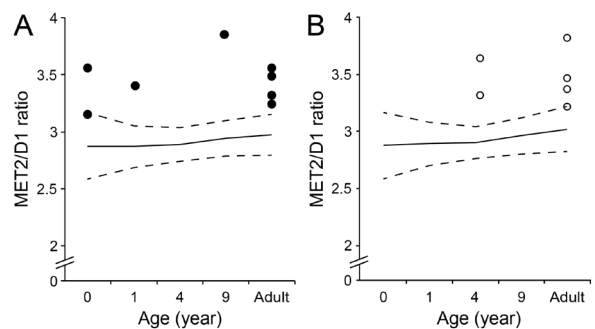


Figure 3. Scatter plots showing the bone length ratio of the second metacarpal bone (MET2) to the distal phalanx of the thumb (D1) in male (A) and female (B) patients with FOP. Solid and dash lines denote the normal value and the standard deviation (SD) of the MET2/D1 ratio, respectively.

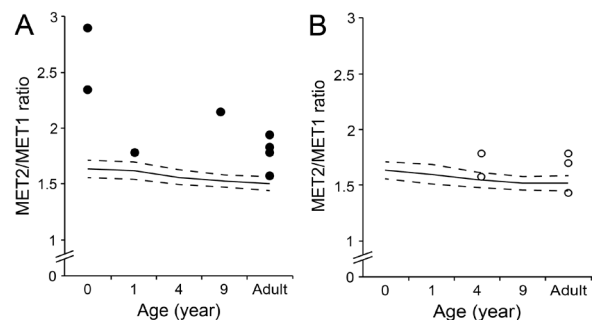


Figure 4. Scatter plots showing the bone length ratio of the second metacarpal bone (MET2) to the first metacarpal bone (MET1) in male (A) and female (B) patients with FOP. Solid and dash lines denote the normal value and the standard deviation (SD) of the MET2/MET1 ratio, respectively.

large ($> +3SD$ of normal controls) (Figure 4A and 4B). The MET2/P1 ratio was higher in infant patients, but it scattered around the mean value with increasing age (data not shown). There were no characteristic features in the values of the MET1/P1, MET1/D1, and P1/D1 ratios in FOP patients, although the MET1/P1 and MET1/D1

Table 2. Mean and standard deviation of normal controls for the (SH+SD)/D ratio of the C5 vertebra

Age group	<1	1-2	2-3	3-4	4-5	5-6	6-7	7-8	8-9	9-10	10-11	11-12	12-13	13-14	14-15	15-16	16-17	17-18	18-19	19-20	20-21
Mean	1.05	1.10	1.09	1.20	1.21	1.43	1.37	1.47	1.33	1.47	1.50	1.53	1.51	1.57	1.69	1.86	1.76	1.73	1.71	1.78	1.86
SD	0.13	0.15	0.15	0.13	0.11	0.18	0.18	0.17	0.19	0.18	0.16	0.18	0.20	0.19	0.12	0.16	0.22	0.22	0.23	0.24	0.25
N	11	21	17	13	6	13	25	19	20	17	16	17	14	20	16	21	23	31	28	38	20

SD denotes standard deviation; N, number of control subjects; SH, height of the spinous process; SD, depth of the spinous process; D, depth of the vertebral body.

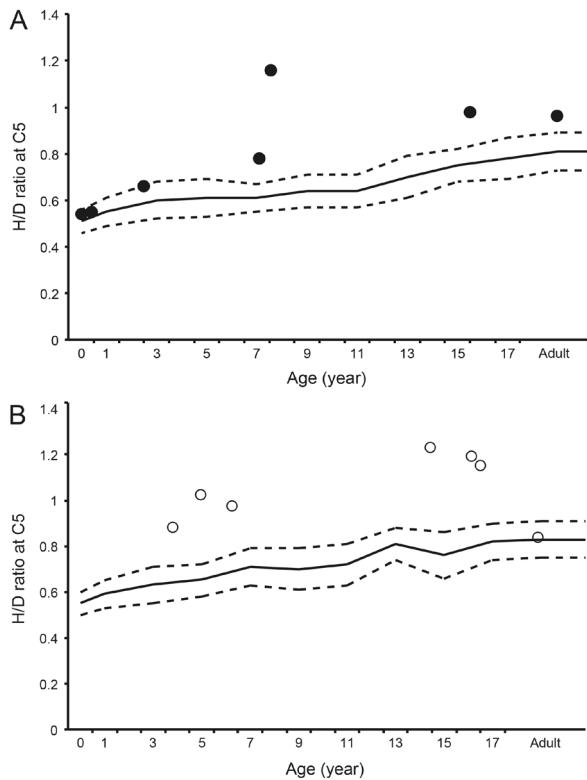


Figure 5. Scatter plots showing the bone length ratio of the C5 vertebral height (H) to depth (D) in male (A) and female (B) patients with FOP. Solid and dashed lines denote the normal value and the standard deviation (SD) of the H/D ratio, respectively.

ratios were relatively small ($< -1SD$ of normal controls) in infant FOP patients (data not shown).

3.3. Radiographic characteristics of the cervical spine

Reference values of the $(SH + SD)/D$ ratio of the C5 vertebra are shown in Table 2. There were 14 (7 males and 7 females) cervical spine radiographs available for analysis. Among them, three radiographs were excluded from analysis of the $(SH + SD)/D$ ratio for insufficient resolution. The H/D ratio of the C5 vertebra exceeded $+2SD$ of normal controls in patients over 4 years of age except one female adult patient (Figure 5A and 5B). Similarly, the $(SH + SD)/D$ ratio of the C5 vertebra was larger than $+2SD$ of normal controls in young patients except one male infant (Figure 6).

4. Discussion

In the present study, we quantitatively proved the hand

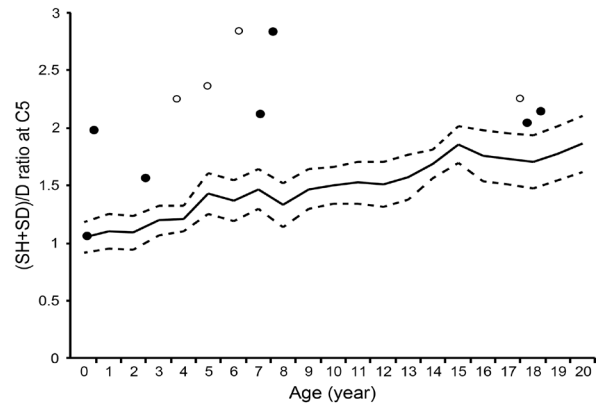


Figure 6. Scatter plots showing the bone length ratio of the C5 spinous process height (SH) + depth (SD) to the C5 vertebral depth (D). Solid and open circles indicate male and female, respectively. Solid and dashed lines denote the normal value and the standard deviation (SD) of the $(SH+SD)/D$ ratio, respectively.

and cervical spine abnormalities in FOP including shortened thumbs as well as tall and narrow vertebral bodies and hypertrophic posterior elements of the cervical spine (7,10). Especially in young patients, shortening of the first metacarpal bone and enlargement of the cervical spinous processes were pathognomonic findings useful for early diagnosis of FOP before the appearance of HO.

Previous studies have reported that thumb shortening was seen in 50% of FOP patients (6). In the present study, all patients had a MET2/D1 ratio larger than $+1SD$ of normal controls, and 85% (11/13) of the patients showed an increased MET2/MET1 ratio. The thumb shortening, therefore, seems to be more common than previous reports in FOP. Furthermore, an extremely high MET2/MET1 ratio in infant patients suggested that disproportionate shortening of the first metacarpal bone was an important early radiographic finding in FOP (Figure 7).

It is an intriguing feature of FOP that thumb morphogenesis is exclusively disrupted in the development of digit formation (11). The thumb is the last digit in the autopod to form, and it is different from other digits in terms of its relative position, shape, size, and number of phalanges. These unique thumb identities may be attributed to the expression profile of *HoxD* genes, which are pivotal transcriptional factors regulating limb patterning and growth (12). All four *HoxD10* to *D13* genes are expressed in the future digit II-V area in the autopod during the hand plate formation, whereas sole expression of the

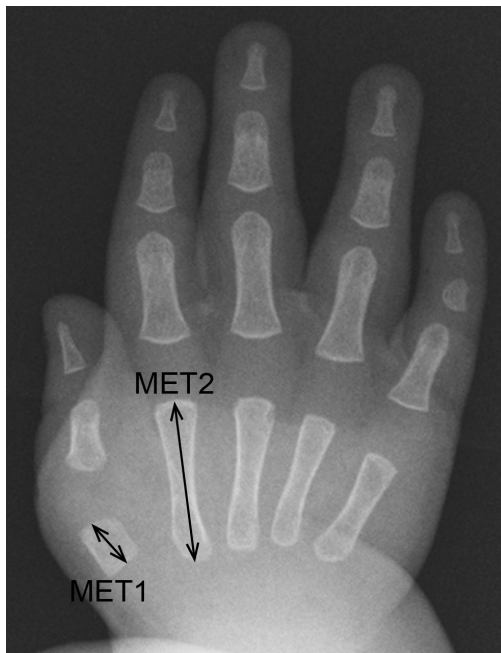


Figure 7. An anteroposterior radiograph of the right hand of Patient 1 at the age of eight months showing marked shortening of the first metacarpal bone. The MET2/MET1 ratio and the corresponding SD value is 2.9 and 16.3, respectively.

HoxD13 gene in the presumptive digit I area is of great significance (13). Mutations in the homeodomain of the *HoxD13* gene cause brachydactyly type D that is characterized by variable shortening of the distal phalanx of the thumb. This mutated *HoxD13* proteins responsible for its decreased affinity for the double-stranded DNA target containing a cognitive sequence of the homeodomain (14). Interestingly, previous research has revealed that BMP signaling-dependent Smad1/4 proteins prevented *HoxD10* and *HoxD13* from binding to DNA targets (15). Constitutively-activated BMP signaling in FOP thus is likely to impair *HoxD13*-mediated transcriptional regulation by direct interactions between BMP-induced Smads and *HoxD13*. Mesenchymal condensation and chondrocyte proliferation of the presumptive digit I area could be suppressed by down-regulated *HoxD13* function, whereas in presumptive digits II to V areas, it could be preserved by compensating expressions of other *HoxD* genes (*HoxD11* and *HoxD12*). Dysregulated BMP signal transduction during embryogenesis seems to cause relative shortening of the first metacarpals and distal phalanges of the thumb in FOP.

More than 90% of adult FOP patients showed fusion of the facet joints, which is a type of orthotopic ossification (6). To our knowledge, however, there are no reports delineating the precise prevalence of tall and narrow vertebral bodies and enlarged posterior elements of the cervical vertebrae. Here we demonstrated that the H/D and (SH + SD)/D ratios in the C5 vertebrae were larger than +2SD of normal values in 64% and 73% of patients, respectively (Figure 8). In addition to

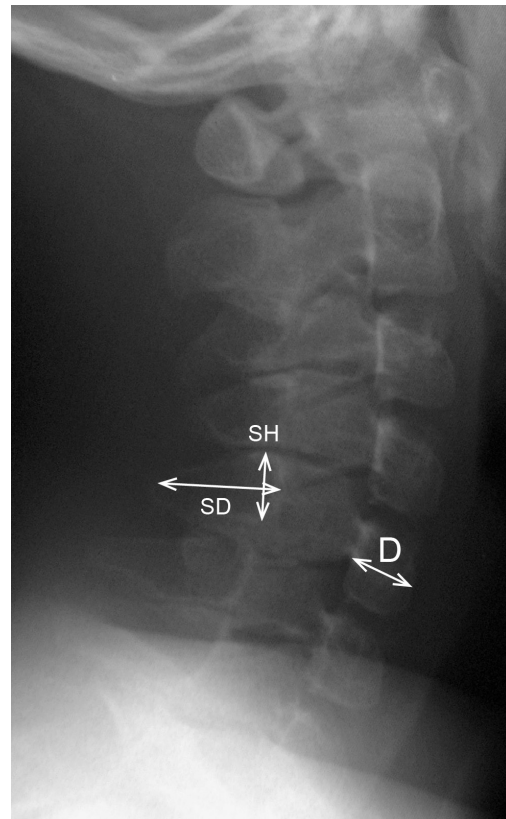


Figure 8. A lateral radiograph of the cervical spine of Patient 16 at the age of eight years showing enlarged spinous process of the C5 vertebra. The (SH+SD)/D ratio and the corresponding SD value is 2.8 and 7.9, respectively.

neck stiffness, which seemed to be an important early clinical sign before the appearance of HO (6), tall and narrow vertebrae and hypertrophic spinous processes of the cervical spine are radiographic characteristics in young FOP patients.

In a previous *in vivo* study, genetically-engineered overexpression of BMP-2/4 both dorsally and laterally to the neural tube manifested combined phenotypes of hypertrophic spinous processes and large deletion of the lateral and ventral parts of vertebral bodies (16). Thus, mesenchymal condensations at the paraxial mesoderm in FOP, where BMP-2 signaling is aberrantly activating, could be responsible for both enlarged spinous processes and relatively tall vertebral bodies.

The common *ACVR1/ALK2* mutation (c.617G > A, p.R206H) shows a homogeneous phenotype including congenital malformation of the great toes and the skeletal features in the thumb and cervical spine (17). In contrast, several atypical mutations in the *ALK2/ACVR1* gene, such as L196P, R258S, R375P, G328R, and P197_F198 del insL, have been identified in patients who showed normal-appearing great toes (18). In this study, one patient (Patient 14) with an atypical mutation (c.774G > C, p.R258S) showed normal-appearing great toes. She also lacked the shortened thumb but exhibited exceptionally tall and narrow vertebral bodies. Another patient (Patient 4) who showed neither malformed great

toes nor shortening of the first metacarpal bone also manifested distinctive features of the cervical spine in spite of the common *ACVR1/ALK2* mutation. We believe that radiographic characteristics of the cervical spine are potent diagnostic clues for FOP especially in cases without typical deformities of the great toes.

Acknowledgements

This work was supported partly by Research Committee on Fibrodysplasia Ossificans Progressiva from the Ministry of Health, Labour and Welfare of Japan.

References

1. Shore EM, Xu M, Feldman GJ, *et al.* A recurrent mutation in the BMP type I receptor *ACVR1* causes inherited and sporadic fibrodysplasia ossificans progressiva. *Nat Genet.* 2006; 38:525-527.
2. Kitterman JA, Kantanie S, Rocke DM, Kaplan FS. Iatrogenic harm caused by diagnostic errors in fibrodysplasia ossificans progressiva. *Pediatrics.* 2005; 116:e654-e661.
3. Kitoh H, Achiwa M, Kaneko H, Mishima K, Matsushita M, Kadono I, Horowitz JD, Sallustio BC, Ohno K, Ishiguro N. Perhexiline maleate in the treatment of fibrodysplasia ossificans progressiva: An open-labeled clinical trial. *Orphanet J Rare Dis.* 2013; 8:163.
4. Pignolo RJ, Shore EM, Kaplan FS. Fibrodysplasia ossificans progressiva: Diagnosis, management, and therapeutic horizons. *Pediatr Endocrinol Rev.* 2013; 10 (Suppl 2):437-448.
5. Nakashima Y, Haga N, Kitoh H, Kamizono J, Tozawa K, Katagiri T, Susami T, Fukushi J, Iwamoto Y. Deformity of the great toe in fibrodysplasia ossificans progressiva. *J Orthop Sci.* 2010; 15:804-809.
6. Kaplan FS, Glaser DL, Shore EM, Deirmengian GK, Gupta R, Delai P, Morhart P, Smith R, Le Merrer M, Rogers JG, Connor JM, Kitterman JA. The phenotype of fibrodysplasia ossificans progressiva. *Clin Rev Bone Miner Metab.* 2005; 3:183-188.
7. Mishima K, Kitoh H, Katagiri T, Kaneko H, Ishiguro N. Early clinical and radiographic characteristics in fibrodysplasia ossificans progressiva: A report of two cases. *J Bone Joint Surg Am.* 2011; 93:e52.
8. Poznanski AK, Garn SM, Holt JF. The thumb in the congenital malformation syndromes. *Radiology.* 1971; 100:115-129.
9. Remes VM, Heinanen MT, Kinnunen JS, Marttinen EJ. Reference values for radiological evaluation of cervical vertebral body shape and spinal canal. *Pediatr Radiol.* 2000; 30:190-195.
10. Kaplan FS, Le Merrer M, Glaser DL, Pignolo RJ, Goldsby RE, Kitterman JA, Groppe J, Shore EM. Fibrodysplasia ossificans progressiva. *Best Pract Res Clin Rheumatol.* 2008; 22:191-205.
11. Pignolo RJ, Shore EM, Kaplan FS. Fibrodysplasia ossificans progressiva: Clinical and genetic aspects. *Orphanet J Rare Dis.* 2011; 6:80.
12. Oberg KC. Review of the molecular development of the thumb: Digit primera. *Clin Orthop Relat Res.* 2014; 472:1101-1105.
13. Deschamps J. Tailored *Hox* gene transcription and the making of the thumb. *Genes Dev.* 2008; 22:293-296.
14. Johnson D, Kan SH, Oldridge M, Trembath RC, Roche P, Esnouf RM, Giele H, Wilkie AO. Missense mutations in the homeodomain of *HOXD13* are associated with brachydactyly types D and E. *Am J Hum Genet.* 2003; 72:984-997.
15. Li X, Nie S, Chang C, Qiu T, Cao X. Smads oppose Hox transcriptional activities. *Exp Cell Res.* 2006; 312:854-864.
16. Monsoro-Burq AH, Duprez D, Watanabe Y, Bontoux M, Vincent C, Brickell P, Le Douarin N. The role of bone morphogenetic proteins in vertebral development. *Development.* 1996; 122:3607-3616.
17. Kaplan FS, Xu M, Glaser DL, Collins F, Connor M, Kitterman J, Sillence D, Zackai E, Ravitsky V, Zasloff M, Ganguly A, Shore EM. Early diagnosis of fibrodysplasia ossificans progressiva. *Pediatrics.* 2008; 121:e1295-e1300.
18. Kaplan FS, Xu M, Seemann P, *et al.* Classic and atypical fibrodysplasia ossificans progressiva (FOP) phenotypes are caused by mutations in the bone morphogenetic protein (BMP) type I receptor *ACVR1*. *Hum Mutat.* 2009; 30:379-390.

(Received April 13, 2014; Revised April 24, 2014; Accepted May 07, 2014)

Radiographic characteristics of the hand and cervical spine in fibrodysplasia ossificans progressiva

Kenichi Mishima¹, Hiroshi Kitoh^{1,2,*}, Nobuhiko Haga², Yasuharu Nakashima², Junji Kamizono², Takenobu Katagiri², Takafumi Susami², Masaki Matsushita¹, Naoki Ishiguro¹

¹Department of Orthopaedic Surgery, Nagoya University Graduate School of Medicine, Nagoya, Aichi, Japan;

²The Research Committee on Fibrodysplasia Ossificans Progressiva, Tokyo, Japan.

Summary

Fibrodysplasia ossificans progressiva (FOP) is a disabling heritable disorder of connective tissue characterized by progressive heterotopic ossification in various extraskelatal sites. Early correct diagnosis of FOP is important to prevent additional iatrogenic harm or trauma. Congenital malformation of the great toes is a well-known diagnostic clue, but some patients show normal-appearing great toes. The thumb shortening and cervical spine abnormalities are other skeletal features often observed in FOP. This study aimed to address the quantitative assessment of these features in a cohort of patients with FOP, which potentially helps early diagnosis of FOP. Radiographs of the hand and cervical spine were retrospectively analyzed from a total of 18 FOP patients (9 males and 9 females) with an average age of 13.9 years (range 0.7-39.3 years). The elevated ratio of the second metacarpal bone to the distal phalanx of the thumb ($> +1SD$) was a consistent finding irrespective of the patient's age and gender. Infant FOP patients, in addition, exhibited an extremely high ratio of the second metacarpal bone to the first metacarpal bone ($> +3SD$). The height/depth ratio of the C5 vertebra increased in patients over 4 years of age ($> +2SD$). Additionally, the ratio of (height+depth) of the C5 spinous process to the C5 vertebral depth was markedly elevated in young patients ($> +2SD$). We quantitatively demonstrated the hand and cervical spine characteristics of FOP. These findings, which can be seen from early infancy, could be useful for early diagnosis of FOP even in patients without great toe abnormalities.

Keywords: Fibrodysplasia ossificans progressiva, early diagnosis, radiographic characteristics

1. Introduction

Fibrodysplasia ossificans progressiva (FOP) is a severely disabling genetic disorder of connective tissues characterized by congenital malformations of the great toes and progressive heterotopic ossification (HO) in various extraskelatal sites including muscles, tendons, ligaments, fascias, and aponeuroses. FOP is caused by a recurrent activating mutation (c.617G > A, p.R206H) in the gene encoding activin receptor IA/activin-like kinase 2 (ACVR1/ALK2), a bone morphogenetic protein (BMP) type I receptor (1). HO typically begins

to form during the first decade of life preceded by painful soft tissue swelling and inflammation (flare-ups), which are sometimes mistaken for aggressive fibromatosis or musculoskeletal tumors. Surgical resection of HO leads to explosive new bone formation (2). Since there is no definitive treatment to prevent progressive HO in FOP to date (3), early correct diagnosis is necessary to maintain their mobility by preventing additional iatrogenic harm (4).

Malformations of the great toes, such as hallux valgus, deformed proximal phalanges and shortened first metatarsal bones, are well-known pre-osseous features of FOP (5). A reported incidence of these deformities is 95%, suggesting that there exists rare FOP cases without the great toe abnormalities (6). We demonstrated additional early radiographic signs of FOP including shortening of the first metacarpal bones and hypertrophy of the posterior element of the cervical

*Address correspondence to:

Dr. Hiroshi Kitoh, Department of Orthopaedic Surgery, Nagoya University Graduate School of Medicine, 65 Tsurumai, Showa-ku, Nagoya, Aichi, 466-8550, Japan.
E-mail: hkitoh@med.nagoya-u.ac.jp

spine (7). Clinical awareness of these deformities can aid clinicians in making early diagnosis of FOP, but quantitative assessment of these deformities has not yet been determined.

In this study, we retrospectively examined radiographs of the hand and cervical spine in FOP patients and demonstrated various abnormal radiographic parameters helpful for early diagnosis of this specific disorder.

2. Materials and Methods

2.1. Demographics

This study represents a retrospective case-control study consisting of Japanese FOP patients followed up at health care facilities where members of the Research Committee on Japanese Fibrodysplasia Ossificans Progressiva practiced. After approval from the Institutional Review Board of the Nagoya University Hospital, we collected the hand and/or cervical spine radiographs from 18 FOP patients (9 males and 9 females) with an average age of 13.9 years (range 0.7-39.3 years) at the time of this study. The patients were diagnosed clinically and radiographically based on various characteristic findings of FOP including deformities of the great toes, extraskeletal HO, joint contractures, cervical fusions, broad femoral necks, and osteochondroma-like lesions. Molecular testing was performed on fourteen patients. Thirteen showed the common *ACVR1/ALK2* mutation within the glycine/serine-rich regulatory (GS) domain (c.617G > A, p.R206H), and one patient had an atypical mutation within the protein kinase domain (c.774G > T, p.R258S). Molecular studies were not conducted for the remaining 4 patients who showed characteristic skeletal features of FOP. We examined anteroposterior (AP) radiographs of the hands and lateral radiographs of the cervical spine in each individual. The earliest hands and cervical spine films were analyzed using image processing and analysis software ImageJ®.

2.2. Radiographic assessment of the hand

According to the measurement method by Poznanski *et al.* (8), the length of each phalanx and metacarpal bone was measured. In brief, the tangent lines were drawn at both ends of each bone, which were perpendicular to the bone axis, and a bone length was defined as the distance between these two lines (Figure 1). We measured a length of the distal (D1) and proximal (P1) phalanges of the thumb as well as that of the first and second metacarpal bones (MET1 and MET2), and calculated the following bone length ratios, MET2/MET1, MET2/P1, MET2/D1, MET1/P1, MET1/D1, and P1/D1. Radiographs of both hands from one patient were separately analyzed to obtain the average value of the measurements. Reference ranges of these

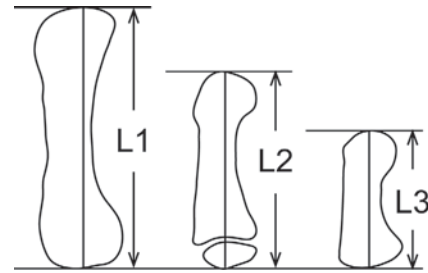


Figure 1. A schematic diagram illustrating the measurement method of bone length in the hand. Bone length was defined as the distance between the tangents drawn to each end of the bone, which were perpendicular to the bone axis. The entire bone length was measured for adults (L1), children (L2), and infants (L3).

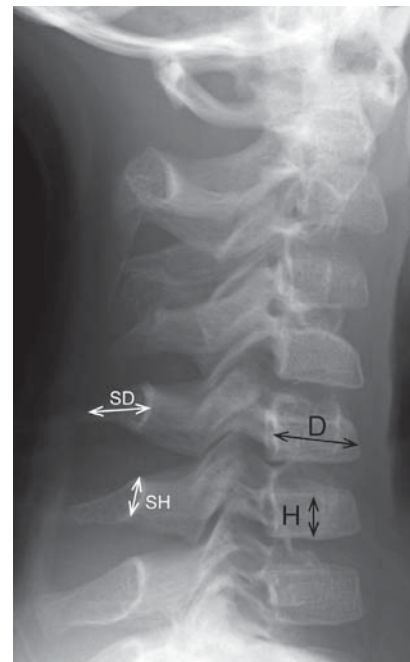


Figure 2. A radiograph depicting the measurements of the bone length in the cervical spine. The height (H) and depth (D) of the C5 vertebral body was measured at the midpoint of the body. The height of the C5 spinous process (SH) was defined as the distance from the cranial to the caudal rim at the juxta-laminar zone. The depth of the spinous process (SD) was measured from the midpoint of the anterior wall to that of the posterior rim.

measurements in different ages and genders were used based on the literature from Poznanski *et al.* (8). The control data of these measurements in infant ($n = 21$) were determined by the radiographic database in Nagoya University Hospital.

2.3. Radiographic assessment of the cervical spine

According to the measurement method proposed by Remes *et al.* (9), the height and depth of the C5 vertebral body were measured. Briefly, vertebral body height (H) was measured at the midpoint of the vertebra, perpendicular to the lower end plate. The vertebral body depth (D) was measured at the midpoint of the body from the anterior wall to the posterior wall (Figure 2). The H/D ratios of the C5 vertebra were then calculated

Table 1. Characteristics and quantitative indices for the study population

Patient	Sex	ALK2 mutation	Age at X-ray (yrs)		Deviation of the bone length ratios (SD)			
			Hand/Cervical spine		MET2/D1	MET2/D1	H/D	(SH+SD)/D
1	M	R206H	0/0		1.0	1.0	0.6	0.1
2	M	R206H	0/0		2.4	2.4	0.6	7.1
3	M	R206H	1/3		3.1	3.1	0.9	2.8
4	F	R206H	5/6		2.8	2.8	3.3	8.3
5	M	R206H	8/7		6.2	6.2	2.8	3.7
6	M	R206H	12/18		4.1	4.1	1.9	1.5
7	F	R206H	17/17		4.0	4.0	4.1	NA
8	F	R206H	20/NA		2.2	2.2	NA	NA
9	M	R206H	29/NA		2.7	2.7	NA	NA
10	M	R206H	34/NA		3.5	3.5	NA	NA
11	F	R206H	36/NA		1.0	1.0	NA	NA
12	M	R206H	39/16		1.9	1.9	3.0	1.8
13	F	R206H	NA/18		NA	NA	0.6	2.4
14	F	R258S	14/14		1.7	1.7	4.9	NA
15	M	ND	NA/4		NA	NA	3.2	8.8
16	F	ND	NA/8		NA	NA	9.2	7.9
17	F	ND	NA/16		NA	NA	4.4	NA
18	F	ND	5/5		5.3	5.3	5.3	5.4

M denotes male; F, female; ND, not determined; NA, not applicable; SD, standard deviation.

and compared to normal reference values established by Remes *et al.* in different age and gender groups (9). In addition, we measured the height and depth of the C5 spinous process. The height of the spinous process (SH) was defined as the distance from the cranial to caudal margin at the junction of the spinous process and lamina. The depth of spinous process (SD) was measured from the midportion of the anterior wall to that of the posterior rim demarcating a thick cortex shadow (Figure 2). The sum of SH and SD measurements was used for the evaluation of spinous process size, then the (SH + SD)/D ratio of the C5 vertebra was calculated. Reference values of the (SH + SD)/D ratio were established from the radiographic database of normal controls in Nagoya University Hospital.

3. Results

3.1. Characteristics of the study cohort

Patients' characteristics and quantitative indices of the measurements are shown in Table 1. Deviation of the bone length ratios in the hand and cervical spine was calculated based on age-matched reference values.

3.2. Radiographic characteristics of the hand

Mean and standard deviation of the MET2/D1 and MET2/MET1 ratio in control infants ($n = 21$) are 2.9 ± 0.29 and 1.64 ± 0.08 , respectively. Twenty-six hand radiographs from 14 patients (8 males and 6 females) were available. Regardless of age and gender, all FOP patients showed a MET2/D1 ratio larger than +1SD of normal controls (Figure 3A and 3B). In infant patients without an epiphyseal ossification center of the first metacarpal bone, the MET2/MET1 ratio was extremely

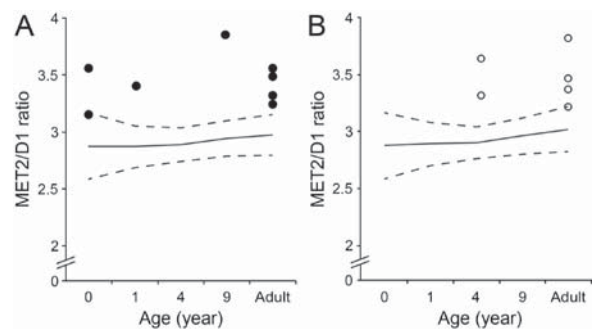


Figure 3. Scatter plots showing the bone length ratio of the second metacarpal bone (MET2) to the distal phalanx of the thumb (D1) in male (A) and female (B) patients with FOP. Solid and dash lines denote the normal value and the standard deviation (SD) of the MET2/D1 ratio, respectively.

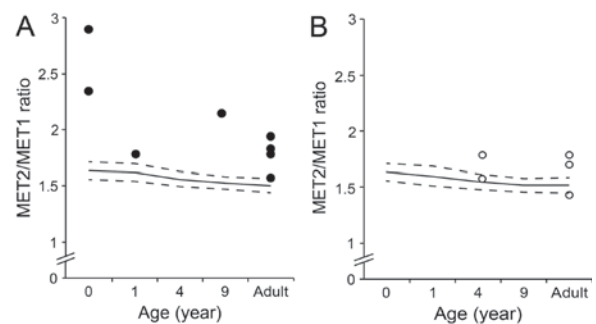


Figure 4. Scatter plots showing the bone length ratio of the second metacarpal bone (MET2) to the first metacarpal bone (MET1) in male (A) and female (B) patients with FOP. Solid and dash lines denote the normal value and the standard deviation (SD) of the MET2/MET1 ratio, respectively.

large ($> +3SD$ of normal controls) (Figure 4A and 4B). The MET2/P1 ratio was higher in infant patients, but it scattered around the mean value with increasing age (data not shown). There were no characteristic features in the values of the MET1/P1, MET1/D1, and P1/D1 ratios in FOP patients, although the MET1/P1 and MET1/D1

Table 2. Mean and standard deviation of normal controls for the (SH+SD)/D ratio of the C5 vertebra

Age group	<1	1-2	2-3	3-4	4-5	5-6	6-7	7-8	8-9	9-10	10-11	11-12	12-13	13-14	14-15	15-16	16-17	17-18	18-19	19-20	20-21
Mean	1.05	1.10	1.09	1.20	1.21	1.43	1.37	1.47	1.33	1.47	1.50	1.53	1.51	1.57	1.69	1.86	1.76	1.73	1.71	1.78	1.86
SD	0.13	0.15	0.15	0.13	0.11	0.18	0.18	0.17	0.19	0.18	0.16	0.18	0.20	0.19	0.12	0.16	0.22	0.22	0.23	0.24	0.25
N	11	21	17	13	6	13	25	19	20	17	16	17	14	20	16	21	23	31	28	38	20

SD denotes standard deviation; N, number of control subjects; SH, height of the spinous process; SD, depth of the spinous process; D, depth of the vertebral body.

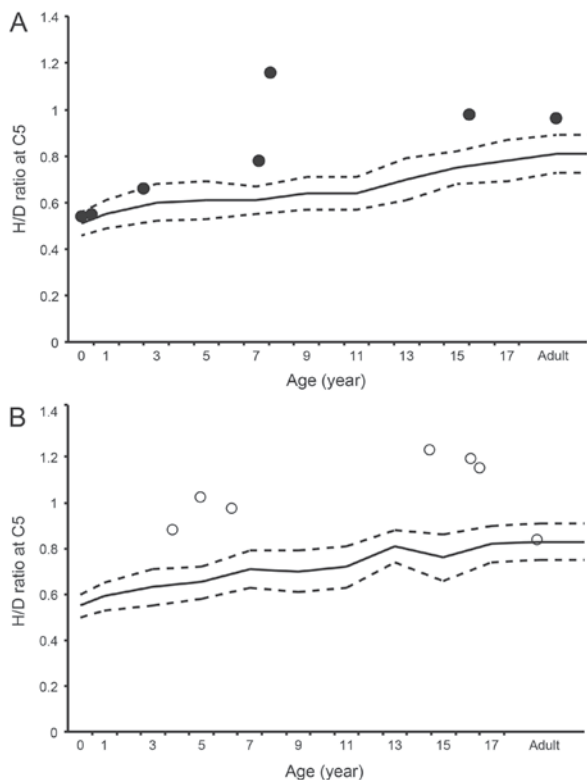


Figure 5. Scatter plots showing the bone length ratio of the C5 vertebral height (H) to depth (D) in male (A) and female (B) patients with FOP. Solid and dashed lines denote the normal value and the standard deviation (SD) of the H/D ratio, respectively.

ratios were relatively small ($< -1SD$ of normal controls) in infant FOP patients (data not shown).

3.3. Radiographic characteristics of the cervical spine

Reference values of the (SH + SD)/D ratio of the C5 vertebra are shown in Table 2. There were 14 (7 males and 7 females) cervical spine radiographs available for analysis. Among them, three radiographs were excluded from analysis of the (SH + SD)/D ratio for insufficient resolution. The H/D ratio of the C5 vertebra exceeded $+2SD$ of normal controls in patients over 4 years of age except one female adult patient (Figure 5A and 5B). Similarly, the (SH + SD)/D ratio of the C5 vertebra was larger than $+2SD$ of normal controls in young patients except one male infant (Figure 6).

4. Discussion

In the present study, we quantitatively proved the hand

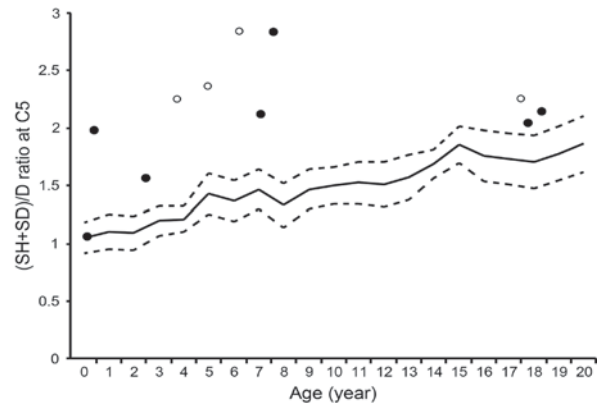


Figure 6. Scatter plots showing the bone length ratio of the C5 spinous process height (SH) + depth (SD) to the C5 vertebral depth (D). Solid and open circles indicate male and female, respectively. Solid and dashed lines denote the normal value and the standard deviation (SD) of the (SH+SD)/D ratio, respectively.

and cervical spine abnormalities in FOP including shortened thumbs as well as tall and narrow vertebral bodies and hypertrophic posterior elements of the cervical spine (7,10). Especially in young patients, shortening of the first metacarpal bone and enlargement of the cervical spinous processes were pathognomonic findings useful for early diagnosis of FOP before the appearance of HO.

Previous studies have reported that thumb shortening was seen in 50% of FOP patients (6). In the present study, all patients had a MET2/D1 ratio larger than $+1SD$ of normal controls, and 85% (11/13) of the patients showed an increased MET2/MET1 ratio. The thumb shortening, therefore, seems to be more common than previous reports in FOP. Furthermore, an extremely high MET2/MET1 ratio in infant patients suggested that disproportionate shortening of the first metacarpal bone was an important early radiographic finding in FOP (Figure 7).

It is an intriguing feature of FOP that thumb morphogenesis is exclusively disrupted in the development of digit formation (11). The thumb is the last digit in the autopod to form, and it is different from other digits in terms of its relative position, shape, size, and number of phalanges. These unique thumb identities may be attributed to the expression profile of *HoxD* genes, which are pivotal transcriptional factors regulating limb patterning and growth (12). All four *HoxD10* to *D13* genes are expressed in the future digit II-V area in the autopod during the hand plate formation, whereas sole expression of the



Figure 7. An anteroposterior radiograph of the right hand of Patient 1 at the age of eight months showing marked shortening of the first metacarpal bone. The MET2/MET1 ratio and the corresponding SD value is 2.9 and 16.3, respectively.

HoxD13 gene in the presumptive digit I area is of great significance (13). Mutations in the homeodomain of the *HoxD13* gene cause brachydactyly type D that is characterized by variable shortening of the distal phalanx of the thumb. This mutated *HoxD13* proteins responsible for its decreased affinity for the double-stranded DNA target containing a cognitive sequence of the homeodomain (14). Interestingly, previous research has revealed that BMP signaling-dependent Smad1/4 proteins prevented *HoxD10* and *HoxD13* from binding to DNA targets (15). Constitutively-activated BMP signaling in FOP thus is likely to impair *HoxD13*-mediated transcriptional regulation by direct interactions between BMP-induced Smads and *HoxD13*. Mesenchymal condensation and chondrocyte proliferation of the presumptive digit I area could be suppressed by down-regulated *HoxD13* function, whereas in presumptive digits II to V areas, it could be preserved by compensating expressions of other *HoxD* genes (*HoxD11* and *HoxD12*). Dysregulated BMP signal transduction during embryogenesis seems to cause relative shortening of the first metacarpals and distal phalanges of the thumb in FOP.

More than 90% of adult FOP patients showed fusion of the facet joints, which is a type of orthotopic ossification (6). To our knowledge, however, there are no reports delineating the precise prevalence of tall and narrow vertebral bodies and enlarged posterior elements of the cervical vertebrae. Here we demonstrated that the H/D and (SH + SD)/D ratios in the C5 vertebrae were larger than +2SD of normal values in 64% and 73% of patients, respectively (Figure 8). In addition to

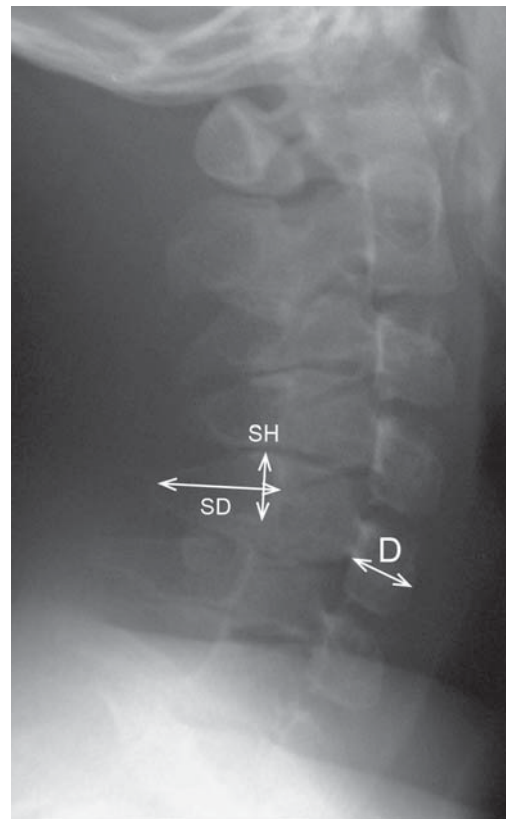


Figure 8. A lateral radiograph of the cervical spine of Patient 16 at the age of eight years showing enlarged spinous process of the C5 vertebra. The (SH+SD)/D ratio and the corresponding SD value is 2.8 and 7.9, respectively.

neck stiffness, which seemed to be an important early clinical sign before the appearance of HO (6), tall and narrow vertebrae and hypertrophic spinous processes of the cervical spine are radiographic characteristics in young FOP patients.

In a previous *in vivo* study, genetically-engineered overexpression of BMP-2/4 both dorsally and laterally to the neural tube manifested combined phenotypes of hypertrophic spinous processes and large deletion of the lateral and ventral parts of vertebral bodies (16). Thus, mesenchymal condensations at the paraxial mesoderm in FOP, where BMP-2 signaling is aberrantly activating, could be responsible for both enlarged spinous processes and relatively tall vertebral bodies.

The common *ACVR1/ALK2* mutation (c.617G > A, p.R206H) shows a homogeneous phenotype including congenital malformation of the great toes and the skeletal features in the thumb and cervical spine (17). In contrast, several atypical mutations in the *ALK2/ACVR1* gene, such as L196P, R258S, R375P, G328R, and P197_F198 del insL, have been identified in patients who showed normal-appearing great toes (18). In this study, one patient (Patient 14) with an atypical mutation (c.774G > C, p.R258S) showed normal-appearing great toes. She also lacked the shortened thumb but exhibited exceptionally tall and narrow vertebral bodies. Another patient (Patient 4) who showed neither malformed great

toes nor shortening of the first metacarpal bone also manifested distinctive features of the cervical spine in spite of the common *ACVR1/ALK2* mutation. We believe that radiographic characteristics of the cervical spine are potent diagnostic clues for FOP especially in cases without typical deformities of the great toes.

Acknowledgements

This work was supported partly by Research Committee on Fibrodysplasia Ossificans Progressiva from the Ministry of Health, Labour and Welfare of Japan.

References

1. Shore EM, Xu M, Feldman GJ, *et al.* A recurrent mutation in the BMP type I receptor *ACVR1* causes inherited and sporadic fibrodysplasia ossificans progressiva. *Nat Genet.* 2006; 38:525-527.
2. Kitterman JA, Kantanie S, Rocke DM, Kaplan FS. Iatrogenic harm caused by diagnostic errors in fibrodysplasia ossificans progressiva. *Pediatrics.* 2005; 116:e654-e661.
3. Kitoh H, Achiwa M, Kaneko H, Mishima K, Matsushita M, Kadono I, Horowitz JD, Sallustio BC, Ohno K, Ishiguro N. Perhexiline maleate in the treatment of fibrodysplasia ossificans progressiva: An open-labeled clinical trial. *Orphanet J Rare Dis.* 2013; 8:163.
4. Pignolo RJ, Shore EM, Kaplan FS. Fibrodysplasia ossificans progressiva: Diagnosis, management, and therapeutic horizons. *Pediatr Endocrinol Rev.* 2013; 10 (Suppl 2):437-448.
5. Nakashima Y, Haga N, Kitoh H, Kamizono J, Tozawa K, Katagiri T, Susami T, Fukushi J, Iwamoto Y. Deformity of the great toe in fibrodysplasia ossificans progressiva. *J Orthop Sci.* 2010; 15:804-809.
6. Kaplan FS, Glaser DL, Shore EM, Deirmengian GK, Gupta R, Delai P, Morhart P, Smith R, Le Merrer M, Rogers JG, Connor JM, Kitterman JA. The phenotype of fibrodysplasia ossificans progressiva. *Clin Rev Bone Miner Metab.* 2005; 3:183-188.
7. Mishima K, Kitoh H, Katagiri T, Kaneko H, Ishiguro N. Early clinical and radiographic characteristics in fibrodysplasia ossificans progressiva: A report of two cases. *J Bone Joint Surg Am.* 2011; 93:e52.
8. Poznanski AK, Garn SM, Holt JF. The thumb in the congenital malformation syndromes. *Radiology.* 1971; 100:115-129.
9. Remes VM, Heinanen MT, Kinnunen JS, Marttinen EJ. Reference values for radiological evaluation of cervical vertebral body shape and spinal canal. *Pediatr Radiol.* 2000; 30:190-195.
10. Kaplan FS, Le Merrer M, Glaser DL, Pignolo RJ, Goldsby RE, Kitterman JA, Groppe J, Shore EM. Fibrodysplasia ossificans progressiva. *Best Pract Res Clin Rheumatol.* 2008; 22:191-205.
11. Pignolo RJ, Shore EM, Kaplan FS. Fibrodysplasia ossificans progressiva: Clinical and genetic aspects. *Orphanet J Rare Dis.* 2011; 6:80.
12. Oberg KC. Review of the molecular development of the thumb: Digit prima. *Clin Orthop Relat Res.* 2014; 472:1101-1105.
13. Deschamps J. Tailored *Hox* gene transcription and the making of the thumb. *Genes Dev.* 2008; 22:293-296.
14. Johnson D, Kan SH, Oldridge M, Trembath RC, Roche P, Esnouf RM, Giele H, Wilkie AO. Missense mutations in the homeodomain of *HOXD13* are associated with brachydactyly types D and E. *Am J Hum Genet.* 2003; 72:984-997.
15. Li X, Nie S, Chang C, Qiu T, Cao X. Smads oppose Hox transcriptional activities. *Exp Cell Res.* 2006; 312:854-864.
16. Monsoro-Burq AH, Duprez D, Watanabe Y, Bontoux M, Vincent C, Brickell P, Le Douarin N. The role of bone morphogenetic proteins in vertebral development. *Development.* 1996; 122:3607-3616.
17. Kaplan FS, Xu M, Glaser DL, Collins F, Connor M, Kitterman J, Sillence D, Zackai E, Ravitsky V, Zasloff M, Ganguly A, Shore EM. Early diagnosis of fibrodysplasia ossificans progressiva. *Pediatrics.* 2008; 121:e1295-e1300.
18. Kaplan FS, Xu M, Seemann P, *et al.* Classic and atypical fibrodysplasia ossificans progressiva (FOP) phenotypes are caused by mutations in the bone morphogenetic protein (BMP) type I receptor *ACVR1*. *Hum Mutat.* 2009; 30:379-390.

(Received April 13, 2014; Revised April 24, 2014; Accepted May 07, 2014)

Meclozine Promotes Longitudinal Skeletal Growth in Transgenic Mice with Achondroplasia Carrying a Gain-of-Function Mutation in the *FGFR3* Gene

Masaki Matsushita^{1,2}, Satoru Hasegawa¹, Hiroshi Kitoh², Kensaku Mori³, Bisei Ohkawara¹, Akihiro Yasoda⁴, Akio Masuda¹, Naoki Ishiguro², Kinji Ohno¹

¹Division of Neurogenetics, Center for Neurological Diseases and Cancer, Nagoya University Graduate School of Medicine, Nagoya, Japan; ²Department of Orthopaedic Surgery, Nagoya University Graduate School of Medicine, Nagoya, Japan; ³Department of Media Science, Graduate School of Information Science, Nagoya University, Nagoya, Japan; ⁴Department of Diabetes, Endocrinology and Nutrition, Kyoto University Graduate School of Medicine, Kyoto, Japan

Key terms: meclozine, achondroplasia, FGFR3

Achondroplasia (ACH) is one of the most common skeletal dysplasias causing short stature owing to a gain-of-function mutation in the *FGFR3* gene, which encodes the fibroblast growth factor receptor 3. We found that meclozine, an over-the-counter drug for motion sickness, inhibited elevated FGFR3 signaling in chondrocytic cells. To examine the feasibility of meclozine administration in clinical settings, we investigated the effects of meclozine on ACH model mice carrying the heterozygous *Fgfr3^{ach}* transgene. We quantified the effect of meclozine in bone explant cultures employing limb rudiments isolated from developing embryonic tibiae from *Fgfr3^{ach}* mice. We found that meclozine significantly increased the full-length and cartilaginous primordia of embryonic tibiae isolated from *Fgfr3^{ach}* mice. We next analyzed the skeletal phenotypes of growing *Fgfr3^{ach}* mice and wild-type mice with or without meclozine treatment. In *Fgfr3^{ach}* mice, meclozine significantly increased the body length after two weeks of administration. At skeletal maturity, the bone lengths, including the cranium, radius, ulna, femur, tibia, and vertebrae were significantly longer in meclozine-treated *Fgfr3^{ach}* mice than in untreated *Fgfr3^{ach}* mice. Interestingly, meclozine also increased bone growth in wild-type mice. The plasma concentration of meclozine during treatment was within the range that has been used in clinical settings for motion sickness. Increased longitudinal bone growth in *Fgfr3^{ach}* mice by oral administration of meclozine in a growth period indicates potential clinical feasibility of meclozine for the improvement of short stature in ACH.

Fibroblast growth factor receptor 3 (FGFR3) is a negative regulator of endochondral bone growth. Gain-of-function mutations in the *FGFR3* gene cause several short-limbed skeletal dysplasias, including achondroplasia (ACH) (1, 2), hypochondroplasia (HCH) (3), severe ACH with developmental delay and acanthosis nigricans (SADDAN) (4), and thanatophoric dysplasia (TD) types I and II (5). In contrast, loss-of-function mutations in *FGFR3* lead to camptodactyly, tall stature, and hearing loss (CATSHL) syndrome (6). ACH is the most common short-limbed skeletal dysplasia, with an incidence of 1 in

16 000 to 26 000 live births (7). Clinical features of ACH include severe short stature with rhizomelic shortening of the extremities, relative macrocephaly with frontal bossing, midface hypoplasia, and increased lumbar lordosis. In addition, foramen magnum stenosis, hydrocephalus, and spinal canal stenosis are potentially serious complications of ACH (8).

Growth hormone has been administered to children with ACH for treatment of short stature in some countries (9), but the response to this therapy is moderate and the long-term effects remain controversial. Limb lengthening

ISSN Print 0013-7227 ISSN Online 1945-7170

Printed in U.S.A.

Copyright © 2014 by the Endocrine Society

Received November 13, 2014. Accepted November 25, 2014.

Abbreviations:

procedures are another therapeutic option to gain bone length (10) but involves significant time and effort. Inhibition of FGFR3 signaling is a therapeutic strategy for ACH and other FGFR3-related skeletal dysplasias (11–13); however, no effective treatments are currently available for these disorders. C-type natriuretic peptide (CNP) is a potent antagonist of *FGFR3* signaling, which alleviates the short-limbed phenotype of transgenic ACH mice through inhibition of the intracellular mitogen-activated protein kinase (MAPK) pathway (14). CNP, however, has a short half-life, and continuous intravenous (IV) infusion is required for in vivo experiments (15). A CNP analog with an extended half-life, BMN-111, has recently been developed, and significant bone growth recovery was demonstrated in a mouse model of ACH by subcutaneous administration of BMN-111 (16). Recent studies using induced pluripotent stem (iPS) cells established from patients with FGFR3-related skeletal dysplasias revealed that statins also rescue the mouse phenotypes (17).

In our previous study, we found that meclozine, an over-the-counter (OTC) H1 receptor inhibitor used to treat motion sickness, inhibited elevated FGFR3 signaling and promoted chondrocyte proliferation and differentiation using various chondrocytic cell lines. We also confirmed that meclozine alleviates FGF2-mediated longitudinal growth inhibition of embryonic tibiae in bone explant cultures (18). In the present study, we orally administered meclozine to immature transgenic mice with ACH and investigated the effects of this drug on longitudinal bone growth and bone-related complications.

Materials and Methods

Mice

Fgfr3^{ach} mice (FVB background) were provided by Dr. David M. Ornitz at Washington University (19). In brief, *Fgfr3^{ach}* mice express activated *FGFR3* in the growth plate using the *Col2a1* promoter. In all experiments, we used transgenic mice carrying the heterozygous *Fgfr3^{ach}* transgene. Due to unavailability of a sufficient number of wild-type FVB mice, we employed BL6J mice to investigate the effect of meclozine on wild-type mice. All experimental procedures were approved by the Animal Care and Use Committee of our institution.

Bone explant cultures

For bone explant cultures, tibiae from *Fgfr3^{ach}* mice embryos were dissected under the microscope on embryonic day 16.5, placed in a 48-well plate, and cultured in BGJb medium (Invitrogen) supplemented with 0.2% bovine serum albumin and 150 mg/ml ascorbic acid in the presence or absence of 20 μ M meclozine (MP Biomedicals). The embryonic tibiae were cultured for 6 days, with daily replenishment of the medium. The longitudinal length of the bone, which was defined as the length

between the proximal and distal articular cartilage, was measured using ImageJ (18).

Oral administration of meclozine to mice

Food containing meclozine, which was prepared by mixing 0.4 g of meclozine with 1 kg of food (Oriental Yeast Co.), was administered ad libitum to (i) wild-type mice from 2 weeks of age, (ii) *Fgfr3^{ach}* and littermate mice from 3 weeks of age, or (iii) pregnant mice carrying wild-type embryos from 14 days of gestation. Body length was measured every week.

Calculation of feed intake

Fgfr3^{ach} male mice and wild-type female mice were allowed to mate and the 3-week-old littermates were divided into treated and untreated groups. Each group shared one cage for 3 weeks, and total food intake for each cage was measured. The measurements were divided by the total body weight of the mice in each cage, and the calculated values between the two groups were compared.

Radiological analysis

At the end of the treatment, *Fgfr3^{ach}* mice were subjected to microcomputed tomography (Micro-CT) scans (0.5 mm Al filter, 50 kV, 500 μ A for 0.054 seconds; SkyScan 1176, Bruker) as well as a soft X-ray (30 kV, 5 mA for 20 seconds; SOFTEX Type CMB-2; SOFTEX, Kanagawa, Japan). Three-dimensional images from the CT scan were reconstructed by an in-house volume-rendering software (20). This software enabled us to render 3D views of the CT scan from arbitrary viewpoints and directions, as well as measure the distance between two specific points. The lengths of various bones, including the cranium, humerus, radius, ulna, femur, tibia, and vertebrae (L1–5) were measured on both the soft X-ray films and the reconstructed 3D images. The areas of the foramen magnum and spinal canal from L3, L4, and L5 vertebrae were measured from the reconstructed 2D images with the CT-Analyzer (Bruker). The total bone volume of each mouse was also measured from the reconstructed 3D images.

Skeletal preparation

Whole skeletons were harvested, stored in 90% ethanol for 3 days, followed by acetone treatment for 2 days (21). Specimens were then stained using Alizarin red to analyze ossified bones, and Alcian blue to analyze cartilage, for 3 days at 37°C. Following incubation, the samples were transferred to 1% KOH and incubated at room temperature for 2 days. The specimens were serially washed with decreasing concentrations (1% to 0%) of KOH and increasing concentrations (0% to 100%) of glycerol by monitoring the intensity of the stain and the amount of tissue remaining on the specimens. Longitudinal bones, including the humerus, radius, ulna, femur, and tibia were dissected under the microscope and their lengths were measured using ImageJ.

Measurement of plasma meclozine concentrations

Cardiac blood samples were collected under anesthesia from 8-week-old BL6J mice fed 0.2 g or 0.4 g meclozine per kilogram food ad libitum for 72 hours, and plasma concentrations of meclozine were measured (Tanabe R&D Service Co.).

Statistical analysis

Data are expressed as mean \pm standard deviation (SD). Statistical analyses were carried out using the paired and unpaired Student's *t*-tests, or two-way ANOVA followed by Fisher's LSD test.

Results

Meclozine attenuated the growth defect in the *Fgfr3^{ach}* tibiae in bone explant culture

We quantified the effect of meclozine in bone explant cultures by using developing embryonic tibiae isolated from limb rudiments in *Fgfr3^{ach}* mice ($n = 5$) at embryonic day 16.5 (E16.5). We added 20 mM meclozine to the culture medium and compared the length of the treated tibia with that of the contralateral untreated tibia from the same mouse. Meclozine significantly increased the full-length and cartilaginous primordia of the tibiae from *Fgfr3^{ach}* mice by 4.6% ($P < .05$) and 8.3% ($P < .01$) as compared with the contralateral untreated tibiae, respectively. In contrast, the bone marrow in the meclozine-treated tibiae was similar to that in untreated tibiae (Figure 1).

Meclozine ameliorated the short stature of *Fgfr3^{ach}* mice

We next examined the effects of meclozine on longitudinal skeletal growth in *Fgfr3^{ach}* mice. 3-week-old littermates comprised of *Fgfr3^{ach}* and wild-type mice, which were born from *Fgfr3^{ach}* male and wild-type female, were randomly divided into two groups (a meclozine-treated group and an untreated group). Thus, a variable combination of four groups was generated for each kinship: (i) meclozine-treated *Fgfr3^{ach}* mice, (ii) meclozine-treated wild-type mice, (iii) untreated *Fgfr3^{ach}* mice, and (iv) un-

treated wild-type mice. *Fgfr3^{ach}* and wild-type littermates were not differentiated when meclozine treatment was started because we genotyped mice using tails at the end of the experiment in order to consecutively measure the total body length. The absolute values of the body length and bone length were compared within a kinship but not between kinships. For comparison across kinships, we used values normalized with wild-type littermates in the same kinship. We analyzed a total of 8 kinships, including 12 *Fgfr3^{ach}* mice and 19 wild-type mice. Food containing 0.4 g meclozine per kilogram was administered ad libitum to 3-week-old littermates in the treated group for 3 weeks. At six weeks, the body length of the untreated *Fgfr3^{ach}* mice was much shorter than that of the gender-matched wild-type littermates. In contrast, the body lengths of the treated *Fgfr3^{ach}* mice were closer to those of gender-matched wild-type littermates. Quantitative measurements demonstrated that meclozine increased the body length of *Fgfr3^{ach}* mice by 5.4% ($P < .05$; Figure 2A). Temporal analyses demonstrated that meclozine had a statistically significant effect on body length after two weeks (Figure 2B). Intake of food by individual mice (per one gram of the body weight) was similar between the treated and untreated groups (Supplemental Figure 1).

Meclozine increased the bone length of *Fgfr3^{ach}* mice

We next quantified the effects of meclozine on the bone growth of *Fgfr3^{ach}* mice using radiological analysis. After 3 weeks of meclozine administration, *Fgfr3^{ach}* mice were subjected to soft X-ray and Micro-CT scan. We measured individual bone lengths based on the 3D images reconstructed from the Micro-CT scan. The bone lengths, including the cranium, radius, ulna, femur, tibia, and ver-

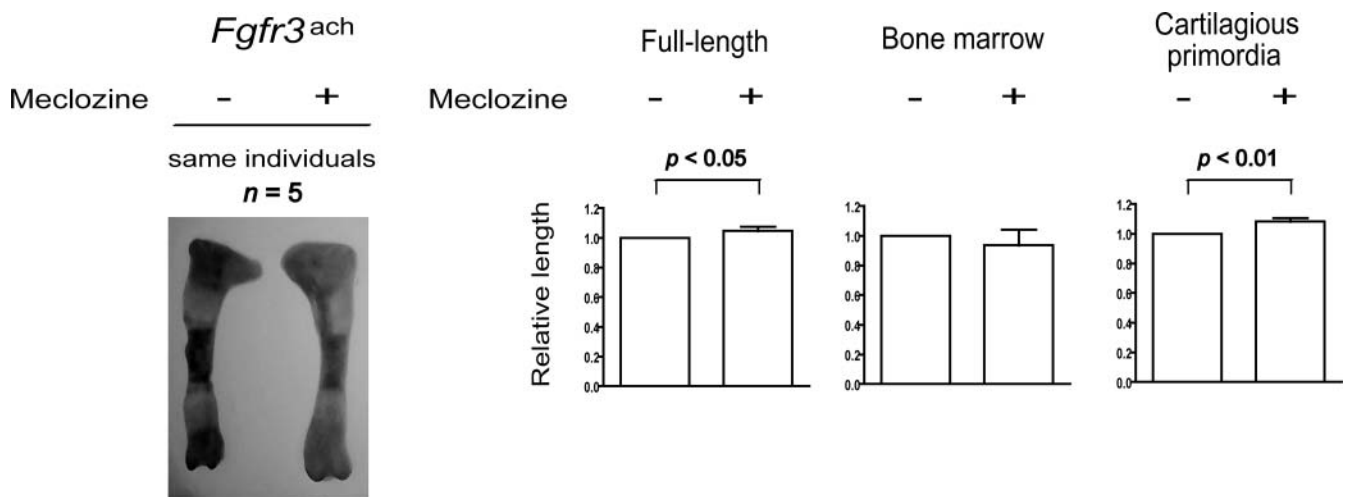


Figure 1. Meclozine enhances bone growth of embryonic tibiae in *Fgfr3^{ach}* mice in explant cultures. Meclozine significantly increased the full-length and cartilaginous primordia of tibiae in *Fgfr3^{ach}* mice but had no effect on the length of bone marrow.

tebrae (L1–5) were significantly longer in meclozine-

treated *Fgfr3^{ach}* mice than in the untreated *Fgfr3^{ach}* mice

(Figure 3A). Similar results were obtained from measurements using the soft X-ray films (Supplemental Figure 2). The bone volumes of the *Fgfr3^{ach}* mice, measured from osseous voxels on the reconstructed images, were significantly increased by meclozine treatment (Figure 3B).

We further analyzed the area of the foramen magnum and lumbar spinal canal in *Fgfr3^{ach}* mice. Meclozine did not increase the area of foramen magnum and lumbar spinal canal in *Fgfr3^{ach}* mice (Supplemental Figure 3 and 4).

Meclozine increased the bone growth in wild-type mice

We further examined the effects of meclozine on bone growth in wild-type mice. Meclozine was administered to 2-week-old wild-type mice for 3 weeks. As wild-type mice were weaned at 2 weeks after birth, we started meclozine treatment 1 week earlier than that for *Fgfr3^{ach}* mice. The body length of meclozine-treated mice was significantly longer than that of untreated mice after 1 week (Figure 4A, B). The bone lengths of the radius, ulna, femur, tibia, and vertebrae (L1–5) of the meclozine-treated mice were significantly longer than the corresponding bone lengths in the untreated mice (Figure 4C).

We next administered meclozine to pregnant wild-type mice to examine the effects of the drug on fetal bone development. After administration of meclozine to wild-type mice at 14 days of gestation, their offspring were subjected to transparent specimen analysis at postnatal day 5. The meclozine-treated offspring were larger than the untreated offspring (Figure 4D). The lengths of the long tubular bones, including the ulna, femur, and tibia, were significantly longer in the meclozine-

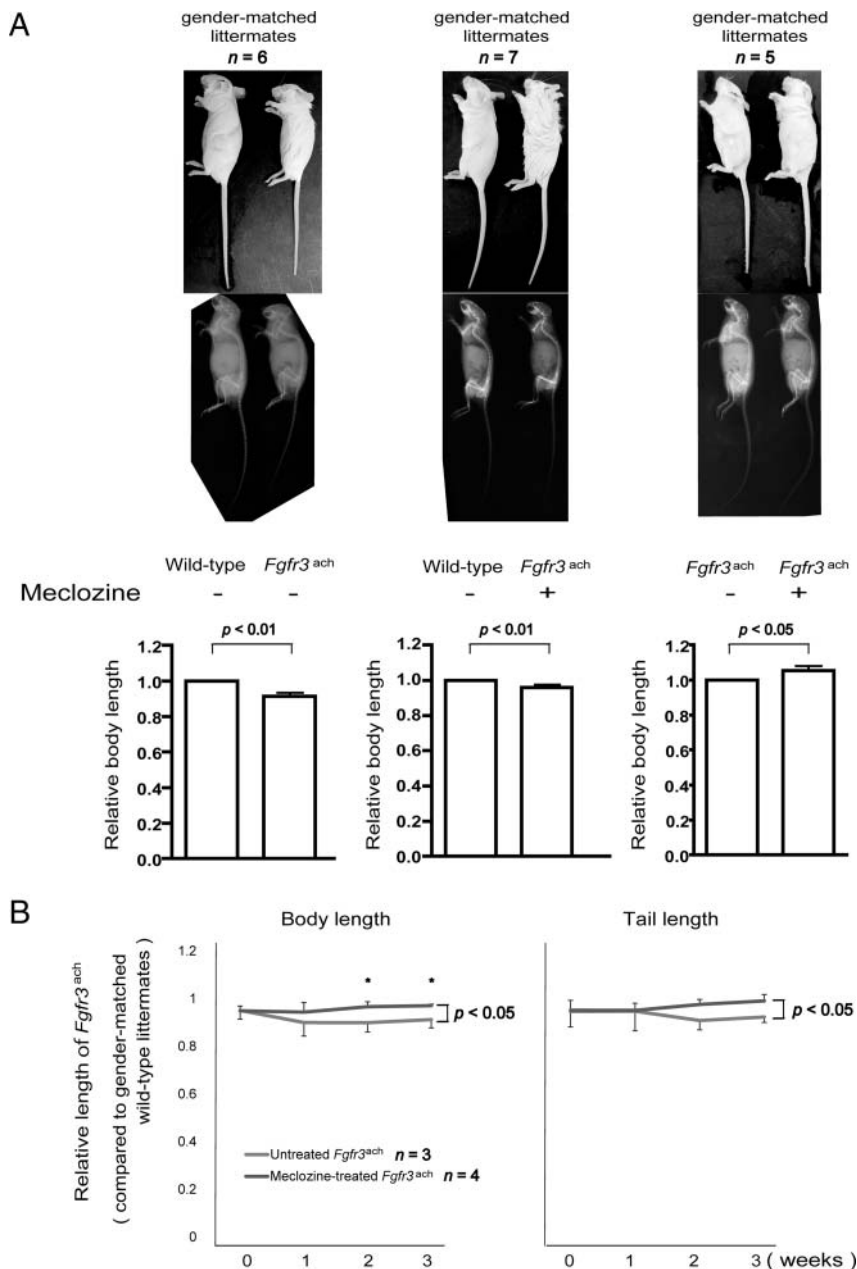


Figure 2. Meclozine reverses the dwarfed phenotype in *Fgfr3^{ach}* mice. A, Meclozine treatment was initiated without prior knowledge of the genotype and administered for 3 weeks. 3 indicated pairs of gender-matched littermates were examined. Body length of the mice was normalized to that of the indicated gender-matched wild-type littermate. Body lengths of *Fgfr3^{ach}* mice without meclozine treatment were 0.913 ± 0.023 of the gender-matched wild-type littermates (left graph). The body lengths of *Fgfr3^{ach}* mice with meclozine treatment were 0.960 ± 0.018 of the gender-matched wild-type littermates (middle graph). Meclozine significantly increased the body length of *Fgfr3^{ach}* mice ($P < .05$ by unpaired *t* test, not shown). In 5 kinships, in which gender-matched *Fgfr3^{ach}* mice were treated with or without meclozine, meclozine increased the body length of *Fgfr3^{ach}* mice to 1.054 ± 0.027 of the untreated *Fgfr3^{ach}* mice (right graph). Left panel, a male pair; middle panel, a female pair and right panel, a male pair. Mean and standard deviation (SD) are indicated in the graphs and the legends. The statistical differences shown on each graph were analyzed by paired *t* test. B, The body and tail lengths of meclozine-treated *Fgfr3^{ach}* mice were significantly longer than those of untreated *Fgfr3^{ach}* mice. The measured lengths of the *Fgfr3^{ach}* mice were normalized to those of the gender-matched wild-type littermates. Statistical significance by two-way ANOVA is shown on the right side of each graph. * $P < .05$ by Fisher's LSD test for each pair.

treated mice than in the untreated-mice (Figure 4E).

The plasma meclozine concentration in the present study is clinically relevant

We next measured the plasma concentrations of meclozine used in the current study (0.2 or 0.4 g of meclozine per kilogram food). Blood samples were collected from 8-week-old wild-type mice after ad libitum intake of meclozine-containing food for 72 hours. The average plasma meclozine concentrations after treatment were within the range used in clinical settings (22) (Figure 5).

Discussion

The small compounds, NF449 (11), A31 (12), and P3 (13), have recently been reported to improve short-stature phenotypes in animal models with accelerated FGFR3 signaling. The safety of these novel compounds in humans, however, remains to be elucidated. Meclozine, an OTC H1 inhibitor, has been safely used for motion sickness for more than 50 years, and its optimal dose and adverse effects have already been established. A previous study indicates that the peak plasma concentration of meclozine is 68.42 ng/ml after a single clinical dose in humans (22). We have demonstrated that oral administration of clinically attainable concentrations of meclozine increased longitudinal bone growth in *Fgfr3^{ach}* mice during the observed growth period. This effect was most likely due to the inhibition of activated FGFR3 signaling, which was previously observed in cultured rat chondrosarcoma cells (18). Currently, distraction osteogenesis is the only available surgical procedures to increase bone length; however, it is a long and invasive treatment that compromises the pa-

tient's quality of life (QOL). The healing index is 36.2 days per cm (23); thus, the patients are forced to attach external fixators for 362 days to increase their height by 10 cm. In contrast, meclozine increased body length of *Fgfr3^{ach}* mice by 5.4% in our study. If the same effect could be observed in patients with ACH, the patients could be expected to increase 6.7 to 7.1 cm in height, based on the average height of adults with ACH. Although further studies are needed to investigate the adverse effects associated with long-term drug administration, meclozine is a potential therapeutic compound for ACH and other FGFR3-related disorders.

To date, CNP, the CNP analog BNM-111, and statins are the only promising compounds that can be applied in clinical practice for FGFR3-related skeletal disorders. Yasoda et al reported that continuous IV administration of CNP rescued the short-limbed phenotype in *Fgfr3^{ach}* mice (15). Lorget et al similarly demonstrated that subcutaneous injection of BNM-111 reversed the dwarfism-related clinical features observed in *Fgfr3^{Y367C/+}* mice (16). Additionally, Yamashita et al identified that intraperitoneal injection of statins, which have been used to lower serum cholesterol levels, rescued the phenotype of *Fgfr3^{ach}* mice using a screen with patient-derived iPS cells (17). Currently, CNP and BNM-111 administration is restricted to injection, which potentially poses physical and psychological burdens on young children. Since meclozine and statins can be administered orally, they are more convenient for children to take. Although the site of action of statins has not been dissected (17), meclozine and statins may have an additive effect on abnormally activated FGFR3 signaling in patients with ACH.

Some ACH patients have neurological complications such as gait disturbance, leg paralysis, hydrocephalus, and

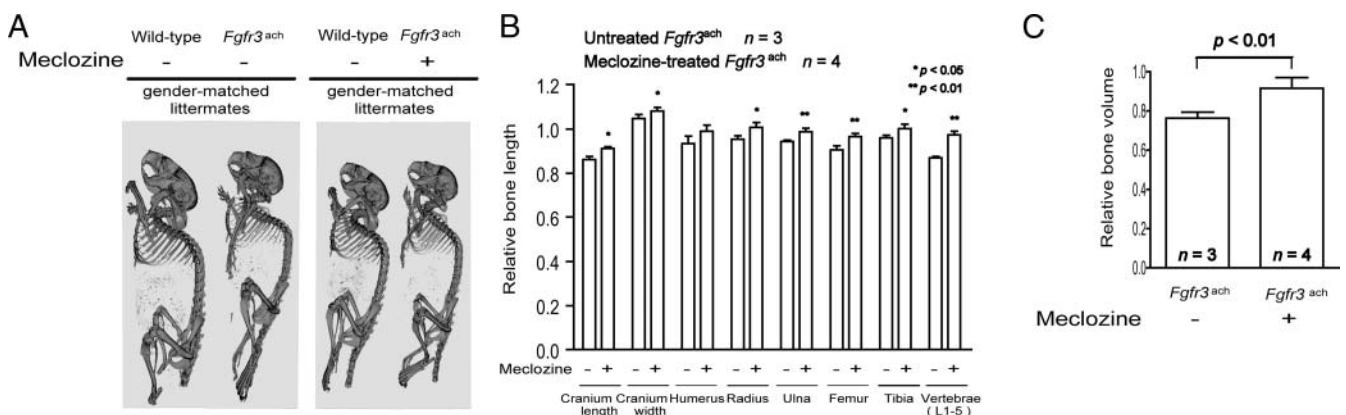


Figure 3. Meclozine increases the longitudinal bone growth of *Fgfr3^{ach}* mice. A, Reconstructed computed tomography (CT) images. Left panel, a male pair; right panel, a female pair. B, Meclozine significantly increased the length of the cranium, radius, ulna, femur, tibia, and vertebrae in *Fgfr3^{ach}* mice. C, The total bone volume of meclozine-treated *Fgfr3^{ach}* mice was significantly increased compared to that of untreated *Fgfr3^{ach}* mice. B and C, Bone lengths and total bone volumes of *Fgfr3^{ach}* mice were normalized to those of the gender-matched wild-type littermates. Statistical significance was analyzed by the unpaired *t* test.

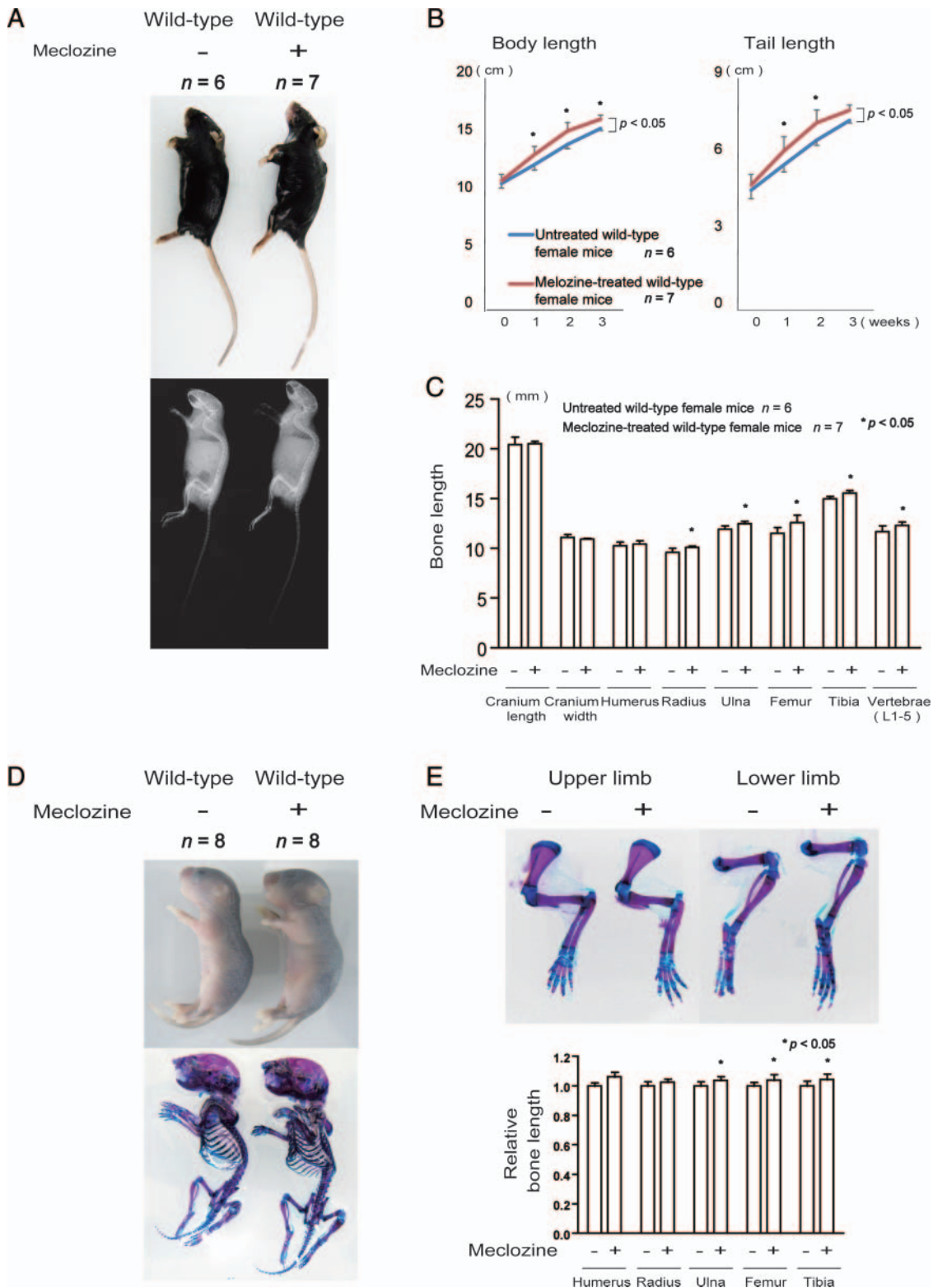


Figure 4. A-C, Wild-type mice were treated with meclozine 2 weeks after birth for 3 weeks. A, Visual images and soft X-ray images of wild-type female mice with or without meclozine. Meclozine-treated mice were larger than the untreated mice. B, Body and tail lengths of meclozine-treated wild-type female mice were significantly longer than those of untreated wild-type female mice. Statistical significance analyzed by two-way ANOVA is shown on the right side of each graph. $*P < .05$ by Fisher's LSD test for each pair. C, The lengths of the radius, ulna, femur, tibia, and vertebrae on the soft X-ray films were significantly increased by meclozine treatment by unpaired *t* test. D and E, Pregnant mice were treated with meclozine from embryonic day 14. D, Visual images and skeletons stained with Alizarin red and Alcian blue of wild-type mice at postnatal day 5, with or without meclozine. Meclozine-treated offspring were larger than untreated offspring. E, The lengths of the ulna, femur, and tibia measured using stained skeletons were significantly increased after meclozine treatment, as assessed by unpaired *t* test.

central hypopnea, in addition to short stature, which is caused by stenosis of the foramen magnum or spinal canal. In the current study, meclozine failed to enhance the growth of the foramen magnum and lumbar spinal canal. Similarly, BMN-111 could not increase the sagittal and lateral diameters of the foramen magnum in *Fgfr3*^{Y367C/+} mice (16). Stenosis of the spinal canal and foramen magnum in patients with ACH is most likely due to premature synchondrosis closure, and any growth-promoting treatment for these stenoses must precede the timing of the synchondrosis closure (24). Jin et al demonstrated that the thanatophoric phenotypes of *Fgfr3*^{K644E/+} mice were rescued by intraperitoneal injection of P3 to the mother (13). Prenatal treatments are generally unrealistic even if the patients get a definite diagnosis of ACH during prenatal periods. Therefore, we tested the effect of meclozine from 3 weeks of age in *Fgfr3*^{ach} mice. In future, we will examine the effect of maternal administration of meclozine using mouse models to treat devastating phenotypes in thanatophoric dysplasia and possibly stenosis of the spinal canal and foramen magnum in ACH.

Acknowledgments

We would like to thank Dr. David M. Ornitz at Washington University for providing *Fgfr3*^{ach} mice. This work was supported by Grants-in-Aid from the Ministry of Education, Culture, Sports, Science, and Technology of Japan, and the Ministry of Health, Labor, and Welfare of Japan.

Address all correspondence and requests for reprints to: Kinji Ohno, MD, PhD, 65 Tsurumai, Showa-ku, Nagoya 466-8550, Japan, Email: ohnok@med.nagoya-u.ac.jp, Phone: +81 52 744 2447, Fax: +81 52 744 2449

Disclosure Summary: The authors have nothing to disclose

This work was supported by **Funding**: This work was supported by Grants-in-Aid from the Ministry of Education, Cul-

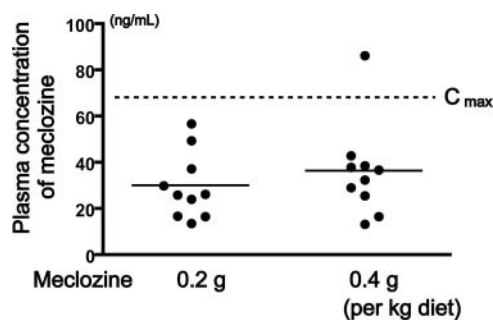


Figure 5. Plasma concentrations of meclozine in 8-week-old wild-type mice fed 0.2 g or 0.4 g meclozine per kilogram diet for 72 hours. The average plasma concentrations were 30.30 ± 14.27 ng/ml and 36.58 ± 20.12 ng/ml for 0.2 g and 0.4 g per kilogram diet, respectively. The mean peak drug concentration (C_{max}) after a single dose of 25 mg of meclozine in human subjects was 68.42 ng/ml (22).

ture, Sports, Science, and Technology of Japan, and the Ministry of Health, Labor and Welfare of Japan.

References

- Rousseau F, Bonaventure J, Legeai-Mallet L, Pelet A, Rozet JM, Maroteaux P, Le Merrer M, Munnich A. Mutations in the gene encoding fibroblast growth factor receptor-3 in achondroplasia. *Nature*. 1994;371:252-254.
- Shiang R, Thompson LM, Zhu YZ, Church DM, Fielder TJ, Bocian M, Winokur ST, Wasmuth JJ. Mutations in the transmembrane domain of FGFR3 cause the most common genetic form of dwarfism, achondroplasia. *Cell*. 1994;78:335-342.
- Prinos P, Costa T, Sommer A, Kilpatrick MW, Tsipouras P. A common FGFR3 gene mutation in hypochondroplasia. *Hum Mol Genet*. 1995;4:2097-2101.
- Tavormina PL, Bellus GA, Webster MK, Bamshad MJ, Fraley AE, McIntosh I, Szabo J, Jiang W, Jabs EW, Wilcox WR, Wasmuth JJ, Donoghue DJ, Thompson LM, Francomano CA. A novel skeletal dysplasia with developmental delay and acanthosis nigricans is caused by a Lys650Met mutation in the fibroblast growth factor receptor 3 gene. *Am J Hum Genet*. 1999;64:722-731.
- Tavormina PL, Shiang R, Thompson LM, Zhu YZ, Wilkin DJ, Lachman RS, Wilcox WR, Rimoin DL, Cohn DH, Wasmuth JJ. Thanatophoric dysplasia (types I and II) caused by distinct mutations in fibroblast growth factor receptor 3. *Nat Genet*. 1995;9:321-328.
- Toydemir RM, Brassington AE, Bayrak-Toydemir P, Krakowiak PA, Jorde LB, Whitby FG, Longo N, Viskochil DH, Carey JC, Bamshad MJ. A novel mutation in FGFR3 causes camptodactyly, tall stature, and hearing loss (CATSHL) syndrome. *Am J Hum Genet*. 2006;79:935-941.
- Waller DK, Correa A, Vo TM, Wang Y, Hobbs C, Langlois PH, Pearson K, Romitti PA, Shaw GM, Hecht JT. The population-based prevalence of achondroplasia and thanatophoric dysplasia in selected regions of the US. *Am J Med Genet A*. 2008;146A:2385-2389.
- Horton WA, Hall JG, Hecht JT. *Achondroplasia*. *Lancet*. 2007;370:162-172.
- Horton WA, Hecht JT, Hood OJ, Marshall RN, Moore WV, Hollowell JG. Growth hormone therapy in achondroplasia. *Am J Med Genet*. 1992;42:667-670.
- Noonan KJ, Leyes M, Forriol F, Canadell J. Distraction osteogenesis of the lower extremity with use of monolateral external fixation. A study of two hundred and sixty-one femora and tibiae. *J Bone Joint Surg Am*. 1998;80:793-806.
- Krejci P, Murakami S, Prochazkova J, Trantirek L, Chlebova K, Ouyang Z, Aklia A, Smutny J, Bryja V, Kozubik A, Wilcox WR. NF449 is a novel inhibitor of fibroblast growth factor receptor 3 (FGFR3) signaling active in chondrocytes and multiple myeloma cells. *J Biol Chem*. 2010;285:20644-20653.
- Jonquoy A, Mugniery E, Benoist-Lasselin C, Kaci N, Le Corre L, Barbault F, Girard AL, Le Merrer Y, Busca P, Schibler L, Munnich A, Legeai-Mallet L. A novel tyrosine kinase inhibitor restores chondrocyte differentiation and promotes bone growth in a gain-of-function *Fgfr3* mouse model. *Hum Mol Genet*. 2012;21:841-851.
- Jin M, Yu Y, Qi H, Xie Y, Su N, Wang X, Tan Q, Luo F, Zhu Y, Wang Q, Du X, Xian CJ, Liu P, Huang H, Shen Y, Deng CX, Chen D, Chen L. A novel FGFR3-binding peptide inhibits FGFR3 signaling and reverses the lethal phenotype of mice mimicking human thanatophoric dysplasia. *Hum Mol Genet*. 2012;21:5443-5455.
- Yasoda A, Komatsu Y, Chusho H, Miyazawa T, Ozasa A, Miura M, Kurihara T, Rogi T, Tanaka S, Suda M, Tamura N, Ogawa Y, Nakao K. Overexpression of CNP in chondrocytes rescues achon-

- droplasia through a MAPK-dependent pathway. *Nat Med*. 2004;10:80–86.
15. Yasoda A, Kitamura H, Fujii T, Kondo E, Murao N, Miura M, Kanamoto N, Komatsu Y, Arai H, Nakao K. Systemic administration of C-type natriuretic peptide as a novel therapeutic strategy for skeletal dysplasias. *Endocrinology*. 2009;150:3138–3144.
 16. Lorget F, Kaci N, Peng J, Benoist-Lasselin C, Mugniery E, Oppeneer T, Wendt DJ, Bell SM, Bullens S, Bunting S, Tsuruda LS, O'Neill CA, Di Rocco F, Munnich A, Legeai-Mallet L. Evaluation of the therapeutic potential of a CNP analog in a Fgfr3 mouse model recapitulating achondroplasia. *Am J Hum Genet*. 2012;91:1108–1114.
 17. Yamashita A, Morioka M, Kishi H, Kimura T, Yahara Y, Okada M, Fujita K, Sawai H, Ikegawa S, Tsumaki N. Statin treatment rescues FGFR3 skeletal dysplasia phenotypes. *Nature*. 2014;513:507–511.
 18. Matsushita M, Kitoh H, Ohkawara B, Mishima K, Kaneko H, Ito M, Masuda A, Ishiguro N, Ohno K. Meclozine facilitates proliferation and differentiation of chondrocytes by attenuating abnormally activated FGFR3 signaling in achondroplasia. *PLoS One*. 2013;8:e81569.
 19. Naski MC, Colvin JS, Coffin JD, Ornitz DM. Repression of hedgehog signaling and BMP4 expression in growth plate cartilage by fibroblast growth factor receptor 3. *Development*. 1998;125:4977–4988.
 20. Mori K, Suenaga Y, Toriwaki J. Fast software-based volume rendering using multimedia instructions on PC platforms and its application to virtual endoscopy. *Proc SPIE*. 2003;5031:111–122.
 21. Wallin J, Wilting J, Koseki H, Fritsch R, Christ B, Balling R. The role of Pax-1 in axial skeleton development. *Development*. 1994;120:1109–1121.
 22. Wang Z, Lee B, Pearce D, Qian S, Wang Y, Zhang Q, Chow MS. Meclozine metabolism and pharmacokinetics: formulation on its absorption. *J Clin Pharmacol*. 2012;52:1343–1349.
 23. Kitoh H, Kitakoji T, Tsuchiya H, Katoh M, Ishiguro N. Distraction osteogenesis of the lower extremity in patients with achondroplasia/hypochondroplasia treated with transplantation of culture-expanded bone marrow cells and platelet-rich plasma. *Journal of pediatric orthopedics*. 2007;27:629–634.
 24. Matsushita T, Wilcox WR, Chan YY, Kawanami A, Bukulmez H, Balmes G, Krejci P, Mekikian PB, Otani K, Yamaura I, Warman ML, Givol D, Murakami S. FGFR3 promotes synchondrosis closure and fusion of ossification centers through the MAPK pathway. *Hum Mol Genet*. 2009;18:227–240.

Nationwide radiation dose survey of computed tomography for fetal skeletal dysplasias

**Osamu Miyazaki, Hideaki Sawai, Jun
Murotsuki, Gen Nishimura & Tetsuya
Horiuchi**

Pediatric Radiology

ISSN 0301-0449

Pediatr Radiol

DOI 10.1007/s00247-014-2916-1



Your article is protected by copyright and all rights are held exclusively by Springer-Verlag Berlin Heidelberg. This e-offprint is for personal use only and shall not be self-archived in electronic repositories. If you wish to self-archive your article, please use the accepted manuscript version for posting on your own website. You may further deposit the accepted manuscript version in any repository, provided it is only made publicly available 12 months after official publication or later and provided acknowledgement is given to the original source of publication and a link is inserted to the published article on Springer's website. The link must be accompanied by the following text: "The final publication is available at link.springer.com".

Nationwide radiation dose survey of computed tomography for fetal skeletal dysplasias

Osamu Miyazaki · Hideaki Sawai · Jun Murotsuki ·
Gen Nishimura · Tetsuya Horiuchi

Received: 13 June 2013 / Revised: 20 November 2013 / Accepted: 30 January 2014
© Springer-Verlag Berlin Heidelberg 2014

Abstract

Background Recently, computed tomography (CT) has been used to diagnose fetal skeletal dysplasia. However, no surveys have been conducted to determine the radiation exposure dose and the diagnostic reference level (DRL).

Objective To collect CT dose index volume (CTDIvol) and dose length product (DLP) data from domestic hospitals implementing fetal skeletal 3-D CT and to establish DRLs for Japan.

Materials and methods Scan data of 125 cases of 20 protocols from 16 hospitals were analyzed. The minimum, first-quartile,

median, third-quartile and maximum values of CTDIvol and DLP were determined. The time-dependent change in radiation dose setting in hospitals with three or more cases with scans was also examined.

Results The minimum, first-quartile, median, third-quartile and maximum CTDIvol values were 2.1, 3.7, 7.7, 11.3 and 23.1 mGy, respectively, and these values for DLP were 69.0, 122.3, 276.8, 382.6 and 1025.6 mGy·cm, respectively. Six of the 12 institutions reduced the dose setting during the implementation period.

Conclusions The DRLs of CTDIvol and DLP for fetal CT were 11.3 mGy and 382.6 mGy·cm, respectively. Institutions implementing fetal CT should use these established DRLs as the standard and make an effort to reduce radiation exposure by voluntarily decreasing the dose.

O. Miyazaki (✉) · T. Horiuchi
Department of Radiology,
National Center for Child Health and Development,
2-10-1 Okura, Setagaya-ku, Tokyo 157-8535, Japan
e-mail: osamu-m@rc4.so-net.ne.jp

H. Sawai
Department of Obstetrics and Gynecology,
Hyogo College of Medicine,
1-1 Mukogawa-cho, Nishinomiya-shi, Hyogo 663-8501, Japan

J. Murotsuki
Department of Maternal and Fetal Medicine,
Miyagi Children's Hospital,
4-3-17 Ochiai, Aoba-ku, Sendai-shi, Miyagi 989-3126, Japan

J. Murotsuki
Department of Advanced Fetal and Developmental Medicine,
Tohoku University Graduate School of Medicine, 1-1 Seiryō-cho,
Sendai-shi, Miyagi 980-8574, Japan

G. Nishimura
Department of Pediatric Imaging,
Tokyo Metropolitan Children's Medical Center,
2-8-29 Musashidai, Fuchu-shi, Tokyo 183-8525, Japan

T. Horiuchi
Department of Medical Physics and Engineering,
Division of Medical Technology and Science,
Course of Health Science, Graduate School of Medicine,
Osaka University, 1-7 Yamadaoka, Suita, Osaka 565-0871, Japan

Keywords Skeletal dysplasia · Prenatal diagnosis · 3-D computed tomography · Diagnostic reference level · Fetus · Fetal computed tomography

Introduction

In recent years, improvements in computed tomography (CT) performance have created various innovative scan techniques and increased the number of indications, such as cardiac CT. One of the new diagnostic methods is to apply CT for the prenatal diagnosis of skeletal dysplasia suspected in a fetus.

According to the latest nosology and classification of genetic skeletal disorders in 2011 [1], 456 skeletal dysplasias have been identified. The overall prevalence of neonatally manifested skeletal dysplasia is approximately 2 out of 10,000, half of them lethal [2]. However, most of these types are so rare that obstetricians never encounter them. These types include various severe diseases, from poor-prognosis diseases causing fetal or postpartum death to favorable-prognosis diseases causing no problems in physiology or intelligence.

Two-dimensional ultrasonography (2-D US) [3] and magnetic resonance imaging (MRI) [4] are conventionally used for evaluating fetal skeletal dysplasia. However, US and MRI have limitations in visualizing the skeletal system compared to radiography, which is better for performing bone surveys. Three-dimensional US [5], which was recently introduced in daily practice, provides higher image quality, but it is highly dependent on the skills of the operator. In particular, when interpreting skeletal findings in patients, the operator must create 3-D images using his/her own judgment based on his/her experience and knowledge of radiological findings. Therefore, prenatal diagnosis of skeletal dysplasia is difficult, and patients, their families and medical practitioners face difficult problems when making decisions regarding antenatal care and delivery.

Recently, fetal CT using a multidetector technique has gained popularity in the prenatal diagnosis of severe skeletal dysplasias [3, 6–11]. A precise diagnosis of skeletal dysplasia requires identification of pathognomonic findings in a constellation of as many abnormal skeletal changes as possible. Pathognomonic findings may be divided into gross changes and important, but subtle, changes. The capability of fetal CT to delineate the fetal skeleton is similar to that of a postnatal full skeletal survey. Fetal US and MRI are only able to detect gross pathognomonic changes, such as shortness, bending and deformity of the long bones, and severe skull deformity [10]. Fetal CT has been found to be highly effective in diagnosing fetal skeletal dysplasia with a diagnostic yield of 90% or higher [7, 10].

The time of 26–30 gestational weeks is recommended for the timing of fetal CT in this scenario because fetal skeletal mineralization is usually sufficient for evaluation by CT at this time [12]. Additionally, the risk of the central nervous system is greatest with exposure at 8–15 weeks of gestation, with no proven risk at greater than 25 weeks of gestation [13].

Despite this benefit, the resulting radiation exposure is disadvantageous. Whether fetal CT can be justified under the ALARA (As Low As Reasonably Achievable) principle of protection against radiation remains controversial [14]. The fetal CT technique should be more strongly justified and optimized than any other X-ray examination on the basis of the linear non-threshold hypothesis that the risk of future carcinogenesis from fetal exposure cannot be completely ruled out [15].

Bach-Segura [16] introduced adequate scan settings for fetal CT and they described an average volume CT dose index (CTDI_{vol}) of 6 mGy at 100 kV and 120 mAs. To date, there is no guideline for fetal CT in Japan and individual hospitals may perform fetal CT according to their own protocol. If radiologists and obstetricians affirm and continue this type of examination, a guideline for fetal CT, including indications and standard protocol, should be established in the near future. In such cases, the concept of diagnostic reference levels (DRLs) is essential.

DRL is a practical tool for promoting the assessment of existing protocols and appropriate development of new and improved protocols at each CT center by facilitating the comparison of doses from present practice. DRLs were first successfully implemented in relation to conventional X-rays in the 1980s and subsequently developed for application to CT in the 1990s [17, 18]. DRLs assist in the optimization of protection by helping to avoid unnecessarily high doses to the patient. The system for using DRLs includes the estimation of patient doses as part of the regular quality assurance program [19].

DRLs are established on the basis of a survey of the standard diagnostic radiation dose that is commonly used. Each hospital can use the established DRL to optimize the diagnostic radiation dose, confirming that the dose is not much different from the DRL. The setting of DRLs and the validation of their compatibility with the clinical dose involve various factors, including the country, region, clinical purpose, guarantee of image quality, optimization of scan settings, scanner design and maintenance. However, each institution should adjust its standard radiation dose if the dose differs from the DRL without a justifiable reason.

DRLs are based on standard phantom or patient measurements under specific conditions at a number of representative clinical facilities. DRLs have been set at approximately the 75th percentile of measured patient or phantom data. This means that procedures performed at 75% of the institutions surveyed have exposure levels at or below the DRL [20]. Twenty-five percent of recorded doses will be above this level. Institutions should receive feedback on their dose levels with respect to the DRLs [21]. Few surveys or studies on fetal CT doses have been conducted [10, 22], and the fetal CT radiation dose distribution throughout Japan is unknown.

The objective of this study was to collect data on CTDI_{vol} and dose-length product (DLP) from domestic hospitals implementing fetal 3-D CT, evaluate their trends and establish DRLs in Japan on the basis of the survey results. The Ministry of Health, Labour and Welfare of Japan (MHLW) H23-Nanchi-Ippan-123 fetal skeletal dysplasia study group takes responsibility for feeding back information to participating institutions regarding local dose levels with respect to DRLs.

Materials and methods

Data collection

We selected hospitals participating in the Japan Forum of Fetal Skeletal Dysplasia (the nation's largest online network intended to support the diagnosis of fetal skeletal dysplasia including mainly obstetricians [53 registrants]) that had already implemented fetal CT. We also selected hospitals that had consulted the Japan Forum of Fetal Skeletal Dysplasia

about fetal CT diagnosis in the past, hospitals that had reported implementation of fetal CT in abstracts issued by Japanese academic societies and scientific meetings, and the members of the MHLW Fetal Skeletal Dysplasia Study Group (grant-in-aid for Scientific Research from the Ministry of Health, Labor and Welfare of Japan H23-Nanchi-Ippan-123). A questionnaire was distributed electronically by e-mail for radiologists or obstetricians.

Thirty-eight hospitals were requested to participate in our study, and 16 of them expressed their intention to do so. These comprised eight university hospitals (Hokkaido University Hospital, Tohoku University Hospital, Yamagata University Hospital, National Defense Medical College Hospital, Hyogo College of Medicine Hospital, Tokushima University Hospital, Hiroshima University Hospital and Kurume University Hospital), five perinatal medical centers or pediatric hospitals (Miyagi Children's Hospital, National Center for Child Health and Development, Nagara Medical Center, Ehime Prefectural Central Hospital, and Perinatal Medical Center for Mother and Child Health, and Yamaguchi Grand Medical Center), and three regional referral hospitals (Aomori Prefectural Central Hospital, Chiba Kaihin Municipal Hospital and Kumamoto City Hospital). All fetuses were suspected of having skeletal dysplasias on the basis of a 2-D US scan or a second- or third-level diagnostic 2-D US performed by experienced fetal medicine physicians. After informed consent, the mothers underwent multidetector CT (mean \pm SD: 30.2 \pm 2.6 weeks of gestation, range: 15–38 weeks, Table 1).

The first half of the distributed questionnaire was associated with epidemiological background, the number of fetal CT scans performed throughout the time span of the study, the timing of gestational week at multidetector CT, experience of a repeat fetal CT scan and control of fetal motion to avoid rescanning. The second half contained detailed questions on the scan conditions, including the specific CT scanner model, tube voltage (kVp), scan field of view, rotation time, number of detector rows, beam width and pitch factor. For Toshiba users, filters and parameters for volume exposure control, such as target standard deviation (SD), slice thickness, reconstruction function, and maximum and minimum tube current (mA), were asked. For GE scanners, parameters for auto mA/smart mA (type of automatic exposure control, noise index, and maximum and minimum mA) were asked. For Siemens scanners, parameters for CARE Dose 4D (quality reference mAs, and minimum and maximum of effective mAs) were asked. For the dose information, CTDIvol and DLP were collected. One hospital (hospital 8 in Table 1) changed its protocols three times during the period. Two hospitals (hospitals 4 and 13 in Table 1) used two different CT scanners, each with its own scan setting. Therefore, these situations were treated as separate protocols in this survey.

The data were entered manually into an Excel spreadsheet (Microsoft Corp., Redmond, WA, USA) by individual CT technologists in each institution, and some data were missing or inadequate in some answers. If the CTDIvol and DLP values were inappropriate, they were calculated as well as

Table 1 Results of the epidemiological background (hospital number and characteristic, number of fetal CT scans performed throughout the time span of the study, timing of gestational week at MDCT, experience of repeat fetal CT scan and fetal motion control to avoid rescanning)

Hospital	Characteristic	Fetal CT cases/years	Gestational week at MDCT (range, mean)	Experience of repeat fetal CT examination	Fetal motion control to avoid rescan
1	University hospital	7/4	25–36, 31	No	No
2	Regional referral hospital	4/3	30–34, 32	No	No
3	Perinatal medical center	4/2	20–34, 29	No	No
4	University hospital	18/6	27–36, 32	No	Mioblock
5	University hospital	5/5	27–35, 31	No	No
6	University hospital	4/5	25–28, 26	No	No
7	Regional referral hospital	2/3	15–33, 24	No	No
8	Perinatal medical center	53/5	15–37, 30	No	No
9	Perinatal medical center	11/3	26–31, 29	1 case	No
10	University hospital	4/3	28–32, 30	No	No
11	University hospital	3/3	28–30, NA	No	No
12	Perinatal medical center	4/3	29–38, 32	No	No
13	University hospital	13/6	20–35, 29	No	No
14	Perinatal medical center	3/4	28–32, 30	No	No
15	University hospital	1/2	34, 34	No	No
16	Regional referral hospital	3/5	32–37, 34	No	No
	Total	139/6	mean \pm SD 30.2 \pm 2.6 weeks		

NA not available

possible using CT Expo software (SASCRA, Buchholz, Germany), a program for dose evaluation in CT. However, six CTDIvol and five DLP values were treated as inappropriate data. Eventually, during a 29-month period, from October 2009 until February 2011, 119 CTDIvol and 120 DLP values from a total of 20 protocols and 125 scan data were available for this audit.

CT dosimetry

The framework for CT dosimetry has already been well established [23]. The monitoring of CT performance as part of routine quality assurance is based on the practical dose qualities of CTDIvol and DLP. These form the basis for the reference dose (and DRLs) set for the purpose of promoting the optimization of patient protection [23]. CTDIvol (units: mGy) is the mean absorbed radiation dose to the patient at a given point of scan volume expressed as a function of kVp, mAs, filtering, collimation and pitch. DLP (units: mGy cm) is an indicator of the mean absorbed dose to the patient of each series in a CT exam and is defined as the product of CTDIvol \times exposed scan length [24]. To establish the DRLs, the minimum, first-quartile (25th percentile), median (50th percentile), third-quartile (75th percentile) and maximum values of CTDIvol and DLP for fetal CT were determined on the basis of all of the scan data [25]. In keeping within the established framework, the national DRLs presented in this survey were determined using the 75th percentile values of CTDIvol and DLP [15]. The median value was compared among all of the protocols ($n=20$) to clarify its tendency. We evaluated the interval change of CTDIvol in the hospitals presenting with three or more cases during the same period, regardless of whether dose reduction was introduced. This study was approved by the institutional review board at the National Center for Child Health and Development, Tokyo, Japan.

Results

Table 1 shows the results of epidemiological background. A total of 139 cases of fetal CT were performed throughout 6 years (range: 1–53 cases). The timing of gestational week at the CT scan ranged from 15 to 38 weeks (mean \pm SD: 30.2 \pm 2.6 weeks). Only one hospital (no. 9) experienced a repeat fetal CT examination, and only hospital 4 had answered yes to use of Mioblock (MSD, Tokyo, Japan) for fetal motion control to avoid rescanning.

Table 2 shows details of 20 CT scan protocols, in which technical conditions included the specific CT scanner model, tube voltage (kVp), scan field of view, rotation time, beam width, detector configuration and pitch factor. The tube voltage was set at 100 kV in all of the cases in one hospital

(hospital 8), at 100 or 120 kV in hospitals 9 and 13, and at 120 kV in all of the cases in the remaining 13 hospitals.

The range of rotation time was 0.37–0.75 s, and 75% (15/20 protocols) were carried out by 0.5 s. The beam width ranged from 10 to 40 mm (mean: 20 mm) and helical pitch ranged from 0.64 to 1.67 (mean: 1.1). For Toshiba CT scanners, variation in filters, target standard deviation, slice thickness, reconstruction function, and maximum and minimum tube current (mA) are summarized. For GE CT scanners, protocol 8c was obtained with iterative reconstruction (ASIR: Adaptive Statistical Iterative Reconstruction). The setting of automatic exposure control, quality reference mAs, and minimum and maximum effective mAs are summarized. For Siemens scanners, parameters for CARE Dose 4D are summarized. Throughout the 20 protocols, iterative reconstruction was only performed in protocol 8c, while the other 19 were carried out without it.

Table 3 shows the data of CTDIvol (median), sample number of CTDIvol, DLP (median), sample number of DLP, scan length (average) mm and interval change of CTDIvol in all of the 20 protocols. Protocol number 8c, which was only performed with iterative reconstruction, showed the lowest median CTDIvol (2.6 mGy). However, there was no other obvious relationship between technical data (number of detectors, reconstruction function and availability of 100 kV) and dose levels. Additionally, data from each scan did not correspond to patients' individual body weight or correct gestational week. Therefore, it was unknown which hospitals used higher doses of radiation to image mothers later in pregnancy. The relationship between maternal girth and weight (and by implication, gestational age), which affected CT parameters used for the examinations, was also unknown.

The scan length greatly varied between institutions (327 \pm 47.7 cm, range: 245–440 cm, Table 3). No institution used bismuth shielding for fetal CT examinations.

Table 4 shows the minimum, first-quartile, median, third-quartile and maximum values of CTDIvol and DLP. The minimum, first-quartile, median, third-quartile and maximum values of CTDIvol were 2.1, 3.7, 7.7, 11.3 and 23.1 mGy, and the corresponding values of DLP were 69.0, 122.3, 276.8, 382.6 and 1025.6 mGy-cm, respectively. The domestic DRLs of CTDIvol and DLP for fetal CT were 11.3 mGy and 382.6 mGy-cm, respectively. The minimum, first-quartile, median, third-quartile and maximum values of scan length were 190, 295, 319, 356 and 476 mm, respectively. In Figs. 1 and 2, all 20 CTDIvol and DLP medians per protocol are plotted in ascending order, respectively. The maximum values of CTDIvol and DLP were approximately 11 and 15 times as high as their minimums, respectively. In the five protocols with a CTDIvol median of 5 mGy or less, the gap between the third- and first-quartiles tended to be smaller, and the radiation dose was similar among the cases. In contrast, the institutions with high CTDIvol medians tended to show variation in their

Table 2 Details of 20 CT protocols (technical conditions of the scan, including the hospital and protocol, specific CT scanner model, tube voltage [kVp], scan FOV, rotation time, beam width, detector configuration, pitch factor, filter, target SD, slice thickness, reconstruction function, maximum and minimum tube current [mA], ASIR, AEC, quality reference mAs, and minimum and maximum effective mAs)

Hospital / protocol	Toshiba CT scanner model	kVp	Scan FOV	Rotation time	Beam width (mm)	Detector configuration (no. of sections × mm)	Pitch factor	Filter	Parameters for volume EC		Reconstruction function	Minimum mAs	Maximum mAs	
									Target SD	Slice thickness (mm)				
1	Aquilion 64	120	L	0.5, 0.75	32	64×0.5	0.64–0.83	None	12	5	FC13	100	350	
6	Aquilion 64	120	L	0.5	32	32×1, 64×0.5	0.7–1.4	2D-Q01	10	5, 7	FC13	10	400	
7	Aquilion 16	120	M	0.5	16	16×1	0.94	QDS+	9, 25	5	FC10	10	400	
11	Aquilion 16	120	M	0.5	16	16×1	0.94	None	7.5	7	FC13	10	400	
14	Aquilion 64	120	M, L	0.5	32	32×1, 64×0.5	0.84	QDS+	8, 15	5, 10	FC13, 15	10	450	
GE Healthcare														
CT scanner model		kVp	Scan FOV	Rotation time	Beam width (mm)	Detector configuration (no. of sections × mm)	Helical pitch	Plus recon	ASIR	Slice thickness (mm)	Parameters for auto mA AEC	Noise index	Minimum mAs	Maximum mAs
2	LightSpeed Ultra 16	120	L	0.6	10	16×0.625	1.37	Yes	None	5	smart mA	8.5	100	423
8 A	LightSpeed Ultra	100	L	0.5–0.7	20	8×2.5	1.67	Yes	None	5	auto mA	8.15	100	420
8 B	LightSpeed Ultra	100	L	0.5	20	8×2.5	1.67	Yes	None	5	auto mA	21	100	175
8 C	Discovery 750HD	100	L	0.4	40	64×0.625	1.37	Yes	50%	5	smart mA	21	10	175
13 A	LightSpeed VCT	100, 120	M	0.4	40	64×0.625	1.37	Yes	None	5	smart mA	7.9–15	100	770
13 B	LightSpeed Ultra 16	120	L	0.6–0.7	10, 20	16×0.625, 16×1.25	1.37	Yes	None	5	smart mA	8–8.5	100	440
Siemens														
CT scanner model		kVp	Rotation time	Beam width (mm)	Helical pitch	Detector configuration (no. of sections × mm)	Slice thickness (mm)	Parameters for CARE Quality Ref. mAs	Dose 4D Minimum effective mAs	Maximum effective mAs				
3	SOMATOM Sensation 16	120	0.5	12	1.25	16×0.75	5.7	NA	36	47				
4 A	SOMATOM Sensation Cardiac	120	0.37	12	1	16×0.75	10	35, 70	NA	NA				
4 B	SOMATOM Definition	120	0.5	19.2	1	64×0.3	10	50–80	NA	NA				
5	SOMATOM Sensation 64	120	0.5	19.2	1.2	64×0.3	5	150	96	261				
9	SOMATOM Definition AS	100, 120	0.5	19.2	0.6	64×0.3	5	230–350	108	271				
10	SOMATOM Sensation 16	120	0.5	12, 24	0.85	16×0.75, 16×1.5	5, 8	220–280	204	500				
12	SOMATOM Sensation 16	120	0.5	12	1.15	16×0.75	5	150	56	181				

Table 2 (continued)

16	SOMATOM Sensation 16 Philips CT scanner model	kV	120	Scan FOV	L	0.5	12	Rotation time	0.5	80	Beam width (mm)	0.9, 1.05	16×0.75	Detector configuration (no. of sections × mm)	128×0.625	0.8	Helical pitch	5	150	Slice thickness (mm)	5	Noise index	NA	68	122	AEC	none	Minimum mA	NA	Maximum mA	402
15	Brilliance iCT	kV	120	Scan FOV	L	0.5	0.5	Rotation time	0.5	80	Beam width (mm)	0.9, 1.05	16×0.75	Detector configuration (no. of sections × mm)	128×0.625	0.8	Helical pitch	5	150	Slice thickness (mm)	5	Noise index	NA	68	122	AEC	none	Minimum mA	NA	Maximum mA	402

FOV field of view, SD standard deviation, AEC automatic exposure control, ASIR Adaptive Statistical Iterative Reconstruction, NA not available

Table 3 Median CTDIvol, CTDIvol sample, median DLP, DLP sample, length and interval change of CTDIvol for 20 protocols

Hospital / protocol	CTDI vol (median) mGy	CTDIvol sample	DLP (median) mGy.cm	DLP sample	Length (ave) mm	Interval change of CTDI vol mGy
1	12.7	7	359.8	7	357	Flat (med)
2	13.3	4	583.9	4	401	Decreased
3	3.4	5	112.2	5	272	Flat (low)
4A	2.8	3	80	5	364	Flat (low)
4B	2.9	4	89.5	4	310	
5	9.3	4	339.5	4	328.5	Increased
6	6.7	1	210	1	266	NA
7	13.6	2	280	2	245	NA
8A	7.7	33	277	33	314	Decreased
8B	3.3	11	107.8	11	314	
8C	2.6	9	101.3	9	328.3	
9	10.8	8	353	7	362	Decreased
10	11.8	4	454.5	4	318	Decreased
11	23.1	3	784	3	300	Flat (high)
12	10.1	3	403	3	440	Flat (med)
13A	10	10	372.2	10	309.5	Decreased
13B	17.7	3	887.2	3	390	
14	10.6	1	323	1	320	NA
15	13.3	1	493.6	1	280	NA
16	8.1	3	270	3	333	Flat (med)

CTDI CT dose index, DLP dose length product, NA not available, med medium

scanning conditions, and the gap between the third- and first quartiles tended to be greater.

Hospitals presenting with low CTDIvol values did not necessarily provide low DLP values because the length settings were different among these hospitals.

Figure 3 shows the interval changes in CTDIvol in the 12 hospitals where fetal CT was performed in three or more cases (hospitals 1–5, 8–13 and 16). Six of these 12 hospitals (hospitals 2, 5, 8, 9, 10 and 13) reduced the radiation dose during the implementation period, probably based on their own judgment. Of the remaining six hospitals, two (hospitals 3 and 4),

Table 4 Summary of the minimum, 25th, 50th, 75th and maximum CTDIvol and DLP values

	CTDI vol (mGy)	DLP (mGy.cm)
Minimum	2.1	69
25th	3.7	122.3
50th	7.7	276.8
75th	11.3	382.6
Maximum	23.1	1025.6

CTDI CT dose index, DLP dose length product

Fig. 1 Comparison of box plots of individual CTDIvol in each of the 20 protocols

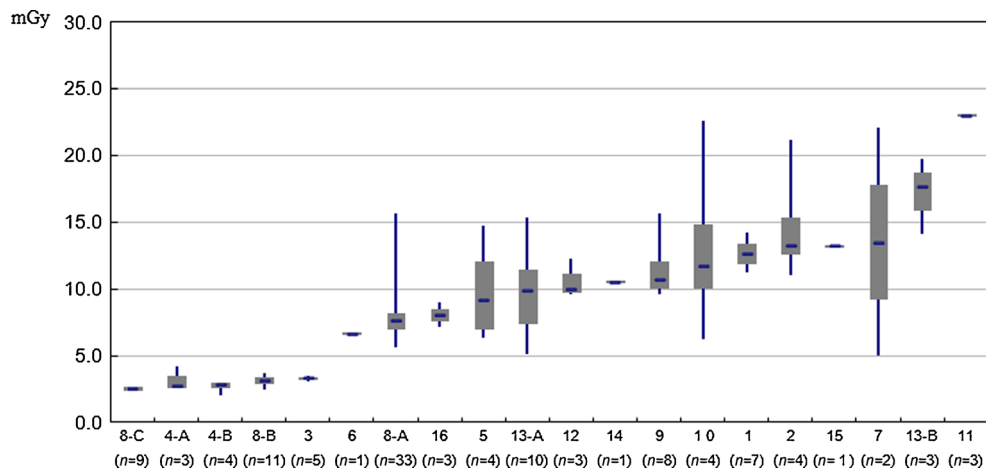
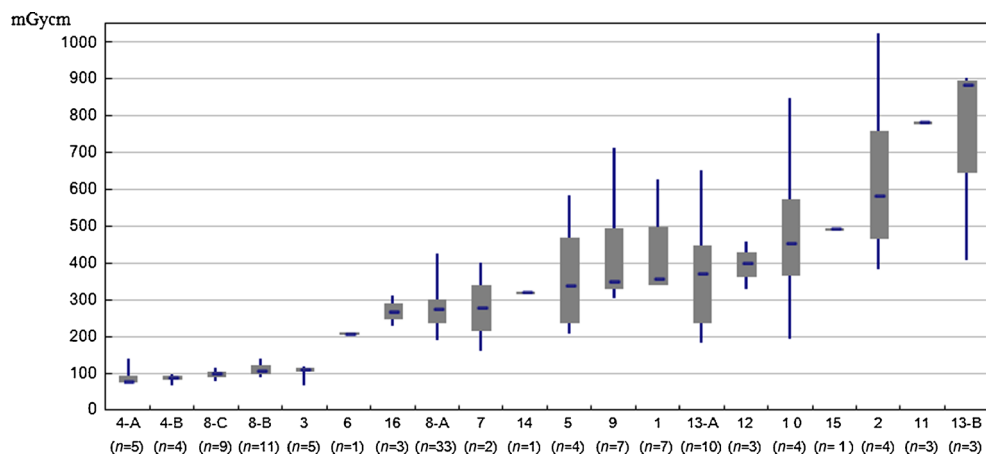


Fig. 2 Comparison of box plots of individual DLP in each of the 20 protocols



three (hospitals 1, 13 and 16), and one (hospital 11) kept the radiation dose low, moderate and high, respectively.

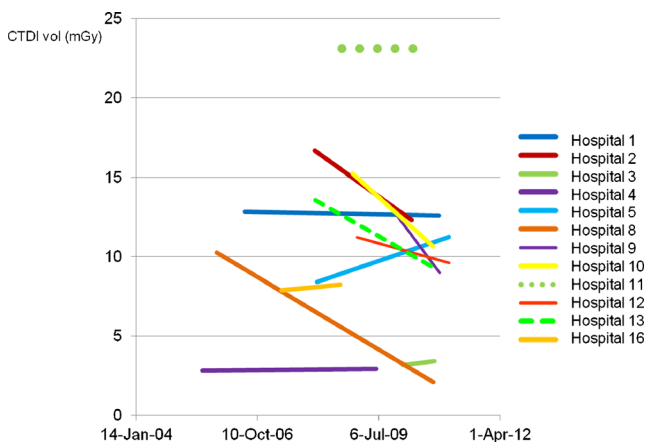


Fig. 3 Interval changes in CTDIvol in the 12 hospitals where fetal CT was performed in three or more cases (hospitals 1-5, 8-13 and 16)

Discussion

CT for fetal skeletal dysplasia was first reported by Shoda et al. [26] in 1997. Since then, the usefulness of this technique has been reported in case reports [27–29], a report comparing it with fetal US [3] and a review [7]. Most of these reports presented cases of monostotic, rare skeletal dysplasia or discussed diagnostic capabilities of bone morphology [6]. The weighted CT dose index of the fetal exposure dose was reported as 3.12 mGy by Cassart et al. [6], 3 mGy by Ruano et al. [3] and 1.9 mGy by Bonnefoy et al. [30]. Recently, the effective dose for low-dose fetal CT was estimated with an ImPACT CT Patient Dosimetry Calculator (CT Scanner Evaluation Center, London, UK) and reported to be 4.8 mSv by

Victoria et al. [22]. However, in their report, neither the CTDIvol nor DLP value during the scan was mentioned.

In the present study, the CTDIvol median was as low as 2.6–3.4 mGy in five protocols of three hospitals (hospitals 3, 4 and 8), and these data are similar to those in the reports mentioned above [3, 6, 30]. In these hospitals, the maximum and minimum values were stable and, therefore, radiation dose control was probably appropriately performed (Figs. 1 and 2). These values are similar to the first-quartile values calculated in this study (3.7 mGy). In these three hospitals, many images were taken at lower dose settings. At this time, a favorable, reasonable dose setting for fetal CT protocol was 3.7 mGy, which corresponds to the first-quartile value obtained in this study.

In our study, the national DRL of CTDIvol for Japanese fetal CT was estimated at 11.3 mGy. Seven hospitals (hospitals 1, 2, 7, 10, 11, 13 and 15) presented with a CTDIvol exceeding this DRL value. Of these hospitals, three (hospitals 2, 10 and 13) had a tendency to reduce the radiation dose over time. Based on our results, our study group advised these seven hospitals to reduce the radiation dose to the DRL or lower.

Concerning a time-dependent change in the exposure dose, six of the 12 hospitals reduced the dose setting during the implementation period. In particular, hospital 8 reduced the dose voluntarily by revising the protocol twice during the surveyed period. Presumably, this hospital had set a higher radiation dose at first because the setting condition was not clear. However, this hospital may have voluntarily attempted to reduce the dose while maintaining image quality. Their efforts should be appreciated in terms of the ALARA principle. Two of the other six hospitals kept the radiation dose at a moderate or high level, and they should change their protocol according to the DRL results.

Our CTDIvol and DLP values were derived from the dose radiated by the equipment and are not equivalent to the fetal exposure dose. The fetal exposure dose cannot be directly measured and must be estimated. If each hospital uses a human pelvis phantom, the fetal exposure dose can be estimated individually. A previously reported technique to estimate the fetal exposure dose was also useful [31]. The easiest method to assess the fetal exposure dose may be to simply use the uterine organ dose calculated with the commercially available Monte Carlo simulation software [22].

In our study, the fetal exposure dose was not estimated for each case. However, this dose should be much lower than the threshold of occurrence of central nervous system anomalies, which is specified in the International Commission on Radiological Protection Publication 87 (100 mGy, first trimester) [32]. In addition, it is difficult to appropriately estimate carcinogenesis due to low-dose exposure in the fetus. Hurwitz et al. [33] estimated the fetal exposure dose in pregnant women subjected to appendicitis or chest CT. They found that the fetal exposure dose was 30 mGy in pregnant women subjected to an appendicitis CT protocol, and the risk of childhood

carcinogenesis from this fetal exposure dose was approximately twice as high as that for natural childhood carcinogenesis (The excess relative risk of developing childhood cancer 2:600) [33]. While the DRL of CTDIvol was estimated as approximately 11 mGy in this study, this value must be converted to the fetal exposure dose. If the fetal exposure dose is approximated at 1.3 times that of CTDIvol [34], the risk of childhood carcinogenesis from this fetal exposure dose may be less than that for the appendicitis CT protocol described above.

Recently, the risk of leukemia and brain tumors from childhood CT exposure has been reported [35], but the risk of future carcinogenesis from fetal CT exposure remains unknown. When state-of-the-art technology, such as iterative reconstruction, is widely used in CT equipment in the near future, the exposure dose for CT scans can be decreased to 1 mSv or less [36]. However, before this is achieved, each hospital should use CT doses as low as possible on the principle of ALARA.

Based on our study results, we should reduce the exposure dose voluntarily and control the exposure dose throughout Japan. Moreover, we should implement a similar study after 3 or 4 years to confirm that the radiation dose has decreased after the establishment of DRLs by the committee of the Japan Society of Obstetrics and Gynecology. Depending on the results of the next study, it may be necessary to review the DRLs and reset them at lower values.

Conclusion

The national DRLs of CTDIvol and DLP for fetal CT in Japan were estimated as 11.3 mGy and 382.6 mGy·cm, respectively. Based on these results, the exposure dose should be voluntarily reduced and the exposure dose should be controlled to continue promoting fetal CT that involves radiation exposure.

Acknowledgments This article was supported by a grant-in-aid for Scientific Research from the Ministry of Health, Labour and Welfare of Japan, H23-Nanchi-Ippan-123.

We very much appreciate the cooperation of the following subgroup members of the above research project: Dr. Yoshihisa Shimanuki, radiologist, and Mr. Kiyooki Sasaki, chief radiological technologist, Miyagi Children's Hospital; Mr. Hiroshi Nagamatsu and Ms. Ayano Shimada, radiological technologists, National Center for Child Health and Development; and Dr. Chihiro Tani, radiologist, and Mr. Masao Kiguchi, radiological technologist, Hiroshima University. Moreover, we very much appreciate the cooperation of all obstetricians, radiologists, and radiological technologists in all 16 hospitals.

Conflict of interest None

References

1. Warman ML, Cormier-Daire V, Hall C et al (2011) Nosology and classification of genetic skeletal disorders: 2010 revision. *Am J Med Genet A* 155:943–948

2. Schumacher R, Seaver LH, Spranger J (2004) Introduction. In: Schumacher R, Seaver LH, Spranger J (eds) *Fetal radiology, a diagnostic atlas*, 1st edn. Springer, Berlin, pp 1–2
3. Ruano R, Molho M, Roume J et al (2004) Prenatal diagnosis of fetal skeletal dysplasias by combining two-dimensional and three-dimensional ultrasound and intrauterine three-dimensional helical computer tomography. *Ultrasound Obstet Gynecol* 24:134–140
4. Suzumura H, Kohno T, Nishimura G et al (2002) Prenatal diagnosis of hypochondrogenesis using fetal MRI: a case report. *Pediatr Radiol* 35:373–375
5. Garjian KV, Pretorius DH, Budorick NE et al (2000) Fetal skeletal dysplasia: three-dimensional US-initial experience. *Radiology* 21: 717–723
6. Cassart M, Massez A, Cos T et al (2007) Contribution of three dimensional computed tomography in the assessment of fetal skeletal dysplasia. *Ultrasound Obstet Gynecol* 29:537–543
7. Cassart M (2010) Suspected fetal skeletal malformations or bone diseases: how to explore. *Pediatr Radiol* 40:1046–1051
8. Boulet S, Althuser M, Nuges F et al (2009) Prenatal diagnosis of achondroplasia: new specific signs. *Prenat Diagn* 29:697–702
9. Victoria T, Epelman M, Coleman BG et al (2013) Low-dose fetal CT in the prenatal evaluation of skeletal dysplasia and other severe skeletal abnormalities. *AJR Am J Roentgenol* 200:989–1000
10. Miyazaki O, Nishimura G, Sago H et al (2012) Prenatal diagnosis of fetal skeletal dysplasia with 3D CT. *Pediatr Radiol* 42:842–852
11. Macé G, Sonigo P, Cormier-Daire V et al (2013) Three-dimensional helical computed tomography in prenatal diagnosis of fetal skeletal dysplasia. *Ultrasound Obstet Gynecol* 42:161–168
12. Guillerman RP (2011) Newer CT applications and their alternatives: what is appropriate in children? *Pediatr Radiol* 41:s534–s548
13. The American College of Obstetrics and Gynecologists (2004) Guidelines for diagnostic imaging pregnancy. ACOG committee opinion No. 299. 104:647–651
14. Slovis TL, Hall ET, Huda W et al (2002) ALARA conference executive summary. *Pediatr Radiol* 32:221
15. Frush DP (2011) Justification and optimization of CT in children: how are we performing? *Pediatr Radiol* 41:s467–s471
16. Bach-Segura P (2006) Etude du squelette fœtal en scanner multibarrette: optimisation du protocole, traitement de l'image. *J Radiol* 87:1358
17. IAEA Radiation Protection of Patients (RPOP). Diagnostic reference levels (DRLs) in CT. https://rpop.iaea.org/RPOP/RPoP/Content/InformationFor/HealthProfessionals/1_Radiology/ComputedTomography/diagnostic-reference-levels.htm
18. Institute of Physics and Engineering in Medicine (IPEM) (2004) Guidance on the establishment and use of diagnostic reference levels for medical X-ray examinations. IPEM report 88.
19. European Commissions. Radiation protection 109. Guidance on diagnostic reference levels (DRLs) for medical exposure. http://ec.europa.eu/energy/nuclear/radiation_protection/doc/publication/109_en.pdf#search='European+Commission+%28EC%29.+Radiation+protection+109.+Guidance+on+diagnostic+reference+levels+%28DRLs%29+for+medical+exposures'
20. ACR–AAPM practice guideline for diagnostic reference levels and achievable dose in medical X-ray imaging. Revised 2013 (Resolution 47). <http://www.acr.org/~media/796DE35AA407447DB81CEB5612B4553D.pdf#search='ACR+PRACTICE+GUIDELINE+FOR+DIAGNOSTIC+REFERENCE+LEVELS+IN+MEDICAL+XRAY+IMAGING%2C+Revised+2008++Resolution+3'>
21. Thomas KE (2011) CT utilization—trends and developments beyond the United States' borders. *Pediatr Radiol* 41:s562–s566
22. Victoria T, Epelman M, Bebbington M et al (2012) Low-dose fetal CT for evaluation of severe congenital skeletal anomalies; preliminary experience. *Pediatr Radiol* 42:s142–s149
23. Shrimpton PC, Hillier MA, Lewis MA et al (2006) National survey of doses from CT in the UK: 2003. *Br J Radiol* 79:968–980
24. Kritsaneepaiboon S, Trinavarat P, Visrutarathna P (2012) Survey of pediatric MDCT radiation dose from university hospitals in Thailand: a preliminary for national dose survey. *Acta Radiol* 52:820–826
25. Watson DJ, Coakley KS (2010) Paediatric CT reference doses based on weight and CT dosimetry phantom size: local experience using a 64-slice CT scanner. *Pediatr Radiol* 40:693–703
26. Shoda S, Hamada H, Oki A et al (1997) Diagnosis of fetal anomalies by three-dimensional imaging using helical computed tomography. *Prenat Diagn* 17:670–674
27. Miyazaki O, Nishimura G, Sago H et al (2007) Prenatal diagnosis of chondrodysplasia punctata tibia-metacarpal type using multidetector CT and three-dimensional reconstruction. *Pediatr Radiol* 37:1151–1154
28. Tsutsumi S, Sawai H, Nishimura G et al (2008) Prenatal diagnosis of thanatophoric dysplasia by 3-D helical computed tomography and genetic analysis. *Fetal Diagn Ther* 24:420–424
29. Yamada T, Nishimura G, Nishida K et al (2011) Prenatal diagnosis of short-rib polydactyly syndrome type 3 (Verma-Naumoff type) by three-dimensional computed tomography. *J Obstet Gynaecol Res* 37:151–155
30. Bonnefoy O, Delbosc JM, Maugey-Laulom B et al (2006) Prenatal diagnosis of hypochondroplasia: three-dimensional multislice computed tomography findings and molecular analysis. *Fetal Diagn Ther* 21:18–21
31. Felmlee JP, Gray JE, Leetzow ML et al (1990) Estimated fetal radiation dose from multislice CT studies. *AJR Am J Roentgenol* 154:185–190
32. ICRP (2000) *Annals of the ICRP publication 84*, 30(1). Elsevier Science Ltd, London
33. Hurwitz LM, Yoshizumi T, Reiman RE et al (2005) Radiation dose to the fetus from body MDCT during early gestation. *AJR Am J Roentgenol* 186:871–876
34. Miyazaki O, Horiuchi T, Akahane M et al (2009) Radiation doses of three-dimensional MDCT for skeletal dysplasia: is the procedure warranted? *Pediatr Radiol* 39:S288–S327
35. Pearce MS, Salotti JA, Little MP et al (2012) Radiation exposure from CT scans in childhood and subsequent risk of leukemia and brain tumors: a retrospective cohort study. *Lancet* 380:499–505
36. <http://www.gehealthcare.com/dose/how-we-can-help/computed-tomography.html>. Accessed 19 Jan 2013

DISEASE MODELS

Statins give bone growth a boost

The development of stem-cell-based models of two diseases that cause dwarfism reveals that statins — drugs that are used to treat high levels of blood cholesterol — may also promote cartilage formation and bone growth.

BJORN R. OLSEN

Many medical conditions can cause short stature, but a faulty gene encoding the protein FGFR3 is responsible for two-thirds of all forms of dwarfism in humans. FGFR3 normally controls a brake signal in the molecular machinery that regulates the growth of limb bones during childhood and adolescence. In 1 in every 10,000–30,000 births, genetic mutations cause FGFR3 to become overactive and so brake too hard. Although our understanding of the cellular processes that go awry in dwarfism is good, development of treatments has been hampered by a lack of efficient methods for screening and testing potential drugs. In a paper published on *Nature's* website today, Yamashita *et al.*¹ report a major step forward in solving this problem, establishing a human-disease-based system for screening potential drugs to treat skeletal-growth defects.

In humans, the most common FGFR3 mutation results in achondroplasia, a disorder that causes short extremities, increased curvature of the spine and distortion of skull growth, resulting in substantial health problems². More-severe mutations in FGFR3 can

cause thanatophoric dysplasia, in which a small chest, and respiratory problems, may cause death either at or shortly after birth³. In both dysplasias, skeletal defects are caused by decreased proliferation and impaired maturation of cartilage-forming cells called chondrocytes within growing regions of bone⁴. It has not previously been possible to obtain chondrocytes from patients, but Yamashita and colleagues took advantage of improved cell-reprogramming techniques⁵ to do just that.

The authors isolated skin cells from three individuals with thanatophoric dysplasia and converted the cells to induced pluripotent stem cells, which can give rise to any cell type in the body. Next, Yamashita and co-workers stimulated the stem cells to become chondrocytes, which had the same genetic make-up as the original patients. They then took advantage of the chondrocytes' ability to aggregate into cartilage-forming particles⁶ to generate a system for analysing particles formed by thanatophoric dysplasia chondrocytes and by controls without the FGFR3 mutation. The authors compared the particles' similarities and differences as the different cells grew and matured over several weeks in culture (Fig. 1).

A major difference was that, compared to

controls, thanatophoric dysplasia particles exhibited impaired maturation associated with degradation of cartilage. Remarkably, reducing FGFR3 levels or adding antibodies to block FGFR3 activity in dysplasia cultures restored growth and maturation of the cartilage-forming particles to normal levels. Yamashita and co-workers used their culture system to assay several molecules that affect either the response of cells to FGFR3 signals or the formation of chondrocytes from stem cells, to determine which could promote cartilage development in dysplastic cells. Molecules that had positive effects included C-type natriuretic peptide (CNP) and several statins, including lovastatin and rosuvastatin.

CNP has a positive effect on bone formation and growth⁴, and its overexpression in chondrocytes counteracts dwarfism in a mouse model of achondroplasia⁷. As a result, CNP has been pursued as a potential achondroplasia treatment, although it is not an ideal candidate. A major obstacle is that the peptide, which must be injected, is degraded within minutes of being administered. A more stable version is effective in mouse models of achondroplasia and is currently in clinical trials, but still requires daily injections⁸. In addition, the effects of CNP on the cardiovascular system and the central nervous system raise the possibility of undesirable side effects if the drug is used long-term in children.

Statins — cholesterol-lowering drugs that are available in tablet form — provide an interesting alternative. Their safety has been evaluated in children with inherited high cholesterol⁹, and evidence¹⁰ suggests that early statin treatment improves the chances of children with this condition reaching the age of 30 without having a heart attack. In addition to their cholesterol-related properties, the drugs stimulate production of chondrocyte

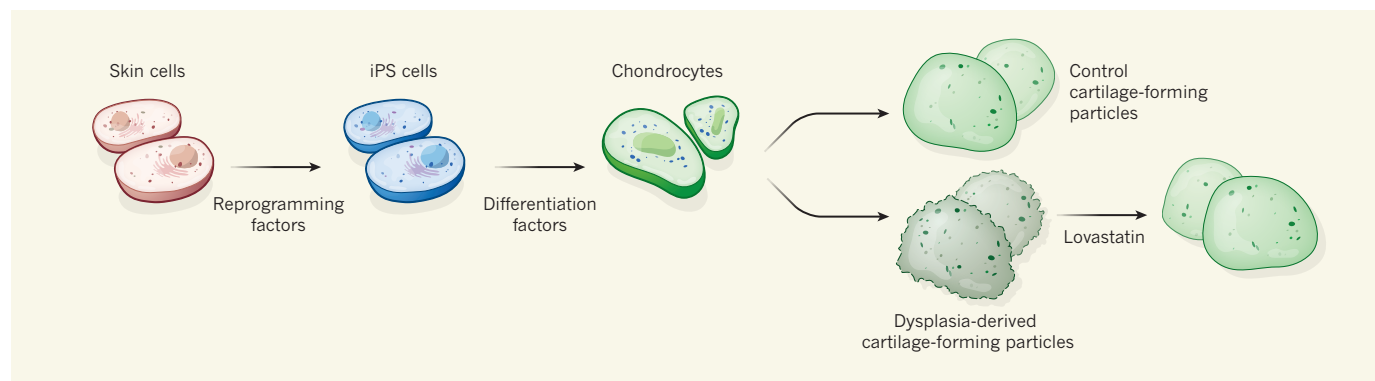


Figure 1 | A cell-based model of impaired bone growth. Yamashita *et al.*¹ isolated skin cells from people with thanatophoric dysplasia and from people with normal bone growth, and reprogrammed them to become induced pluripotent stem cells (iPS cells), which can give rise to every cell type of the body. They then added factors that caused the cells to differentiate into

cartilage-forming cells called chondrocytes. Chondrocytes derived from controls produced normal cartilage-forming particles, but the particles formed from dysplasia-derived chondrocytes showed impaired growth and maturation. However, normal particle formation was restored when the drug lovastatin was added to the culture dish, highlighting a possible treatment for this disease.

molecules that make up the structure of cartilage¹¹, and repress production of cartilage-degrading enzymes¹². In a series of compelling experiments, Yamashita *et al.* demonstrated that lovastatin stimulates production of cartilage components in thanatophoric dysplasia chondrocytes, and promotes the formation of chondrocytes from stem cells. It also restores cartilage formation by chondrocytes derived from people with achondroplasia. Finally, the authors showed that injecting rosuvastatin into mice with an achondroplasia-causing defect in FGFR3 partially restored bone growth in the limbs and head.

What are the mechanisms underlying these striking effects? Yamashita and colleagues' study does not provide the full answer. However, the authors do find that high levels of FGFR3 protein, but not messenger RNA, are reduced to normal levels when lovastatin is added to cultures of particles derived from people with either form of dysplasia. This suggests that statins stimulate degradation of FGFR3. Cellular protein-degradation machines called proteasomes might be involved, because adding a proteasome inhibitor to lovastatin-containing cultures increased levels of FGFR3. The researchers speculate that this is related to the ability of statins to lower cholesterol in cells, and to destabilize cell membranes so

that FGFR3 (which spans the membrane) is more easily internalized and degraded, but this remains to be determined.

If the ability of statins to restore cartilage-particle growth is found to be independent of their cholesterol-lowering properties, it may be possible to modify the drugs such that these two effects are separated. However, if the cartilage-promoting effect of statins is a direct consequence of a decrease in cholesterol, extreme care is needed before using the drugs to treat children with achondroplasia. It will be crucial to ensure that cholesterol levels in these children are maintained at reasonable levels.

Between the ages of 25 and 35, mortality related to heart disease is more than 10 times higher in people with achondroplasia than in the general population^{13,14}. The reasons for this are not understood, and limited data suggest that serum cholesterol levels in children with achondroplasia are in the high normal range¹⁵. Whether statin treatment would help to reduce this mortality is therefore unclear.

In summary, Yamashita *et al.* have established a disease model of achondroplasia and related dysplasias based on pluripotent stem cells. The results of the study raise the possibility that statins might be effective in treating children with these disorders. Furthermore, the authors' system allows screening of

additional compounds in the search for even safer drugs. ■

Bjorn R. Olsen is in the Department of Cell Biology, Harvard Medical School, Boston, Massachusetts 02115, USA.
e-mail: bjorn_olsen@hms.harvard.edu

1. Yamashita, A. *et al.* *Nature* <http://dx.doi.org/10.1038/nature13775> (2014).
2. Shiang, R. *et al.* *Cell* **78**, 335–342 (1994).
3. Tavormina, P. L. *et al.* *Am. J. Hum. Genet.* **64**, 722–731 (1999).
4. Laederich, M. B. & Horton, W. A. *Curr. Opin. Pediatr.* **22**, 516–523 (2010).
5. Okita, K. *et al.* *Nature Methods* **8**, 409–412 (2011).
6. Koyama, N. *et al.* *Stem Cells Dev.* **22**, 102–113 (2013).
7. Yasoda, A. *et al.* *Nature Med.* **10**, 80–86 (2004).
8. Lorget, F. *et al.* *Am. J. Hum. Genet.* **91**, 1108–1114 (2012).
9. Eiland, L. S. & Luttrell, P. K. *J. Pediatr. Pharmacol. Ther.* **15**, 160–172 (2010).
10. Braamskamp, M. J. *et al.* *Circulation* **128**, A17837 (2013).
11. Hatano, H., Maruo, A., Bolander, M. E. & Sarkar, G. *J. Orthop. Sci.* **8**, 842–848 (2003).
12. Simopoulou, T., Malizos, K. N., Poultsides, L. & Tsezou, A. *J. Orthop. Res.* **28**, 110–115 (2010).
13. Hunter, A. G., Hecht, J. T. & Scott, C. I. *Jr Am. J. Med. Genet.* **62**, 255–261 (1996).
14. Wynn, J., King, T. M., Gambello, M. J., Waller, D. K. & Hecht, J. T. *Am. J. Med. Genet. A* **143A**, 2502–2511 (2007).
15. Collipp, P. J., Sharma, R. K., Thomas, J., Maddaiah, V. T. & Chen, S. Y. *Am. J. Dis. Child.* **124**, 682–685 (1972).

Statin treatment rescues FGFR3 skeletal dysplasia phenotypes

Akihiro Yamashita¹, Miho Morioka¹, Hiromi Kishi¹, Takeshi Kimura^{1,2}, Yasuhito Yahara¹, Minoru Okada¹, Kaori Fujita¹, Hideaki Sawai³, Shiro Ikegawa⁴ & Noriyuki Tsumaki^{1,5}

Gain-of-function mutations in the fibroblast growth factor receptor 3 gene (*FGFR3*) result in skeletal dysplasias, such as thanatophoric dysplasia and achondroplasia (ACH). The lack of disease models using human cells has hampered the identification of a clinically effective treatment for these diseases. Here we show that statin treatment can rescue patient-specific induced pluripotent stem cell (iPSC) models and a mouse model of *FGFR3* skeletal dysplasia. We converted fibroblasts from thanatophoric dysplasia type I (TD1) and ACH patients into iPSCs. The chondrogenic differentiation of TD1 iPSCs and ACH iPSCs resulted in the formation of degraded cartilage. We found that statins could correct the degraded cartilage in both chondrogenically differentiated TD1 and ACH iPSCs. Treatment of ACH model mice with statin led to a significant recovery of bone growth. These results suggest that statins could represent a medical treatment for infants and children with TD1 and ACH.

Achondroplasia (ACH) is the most common skeletal dysplasia, and the condition leads to disproportionate short-limb dwarfism. Mutations in the gene encoding fibroblast growth factor receptor 3 (*FGFR3*) were identified in patients with ACH (refs 1, 2). *FGFR3* mutations were subsequently found in patients with thanatophoric dysplasia, of which there are two types that can be distinguished by the radiographic findings and the results of a molecular analysis: thanatophoric dysplasia type I (TD1) and II (TD2). The phenotype of thanatophoric dysplasia is more severe than that of ACH, and the condition is lethal due to respiratory insufficiency, which is secondary to an abnormal chest wall skeleton. Owing to recent progress in respiratory management, infants with thanatophoric dysplasia can survive for several months to years. *FGFR3* mutations have also been found in some other conditions, which are collectively called *FGFR3* chondrodysplasias³. Mice that are deficient for *FGFR3* show skeletal overgrowth⁴. This mouse phenotype suggests that *FGFR3* is a negative regulator of endochondral bone formation, confirming that the mutations causing *FGFR3* chondrodysplasias are gain-of-function mutations.

FGFR3 functions as a transmembrane receptor tyrosine kinase. Therapeutic strategies aimed at decreasing excessive *FGFR3* signals have been investigated⁵. The application of c-type natriuretic peptide (CNP)⁶, a CNP analogue⁷, parathyroid hormone⁸, a *FGFR3*-binding peptide⁹ and soluble *FGFR3* (ref. 10) led to a recovery of bone growth in a genetically manipulated mouse model of *FGFR3* chondrodysplasia. CNP attenuates the mitogen-activated protein kinase (MAPK) signals which are activated by *FGFR3*. The efficacy of all of these treatments remains to be tested in appropriate human cell models, which have not been available for *FGFR3* chondrodysplasia. In addition, the safety of these treatments needs to be confirmed through additional pre-clinical and clinical tests before wide clinical use can be advocated. The mechanism(s) by which *FGFR3* mutations cause cartilage abnormalities have been investigated by transducing cells with mutant *FGFR3* *in vitro*, and generating a genetically engineered mouse model *in vivo*⁵. The former approach provides information on the impact of *FGFR3* mutations on the receptors, such as receptor stabilization and turnover¹¹. The latter approach has revealed

the impact of *FGFR3* mutations on the growing skeleton and indicated that the endochondral bone formation process is disturbed¹². In addition to these two approaches, recent progress in cell reprogramming technologies is beginning to offer a new disease model: induced pluripotent stem cells (iPSCs). The iPSCs are generated from dermal fibroblasts or blood cells from patients, followed by differentiation into cell types of interest, such as chondrocytes in the case of *FGFR3* chondrodysplasias. This process may provide human cell types and tissues that can allow investigation of the mechanism(s) underlying the onset and progression of disease, and drug screening.

Generation of TD1-specific iPSCs

Human dermal fibroblasts (HDFs) were obtained from three TD1 patients (TD1-714, TD1-10749 and TD1-315H) (Extended Data Fig. 1a). A sequencing analysis of the genomic DNA extracted from the patients' HDFs revealed a heterozygous mutation (R248C) in the *FGFR3* gene in all three TD1 patients (Extended Data Fig. 1a). We established more than three iPSC lines for each TD1 patient and analysed one TD1 iPSC line (TD1-714-3, TD1-10749-1 and TD1-315H-2) derived from the HDFs of each patient. Wild-type iPSC lines (409B2 (ref. 13), KF4009-1 and HDF-11) derived from three control individuals were prepared. We confirmed that all iPSC lines expressed SSEA4 and TRA1-60, and formed teratomas containing all three germ layers (Extended Data Fig. 1a–c).

Abnormal cartilage formation from TD1 iPSCs

We differentiated TD1 and wild-type iPSCs towards chondrocytes. The iPSCs were differentiated into chondrogenic cells in the presence of chondrogenic supplementation on dishes for 14 days, and then were transferred into suspension culture to form cartilaginous particles following the previously described method¹⁴, with modifications. The wild-type iPSCs formed particles composed of cells scattered in a cartilaginous extracellular matrix, as indicated by positive Safranin O staining on day 42. TD1 iPSCs formed particles that did not appear to be stained with Safranin O, indicating that the extracellular matrix contained little glycosaminoglycan (Fig. 1a and Extended Data Fig. 2). The presence of glycosaminoglycan

¹Cell Induction and Regulation Field, Department of Cell Growth and Differentiation, Center for iPS Cell Research and Application, Kyoto University, Kyoto 606-8507, Japan. ²Department of Pediatrics, Osaka University Graduate School of Medicine, Osaka 565-0871, Japan. ³Department of Obstetrics and Gynecology, Hyogo College of Medicine, Hyogo 663-8501, Japan. ⁴Laboratory of Bone and Joint Diseases, Center for Integrated Medical Sciences, RIKEN, Tokyo 108-8639, Japan. ⁵Japan Science and Technology Agency, CREST, Tokyo 102-0075, Japan.

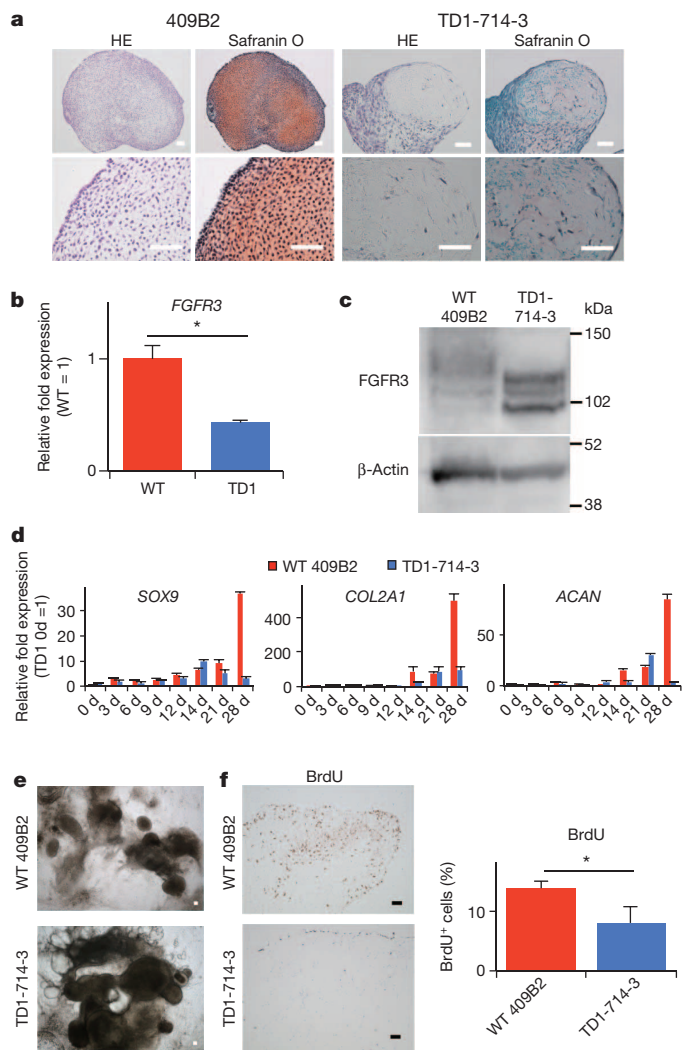


Figure 1 | Chondrogenic differentiation of wild-type iPSCs and TD1 iPSCs. **a**, Histology of iPSC-derived cartilaginous particles on day 42. The images are representative of three independent experiments. HE, haematoxylin and eosin staining. **b**, Results of a real-time RT-PCR expression analysis of *FGFR3* mRNA in chondrogenically differentiated iPSC lines on day 28 ($n = 3$ independent iPSC lines). WT, wild type. **c**, Results of an immunoblot analysis of the *FGFR3* protein in chondrogenically differentiated iPSCs on day 28. The images are representative of three independent experiments. **d**, Time course of the changes in the expression of markers in iPSCs subjected to chondrogenic differentiation, as determined by real-time RT-PCR ($n = 3$ technical replicates). **e**, Phase microscopic images of chondrogenically differentiated iPSCs in adhesion culture on day 14. The images are representative of three independent experiments. **f**, iPSC-derived cartilaginous particles on day 28 were treated with BrdU. Left: histological sections were immunostained with anti-BrdU antibodies. Right: the number of BrdU-positive cells were divided by the total number of cells ($n = 3$ particles). The data are representative of two independent experiments. The error bars denote the means \pm s.d. * $P < 0.05$ by the t -test. Scale bars, 50 μ m.

is important for the mechanical properties of cartilage. Messenger RNA expression analysis showed that there were decreased expression levels of chondrocyte markers and increased expression levels of type I collagen genes in chondrogenically differentiated TD1 iPSCs on day 28 (Extended Data Fig. 3a). Immunohistochemical analysis showed that the TD1-iPSC-derived particles expressed more type I collagen and less type II collagen than the wild-type-iPSC-derived particles on day 42 (Extended Data Fig. 3b, c). Focal deposition of type II collagen in the TD1-iPSC-derived particles (Extended Data Fig. 3c, lower panels) suggests that there was limited cartilage formation or remnant cartilage which

was formed in earlier stages that was subsequently degraded. Markers of pluripotency (SSEA4 and TRA1-60) were not detected in either the chondrogenically differentiated wild-type or TD1 iPSCs on day 42 (Extended Data Fig. 3d). The expression level of *FGFR3* mRNA in chondrogenically differentiated TD1 iPSCs was significantly lower than in chondrogenically differentiated wild-type iPSCs (Fig. 1b), probably because of the negative feedback transcriptional regulation due to the gain-of-function mutation of *FGFR3* in the TD1 cells. Immunoblot analysis showed that the amount of *FGFR3* protein in the chondrogenically differentiated TD1 iPSCs was higher than in the chondrogenically differentiated wild-type iPSCs (Fig. 1c), supporting the notion that the mutant *FGFR3* receptor is resistant to degradation, leading to persistent activation of the receptor's signal transduction^{11,15–17}.

To examine how the chondrogenic differentiation of TD1 iPSCs resulted in the formation of abnormal particles, we analysed the time course of the changes in expression of markers in wild-type iPSCs and TD1 iPSCs subjected to chondrogenic differentiation (Fig. 1d and Extended Data Fig. 4a). Expression of *OCT4* (also called *POU5F1*), a marker of pluripotency, decreased rapidly on day 3, and expression of mesodermal/mesodermal markers *T* and *KDR* was transiently increased around days 3–9 in both chondrogenically differentiated wild-type and TD1 iPSCs. Expression of chondrogenic transcription factors *SOX9*, *SOX5* and *SOX6* was activated and increased gradually in both chondrogenically differentiated wild-type and TD1 iPSCs until day 14. Expression levels of *SOX9*, *SOX5* and *SOX6* continued to increase in the chondrogenically differentiated wild-type iPSCs, whereas they decreased gradually after day 14 in the chondrogenically differentiated TD1 iPSCs.

The expression of these chondrogenic transcription factors was followed by expression of their target genes encoding cartilage matrix proteins. Expression of type II collagen gene (*COL2A1*) and aggrecan gene (*ACAN*) was activated on day 14, and increased gradually in both chondrogenically differentiated wild-type and TD1 iPSCs until day 21. The expression levels of *COL2A1* and *ACAN* continued to increase until day 28 in chondrogenically differentiated wild-type iPSCs, whereas they were not changed or were decreased on day 28 in chondrogenically differentiated TD1 iPSCs. These findings suggest that both wild-type iPSCs and TD1 iPSCs were similarly differentiated into chondrocytes until days 14–21. This interpretation was supported by phase microscopic observation, which revealed that the wild-type iPSC and TD1 iPSC cultures similarly produced cell nodules by day 14 (Fig. 1e), because the formation of cell nodules is a typical characteristic of cultured chondrocytes.

Reduced expression of cartilage matrix genes (*COL2A1* and *ACAN*) on day 28, however, indicated that chondrocyte maturation was disturbed in the chondrogenically differentiated TD1 iPSCs after their differentiation into chondrocytes. Previous studies have revealed that chondrocyte proliferation is disturbed in ACH model mice¹² and in chondrocytic cells transduced with *FGFR3* carrying thanatophoric dysplasia and ACH mutations¹⁸, and that chondrocyte apoptosis is increased in thanatophoric dysplasia patients and in chondrogenic cells transduced with *FGFR3* carrying thanatophoric dysplasia and ACH mutations^{16,19,20}. Labelling cells with 5-bromodeoxyuridine (BrdU) revealed that the proliferation rate of the chondrogenically differentiated TD1 iPSCs was decreased compared with that of the chondrogenically differentiated wild-type iPSCs on day 28 (Fig. 1f). The chondrogenically differentiated TD1 iPSCs showed increased numbers of TUNEL-positive cells (Extended Data Fig. 4b, c) and increased immunoreactivity for cleaved-caspase 3 (Extended Data Fig. 4d), suggesting that they had increased apoptosis compared with chondrogenically differentiated wild-type iPSCs. Chondrogenically differentiated TD1 iPSCs showed increased expression levels of p21 (Extended Data Fig. 4e). Together these results suggest that the chondrogenically differentiated TD1 iPSC model recapitulates the two primary abnormalities which are found in *FGFR3*-related disease patients and models: decreased proliferation and increased apoptosis of chondrocytes. These two abnormalities might be responsible for the degraded cartilage tissue found in TD1-iPSC-derived particles on day 42.

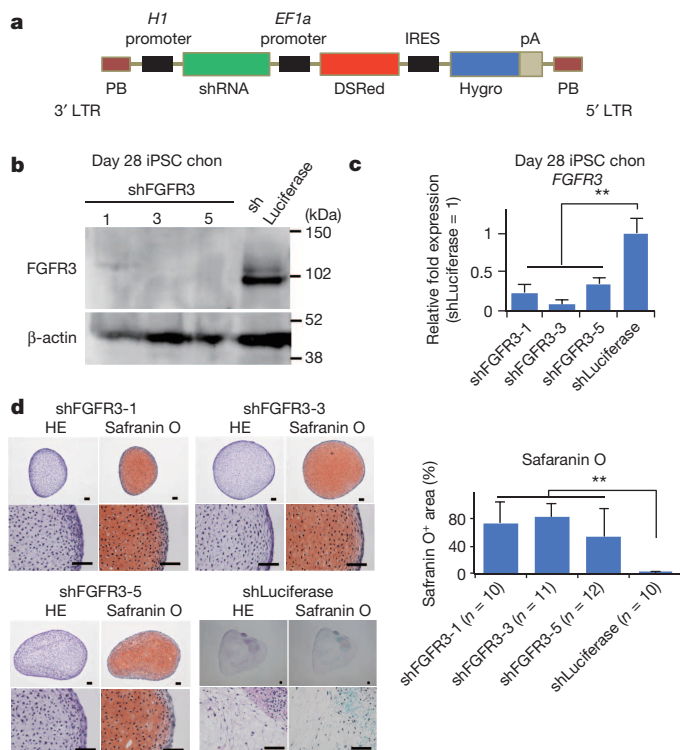


Figure 2 | Results of an analysis of *FGFR3* knockdown in TD1 iPSCs (TD1-714-3) subjected to chondrogenic differentiation. The data were collected from three independent clones respectively bearing three different *FGFR3* shRNAs. **a**, The *FGFR3* shRNA piggyBac (PB) vector. **b**, Results of an immunoblot analysis of *FGFR3* on day 28. iPS chon, chondrogenically differentiated iPSCs. **c**, The results of a real-time RT-PCR expression analysis of *FGFR3* on day 28 ($n = 3$ technical replicates). **d**, Histological analysis on day 42. Scale bars, 50 μm . The right panel shows the area of the Safranin-O-positive region in the particles. The number of particles examined is indicated at the bottom. Error bars denote the means \pm s.d. $**P < 0.01$ by the Tukey-Kramer post-hoc test.

FGFR3 inactivation rescues TD1 iPSC cartilage

To confirm that TD1 iPSCs cannot produce cartilaginous particles due to the gain-of-function mutation of *FGFR3*, we knocked down *FGFR3* in TD1 iPSCs (TD1-714-3) using piggyBac short hairpin RNA (shRNA) vectors (Fig. 2a). Expression of *FGFR3* mRNA and protein was effectively knocked down in the chondrogenically differentiated TD1 iPSCs bearing each of three types of *FGFR3* shRNA (Fig. 2b, c). The TD1 iPSCs transfected with *FGFR3* shRNA formed cartilaginous particles that were positively stained by Safranin O (Fig. 2d). Expression analysis showed that chondrogenically differentiated TD1 iPSCs transduced with *FGFR3* shRNA had increased expression of chondrocyte marker genes and decreased expression of fibroblast marker genes compared with chondrogenically differentiated TD1 iPSCs bearing control shRNA targeting the luciferase gene sequence (Extended Data Fig. 5a).

Furthermore, treatment of chondrogenically differentiated TD1 iPSCs with *FGFR3* neutralizing antibody resulted in partial recovery of cartilage formation (Extended Data Fig. 5b). Expression analysis showed that addition of the *FGFR3* neutralizing antibody increased the expression of chondrocyte marker genes and decreased the expression of fibroblast marker genes in the chondrogenically differentiated TD1 iPSCs (Extended Data Fig. 5c).

These results suggest that the formation of degraded cartilage by TD1 iPSCs is caused by the gain-of-function mutation of *FGFR3*.

Statins rescue TD1-iPSC-derived cartilage

To find effective drugs to treat *FGFR3* chondrodysplasias, we screened molecules for their ability to rescue chondrogenically differentiated TD1 iPSCs from the degraded cartilage phenotype. We selected molecules that had previously been reported to affect *FGFR3* signalling and/or chondrocyte differentiation. Chondrogenically differentiated TD1 iPSCs were rescued by the addition of CNP but not by the addition of an *FGFR3* inhibitor or the G-protein antagonist NF449 (Extended Data Fig. 6).

We included statins in the candidate molecules because they have been reported to have anabolic effects on chondrocytes^{21–23}. The statins compose a drug class broadly characterized as lipid-lowering agents. Statins inhibit mevalonic acid synthesis, and as a consequence lead to a decrease in the amount of total cholesterol and decreased levels of low-density lipoproteins. Statins have favourable effects on cardiovascular disease, the nervous system, the immune system, the skeletal system and tumour growth^{24–27}, and there is emerging interest in the pleiotropic

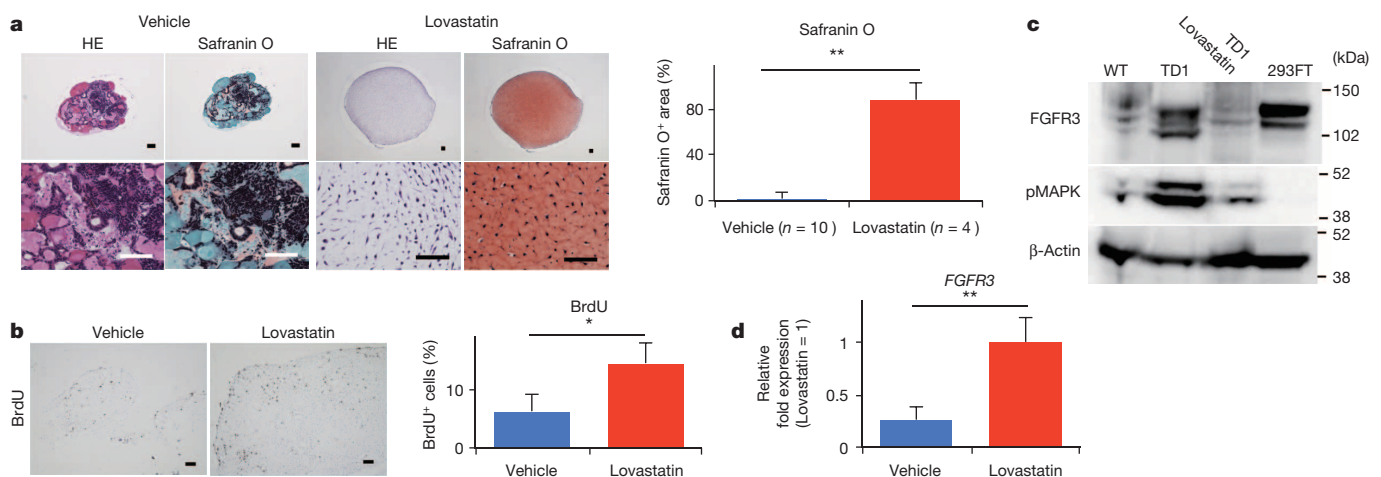


Figure 3 | TD1 (TD1-714-3) iPSCs were chondrogenically differentiated to produce particles in the presence or absence of lovastatin (1 μM). **a**, Left: histology of the particles on day 42. Right: area of the Safranin-O-positive region in the particles. The number of particles examined is indicated at the bottom. The data are representative of three independent experiments. **b**, Particles on day 28 were treated with BrdU. Left: histological sections were immunostained with anti-BrdU antibodies. Right: number of BrdU-positive cells were divided by the total number of cells ($n = 3$ particles). The data are

representative of two independent experiments. **c**, Results of an immunoblot analysis of *FGFR3* and phosphorylated MAPK on day 28. WT, wild-type (409B2)-iPSC-derived particles. 293FT, 293FT cells. The images are representative of three independent experiments. **d**, Results of a real-time RT-PCR expression analysis of *FGFR3* on day 28 ($n = 3$ technical replicates). The data are representative of two independent experiments. Error bars denote the means \pm s.d. $*P < 0.5$; $**P < 0.01$ by the t -test. Scale bars, 50 μm .

effects of statins. We found that the addition of lovastatin recovered the cartilage formation of chondrogenically differentiated TD1 iPSCs (Fig. 3a). An expression analysis showed that the addition of lovastatin increased the expression of a chondrogenic transcription factor (SOX9) and cartilage extracellular components (*COL2A1* and *ACAN*) in chondrogenically differentiated TD1 iPSCs (Extended Data Fig. 7a). Labelling TD1-iPSC-derived particles cultured in the presence or absence of lovastatin with BrdU revealed that the addition of lovastatin increased the proliferation rates of chondrogenically differentiated TD1 iPSCs in the particles (Fig. 3b). Furthermore, we confirmed that addition of mevastatin, atorvastatin, pravastatin, rosuvastatin and fluvastatin also recovered the cartilage formation of chondrogenically differentiated TD1 iPSCs (Extended Data Fig. 7b). These results suggest that various statins can rescue chondrogenically differentiated TD1 iPSCs.

To gain insight into the mechanism(s) by which statins rescue the FGFR3 chondrodysplasia models, we examined the expression levels of FGFR3 protein and mRNA. Immunoblot analysis revealed that application of lovastatin rescued chondrogenically differentiated TD1 iPSCs from the increased amount of FGFR3 protein (Fig. 3c). Accordingly, application of lovastatin rescued chondrogenically differentiated TD1 iPSCs from an increased amount of phosphorylated MAPK, a downstream target of FGFR3 signalling. The changes in the amount of FGFR3 protein were not regulated at the mRNA expression level, because the *FGFR3* mRNA expression levels were increased by lovastatin application in chondrogenically differentiated TD1 iPSCs (Fig. 3d), suggesting that statin treatment may accelerate the degradation of FGFR3 protein in chondrogenically differentiated TD1 iPSCs.

Statin exposure rescues ACH iPSC cartilage

We next investigated whether lovastatin could rescue another FGFR3 chondrodysplasia: ACH. We generated iPSCs from HDFs obtained from two individuals with ACH and one individual who was homozygous for an ACH mutation (ACHhomo). The chondrogenic differentiation of ACH iPSCs and ACHhomo iPSCs resulted in the formation of particles that lacked the cartilaginous element, as indicated by negative Safranin O staining. Addition of lovastatin to the culture media recovered the cartilage formation of chondrogenically differentiated ACH iPSCs and ACHhomo iPSCs (Extended Data Fig. 8).

Statins cause bone elongation in ACH mice

We examined whether statin treatment could rescue *Fgfr3^{Ach}* transgenic mice from the FGFR3 chondrodysplasia phenotype *in vivo*. The *Fgfr3^{Ach}* transgenic mice¹² express *Fgfr3* with an ACH mutation in chondrocytes under the control of the *Col2a1* promoter/enhancer sequences. *Fgfr3^{Ach}* transgenic mice show dwarfism, short limb bones and a short snout. Daily intraperitoneal injections of rosuvastatin significantly increased the anteroposterior lengths of the skulls and the lengths of the ulnas, femurs and tibiae in the *Fgfr3^{Ach}* mice when they were 15 days old (Fig. 4 and Extended Data Fig. 9). There were no significant differences in the lengths of the ulnas and tibiae between *Fgfr3^{Ach}* mice receiving rosuvastatin and wild-type mice receiving vehicle.

The lengths of primordial cartilage in *Fgfr3^{Ach}* mice increased more in organ culture in the presence of lovastatin than in the absence of lovastatin (Extended Data Fig. 10a), indicating that lovastatin acts on the cartilage directly to induce its elongation. Labelling the primordial cartilage with BrdU revealed that lovastatin increased the proliferation rate of chondrocytes in the *Fgfr3^{Ach}* primordial cartilage (Extended Data Fig. 10b).

The pellets of *Fgfr3^{Ach}* primary chondrocytes cultured in the presence of lovastatin showed more intense Safranin O staining than did the pellets of *Fgfr3^{Ach}* primary chondrocytes in the absence of lovastatin (Extended Data Fig. 10c). *Fgfr3^{Ach}* pellets cultured in the presence of lovastatin showed increased expression levels of *Sox9*, *Col2a1* and *Acan* at 2 weeks after the start of pellet culture, as well as increased expression levels of *Runx2* and *Col10a1* at 4 weeks after the start of pellet culture, compared with those cultured in the absence of lovastatin (Extended

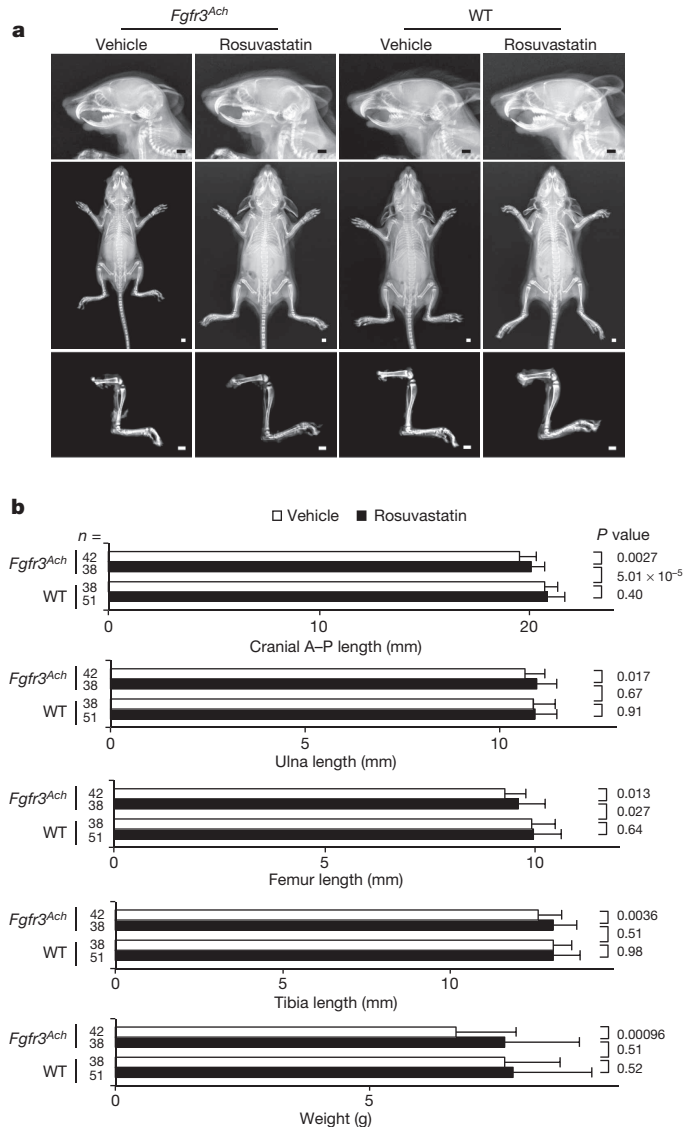


Figure 4 | Rescuing ACH model (*Fgfr3^{Ach}*) mice from reduced bone growth by intraperitoneal injection of rosuvastatin. a, Top: X-ray images of heads. Lateral views. Middle: X-ray images of bodies. Anterior–posterior view. Bottom: X-ray images of the hindlimb skeletons. Scale bars, 2 mm. b, Measurements of the anteroposterior (A–P) length of the heads and the length of the ulnas, femurs and tibiae in X-ray images and weights. The numbers of mice for each group were: *Fgfr3^{Ach}* mice treated with vehicle, $n = 42$; *Fgfr3^{Ach}* mice treated with statin, $n = 38$; wild-type mice treated with vehicle, $n = 38$; wild-type mice treated with statin, $n = 51$. The error bars represent the means \pm s.d. *t*-test *P* values are indicated.

Data Fig. 10d). These results suggest that statin treatment stimulated both chondrocytic differentiation and maturation towards hypertrophy by increasing the expression of *Sox9* and *Runx2*, respectively.

Immunoblot analysis of primary chondrocytes showed that a larger amount of FGFR3 was detected in the *Fgfr3^{Ach}* chondrocytes than in the wild-type chondrocytes (Extended Data Fig. 10e), probably due to overexpression of the *Fgfr3^{Ach}* transgene and inhibited degradation of the mutant FGFR3. Addition of lovastatin to the culture decreased the amount of FGFR3 in the *Fgfr3^{Ach}* chondrocytes, and addition of MG132 increased the amount of FGFR3 in *Fgfr3^{Ach}* chondrocytes which were cultured in the presence of lovastatin. The expression of FGFR3 was slightly increased in *Fgfr3^{Ach}* chondrocytes by the addition of bafilomycin A1 in the presence of lovastatin in the cultures. These results suggest that statin treatment induced the degradation of mutant FGFR3, mainly through a proteasomal pathway.

Discussion

The degree of abnormality in the histology of the resultant TD1-iPSC- and ACH-iPSC-derived cartilaginous particles on day 42 appeared to be more severe than that observed in the cartilage of patients with TD1 and ACH, respectively. One of the reasons for this discrepancy may be that the *in vitro* culture environment lacks any compensatory machinery to adapt skeletal tissues to the malfunction of chondrocytes caused by FGFR3 mutations. The exaggeration of phenotypes has been recognized in iPSC models of other diseases, including Alzheimer's disease²⁸. This exaggeration of the phenotype exhibited by TD1-iPSC-derived chondrocytes may be advantageous for screening drugs, because it may decrease the occurrence of false-negative events.

We injected ACH model mice with 1.0 mg kg⁻¹ rosuvastatin, which is equivalent to 70 mg per day in a 70 kg human. A dose of 80 mg per day of rosuvastatin was studied in a clinical trial and found to be associated with an increased risk of muscle toxicity and renal toxicity compared with a dose of 40 mg per day²⁹. However, a dose of 1.0 mg per kg rosuvastatin is not always intolerable. It is important to note that when rosuvastatin was administered at this dose it was able to elongate the skeletal elements of the ACH model mice, because a considerable proportion of the statin administered was removed by the liver. It remains to be determined which statin is the most effective and what dose is needed. The precise mechanism(s) by which statin treatment can rescue the chondrocyte abnormalities associated with FGFR3 diseases remain to be elucidated, although we have obtained some insights into the statin-induced promotion of FGFR3 degradation, which is inhibited in cases with mutant FGFR3 (see Supplementary Discussion for further information).

Because statins have been administered to large numbers of human patients for many years, there is abundant information available on their safety, although their effects on infants and juvenile patients are still largely unknown. The fact that the treatment rescued both human iPSC disease models and mouse disease models suggests that statins might be effective and applicable for patients with TD1 and ACH.

Online Content Methods, along with any additional Extended Data display items and Source Data, are available in the online version of the paper; references unique to these sections appear only in the online paper.

Received 1 February; accepted 19 August 2014.

Published online 17 September 2014.

- Rousseau, F. *et al.* Mutations in the gene encoding fibroblast growth factor receptor-3 in achondroplasia. *Nature* **371**, 252–254 (1994).
- Shiang, R. *et al.* Mutations in the transmembrane domain of FGFR3 cause the most common genetic form of dwarfism, achondroplasia. *Cell* **78**, 335–342 (1994).
- Warman, M. L. *et al.* Nosology and classification of genetic skeletal disorders: 2010 revision. *Am. J. Med. Genet. A* **155**, 943–968 (2011).
- Deng, C., Wynshaw-Boris, A., Zhou, F., Kuo, A. & Leder, P. Fibroblast growth factor receptor 3 is a negative regulator of bone growth. *Cell* **84**, 911–921 (1996).
- Laederich, M. B. & Horton, W. A. Achondroplasia: pathogenesis and implications for future treatment. *Curr. Opin. Pediatr.* **22**, 516–523 (2010).
- Yasoda, A. *et al.* Systemic administration of C-type natriuretic peptide as a novel therapeutic strategy for skeletal dysplasias. *Endocrinology* **150**, 3138–3144 (2009).
- Lorget, F. *et al.* Evaluation of the therapeutic potential of a CNP analog in a Fgfr3 mouse model recapitulating achondroplasia. *Am. J. Hum. Genet.* **91**, 1108–1114 (2012).
- Xie, Y. *et al.* Intermittent PTH (1–34) injection rescues the retarded skeletal development and postnatal lethality of mice mimicking human achondroplasia and thanatophoric dysplasia. *Hum. Mol. Genet.* **21**, 3941–3955 (2012).
- Jin, M. *et al.* A novel FGFR3-binding peptide inhibits FGFR3 signaling and reverses the lethal phenotype of mice mimicking human thanatophoric dysplasia. *Hum. Mol. Genet.* **21**, 5443–5455 (2012).

- Garcia, S. *et al.* Postnatal soluble FGFR3 therapy rescues achondroplasia symptoms and restores bone growth in mice. *Sci. Transl. Med.* **5**, 203ra124 (2013).
- Monsonego-Ornan, E., Adar, R., Feferman, T., Segev, O. & Yayon, A. The transmembrane mutation G380R in fibroblast growth factor receptor 3 uncouples ligand-mediated receptor activation from down-regulation. *Mol. Cell. Biol.* **20**, 516–522 (2000).
- Naski, M. C., Colvin, J. S., Coffin, J. D. & Ornitz, D. M. Repression of hedgehog signaling and BMP4 expression in growth plate cartilage by fibroblast growth factor receptor 3. *Development* **125**, 4977–4988 (1998).
- Okita, K. *et al.* A more efficient method to generate integration-free human iPSCs. *Nature Methods* **8**, 409–412 (2011).
- Oldershaw, R. A. *et al.* Directed differentiation of human embryonic stem cells toward chondrocytes. *Nature Biotechnol.* **28**, 1187–1194 (2010).
- Cho, J. Y. *et al.* Defective lysosomal targeting of activated fibroblast growth factor receptor 3 in achondroplasia. *Proc. Natl Acad. Sci. USA* **101**, 609–614 (2004).
- Harada, D. *et al.* Sustained phosphorylation of mutated FGFR3 is a crucial feature of genetic dwarfism and induces apoptosis in the ATDC5 chondrogenic cell line via PLC γ -activated STAT1. *Bone* **41**, 273–281 (2007).
- Guo, C. *et al.* Sprouty 2 disturbs FGFR3 degradation in thanatophoric dysplasia type II: a severe form of human achondroplasia. *Cell. Signal.* **20**, 1471–1477 (2008).
- Krejci, P. *et al.* Analysis of STAT1 activation by six FGFR3 mutants associated with skeletal dysplasia undermines dominant role of STAT1 in FGFR3 signaling in cartilage. *PLoS ONE* **3**, e3961 (2008).
- Legeai-Mallet, L., Benoist-Lasselin, C., Delezoide, A. L., Munnich, A. & Bonaventure, J. Fibroblast growth factor receptor 3 mutations promote apoptosis but do not alter chondrocyte proliferation in thanatophoric dysplasia. *J. Biol. Chem.* **273**, 13007–13014 (1998).
- Yamanaka, Y., Tanaka, H., Koike, M., Nishimura, R. & Seino, Y. PTHrP rescues ATDC5 cells from apoptosis induced by FGF receptor 3 mutation. *J. Bone Miner. Res.* **18**, 1395–1403 (2003).
- Yudoh, K. & Karasawa, R. Statin prevents chondrocyte aging and degeneration of articular cartilage in osteoarthritis (OA). *Aging* **2**, 990–998 (2010).
- Simopoulou, T., Malizos, K. N., Poultides, L. & Tsezou, A. Protective effect of atorvastatin in cultured osteoarthritic chondrocytes. *J. Orthop. Res.* **28**, 110–115 (2010).
- Baker, J. F., Walsh, P. M., Byrne, D. P. & Mulholland, K. J. Pravastatin suppresses matrix metalloproteinase expression and activity in human articular chondrocytes stimulated by interleukin-1 β . *J. Orthopaed. Traumatol.* **13**, 119–123 (2012).
- Mundy, G. *et al.* Stimulation of bone formation *in vitro* and in rodents by statins. *Science* **286**, 1946–1949 (1999).
- Millar, P. J. & Floras, J. S. Statins and the autonomic nervous system. *Clinical Sci.* **126**, 401–415 (2014).
- Olivieri, F. *et al.* Telomere/telomerase system: a new target of statins pleiotropic effect? *Curr. Vasc. Pharmacol.* **10**, 216–224 (2012).
- Zhang, J. *et al.* Statins, autophagy and cancer metastasis. *Int. J. Biochem. Cell Biol.* **45**, 745–752 (2013).
- Israel, M. A. *et al.* Probing sporadic and familial Alzheimer's disease using induced pluripotent stem cells. *Nature* **482**, 216–220 (2012).
- Wolfe, S. M. Dangers of rosuvastatin identified before and after FDA approval. *Lancet* **363**, 2189–2190 (2004).

Supplementary Information is available in the online version of the paper.

Acknowledgements We thank H. Ohashi, J. Murotsuki, T. Yamada and K. Ozono for preparation of the dermal fibroblasts from a patient and discussion. We thank D. Ornitz and A. Yasoda for the *Fgfr3^{Ach}* mice. We thank K. Okita and S. Yamanaka for providing the hiPSC line 409B2, and A. Hotta for transducing the piggyBac vectors. We thank A. Motomura, X. Chen, Y. Minegishi, M. Nishino, T. Kobayashi, N. Oda, E. Ikeda and Y. Makita for their assistance. This study was supported in part by the Japan Science Technology Agency (JST), CREST (to N.T.) and Research Center Network for Realization of Regenerative Medicine (to N.T.), and Scientific Research Grant No. 24890101 (to A.Y.) and 26861716 (to A.Y.) and No. 24390354 (to N.T.) from MEXT.

Author Contributions A.Y. was involved in most of the experiments. M.M. performed the immunohistological and immunoblot analyses, as well as the DNA construction. H.K., T.K. and Y.Y. performed the mouse experiments. M.O. contributed to the generation of iPSCs. H.S. and S.I. were involved in the study design. K.F. performed the immunoblot analyses. N.T. designed the study. A.Y. and N.T. wrote the paper.

Author Information Reprints and permissions information is available at www.nature.com/reprints. The authors declare no competing financial interests. Readers are welcome to comment on the online version of the paper. Correspondence and requests for materials should be addressed to N.T. (ntsumaki@cira.kyoto-u.ac.jp).

METHODS

Ethics statement. All experiments were approved by the institutional review board, institutional animal committee (as appropriate) and the institutional biosafety committee of Kyoto University.

Generation of patient-specific iPSCs. HDFs derived from six patients (Extended Data Fig. 1a) were obtained from the cell banks of the Coriell Institute and Saitama Children's Medical Center. Control HDFs from two different neonates were purchased from KURABO (strain 01491 and 01439). HDFs were cultured in DMEM (Sigma) with 10% FBS (Invitrogen), 50 U ml⁻¹ penicillin and 50 µg ml⁻¹ streptomycin. To generate iPSCs, episomal plasmid vectors (Mixture Y4: *OCT4*, *SOX2*, *KLF4*, *L-MYC*, *LIN28* and *p53* shRNA) were electroporated into HDFs with the Neon transfection system (Invitrogen)¹³. One week after transduction, 1 × 10⁵ cells were re-seeded into 100 mm dishes with feeder cells. The cells were subsequently cultured in hiPSC medium. The 409B2 cells used as the control iPSCs were a gift from K. Okita and S. Yamanaka (Center for iPS Cell Research and Application (CiRA), Kyoto University, Kyoto, Japan)¹³. All cells were negative for mycoplasma contamination.

Chondrogenic differentiation of hiPSCs. The hiPSCs were transferred and then maintained in a feeder-free medium, Essential 8 (Invitrogen) with 50 units ml⁻¹ penicillin and 50 mg ml⁻¹ streptomycin, in 3.5-cm Matrigel-coated dishes. The hiPSCs formed high-density cell colonies which consisted of 1–2 × 10⁵ cells 10–15 days after the start of maintenance under the feeder-free culture conditions. Subsequently, the chondrogenic differentiation of iPSCs was performed following the previously described method¹⁴, with modifications. The hiPSCs were initially differentiated into mesendodermal cells in DMEM/F12 (Sigma) with 10 ng ml⁻¹ of Wnt3A (R&D), 10 ng ml⁻¹ of Activin A (R&D), 1% ITS (Invitrogen), 1% FBS and 50 units and 50 mg ml⁻¹ of penicillin and streptomycin, respectively (Invitrogen) for 3 days. On day 3, the medium was changed to the basal medium (DMEM (Sigma) with 1% ITS, 1% FBS, 2 mM L-glutamine (Invitrogen), 1 × 10⁻⁴ M non-essential amino acids (Invitrogen), 1 mM Na pyruvate (Invitrogen), 50 units of penicillin and 50 mg ml⁻¹ of streptomycin) supplemented with 50 µg ml⁻¹ of ascorbic acid (Nacalai), 10 ng ml⁻¹ of BMP2 (Peprotech), 10 ng ml⁻¹ of TGFβ1 (Peprotech) and 10 ng ml⁻¹ of GDF5 (PTT), which was intended to commit the cells to the chondrocytic lineage. A total of 10 ng ml⁻¹ of bFGF (WAKO) was added to the chondrogenic medium from day 3 to day 14 to increase the cell proliferation. Chondrogenic cells form multilayered nodules by day 14. The nodules were physically separated from the bottom of the dishes to form particles, which were then transferred to a suspension culture in 3.5-cm Petri dishes on day 14. The cells in the particles produce cartilaginous extracellular matrix, resulting in the particles becoming cartilaginous tissue in suspension culture. Particles were harvested on days 28 and 42 for the analyses. The culture medium was changed every 2–7 days.

Histological analysis. The particles in the suspension culture, metatarsals in the organ culture and pellets in the pellet culture were collected, fixed with 4% paraformaldehyde, processed and embedded in paraffin. For some experiments (the results of which are shown in Figs 1f and 3b), the particles were immediately embedded in SCEM compound (SECTION-LAB) and subjected to frozen sectioning according to the method described by Kawamoto³⁰. Semi-serial sections were prepared and stained with haematoxylin and eosin (HE) or Safranin-O-fast green-iron haematoxylin (Safranin O) or were immunostained with specific antibodies.

The area of the Safranin-O-positive region and the total area of the particle were measured. The measurements of these areas were performed in a blinded manner. The area of the Safranin-O-positive region was divided by the total area of the particle.

For the anti-type I collagen antibody (Southern Biotech, 1320-01), immune complexes were detected by using N-Histofine Simple Stain MAX PO (GO) (Nichirei Biosciences, 414351) and DAB (DAKO, K3468) as a chromogen. For the anti-SSEA4 antibodies (Santa Cruz, sc-5279), anti-TRA1-60 antibodies (Abcam, ab16287), anti-type II collagen (Thermo MS-235) and cleaved caspase 3 (Cell signalling, Asp175), immune complexes were detected using secondary antibodies conjugated to Alexa Fluor 488 or 546.

For the TUNEL assay, an *in situ* cell death detection kit (TMR red; Roche) was used according to the manufacturer's instructions.

For BrdU labelling, samples were treated with BrdU overnight before collection. The incorporated BrdU was detected using a BrdU staining kit (Invitrogen). The numbers of BrdU-positive cells and total cells were counted in a blinded manner. The number of BrdU-positive cells was divided by the total number of cells.

RNA isolation and quantitative real-time RT-PCR. Total RNA was isolated from whole-cell lysates using the RNeasy Mini kit (Qiagen) according to the manufacturer's instructions with on-column DNase I digestion. The total RNAs prepared from the re-differentiated human fetal chondrocytes were purchased from Cell Applications, Inc. (402RD-R10f). A total of 500 ng of total RNA was used as a template for cDNA synthesis using the ReverTra Ace system (TOYOBO). The amplified products were used to derive standard curves for quantitative real-time PCR. Real-time PCR was performed in a Step One system (ABI) using a KAPA SYBR FAST qPCR kit Master Mix and the ABI prism (KAPA BIOSYSTEMS). The expression

levels were normalized to the level of β-actin for human expression studies and *Gapdh* for the mouse mRNA expression levels. The primer sequences are shown in Supplementary Tables 1 and 2.

Immunoblot analysis. Cell lysates were subjected to SDS-PAGE. The separated proteins were then electroblotted and immunostained with the anti-FGFR3 antibody (Cell Signaling, 4574), anti-phosphorylated MAPK antibody (Cell Signaling, 9109) and anti β-actin antibody (Cell Signaling, 49776). FGFR3 migrates on SDS-PAGE as several bands due to the different levels of post-translational modification¹¹.

FGFR3 shRNA. Three short hairpin RNAs (shRNA) targeting different sites of *FGFR3* (shFGFR3-1, -3 and -5) were cloned into piggyBac vectors (Fig. 2a). A shRNA targeting the luciferase sequence was used as a control. The target sequences are shown in Supplementary Table 3. The *FGFR3* shRNA piggyBac vector and transposase expression vector (PBaseII, P16-25)—a gift from A. Hotta (Center for iPS Cell Research and Application (CiRA), Kyoto University, Kyoto, Japan)—were introduced into the TD1-iPSCs (TD1-714-3) using nucleofection technology according to the manufacturer's instructions (Amaxa). TD1 iPSC lines bearing the *FGFR3* shRNA sequence were established.

FGFR3 neutralizing antibody. The FGFR3 neutralizing antibody was purchased from Santa Cruz (sc-13121). A total of 1 µl of the antibody solution was added to 1 ml of cell culture medium (200 ng ml⁻¹) during the chondrogenic differentiation of TD1 iPSCs. As a control, we used IgG (Cell Signaling, #27295), and 1 µl of the IgG solution was added to 1 ml of medium.

Preparation of test molecules. The stock CNP (Sigma, N8768), NF449 (Abcam, ab120415) and FGFR inhibitor (PD 173047, Cayman) solutions were prepared at a concentration of 100 µM, 50 mM and 1 mM, respectively. The final concentrations of CNP, NF449 and the FGFR inhibitor were 100 nM, 25 µM and 1 µM, respectively. The stock lovastatin (TCI, L0214), mevastatin (Cayman, 10010340), atorvastatin (LKT A7658), pravastatin (Cayman, 10010343), rosuvastatin (BioVision, 1995-5) and fluvastatin (Cayman, 10010337) solutions were prepared by dissolving them in DMSO at a concentration of 10 mM. The final concentrations of all statin solutions were 1 µM. Aliquots of stock solutions were added to the culture medium. As a control, an equal amount of water or DMSO was added to the medium (vehicle).

Fgfr3^{Ach} mice. The *Fgfr3^{Ach}* transgenic mice¹² were a gift from D. Ornitz (Washington University School of Medicine). We produced a large number of mice by *in vitro* fertilization³¹. Spermatozoa were collected from male heterozygous *Fgfr3^{Ach}* mice (FVB strain). Oocytes were collected from superovulated wild-type female mice (C57BL/6 mice). The spermatozoa were added to the oocytes. Fertilized oocytes were transferred into pseudopregnant mice (ICR). A total of 172 pups from a total of 13 litters were obtained on the same day. The pups were F₁ hybrid mice, and were genetically uniform. All 172 pups were included in the study. Rosuvastatin was dissolved in phosphate-buffered saline (PBS). A total of seven and six litters, with a total of 90 and 82 pups, were treated with rosuvastatin (1.0 mg kg⁻¹) or vehicle (PBS), respectively. We injected the solution (statin or PBS) into the peritoneal space of pups six times per week from 3 days after birth (day 3) until day 14. One mouse receiving rosuvastatin was found dead on day 14. Mice receiving PBS were found dead on days 3 and day 4 (one mouse each day). The dead mice were thought to have been lost due to having been eaten, and were not able to be subjected to any of the analyses, including genotyping. The remaining 169 mice were killed on day 15, and then were subjected to X-ray imaging (Faxitron DX-50). Measurements of the lengths of skeletal components on X-ray images were performed in a blinded manner. Genomic DNA was extracted from the toes of each mouse and subjected to a genotype analysis, as reported previously¹². The post-hoc power analysis comparing the *Fgfr3^{Ach}* mice treated with vehicle and the *Fgfr3^{Ach}* mice treated with statin was performed using the G*Power 3.1 software program³². The effect size, *d*, was 0.64, as a function of the two-tailed *t*-test, with power (1 - β) = 0.8, α = 0.05, *n*₁ = 38 and *n*₂ = 42.

Organ culture of the metatarsal primordial cartilage from *Fgfr3^{Ach}* mice. To examine whether the statin affected the cartilage directly or indirectly, we performed organ culture of metatarsal primordial cartilage prepared from *Fgfr3^{Ach}* transgenic mice in the presence or absence of lovastatin for 7 days. Metatarsals were collected from 15.5 d.p.c. mouse embryos with a mixed FVB × C57BL/6 genetic background, and were subjected to organ culture as described previously³³. After the genotypes of the pups were determined, the metatarsals from *Fgfr3^{Ach}* embryos were treated with 1 µM lovastatin or vehicle. The measurements of the lengths of the metatarsals were performed in a blinded manner.

Preparation of primary chondrocytes from *Fgfr3^{Ach}* mice. The primary chondrocytes were prepared from newborn mice with a mixed FVB × C57BL/6 genetic background as described previously³⁴. After the genotypes of pups were determined, the primary chondrocytes from *Fgfr3^{Ach}* animals or those from wild-type animals were trypsinized and mixed, respectively. The cells were subsequently used for pellet culture to analyse the effects of statin treatment on the differentiation and maturation of *Fgfr3^{Ach}* chondrocytes or were subjected to monolayer culture to analyse the degradation of FGFR3 in *Fgfr3^{Ach}* chondrocytes.

Pellet culture of primary chondrocytes from *Fgfr3^{Ach}* mice. To analyse how the statin affected the differentiation of chondrocytes, we performed pellet culture of the chondrocytes prepared from *Fgfr3^{Ach}* transgenic mice. Chondrocytes normally undergo differentiation and maturation towards hypertrophy in pellet culture. A total of 5×10^5 primary chondrocytes prepared from *Fgfr3^{Ach}* mice were transferred into a 15-ml tube (Falcon) and centrifuged at 200g for 10 min³⁵. The resulting cell pellet was incubated for 2 or 4 weeks in the presence or absence of 1 μ M lovastatin.

Monolayer culture of primary chondrocytes from *Fgfr3^{Ach}* mice in the presence of MG132 or bafilomycin A1. To examine how the statin treatment affected the degradation of the FGFR3 protein, we analysed the effects of a proteasome inhibitor, MG132, and a lysosome inhibitor, bafilomycin A1, on the amounts of FGFR3 protein. We prepared primary chondrocyte cultures from wild-type and *Fgfr3^{Ach}* mice. A total of 2.5×10^5 primary chondrocytes were plated in each well of a six-well plate, and were cultured in the presence or absence of 1 μ M lovastatin for 2 days. Next, the culture was supplemented with 10 mM MG132 (Sigma, M7449), 100 nM bafilomycin A1 (Sigma, B1793) or vehicle. Two hours later, the culture was further supplemented with 50 ng ml⁻¹ FGF9 (Peprotech) and incubated at 4 °C for 2 h. Then cells were collected and subjected to an immunoblot analysis using an anti-FGFR3 antibody.

Statistical analysis. The data are shown as averages and standard deviations. We used ANOVA followed by the Tukey–Kramer post-hoc test. In Figs 1b, f, 3a, b, d and 4b and in Extended Data Figs 4c, 5c, 10a, b, d, homogenous variances were assumed by the *F* test and the Student's *t*-test (two-sided) was used. *P* values <0.05 were considered to be statistically significant.

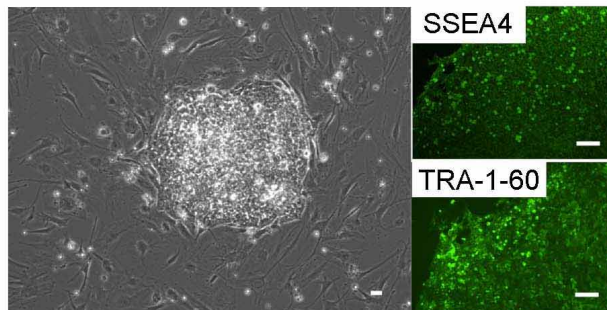
30. Kawamoto, T. Use of a new adhesive film for the preparation of multi-purpose fresh-frozen sections from hard tissues, whole-animals, insects and plants. *Arch. Histol. Cytol.* **66**, 123–143 (2003).
31. Takeo, T. *et al.* Birth of mice from vitrified/warmed 2-cell embryos transported at a cold temperature. *Cryobiology* **58**, 196–202 (2009).
32. Faul, F., Erdfelder, E., Lang, A. G. & Buchner, A. G*Power 3: a flexible statistical power analysis program for the social, behavioral, and biomedical sciences. *Behav. Res. Methods* **39**, 175–191 (2007).
33. Ikegami, D. *et al.* Identification of small molecular compounds and fabrication of its aqueous solution by laser-ablation, expanding primordial cartilage. *Osteoarth. Cartil.* **19**, 233–241 (2011).
34. Gosset, M., Berenbaum, F., Thirion, S. & Jacques, C. Primary culture and phenotyping of murine chondrocytes. *Nature Protocols* **3**, 1253–1260 (2008).
35. Hiramatsu, K. *et al.* Generation of hyaline cartilaginous tissue from mouse adult dermal fibroblast culture by defined factors. *J. Clin. Invest.* **121**, 640–657 (2011).

a

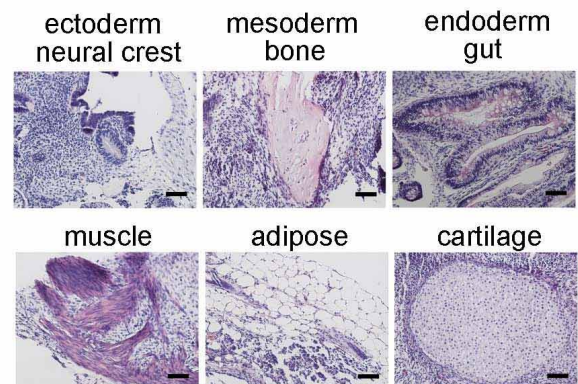
iPSC line	Sex	Age at sampling	Race	ID (cell bank) / lot (company)	origin	FGFR3 mutations	iPSCs	
							hESC markers	Teratomas
TD1-714-3	M	1d	Caucasian	GM00714 (Coriell)	Fibroblast	742C>T [Arg248Cys]	Yes	Yes
TD1-10749-2	M	1d	Caucasian	GM10749 (Coriell)	Fibroblast	742C>T [Arg248Cys]	Yes	Yes
TD1-315H-2	F	21 weeks and 4 days gestation	Japanese	S2012 (Saitama ¹)	Fibroblast	742C>T [Arg248Cys]	Yes	Yes
ACH-8857-1	M	34y	Caucasian	GM08857 (Coriell)	Fibroblast	1138G>A [Gly380Arg]	Yes	Yes
ACH-8858-6	F	30y	Caucasian	GM08858 (Coriell)	Fibroblast	1138G>A [Gly380Arg]	Yes	Yes
ACHhomo-8859-3	F	1m	Caucasian	GM08859 (Coriell)	Fibroblast	1138G>A [Gly380Arg] homozygous	Yes	Yes
409B2	F	36y	Caucasian	HDF1388	Fibroblast	No	Yes	Yes
KF4009-1	M	Newborn	Asian/Caucasian	01491 (Kurabo)	Fibroblast	No	Yes	Yes
HDF-11	M	Newborn	Asian	01439 (Kurabo)	Fibroblast	No	Yes	Yes

¹Saitama, Saitama Children's Medical Center, Japan. ²CiRA, Center for iPS Cell Research and Application.

b

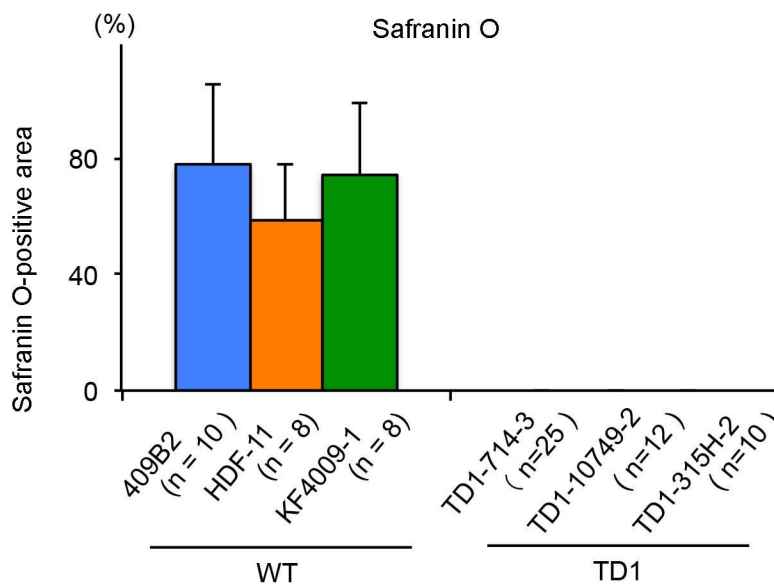
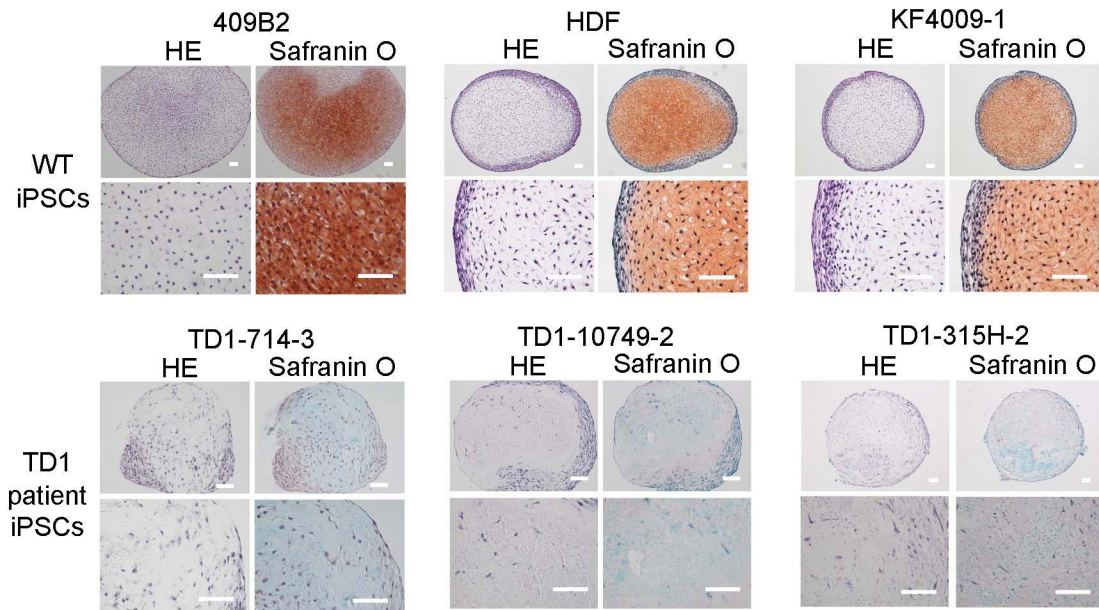


c



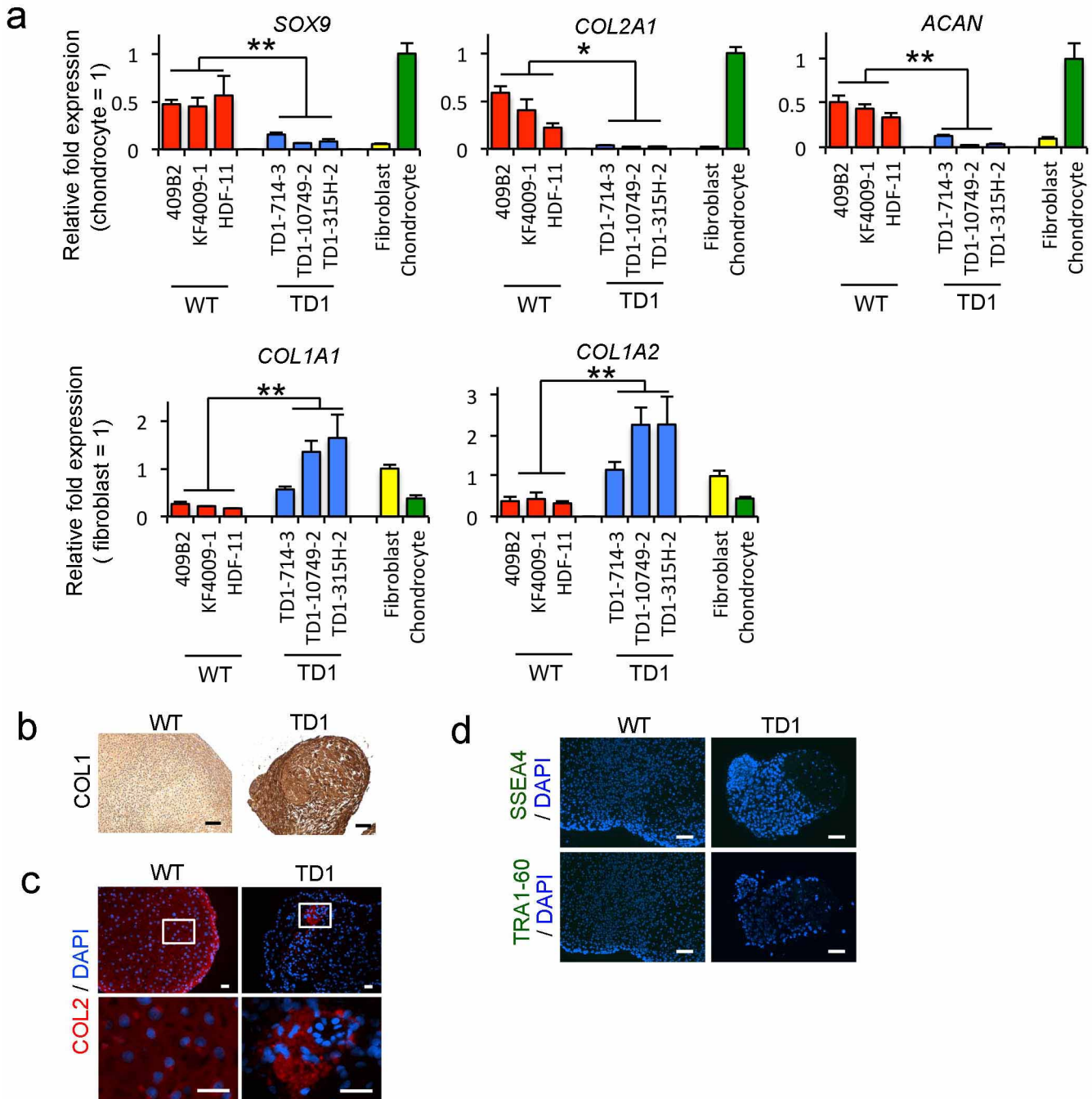
Extended Data Figure 1 | Characterization of the TD1 and ACH iPSCs.
a, Donor information and characterization of iPSCs. **b**, Left: a phase contrast image of TD1 iPSCs (TD1-714-3). Right: immunocytochemical staining of TD1 iPSCs (TD1-714-3) for SSEA4 and TRA1-60. The images are

representative of two independent experiments. **c**, The histology of teratomas formed after implantation of TD1 iPSCs (TD1-10749-2) into SCID mice. The images are representative of experiments using three TD1 iPS clones established from three different patients. Scale bars, 50 μ m.



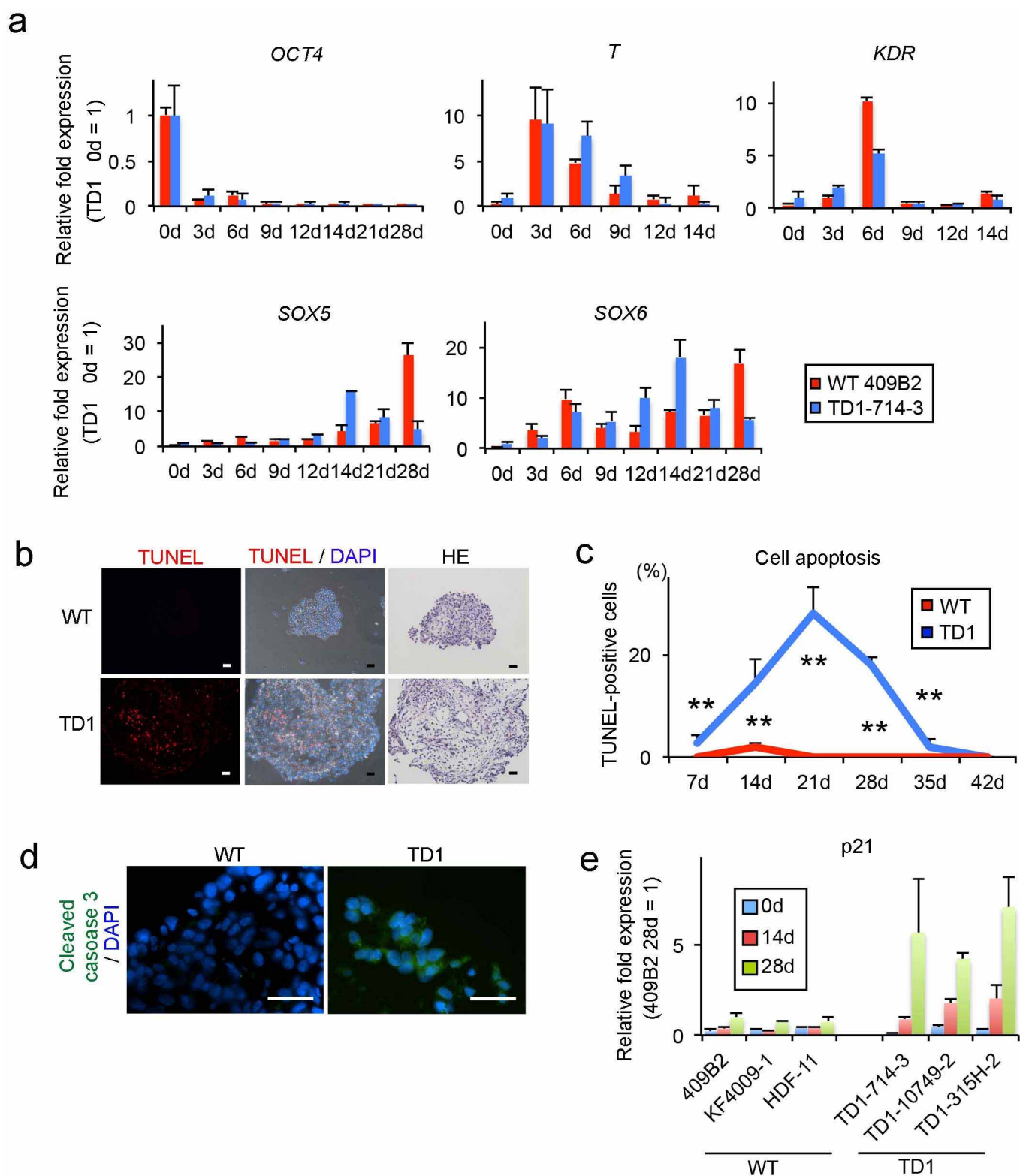
Extended Data Figure 2 | The results of a histological analysis of particles formed by chondrogenically differentiated wild-type and TD1 iPSCs on day 42. The data were collected from three independent wild-type and three independent TD1 iPSC lines which were derived from three individuals, respectively. Top: three iPSC lines established from different control individuals all formed cartilaginous particles (top panels), whereas three iPSC

lines established from different patients formed particles which lacked cartilaginous elements (bottom panels). Scale bars, 50 μ m. Bottom: the area of the Safranin-O-positive region was divided by the total area of the particle. The error bars denote the means \pm s.d. The number of particles examined is indicated at the bottom.



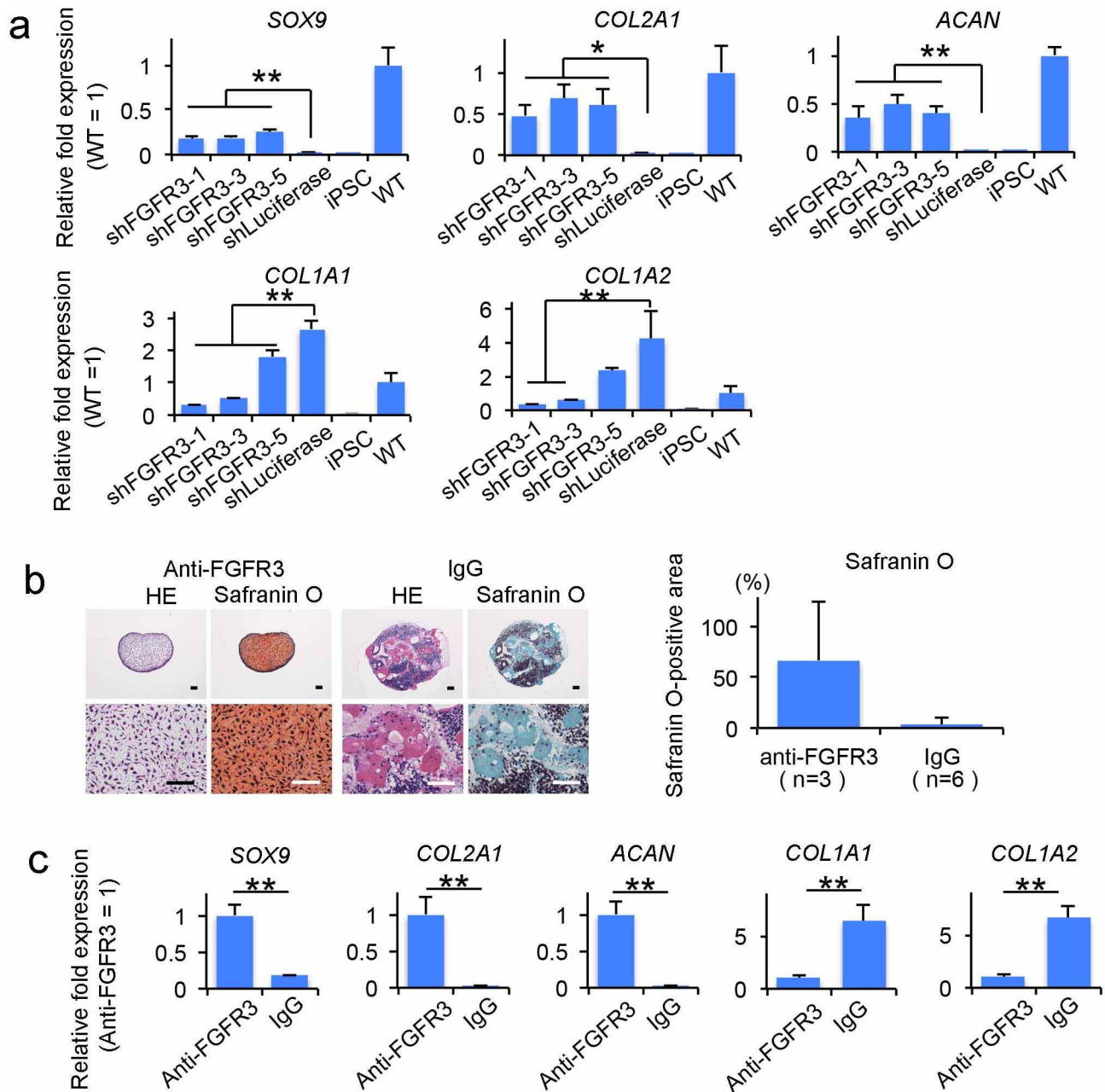
Extended Data Figure 3 | Results of the expression analysis of chondrogenically differentiated wild-type iPSCs and TD1 iPSCs. **a**, The results of a real-time RT-PCR expression analysis of marker genes in chondrogenically differentiated iPSCs lines on day 28. The data were collected from three independent wild-type and three independent TD1 iPSC lines which were derived from three individuals, respectively. Chondrocytes, re-differentiated human fetal chondrocytes; fibroblasts, dermal fibroblasts. * $P < 0.05$ and ** $P < 0.01$ ($n = 3$ technical replicates) by the

Tukey-Kramer post-hoc test. The error bars denote the means \pm s.d. **b-d**, Immunohistochemical detection of the expression of type I collagen (**b**), type II collagen (**c**), SSEA4 (**d**, upper panels) and TRA1-60 (**d**, lower panels) in the particles formed by chondrogenically differentiated wild-type iPSCs (409B2) and TD1 iPSCs (TD1-714-3) on day 42. **b**, **c**, The images are representative of three independent experiments. **d**, The images are representative of experiments using three TD1-iPS clones established from three different patients. Scale bars, 50 μ m (**b**, **d**); 25 μ m (**c**).



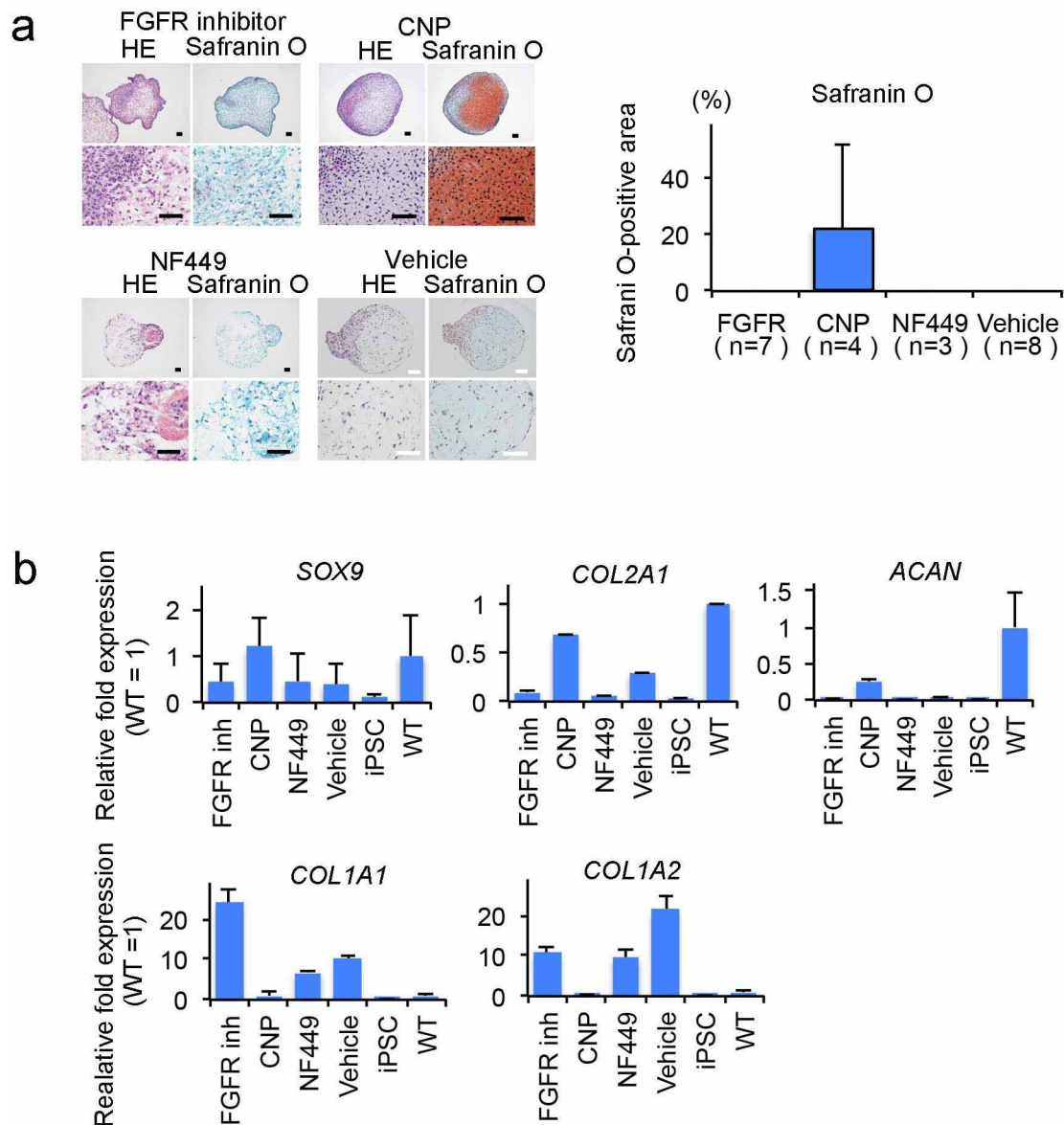
Extended Data Figure 4 | Expression levels of markers and apoptosis in chondrogenically differentiated wild-type and TD1 iPSCs. **a**, Time course of the changes in the expression of markers in iPSCs subjected to chondrogenic differentiation, as determined by real-time RT-PCR ($n = 3$ technical replicates). **b**, The results of the TUNEL assay of particles formed by chondrogenically differentiated iPSCs (409B2 and TD1-714-3) on day 21. Scale bars, 50 μm . The images are representative of two independent experiments. **c**, The ratio of the numbers of TUNEL-positive cells per the total cell number during the chondrogenic differentiation of wild-type iPSCs (409B2) and TD1 iPSCs (TD1-714-3). ****** $P < 0.01$ for TD1-iPSC-derived cells compared to

wild-type iPSC-derived cells on each day after chondrogenic differentiation ($n = 3$ particles), t -test. **d**, Immunohistochemical findings of the expression of cleaved-caspase 3 in the particles formed by chondrogenically differentiated wild-type iPSCs (409B2) and TD1 iPSCs (TD1-714-3) on day 28. Scale bars: 25 μm . The images are representative of two independent experiments. **e**, The results of a real-time RT-PCR expression analysis of p21 in chondrogenically differentiated TD1 iPSCs on days 0, 14 and 28 ($n = 3$ technical replicates). The data were collected from three independent wild-type and three independent TD1 iPSC lines which were respectively derived from three individuals. The error bars denote the means \pm s.d.



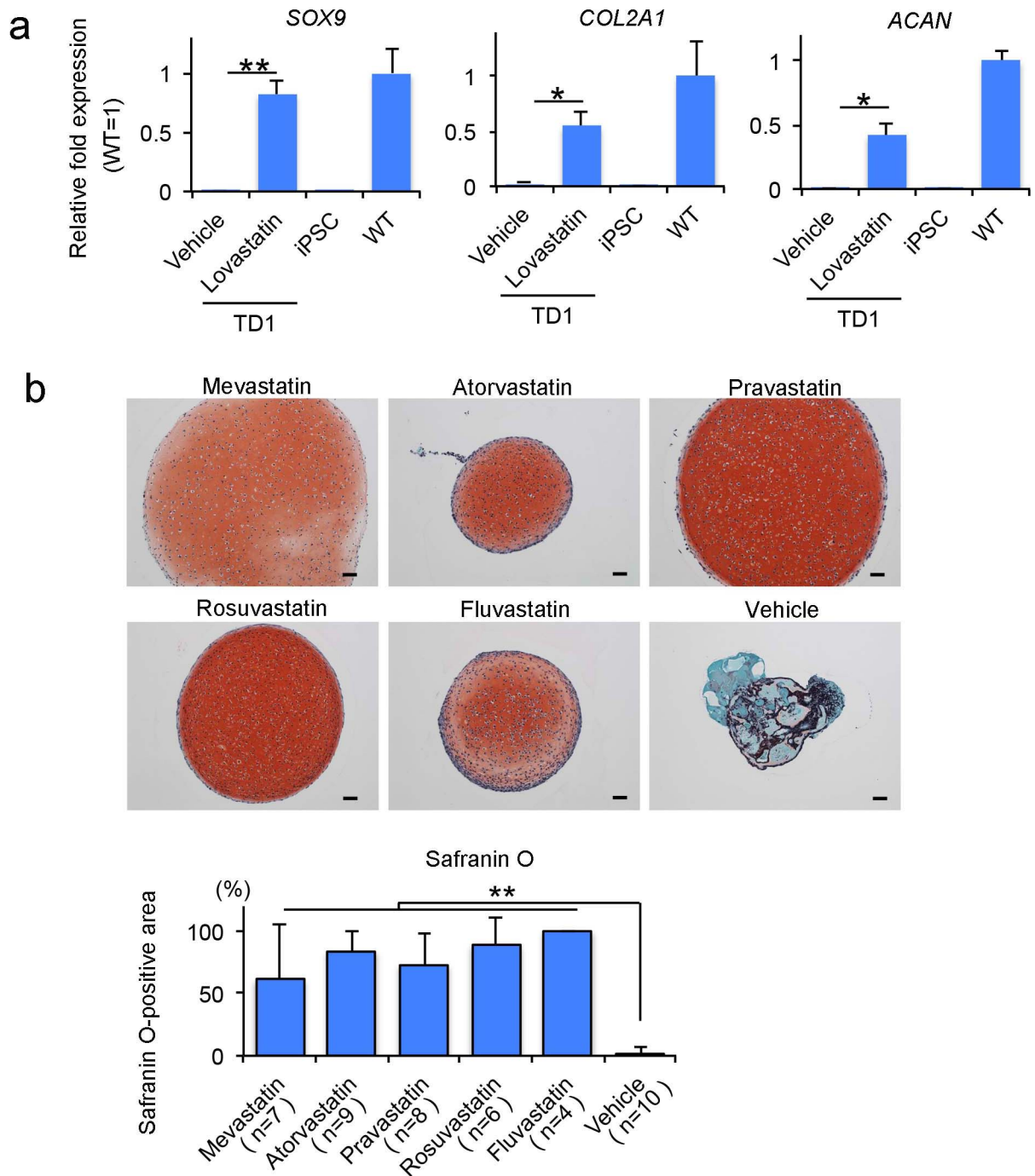
Extended Data Figure 5 | Rescuing the chondrogenically differentiated TD1 iPSCs (TD1-714-3) by *FGFR3* knockdown and treatment with a *FGFR3* neutralizing antibody. **a**, Results of a real-time RT-PCR expression analysis of marker genes on day 28. iPSC, undifferentiated TD1 iPSCs; WT, chondrogenically differentiated wild-type iPSCs (409B2) on day 28. * $P < 0.05$; ** $P < 0.01$, Tukey-Kramer post-hoc test ($n = 3$ technical replicates). The data were collected from three independent clones respectively bearing three different *FGFR3* shRNAs. **b**, A *FGFR3* neutralizing antibody was added to the medium during the chondrogenic differentiation of TD1 iPSCs to induce the

formation of cartilaginous particles. IgG was added as a control. The results of a histological analysis of the particles. Left: histological sections of particles were stained with haematoxylin and eosin or Safranin O. Scale bars, 50 μm . Right: the area of the Safranin-O-positive region was divided by the total area of the particle. The number of particles examined is indicated at the bottom. **c**, The results of a real-time RT-PCR expression analysis of marker genes in chondrogenically differentiated TD1 iPSCs treated with the *FGFR3* neutralizing antibody on day 28. * $P < 0.05$; ** $P < 0.01$ by the t -test ($n = 3$ technical replicates). Error bars denote the means \pm s.d.



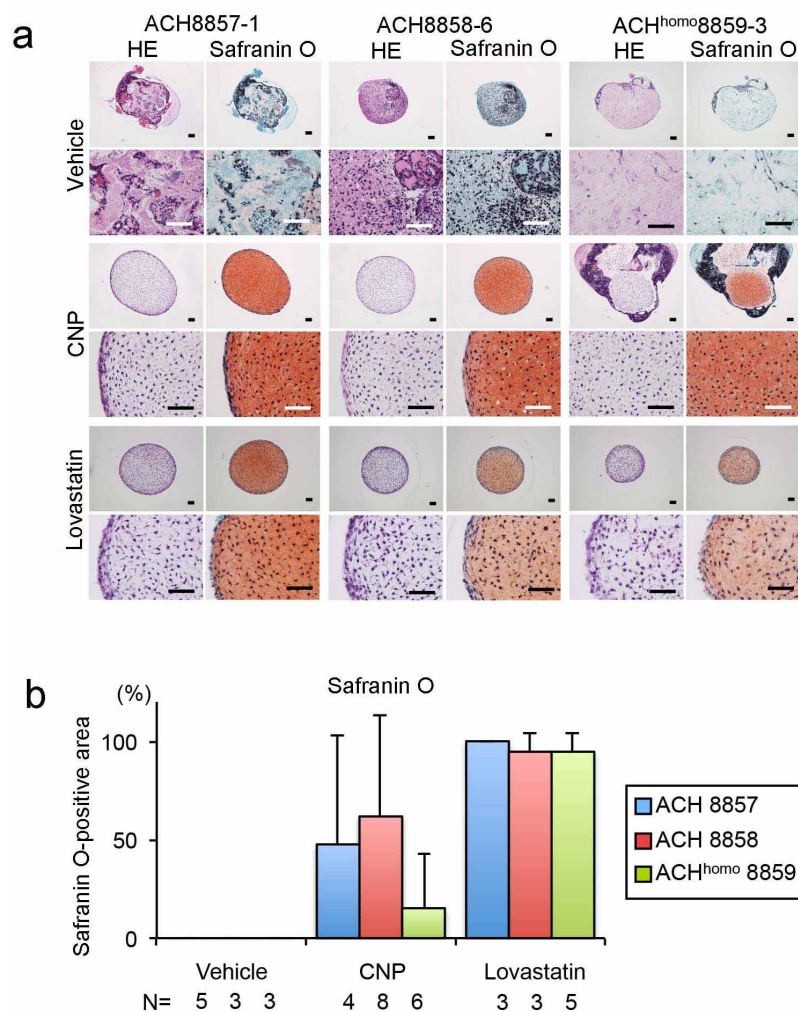
Extended Data Figure 6 | Screening for molecules that rescue chondrogenically differentiated TD1 iPSCs (TD1-714-3). **a**, Candidate molecules or vehicle were added to the medium during the chondrogenic differentiation of TD1 iPSCs. The histology of the particles was examined on day 42. Left: histological sections of particles were stained with haematoxylin and eosin or Safranin O. The addition of a FGFR inhibitor and a G-protein antagonist, NF449, failed to recover the cartilage formation of chondrogenically differentiated TD1 iPSCs under the conditions examined. The FGFR inhibitor used in this experiment inhibits not only FGFR3 but also FGFR1 and FGFR2, which might have adversely affected the cartilage formation. The addition of CNP led to the partial recovery of cartilage formation. Scale bars, 50 μ m. Right:

the area of the Safranin O-positive region was divided by the total area of the particle. The number of particles examined is indicated at the bottom. The data are representative of two independent experiments. **b**, The results of a real-time RT-PCR expression analysis of marker genes in chondrogenically differentiated TD1 iPSCs treated with various factors on day 28. The addition of CNP increased the expression of chondrocyte marker genes and decreased the expression of fibroblast marker genes in the chondrogenically differentiated TD1 iPSCs. iPSC, undifferentiated TD1 iPSCs; WT, chondrogenically differentiated wild-type iPSCs (409B2) on day 28. The final concentrations of each molecule were: FGF inhibitor, 1 μ M; NF449, 25 μ M; and CNP, 100 nM ($n = 3$ technical replicates). Error bars denote the means \pm s.d.



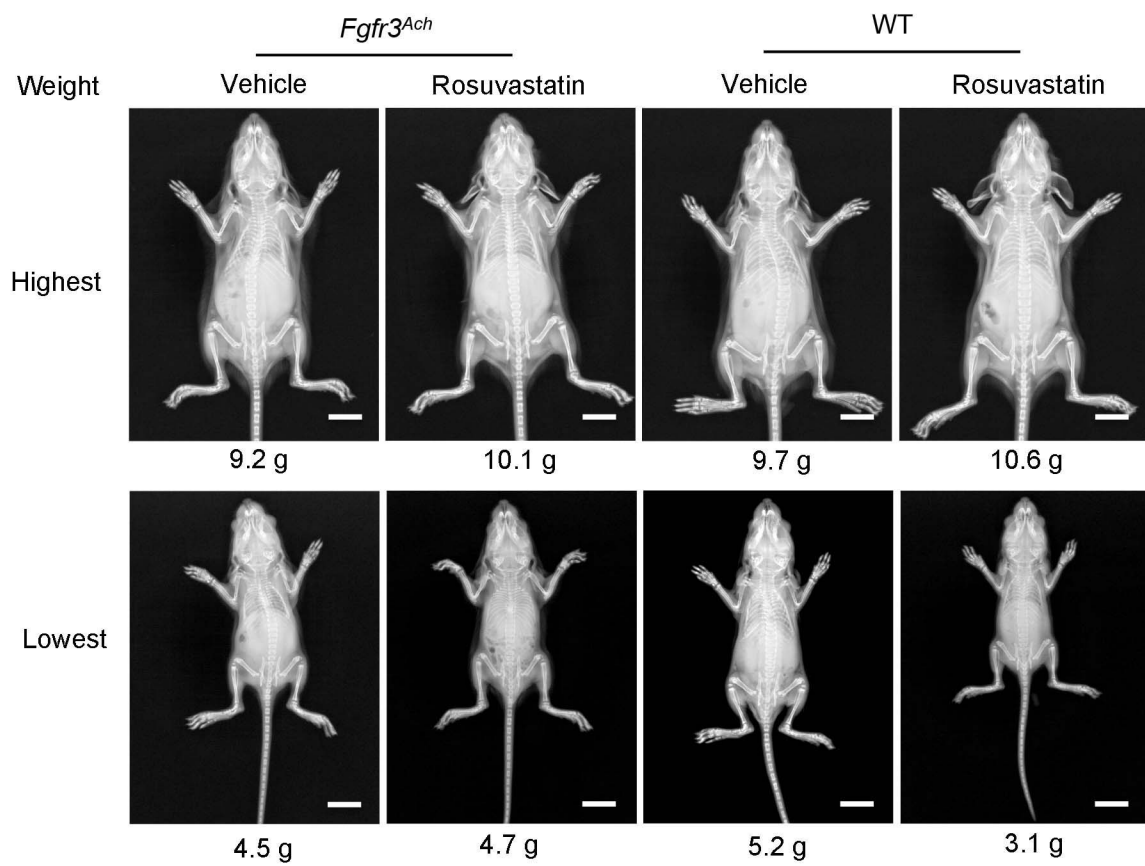
Extended Data Figure 7 | Effects of statins on chondrogenically differentiated TD1 iPSCs. **a**, The results of a real-time RT-PCR expression analysis of marker genes on day 28. TD1 (TD1-714-3) and wild-type (409B2) iPSCs were chondrogenically differentiated in the presence or absence of lovastatin (1 μ M). TD1, chondrogenically differentiated TD1 iPSCs; iPSC, undifferentiated TD1 iPSCs; WT, chondrogenically differentiated wild-type iPSCs ($n = 3$ technical replicates). The data are representative of two independent experiments. **b**, Rescue of chondrogenically differentiated TD1 iPSCs by statin treatment. Mevastatin, atorvastatin, pravastatin, rosuvastatin or

fluvastatin (each 1 μ M) was added to the medium during the chondrogenic differentiation of TD1 iPSCs. On day 42, the particles were subjected to a histological analysis. Top: histological sections of particles were stained with haematoxylin and eosin or Safranin O. Scale bars, 50 μ m. Bottom: the area of the Safranin-O-positive region was divided by the total area of the particle. The number of particles examined is indicated at the bottom. The data are representative of three independent experiments. The error bars denote the means \pm s.d. * $P < 0.05$; ** $P < 0.01$ by the Tukey-Kramer post-hoc test.

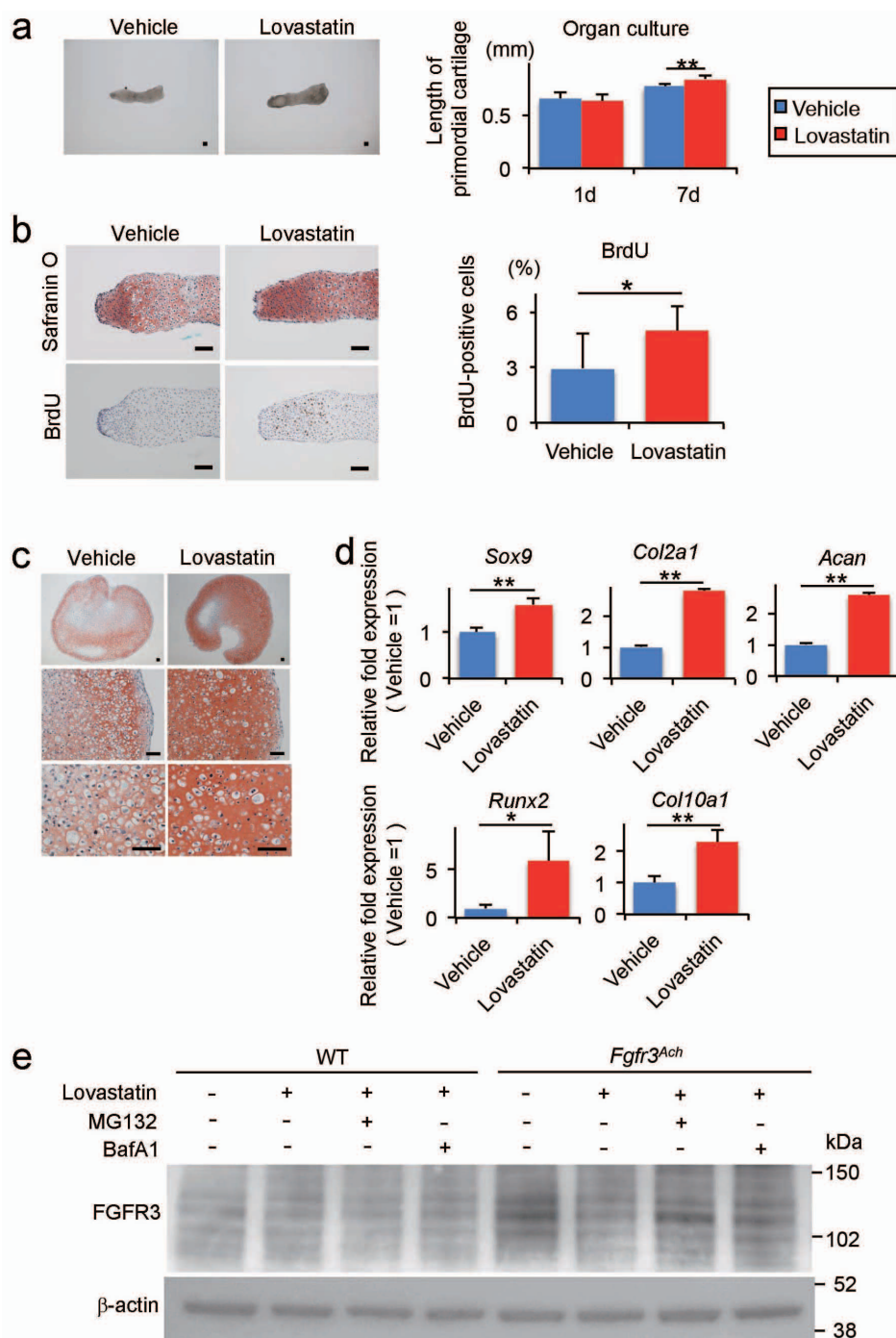


Extended Data Figure 8 | Rescue of chondrogenically differentiated ACH iPSCs by statin treatment. HDFs were obtained from two ACH patients (ACH-8857 and ACH-8858) bearing a heterozygous G380R mutation in the *FGFR3* gene (Extended Data Fig. 1a). HDFs were also obtained from an individual (ACH^{homo}-8859) whose parents both had ACH, who showed a more severe phenotype of chondrodysplasia than typical ACH, and who was homozygous for the G380R mutation in the *FGFR3* gene. We generated more than three iPSC lines for each patient and analysed one iPSC line (ACH-8857-1, ACH-8858-6 and ACH^{homo}-8859-3) derived from each patient's HDFs.

We confirmed that all iPSC lines expressed SSEA4 and TRA1-60, and formed teratomas containing all three germ layers in mice. Lovastatin and CNP were added to the medium during the chondrogenic differentiation of ACH iPSCs. The histology of particles was examined on day 42. **a**, Histological sections of particles were stained with haematoxylin and eosin or Safranin O. Scale bars, 50 μ m. **b**, The area of the Safranin-O-positive region was divided by the total area of the particle. The number of particles examined is indicated at the bottom. The error bars denote the means \pm s.d.



Extended Data Figure 9 | X-ray images of *Fgfr3^{Ach}* and wild-type mice treated with rosuvastatin or vehicle. The images of the mice with lowest and highest weights in each group are shown. The weight (g) of each mouse is indicated at the bottom of each panel. Scale bars, 10 mm.



Extended Data Figure 10 | Organ culture of metatarsal primordal cartilage (a, b), pellet culture of primary chondrocytes (c, d) and culture of primary chondrocytes (e) from *Fgfr3^{Ach}* mice in the presence or absence of lovastatin. **a**, Left: images of cartilage on day 7. Right: mean lengths of the cartilage on day 1 and day 7 ($n = 8$ cartilage samples). **b**, Cartilage on day 7 was treated with BrdU. Left: histological sections were stained with Safranin O and immunostained with BrdU. Right; number of BrdU-positive cells were divided by the total number of cells ($n = 7$ cartilage samples). **c**, Histological sections of pellets cultured for 14 days. The images are representative of three pellets.

d, The results of the real-time RT-PCR expression analysis of pellets cultured for 14 days (*Sox9*, *Col2a1* and *Acan*) and 28 days (*Runx2* and *Col10a1*) ($n = 3$ technical replicates). The data are representative of two independent experiments. **e**, Primary chondrocytes from wild-type and *Fgfr3^{Ach}* mice were cultured in the presence or absence of lovastatin, MG132 or bafilomycin A1, and were subjected to an immunoblot analysis using an anti-FGFR3 antibody. The images are representative of two independent experiments. Error bars denote the means \pm s.d. * $P < 0.5$; ** $P < 0.01$ by the *t*-test. Scale bars, 50 μ m.

Overgrowth Syndrome Associated With a Gain-of-Function Mutation of the Natriuretic Peptide Receptor 2 (*NPR2*) Gene

Kohji Miura,¹ Ok-Hwa Kim,² Hey Ran Lee,³ Noriyuki Namba,¹ Toshimi Michigami,⁴ Won Joon Yoo,³ In Ho Choi,³ Keiichi Ozono,¹ and Tae-Joon Cho^{3*}

¹Department of Pediatrics, Osaka University Graduate School of Medicine, Osaka, Japan

²Department of Radiology, Ajou University Hospital, Suwon, Republic of Korea

³Division of Pediatric Orthopaedics, Seoul National University Children's Hospital, Seoul, Republic of Korea

⁴Department of Bone and Mineral Research, Osaka Medical Centre and Research Institute for Maternal and Child Health, Osaka, Japan

Manuscript Received: 11 March 2013; Manuscript Accepted: 8 August 2013

The signal pathway of the C-type natriuretic (CNP) and its receptor, natriuretic peptide receptor 2 (NPR2) is involved in the longitudinal growth of long bones. Loss of function mutations at NPR2 cause acromesomelic dysplasia, type Maroteaux, while overproduction of CNP by chromosomal translocation and a gain-of-function mutation at NPR2 have been reported to be responsible for an overgrowth syndrome in three cases and one family, respectively. We identified a four-generation family with an overgrowth syndrome characterized by tall stature, macrodactyly of the great toes, scoliosis, coxa valga and slipped capital femoral epiphysis, similar to those previously reported in association with CNP/NPR2 overactivity. The serum level of amino-terminal proCNP was normal in the proband. A novel missense mutation of *NPR2*, c.1462G>C (p.Ala488Pro) was found to cosegregate with the phenotype in this family. In vitro transfection assay of the mutant NPR2 revealed overactivity of the mutant receptor at baseline as well as with the ligand. This overgrowth syndrome caused by a gain-of-function mutation at *NPR2* should be differentiated from Marfan or related syndromes, and may be categorized along with the overgrowth syndrome caused by overproduction of CNP due to its phenotypical similarity as overgrowth CNP/NPR2 signalopathy. © 2013 Wiley Periodicals, Inc.

Key words: tall stature; CNP signal; scoliosis; macrodactyly of the big toe; slipped capital femoral epiphysis

INTRODUCTION

Natriuretic peptides are a family of hormones/paracrine factors regulating blood volume, blood pressure, ventricular hypertrophy, pulmonary hypertension, fat metabolism, and long bone growth [Potter et al., 2006]. They include atrial natriuretic peptide (ANP; OMIM 600296). CNP binds to a homodimeric transmembrane receptor, natriuretic peptide receptor B/guanylate cyclase B (NPR2; OMIM108961) to increase intracellular level of cyclic guanosine monophosphate (cGMP) [Schulz, 2005]. Several lines of evidence

How to Cite this Article:

Miura K, Kim O-H, Lee HR, Namba N, Michigami T, Yoo WJ, Choi IH, Ozono K, Cho T-J. 2014. Overgrowth syndrome associated with a gain-of-function mutation of the natriuretic peptide receptor 2 (NPR2) gene.

Am J Med Genet Part A 164A:156–163.

indicate that CNP-NPR2 signaling plays an important role in endochondral ossification [Yasoda et al., 1998; Teixeira et al., 2008]. Inactivation of CNP-NPR2 signaling resulted in dwarfism in both mouse and human. CNP knock-out mice (*Nppc*^{-/-}) or mice with homozygous loss-of-function mutations in *Npr2* result in undergrowth of the skeletal system [Chusho et al., 2001; Tsuji and Kunieda, 2005]. In humans, an autosomal recessive skeletal dysplasia, acromesomelic dysplasia, type Maroteaux (AMDM) characterized by disproportionately mesomelic shortening of the limbs and severe brachydactyly of the hands and feet is caused by homozygous or compound heterozygous loss-of-function mutations in *NPR2* [Bartels et al., 2004]. On the other hand, chronically elevated plasma level of CNP stimulates skeletal

Kohji Miura and Ok-Hwa Kim contributed equally to this work.

Grant sponsor: Ministry for Health, Welfare and Family Affairs Republic of Korea; Grant number: A080588; Grant sponsor: Ministry of Health, Labour and Welfare of Japan; Grant number: KH20Q007a-1.

*Correspondence to:

Tae-Joon Cho, M.D., Division of Pediatric Orthopaedics, Seoul National University Children's Hospital, 101 Daehang-ro Jongno-gu, Seoul 110-744, Republic of Korea.

E-mail: tjcho@snu.ac.kr

Article first published online in Wiley Online Library (wileyonlinelibrary.com): 20 November 2013

DOI 10.1002/ajmg.a.36218

growth in CNP-overproducing transgenic mice [Kake et al., 2009]. In humans, overproduction of CNP due to a chromosomal translocation causes an overgrowth syndrome [Bocciardi et al., 2007; Moncla et al., 2007]. A three-generation Japanese family was recently reported, with an overgrowth syndrome caused by a gain-of-function mutation in *NPR2* [Miura et al., 2012]. We identified and report a four-generation Korean family with similar phenotype and a novel gain-of-function mutation in *NPR2*.

MATERIALS AND METHODS

Clinical Report

This study was approved by the ethics committee at Seoul National University Hospital, and written informed consent was obtained from the proband and family members. An 8-year-old boy visited orthopedic clinic for awkward ambulation and ankle pain on walking. He was a product of normal full term pregnancy with a birth weight 3.2 kg and height 50 cm ($z = -0.04$). His macrodactyly of the big toe was observed since birth, something familiar to his family (Figs. 1 and 2). Developmental milestones were within normal limits. He was recognized as bigger than his age group after the neonatal period. On physical examination at 8 years of age, the height was 145 cm ($z = +3.67$), and weight was 40 kg (>97 th centile). He had Marfanoid habitus and arachnodactyly. Neurologic examination was free of abnormal findings. At age 12 years, an unstable slipped capital femoral epiphysis (SCFE) developed on the left hip. Physical examination at this age revealed height 183 cm ($z = +5.19$), weight 71 kg (>97 th centile), BMI 21.2 kg/m². He showed long and slender fingers and toes, the hallux being remarkably longer than the other toes, ankle valgus deformity, and scoliosis. No anomalies of cardiac valves or the aorta were found on echocardiogram. Blood pressure was within normal limits. No abnormality was observed in ophthalmic and otologic examinations. Hematological, biochemical and endocrinological

values including insulin-like growth factor-I (IGF-I) were within normal ranges. However, bone formation and resorption markers were increased—osteocalcin, 118 ng/ml (reference range, 8–50); urinary cross-linked N-telopeptide of type I collagen, 969 BCE/mM creatinine (reference range, 21–83). Bone mineral density of L2–4 as measure by dual energy X-ray absorptiometry (Lunar Prodigy Advance, GE Healthcare, Waukesha, WI) was 0.791g/cm² ($z = -0.3$). Considering the tall stature of this patient, this BMD result may suggest presence of more severe osteopenia. Radiological survey of the skeleton showed coxa valga deformity of the femora, slipped capital femoral epiphysis, and lumbar scoliosis (Fig. 3). Arachnodactyly of all fingers and toes; of these, disproportionately long and large great toes were observed. Investigation of the family history revealed a four-generation family with 11 family members including the proband that could be considered to have the same phenotype. Five of 11 affected members were examined. They were characterized by tall stature (exceeded +4 SD compared to age matched control height of Korean population) and markedly long big toes. All of them showed coxa valga deformity with epiphyseal dysplasia of the femoral capital epiphyses and two had SCFE (Fig. 4). Three of them had lumbar scoliosis. The vertebral bodies were tall and showing endplate irregularities and narrowing of the intervertebral disc spaces in four of them. As seen in the clinical phenotype, radiograph of the feet showed extremely elongated metatarsals and assorted phalanges of the great toe symmetrically. The hands of all affected individuals showed arachnodactyly without elongation of specific fingers.

Mutation Analysis

Genomic DNA was extracted from the circulating leukocytes from the proband and family members available (Fig. 1). All the exons of *CNP*, *NPR2*, Natriuretic peptide receptor C (*NPR3*; MIM108962), and fibroblast growth factor receptor 3 (*FGFR3*; MIM134934) were

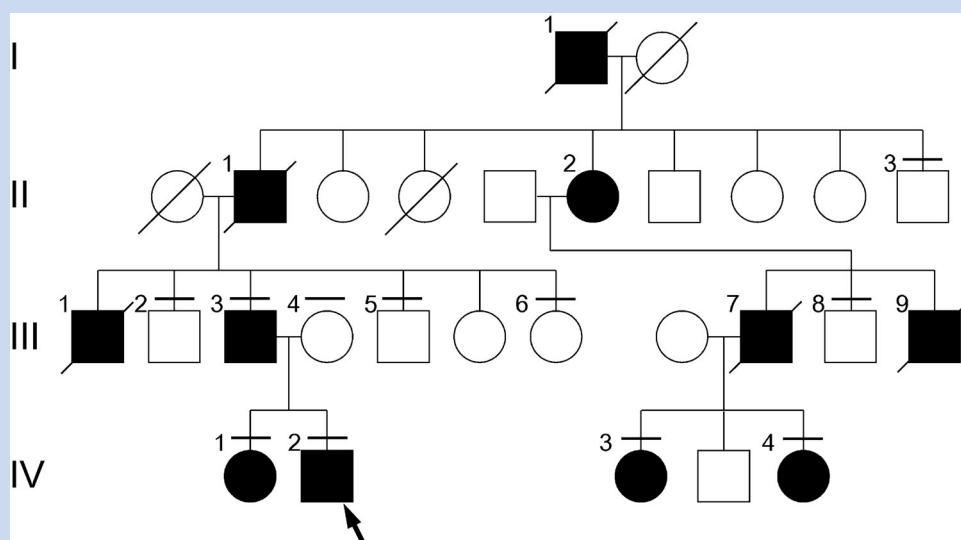


FIG. 1. Pedigree of the family. There are several father-to-son transmissions of the phenotype, revealing autosomal dominant inheritance pattern. Transverse bars above the circles or rectangles denote those who underwent mutation study. An arrow indicates the proband.



FIG. 2. Photographs of the feet of the affected family members. A: III-3, [B] IV-1, [C] IV-2, [D] IV-3, [E] IV-4. Patients IV-3 and IV-4 show relatively mild macrodactyly of the big toes as compared with the others.

amplified using specific primers [Miura et al., 2012] flanking the intron–exon boundaries according to published human genomic DNA sequences (UCSC genome browser: uc002vsl.1 at chromosome 2, 232498379–232499203; uc003zyd.1 at chromosome 9, 35782406–35799728; uc003jyv.2 at chromosome 5, 32711665–32787252; uc003gds.2 at chromosome 4, 1764337–1780396, respectively). Polymerase chain reaction (PCR) products was sequenced using a Big Dye terminator cycle sequencing kit (version 3.1; Applied Biosystems, Foster City, CA) and an ABI 3130 automated sequencer (Applied Biosystems).

Measurement of Serum Amino-Terminal (NT) proCNP Concentrations

Serum of IV-2 and III-3 were separated and collected, and NT-proCNP was assayed using an enzyme immunoassay (BIOMED-ICA, Vienna, Austria) according to the instructions provided. As a control, samples from eight healthy Japanese teenager boys and five women were also measured.

In Vitro Transfection Assay of Mutant NPR2

The pcDNA3.1(+)/hemagglutinin (HA)-tagged human NPR2 wild-type vector (HA-WT) was a gift from Dr. Yoshihiro Ogawa (Tokyo Medical and Dental University, Japan) [Hachiya et al., 2007]. The construct encoding the mutant p.Ala488Pro,

pcDNA3.1(+)/HA-human NPR-2 Ala488Pro (HA-Ala488Pro), was generated by PCR-based mutagenesis using HA-WT as the template, and primers containing the nucleotide change. All vector constructs were verified by bidirectional DNA sequencing.

HEK293A cells at confluence were transfected with empty vector containing green fluorescent protein (GFP), HA-WT, and HA-Ala488Pro using the liposomal transfection reagent FuGENE6 (Reagent: DNA = 3 μ l: 0.5 μ g, Roche, Indianapolis, IN, 12-well plate), according to the manufacturer's instructions. In 48 hr, cell lysate was harvested and immunoblot was performed to compare the expression of transfected genes, using a mouse monoclonal antibody against HA-tag (6E2, 1:1,000; Cell Signaling Technology, Boston, MA) as the primary antibody. As an internal control, β -actin in each sample was detected with a monoclonal anti- β -actin antibody (1:5,000; SIGMA-ALDRICH, Saint Louis, MO).

Transfected cells were serum-starved for 24 hr before the cGMP assay and then incubated at 37°C with 5% CO₂ in DMEM containing 0.5 mM IBMX (3-isobutyl-1-methylxanthine) (Wako, Osaka, Japan) for 10 min. The cells were next treated with vehicle (water) or 1 \times 10⁻⁷ M CNP-22 (Biochem Life Sciences, New Delhi, India) and incubated for another 10 min. The reaction was terminated with 300 μ l of 0.1 M HCl, and the cGMP concentration was measured by a competitive enzyme immunoassay (Cayman Chemical, Ann Arbor, MI). Results are presented as the mean \pm SD. Student's *t* test was used for statistical analyses.



FIG. 3. Skeletal survey of the proband at age 12 years. A,B: Anteroposterior and lateral spine show lumbar scoliosis, slightly tall vertebral bodies with irregular end-plates, and narrowing of the intervertebral disc spaces. C: Pelvis shows coxa valga deformity and slipped femoral capital epiphysis on the left hip. D: Lower extremity demonstrates long and slender long bones with thin cortices. Mild inward bowing of the tibial and fibular diaphysis and ankle valgus deformity are noted. E: Feet show exceedingly long and large metatarsals and phalanges of the great toes symmetrically. F: Hands show overall arachnodactyly without specific digit elongation. Carpal bone age is advanced, measuring approximately 14 years of age.

RESULTS

Identification of a Novel Missense Mutation p.Ala488Pro in *NPR2*

On screening the sequences of exons of *CNP*, *NPR2*, *NPR3*, and *FGFR3* in the proband and family members as depicted on Figure 1, we identified a novel heterozygous sequence variation c. 1462G>C at *NPR2* in those who shared the similar phenotype (III-3, IV-1, IV-2, IV-3, and IV-4), but not in the remaining unaffected family members. The sequence variation eliminates an *NheI* cleavage site. PCR product of wild type containing this site (484 bp) would be cut into 95 and 389 bp fragments. Hence, these PCR products from all the patients tested were incubated with *NheI* (New England BioLabs, Ipswich, MA) overnight and run on an agarose gel to confirm the presence of this sequence variation. It showed that this sequence variation perfectly co-segregated with the phenotype in this family. It was predicted to substitute alanine for proline (p. Ala488Pro). This variant was not registered in the dbSNP (build 137) (<http://www.ncbi.nlm.nih.gov/projects/SNP/>) nor in the

NHLBI Exome Sequencing Project (ESP) (<http://evs.gs.washington.edu/EVS/>). It was not found in 400 alleles from healthy Korean or Japanese controls, either. Amino acid Ala488 is located in a highly conserved region of the juxtamembranous cytoplasmic domain of *NPR2* and is conserved across species (Fig. 5). No mutations were found in *CNP*, *NPR3*, or *FGFR3*.

CNP Was Not Overproduced in the Proband

Serum NT-proCNP levels of the proband (IV-2) and his mother were measured 9.68 and 2.65 pmol/L, respectively. Those of eight Japanese teenager boys of age ranging from 12 to 14 years averaged 6.0 ± 3.4 pmol/L (mean \pm standard deviation), and of five Japanese female adults of age ranging from 32 to 48 averaged 4.0 ± 0.9 pmol/L (unpublished data).

p.Ala488Pro Is a Gain-of-Function Mutation

To investigate the pathogenic significance of the p.Ala488Pro mutation, an in vitro functional assay was performed. HEK293A

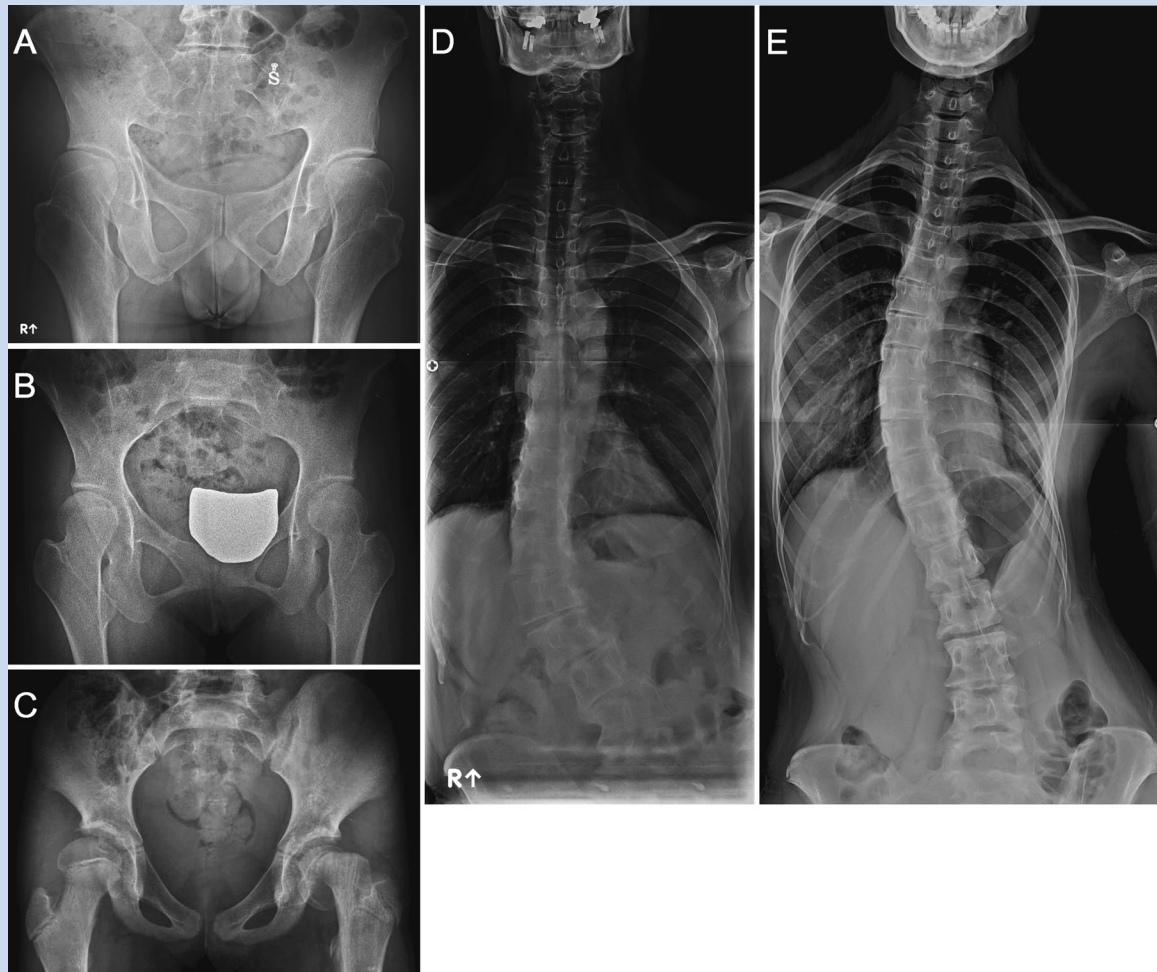


FIG. 4. Radiographs of the pelvis and spine of the other affected family members. Marked coxa valga deformity and residual valgus slipped capital femoral epiphysis are seen in Patients III-3 (A) and IV-1 (B). C: Coxa valga deformity and unstable aggravation of the slipped capital femoral epiphysis at the left hip are seen in Patient IV-3 at age 11 years. D: Patient III-3 and (E) Patient IV-1 show thoracolumbar scoliosis. The vertebral bodies are tall and narrowing of the disc spaces is noted.

cells were transfected with the GFP, HA-WT, and HA-Ala488Pro. The Western blot analysis using anti-HA antibody confirmed that HA-WT and HA-Ala488Pro were expressed at comparable levels, with an approximate molecular size of 120 kDa (Fig. 6A). cGMP production in the cells expressing HA-WT, and HA-Ala488Pro was also examined. cGMP was produced in Ala488Pro-expressing cells, even in the absence of CNP, while no production was observed in HA-WT-expressing cells. Treatment with CNP-22 at a dose of 1×10^{-7} M increased intracellular cGMP levels with concentrations significantly higher in HA-Ala488Pro than in HA-WT-expressing cells (Fig. 6B). These results indicate that p.Ala488Pro is a gain-of-function type mutation.

DISCUSSION

The CNP/NPR2 signal pathway is involved in the longitudinal growth of skeletal system [Yasoda et al., 1998; Chusho et al., 2001;

Bartels et al., 2004; Tsuji and Kunieda, 2005; Bocciardi et al., 2007; Moncla et al., 2007; Teixeira et al., 2008; Kake et al., 2009]. Miura et al. [2012] reported a Japanese family with an overgrowth syndrome caused by a gain-of-function mutation at *NPR2*. The current study reports a second family showing a similar phenotype inherited as an autosomal dominant trait. The affected family members harbor a novel gain-of-function mutation at *NPR2*, c.1462G>C (p.Ala488Pro).

The mutation of the current family is located at a topological domain between transmembrane and protein kinase domainsrot[UniProtKB[Internet]], while the previously reported gain-of-function mutation was at the guanylate cyclase domain [Miura et al., 2012]. Although the current mutation does not exist at the guanylate cyclase domain, it must bring conformational change at the 3D structure of guanylate cyclase domain to enhance its enzymatic activity with or without binding the ligand.

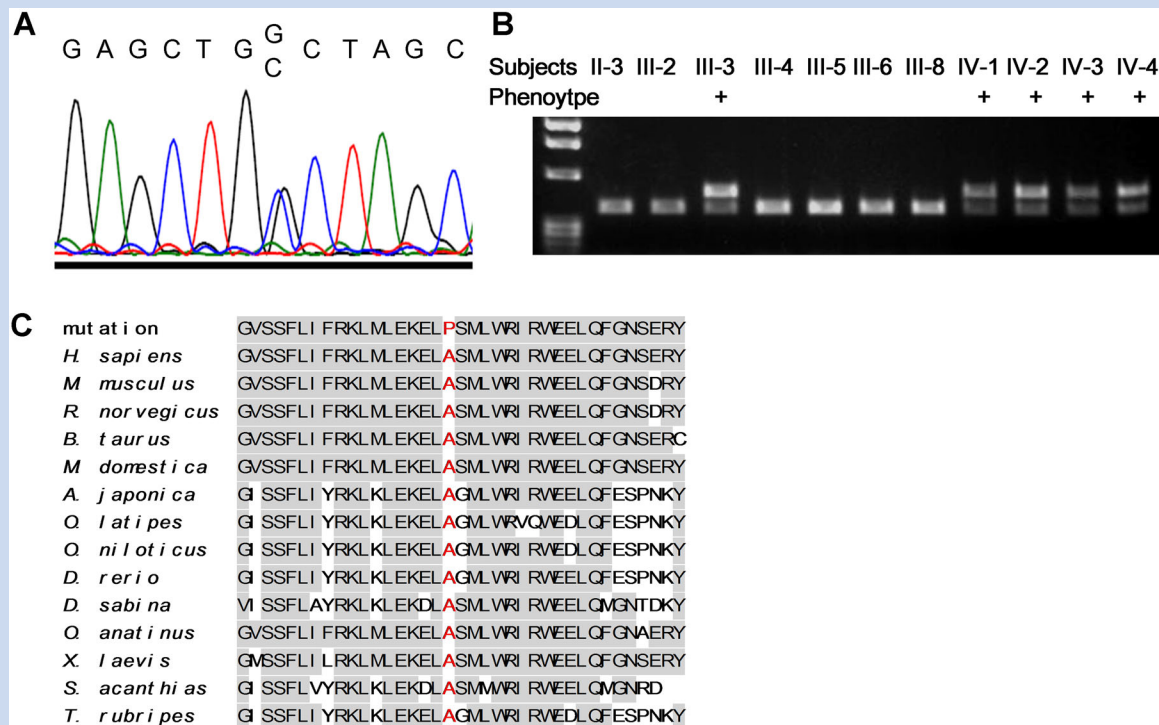


FIG. 5. Identification of the *Npr2* mutation. Sanger sequencing of the *NPR2* revealed a novel G → C missense mutation at nucleotide +1,462 creates a substitution, proline for alanine, at codon 488 in a heterozygous state. Among the subjects tested, this mutation was present in all the patients having the phenotype, and absent in all those who did not (A). This mutation eliminated the cleavage site of *NheI*, producing two bands on gel electrophoresis when treated with *NheI* (B). Amino acid alignment of *NPR2* among various species. Alanine at codon 488 is located in a highly conserved cytoplasmic region between the transmembrane and protein kinase domains of *NPR2* (C).

NPR2 is an interesting example of phenotypes contrasting between gain-of-function versus loss-of-function mutations at a gene encoding a receptor protein. Homozygous or compound heterozygous loss-of-function mutations of *NPR2* in humans cause a specific skeletal dysplasia, AMDM, characterized by marked short stature as well as short fingers and toes. The overgrowth syndrome by gain-of-function mutation seems to have phenotype opposite to that of AMDM. It is also interesting to note that the increased *NPR2* activity did not suppress CNP production, maintaining its serum level within normal limit. The same unsuppressed CNP production was also observed in the previous cases of gain-of-function mutation at *NPR2* [Miura et al., 2012], suggesting lack of feedback loop between the *NPR2* activity and CNP production.

This family has noticed 11 affected members by tall stature and long big toes through four generations. Neither macrodactyly of the big toe and ankle valgus deformity nor scoliosis and residual proximal femoral deformity of SCFE interferes with their daily living activities. One of them (IV-3) had even played basketball in a high school varsity team. However, development of unstable SCFE threatened function of the hip joint, and the proband was required to have major hip surgeries. SCFE is a chronic, gradual displacement of the femoral head at the proximal femoral physis. It may remain silent until physeal closure, and end up with residual deformity at the proximal femur as in the Patients III-3 and IV-

1 (Fig. 4). However, in some cases, the SCFE could aggravate suddenly, resulting in unstable separation of the femoral head as in Patients IV-2 and IV-4 (Figs. 3 and 4), which is an orthopedic emergency requiring surgical intervention to stabilize the femoral head and to preserve its viability. Hence, once this disease entity is recognized, the patient should have an orthopedic consultation to monitor development and progress of SCFE, which was exclusively harbored by the affected members in this family. It is noteworthy that a residual deformity of silent SCFE showed posterolateral displacement of the femoral head (Fig. 4), a rare subtype of SCFE [Loder et al., 2006]. Scoliosis did not require any intervention in these affected family members. Macrodactyly of the big toes were not complained of in shoe fitting or cosmesis in the proband and affected family members.

The characteristic clinical and radiological findings make it a specific, discernible clinical disease entity, which can be differentiated from Marfan or other related syndromes. However, it is very similar to a phenotype caused by chromosomal translocation of 2q37 and subsequent CNP overproduction [Boccardi et al., 2007; Moncla et al., 2007]. Hence, CNP overproduction and its receptor gene gain-of-function mutation may be categorized into a disease entity, that is, overgrowth CNP/*NPR2* signalopathy, which should be included in differential diagnosis of the overgrowth syndrome.

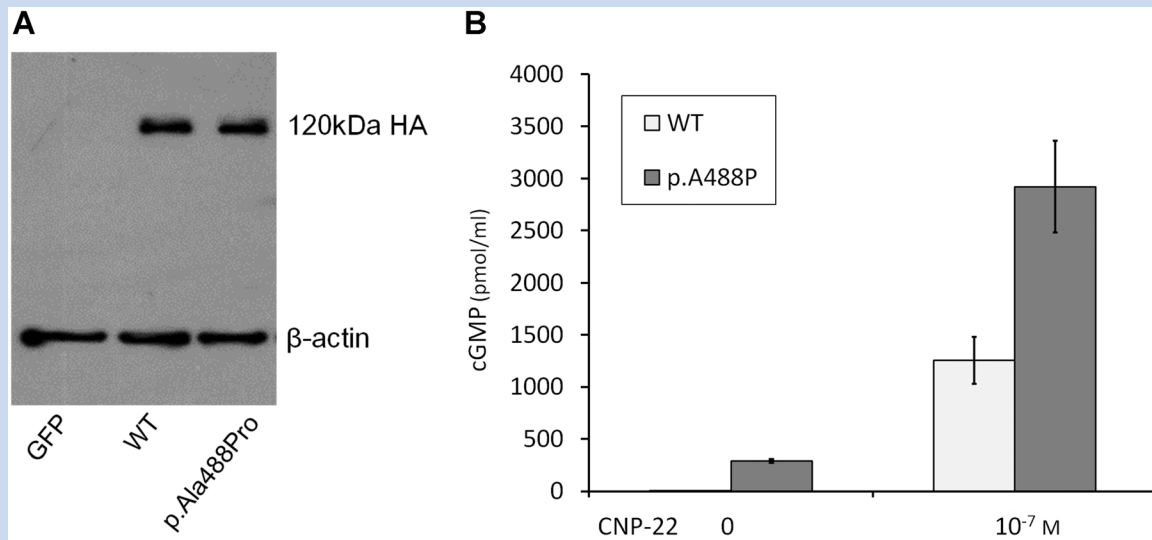


FIG. 6. NPR2 mutation of p.Ala488Pro is a gain-of-function mutation. **A:** Western blot analysis confirmed the comparable expression of HA-WT (WT) and HA-Ala488Pro. As an internal control, β -actin in each sample was detected with anti- β -actin antibody. **B:** Increased cGMP production in the HEK293A cells transfected with the p.Ala488Pro mutant compared to that in wild-type cells (WT). Forty-eight hours after the transfection, the cells were serum-starved for 24 hr, and then treated with the indicated concentrations of CNP-22 for 10 min, before cGMP production was assayed. Results are presented as the mean \pm SD (N = 3, *P < 0.05).

In summary, we report on a family with an overgrowth syndrome inherited as autosomal dominant trait, which is caused by a gain-of-function mutation at *NPR2*. This is a distinct clinical entity that can be differentiated from other overgrowth syndromes by its clinical and radiological manifestations. Recognition of this specific disease entity will lead to targeted molecular study for confirmation, and will alert the clinician for potentially serious complication such as unstable SCFE.

ACKNOWLEDGMENTS

This study was supported in part by a grant from Ministry for Health, Welfare and Family Affairs, Republic of Korea (A080588) and in part by Grants-in-aid from the Ministry of Health, Labour and Welfare of Japan (KH20Q007a-1).

REFERENCES

- Bartels CF, Bukulmez H, Padayatti P, Rhee DK, van Ravenswaaij-Arts C, Pauli RM, Mundlos S, Chitayat D, Shih LY, Al-Gazali LI, Kant S, Cole T, Morton J, Cormier-Daire V, Faivre L, Lees M, Kirk J, Mortier GR, Leroy J, Zabel B, Kim CA, Crow Y, Braverman NE, van den Akker F, Warman ML. 2004. Mutations in the transmembrane natriuretic peptide receptor NPR-B impair skeletal growth and cause acromesomelic dysplasia, type Maroteaux. *Am J Hum Genet* 75:27–34.
- Boccardi R, Giorda R, Buttgerit J, Gimelli S, Divizia MT, Beri S, Garofalo S, Tavella S, Lerone M, Zuffardi O, Bader M, Ravazzolo R, Gimelli G. 2007. Overexpression of the C-type natriuretic peptide (CNP) is associated with overgrowth and bone anomalies in an individual with balanced t(2;7) translocation. *Hum Mutat* 28:724–731.
- Chusho H, Tamura N, Ogawa Y, Yasoda A, Suda M, Miyazawa T, Nakamura K, Nakao K, Kurihara T, Komatsu Y, Itoh H, Tanaka K, Saito Y, Katsuki M. 2001. Dwarfism and early death in mice lacking C-type natriuretic peptide. *Proc Natl Acad Sci USA* 98:4016–4021.
- Hachiya R, Ohashi Y, Kamei Y, Suganami T, Mochizuki H, Mitsui N, Saitoh M, Sakuragi M, Nishimura G, Ohashi H, Hasegawa T, Ogawa Y. 2007. Intact kinase homology domain of natriuretic peptide receptor-B is essential for skeletal development. *J Clin Endocrinol Metab* 92:4009–4014.
- Take T, Kitamura H, Adachi Y, Yoshioka T, Watanabe T, Matsushita H, Fujii T, Kondo E, Tachibe T, Kawase Y, Jishage K, Yasoda A, Mukoyama M, Nakao K. 2009. Chronically elevated plasma C-type natriuretic peptide level stimulates skeletal growth in transgenic mice. *Am J Physiol Endocrinol Metab* 297:E1339–E1348.
- Loder RT, O'Donnell PW, Didelot WP, Kayes KJ. 2006. Valgus slipped capital femoral epiphysis. *J Pediatr Orthop* 26:594–600.
- Miura K, Namba N, Fujiwara M, Ohata Y, Ishida H, Kitaoka T, Kubota T, Hirai H, Higuchi C, Tsumaki N, Yoshikawa H, Sakai N, Michigami T, Ozono K. 2012. An overgrowth disorder associated with excessive production of cGMP due to a gain-of-function mutation of the natriuretic peptide receptor 2 gene. *PLoS ONE* 7:e42180.
- Moncla A, Missirian C, Cacciagli P, Balzamo E, Legeai-Mallet L, Jouve JL, Chabrol B, Le Merrer M, Plessis G, Villard L, Philip N. 2007. A cluster of translocation breakpoints in 2q37 is associated with overexpression of NPPC in patients with a similar overgrowth phenotype. *Hum Mutat* 28:1183–1188.
- Potter LR, Abbey-Hosch S, Dickey DM. 2006. Natriuretic peptides, their receptors, and cyclic guanosine monophosphate-dependent signaling functions. *Endocr Rev* 27:47–72.

- Schulz S. 2005. C-type natriuretic peptide and guanylyl cyclase B receptor. *Peptides* 26:1024–1034.
- Teixeira CC, Agoston H, Beier F. 2008. Nitric oxide, C-type natriuretic peptide and cGMP as regulators of endochondral ossification. *Dev Biol* 319:171–178.
- Tsuji T, Kunieda T. 2005. A loss-of-function mutation in natriuretic peptide receptor 2 (Npr2) gene is responsible for disproportionate dwarfism in *cn/cn* mouse. *J Biol Chem* 280:14288–14292.
- UniProtKB[Internet]. UniProt Consortium (EMBL-EBI, PIR, and SIB) [2002]. P20594(ANPRB_HUMAN) [updated January 9, 2013 Version 151, Cited January 12, 2013]. Available from <http://www.uniprot.org/uniprot/P20594>
- Yasoda A, Ogawa Y, Suda M, Tamura N, Mori K, Sakuma Y, Chusho H, Shiota K, Tanaka K, Nakao K. 1998. Natriuretic peptide regulation of endochondral ossification. Evidence for possible roles of the C-type natriuretic peptide/guanylyl cyclase-B pathway. *J Biol Chem* 273:11695–11700.

A case of severe proximal focal femoral deficiency with overlapping phenotypes of Al-Awadi-Raas-Rothschild syndrome and Fuhrmann syndrome

Masaki Matsushita · Hiroshi Kitoh · Kenichi Mishima · Yoshihiro Nishida · Naoki Ishiguro

Received: 6 January 2014 / Revised: 2 April 2014 / Accepted: 23 April 2014
© Springer-Verlag Berlin Heidelberg 2014

Abstract Proximal focal femoral deficiency (PFFD) is a heterogeneous disorder characterized by various degrees of femoral deficiencies and associated anomalies of the pelvis and lower limbs. The etiology of the disease has not been determined. We report on a 3-year-old boy with severe PFFD, who showed almost completely absent femora and fibulae, malformed pelvis and ectrodactyly of the left foot. These features were partially overlapped with those of Al-Awadi-Raas-Rothschild syndrome or Fuhrmann syndrome, both of which are caused by *WNT7A* mutations. Molecular analysis of our case, however, demonstrated no disease-causing mutations in the *WNT7A* gene.

Keywords Proximal focal femoral deficiency · Al-Awadi-Raas-Rothschild syndrome · Fuhrmann syndrome · *WNT7A* · Molecular analysis · Radiography · Child

Introduction

Proximal focal femoral deficiency (PFFD) is a rare congenital anomaly of the pelvis and proximal femur with several degrees of shortening of the involved lower limb. The condition may be unilateral or bilateral and is often associated with other congenital anomalies. The cause of PFFD is uncertain, but several etiological factors have been suggested, including poor diabetic control, exposure to drugs (thalidomide), viral infections, radiation, focal ischemia and trauma between the 4th and 8th weeks of gestation [1]. The Aitken classification is

the most widely used system for classifying PFFD based on the radiographic appearance ranking from a benign form (Type A) to a severe form (Type D) according to the extent of femoral deficiency [2]. In Type D, the femoral head and acetabulum are absent, and the shaft of the femur is extremely short or absent. There is a phenotypic similarity between the cases with Type D PFFD and those with Al-Awadi-Raas-Rothschild syndrome or Fuhrmann syndrome. These two syndromes have recently been reported to be associated with the *WNT7A* mutations. Both syndromes share similar clinical features, but the phenotype in Fuhrmann syndrome is less severe [3].

Here, we report on a 3-year-old boy who showed severe malformations of the pelvis and bilateral lower limbs without associated severe upper limbs anomalies. The findings of our case were similar to those of Fuhrmann syndrome rather than those of Al-Awadi-Raas-Rothschild syndrome. Molecular analyses, however, demonstrated negative for the *WNT7A* mutations in the present case.

Case report

The proband, a Japanese boy, was the first child born to healthy, nonconsanguineous parents. His mother did not suffer from diabetes mellitus. His younger brother was normal. Family history of skeletal dysplasia was negative. Bilateral femoral deficiencies were found at his second trimester. He was delivered at 36 weeks of gestation with a birth weight of 1,884 g (−1.8 SD for gestational age) and a height of 36 cm (−4.2 SD for gestational age) by Cesarean section. The Apgar score was 6 at 1 min.

He was referred to us at age 12 days for severe malformations of bilateral lower limbs. On physical examinations, bilateral thighs were extremely short so that the lower

M. Matsushita · H. Kitoh (✉) · K. Mishima · Y. Nishida · N. Ishiguro
Department of Orthopaedic Surgery,
Nagoya University Graduate School of Medicine,
65 Tsurumai, Showa-ku, Nagoya, Aichi 466-8550, Japan
e-mail: hkitoh@med.nagoya-u.ac.jp

legs seemed to be connected with the pelvis. There was a varus deformity in the right foot associated with syndactyly of the third and fourth toes and a valgus deformity in the left foot (Fig. 1). He showed flexion contracture of the proximal interphalangeal joint in his left middle and ring fingers. Facial appearance seemed to be normal. Radiographic examinations at the age of 4 months revealed hypoplastic ilia, absent acetabula, and malformed pubic and ischial bones. The left femur was absent, while there was a rudimentary distal femur in the right. Bilateral fibulae were also absent. Bilateral tibiae were slender and there was a large round epiphysis in the left proximal tibia (Fig. 2). The tarsal bones were unremarkable but an ectrodactyly of the left foot was observed (Fig. 2). The spine, thorax and upper limbs were unremarkable. Chromosomal analysis was also normal.

Extraskelletal abnormalities included a left inguinal hernia that was surgically treated at the age of 2 months and an abdominal pressure-induced incontinence with no association of hydronephrosis and ureteral dilatation. Magnetic resonance imaging (MRI) of the whole spine showed no abnormalities. His cognitive development was normal. Varus deformity of his right foot was treated with serial casting and subsequent bracing, while his left valgus foot was spontaneously corrected. Flexion contracture of his left fingers was healed by an application of splinting. He could walk with two Lofstrand crutches at 3 years old. He was diagnosed to have PFFD Type D but his clinical and radiographic features were partially overlapped with those of Al-Awadi-Raas-Rothschild syndrome or Fuhrmann syndrome (Table 1).

After informed consent was obtained from his family, genomic DNA from peripheral blood of the proband was extracted using the QIAampDNABlood Midi kit (Qiagen Inc., Valencia, CA). Direct sequencing of the complete coding regions and exon-intron boundaries of the *WNT7A* gene was performed using the CEQ 8000 Sequencer (Beckman Coulter, Fullerton, CA) according to the manufacturer's instructions. The primers used for amplification and sequencing of the



Fig. 1 A clinical photo of the lower limbs and trunk at the age of 5 months. Marked shortening of bilateral lower limbs, varus foot with syndactyly of the third and fourth toes in the right, and valgus foot in the left are demonstrated

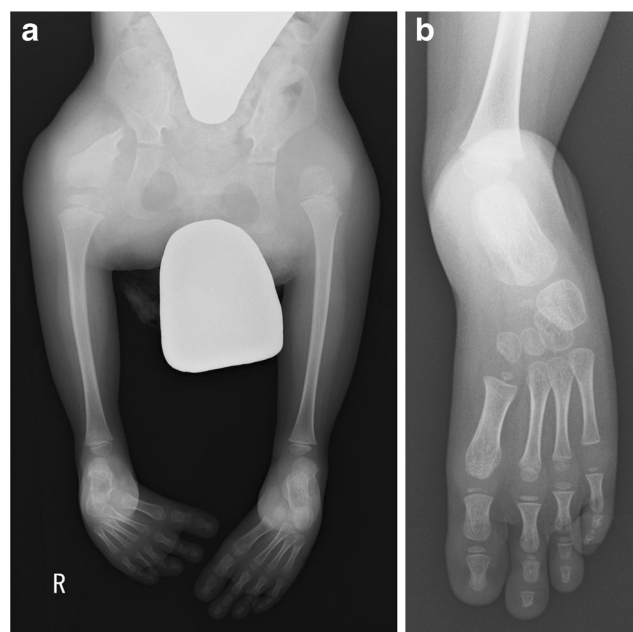


Fig. 2 Anteroposterior radiographs at the age of 3.5 years. **a** The pelvis and lower limbs demonstrate small and narrow ilia, malformed ischiopubic bones, deficient acetabula, complete absence of the left femur, rudimentary right femur, absent fibulae and slender tibiae with ball-shaped large epiphysis of the left tibia. **b** The left foot demonstrates four pairs of metatarsals and phalanges without deformity of tarsal bones

WNT7A gene were described previously [4]. Two reported heterozygous variants, c.315G>A and c.459 T>C in exon 3 of the *WNT7A*, both of which are known synonymous single-nucleotide polymorphisms (SNPs), were found in the proband.

Table 1 Comparison of phenotypes among Al-Awadi-Raas-Rothschild syndrome and Fuhrmann syndrome and present case

Al-Awadi-Raas-Rothschild syndrome and Fuhrmann syndrome		Present case syndrome
Facial dysmorphism	±	–
Thorax anomaly	±	–
Upper limb anomaly	+	±
Urinary tract anomaly	±	±
Pelvis dysplasia	+	+
Lower limbs		
Aplastic/hypoplastic femur	+	+
Aplastic/hypoplastic fibula	+	+
Aplastic/hypoplastic tibia	+	–
Bilateral involvement	+	+
Stick-like appendage	+	–
Feet		
Ectrodactyly	+	+
Hypoplastic nails	+	–

+positive, ± occasionally positive or suspected, – negative

Discussion

Congenital femoral deficiencies can be seen in a variety of diseases including PFFD, femoral hypoplasia-unusual facies syndrome [5], femur-fibula-ulna syndrome [6], Al-Awadi-Raas-Rothschild syndrome and Fuhrmann syndrome [7]. The absence of craniofacial anomalies and upper limb malformations distinguishes our case from femoral hypoplasia-unusual facies syndrome and femur-fibula-ulna syndrome. Al-Awadi-Raas-Rothschild syndrome and Fuhrmann syndrome, both of which are known to be associated with the *WNT7A* mutations, have similar clinical features including limb and pelvic deficiencies and abnormal genitalia. Generally, more severe defects of the upper limbs are seen in Al-Awadi-Raas-Rothschild syndrome than in Fuhrmann syndrome. There is complete and partial loss of *WNT7A* function in these two syndromes, respectively [3]. *WNT7A* molecules regulate the dorsal-ventral and anterior-posterior axes and outgrowth of limbs. The anterior-posterior axis determines the development of fibulo-tibial structures in the foot/leg. Absent femora and fibulae, ectrodactyly of the foot and pelvic dysplasia found in the present case seemed to result from the impairment of anterior-posterior patterning and outgrowth of limbs. Our case, however, only showed minimal upper limb abnormalities (mild contracture of fingers) and lacked the phenotypes of dorsal-ventral axis deficiency such as hypoplastic nails. Negative *WNT7A* mutations could differentiate our PFFD case from Al-Awadi-Raas-Rothschild syndrome or Fuhrmann syndrome, although minor deletions or duplications within the *WNT7A* gene could not be ruled out in the present study.

Kantaputra and Tanpaiboon [8] reported on a 3-year-old Thai boy with severe malformations of the upper and lower limbs, pelvis and genital organs. The majority of findings overlapped with those of Al-Awadi-Raas-Rothschild syndrome, but the presence of humeroulnar synostosis and predominant radial ray abnormalities and absence of nail dysplasia were different features from typical cases of Al-Awadi-

Raas-Rothschild syndrome [8]. Except the upper limb deficiencies, their case had similar phenotypes to our case including hypoplastic ilium, poorly formed acetabula, absent femora and fibulae, slender tibiae with malformed proximal epiphysis and normal facial appearance. These cases may be included in the entity of diseases in the limb-pelvis developmental field.

In conclusion, we present a case of severe PFFD with some overlapping phenotypes of Al-Awadi-Raas-Rothschild syndrome and Fuhrmann syndrome without associated *WNT7A* mutation. Further molecular studies will be needed to determine the basic defects of our case.

Conflicts of interest None.

References

1. Epps CH Jr (1983) Proximal femoral focal deficiency. *J Bone Joint Surg Am* 65:867–870
2. Aitken GT (1969) In: Aitken GT (ed) Proximal femoral focal deficiency: definition, classification, and management. National Academy of Sciences, Washington, pp 1–22
3. Woods CG, Stricker S, Seemann P et al (2006) Mutations in *WNT7A* cause a range of limb malformations, including Fuhrmann syndrome and Al-Awadi/Raas-Rothschild/Schinzel phocomelia syndrome. *Am J Hum Genet* 79:402–408
4. Shyy W, Dietz F, Dobbs MB et al (2009) Evaluation of *CAND2* and *WNT7a* as candidate genes for congenital idiopathic clubfoot. *Clin Orthop Relat Res* 467:1201–1205
5. Daentl DL, Smith DW, Scott CI et al (1975) Femoral hypoplasia-unusual facies syndrome. *J Pediatr* 86:107–111
6. Lenz W, Zygulska M, Horst J (1993) FFU complex: an analysis of 491 cases. *Hum Genet* 91:347–356
7. AlQattan MM, AlAbdulkareem I, Ballow M et al (2013) A report of two cases of Al-Awadi Raas-Rothschild syndrome (AARRS) supporting that “apparent” Phocomelia differentiates AARRS from Schinzel Phocomelia syndrome (SPS). *Gene* 527:371–375
8. Kantaputra PN, Tanpaiboon P (2005) A newly recognized syndrome involving limbs, pelvis, and genital organs or a variant of Al-Awadi/Raas-Rothschild syndrome? *Am J Med Genet A* 132:63–67

RESEARCH

Open Access

Japanese founder duplications/triplications involving *BHLHA9* are associated with split-hand/foot malformation with or without long bone deficiency and Gollop-Wolfgang complex

Eiko Nagata^{1†}, Hiroki Kano^{2†}, Fumiko Kato¹, Rie Yamaguchi¹, Shinichi Nakashima¹, Shinichiro Takayama³, Rika Kosaki⁴, Hidefumi Tonoki⁵, Seiji Mizuno⁶, Satoshi Watanabe⁷, Koh-ichiro Yoshiura⁷, Tomoki Kosho⁸, Tomonobu Hasegawa⁹, Mamori Kimizuka¹⁰, Atsushi Suzuki¹¹, Kenji Shimizu¹¹, Hirofumi Ohashi¹¹, Nobuhiko Haga¹², Hironao Numabe¹³, Emiko Horii¹⁴, Toshiro Nagai¹⁵, Hiroshi Yoshihashi¹⁶, Gen Nishimura¹⁷, Tatsushi Toda¹⁸, Shuji Takada¹⁹, Shigetoshi Yokoyama^{19,22}, Hiroshi Asahara^{19,20}, Shinichiro Sano^{1,21}, Maki Fukami²¹, Shiro Ikegawa² and Tsutomu Ogata^{1*}

Abstract

Background: Limb malformations are rare disorders with high genetic heterogeneity. Although multiple genes/loci have been identified in limb malformations, underlying genetic factors still remain to be determined in most patients.

Methods: This study consisted of 51 Japanese families with split-hand/foot malformation (SHFM), SHFM with long bone deficiency (SHFLD) usually affecting the tibia, or Gollop-Wolfgang complex (GWC) characterized by SHFM and femoral bifurcation. Genetic studies included genomewide array comparative genomic hybridization and exome sequencing, together with standard molecular analyses.

Results: We identified duplications/triplications of a 210,050 bp segment containing *BHLHA9* in 29 SHFM patients, 11 SHFLD patients, two GWC patients, and 22 clinically normal relatives from 27 of the 51 families examined, as well as in 2 of 1,000 Japanese controls. Families with SHFLD- and/or GWC-positive patients were more frequent in triplications than in duplications. The fusion point was identical in all the duplications/triplications and was associated with a 4 bp microhomology. There was no sequence homology around the two breakpoints, whereas rearrangement-associated motifs were abundant around one breakpoint. The rs3951819-D17S1174 haplotype patterns were variable on the duplicated/triplicated segments. No discernible genetic alteration specific to patients was detected within or around *BHLHA9*, in the known causative SHFM genes, or in the exome.

(Continued on next page)

* Correspondence: tomogata@hama-med.ac.jp

†Equal contributors

¹Department of Pediatrics, Hamamatsu University School of Medicine, Hamamatsu 431-3192, Japan

Full list of author information is available at the end of the article

(Continued from previous page)

Conclusions: These results indicate that *BHLHA9* overdosage constitutes the most frequent susceptibility factor, with a dosage effect, for a range of limb malformations at least in Japan. Notably, this is the first study revealing the underlying genetic factor for the development of GWC, and demonstrating the presence of triplications involving *BHLHA9*. It is inferred that a Japanese founder duplication was generated through a replication-based mechanism and underwent subsequent triplication and haplotype modification through recombination-based mechanisms, and that the duplications/triplications with various haplotypes were widely spread in Japan primarily via clinically normal carriers and identified via manifesting patients. Furthermore, genotype-phenotype analyses of patients reported in this study and the previous studies imply that clinical variability is ascribed to multiple factors including the size of duplications/triplications as a critical factor.

Keywords: *BHLHA9*, Split-hand/foot malformation, Long bone deficiency, Gollop-Wolfgang complex, Expressivity, Penetrance, Susceptibility, Japanese founder copy number gain

Introduction

Split-hand/foot malformation (SHFM), also known as ectrodactyly, is a rare limb malformation involving the central rays of the autopod [1,2]. It presents with median clefts of the hands and feet, aplasia/hypoplasia of the phalanges, metacarpals, and metatarsals, and syndactyly. SHFM results from failure to maintain the central portion of the apical ectodermal ridge (AER) in the developing autopod [1,2]. SHFM is divided into two forms: a non-syndromic form with limb-confined manifestations and a syndromic form with extra-limb manifestations [2]. Furthermore, non-syndromic SHFM can occur as an isolated abnormality confined to digits (hereafter, SHFM refers to this type) or in association with other limb abnormalities as observed in SHFM with long bone deficiency (SHFLD) usually affecting the tibia and in Gollop-Wolfgang complex (GWC) characterized by femoral bifurcation [1,2]. Both syndromic and non-syndromic forms are associated with wide expressivity and penetrance even among members of a single family and among limbs of a single patient [2].

SHFM and SHFLD are genetically heterogeneous conditions reviewed in ref. [2]. To date, SHFM has been identified in patients with heterozygous deletions or translocations involving the *DLX5-DLX6* locus at 7q21.2–21.3 (SHFM1) [3] (*DLX5* mutations have been detected recently), heterozygous duplications at 10q24 (SHFM3), heterozygous mutations of *TP63* at 3q27 (SHFM4), heterozygous deletions affecting *HOXD* cluster at 2q31 (SHFM5), and biallelic mutations of *WNT10B* at 12q31 (SHFM6); in addition, SHFM2 has been assigned to Xq26 by linkage analyses in a large Pakistani kindred [2]. Similarly, a genomewide linkage analysis in a large consanguineous family has identified two SHFLD susceptibility loci, one at 1q42.2–q43 (SHFLD1) and the other at 6q14.1 (SHFLD2); furthermore, after assignment of another SHFLD locus to 17p13.1–13.3 [4], duplications at 17p13.3 (SHFLD3) have been found in patients with SHFLD reviewed in ref. [2]. However, the GWC locus (loci) remains unknown at present.

The duplications at 17p13.3 identified to date are highly variable in size, and harbor *BHLHA9* as the sole gene within the smallest region of overlap [5-9]. *Bhlha9/bhlha9* is expressed in the limb bud mesenchyme underlying the AER in mouse and zebrafish embryos, and *bhlha9* knockdown has resulted in shortening of the pectoral fins in zebrafish [6]. Furthermore, *BHLHA9*-containing duplications have been identified not only in patients with SHFLD but also in those with SHFM and clinically normal family members [4-10]. These findings argue for a critical role of *BHLHA9* duplication in the development of SHFM and SHFLD, with variable expressivity and incomplete penetrance.

In this study, we report on *BHLHA9*-containing duplications/triplications with an identical fusion point and various haplotype patterns that were associated with a range of limb malformations including GWC, and discuss on characteristic clinical findings, genomic basis of Japanese founder copy number gains, and underlying factors for phenotypic variability.

Materials and methods

Patients/subjects

We studied 68 patients with SHFM (n = 55), SHFLD (n = 11), or GWC (n = 2), as well as 60 clinically normal relatives, from 51 Japanese families; the pedigrees of 27 of the 51 families and representative clinical findings are shown in Figure 1. All the probands 1–51 had a normal karyotype. Southern blot analysis for SHFM3 locus had been performed in 28 probands with SHFM, indicating 10q24 duplications in two of them [11]. Clinical features including photographs and roentgenograms of a proband with GWC and his brother with SHFLD (family 23 in Figure 1A) were as described previously [12]. The residencies of families 1–51 were widely distributed throughout Japan.

Ethical approval and samples

This study was approved by the Institutional Review Board Committees of Hamamatsu University School of

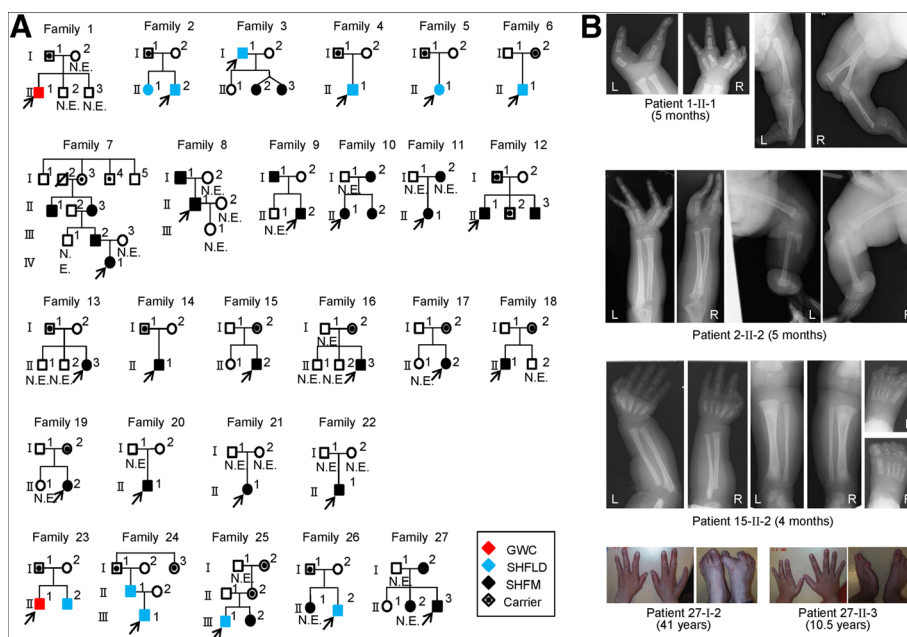


Figure 1 Clinical summary. **A.** Pedigrees of 27 Japanese families with duplications (families 1–22) and triplications (families 23–27) of a ~200 kb region involving *BHLHA9*. The duplications/triplications are associated with GWC, SHFLD, SHFM, or normal phenotype (carriers). N.E.: Not examined molecularly. **B.** Representative clinical findings. Each patient is indicated by a family-generation-individual style and corresponds to the patient/subject shown in Figure 1A and Additional file 5. The top panel: GWC with right bifid femur; the second panel: SHFLD with bilateral tibial deficiencies, the third panel: SHFM with polydactyly; and the bottom panel: SHFM.

Medicine, RIKEN, and National Center for Child Health and Development, and was performed using peripheral leukocyte samples after obtaining written informed consent for the molecular analysis and the publication of genetic and clinical data after removing information for personal identification (e.g., name, birthday, and facial photograph) from the adult subjects (³ 20 years) or from the parents of the child subjects (below 20 years). Furthermore, informed assent was also obtained from child subjects between 6–20 years.

Samples and primers

The primers utilized in this study are summarized in Additional file 1.

Molecular studies

Sanger sequencing, fluorescence *in situ* hybridization (FISH), microsatellite genotyping, Southern blotting, and bisulfite sequencing-based methylation analysis were performed by the standard methods, as reported previously [13]. Quantitative real-time PCR (qPCR) analysis was carried out by the SYBR Green methods on StepOnePlus system, using *RNaseP* as an internal control (Life Technologies). Genomewide oligonucleotide-based array comparative genomic hybridization (CGH) was performed with a catalog human array (4 × 180 K format, ID G4449A) according to the manufacturer's instructions (Agilent Technologies),

and obtained copy number variants/polymorphisms were screened with Agilent Genomic Workbench software using the Database of Genomic Variants (<http://dgv.tcag.ca/dgv/app/home>). Sequencing of a long region encompassing *BHLHA9* was performed with the Nextera XT kit on MiSeq (Illumina), using SAMtools v0.1.17 software (<http://samtools.sourceforge.net/>). Exome sequencing was performed as described previously [14].

Assessment of genomic environments around the fusion points

Repeat elements around the fusion point were searched for using Repeatmasker (<http://www.repeatmasker.org>). Rearrangement-inducing DNA features were investigated for 300 bp regions at both the proximal and the distal sides of each breakpoint, using GEECEE (<http://emboss.bioinformatics.nl/cgi-bin/emboss/geecce>) for calculation of the average GC content, PALINDROME (<http://mobyle.pasteur.fr/cgi-bin/portal.py#forms::palindrome>) and Non-B DB (<http://nonb.abcc.ncifcrf.gov>) for the examination of the palindromes and non-B (non-canonical) structures, and Fuzznuc (<http://emboss.bioinformatics.nl/cgi-bin/emboss/fuzznuc>) for the assessment of rearrangement-associated sequence motifs and tri/tetranucleotides [15–20]. For controls, we examined 48 regions of 600 bp long selected at an interval of 1.5 Mb from the entire chromosome 17.

Statistical analysis

The statistical significance of the frequency was analyzed by the two-sided Fisher's exact probability test.

Results

Sequence analysis of the known causative/candidate genes

We performed direct sequencing for the previously known causative genes (*DLX5*, *TP63*, and *WNT10B*) reviewed in ref. [2] in the probands 1–51. Although no pathologic mutation was identified in *DLX5* and *TP63*, the previously reported homozygous missense mutation of *WNT10B* (c.944C > T, p.R332W) [21] was detected in the proband 48 with SHFM who was born to healthy consanguineous parents heterozygous for this mutation. In addition, while no variation was detected in *DLX5* and *WNT10B*, rs34201045 (4 bp insertion polymorphism) in *TP63* [21] was detected with an allele frequency of 61%.

We also examined *BHLHA9*, because gain-of-function mutations of *BHLHA9* as well as *BHLHA9*-harboring duplications may lead to limb malformations. No sequence variation was identified in the 51 probands.

Array CGH analysis

Array CGH analysis was performed for the probands 1–51, showing increased copy numbers at 17p13.3 encompassing *BHLHA9* (SHFLD3) in the probands 1–27 from families 1–27 (Figure 1A). Furthermore, heterozygous duplications at 10q24 (SHFM3) were detected in the probands 49–51, i.e., a hitherto unreported patient with paternally inherited SHFM (his father also had the duplication) and the two patients who had been indicated to have the duplications by Southern blot analysis [11]. No copy number alteration was observed at other SHFM/SHFLD loci in the probands 1–27 and 49–51. In the remaining probands 28–48, there was no copy number variation that was not registered in the Database of Genomic Variants.

Identical fusion points in *BHLHA9*-containing duplications/triplications

The array CGH indicated that the increased copy number regions at 17p13.3 were quite similar in the physical size in the probands 1–27 and present in three copies in the probands 1–22 and in four copies in the probands 23–27 (Figure 2A). Thus, FISH analysis was performed using 8,259 bp PCR products amplified from this region, showing two signals with a different intensity that was more obvious in the probands 23–27 (Figure 2A).

We next determined the fusion points of the duplications/triplications (Figure 2B). PCR products of 2,195 bp long were obtained with P1/P2 primers in the probands 1–27, and the fusion point was determined by direct sequencing for 418 bp PCR products obtained with P3/P4

primers. The fusion point was identical in all the probands 1–27; it resided on intron 1 of *ABR* and intron 1 of *YWHAE*, and was associated with a 4 bp microhomology.

Then, we performed qPCR analysis for a 214 bp region harboring the fusion point, using P5/P6 primers (Figure 2C and Additional file 2). The fusion point was present in a single copy in the probands 1–22 and in two copies in the probands 23–27. The results showed that the identical genomic segment harboring *BHLHA9* was tandemly duplicated in the probands 1–22 and triplicated in the probands 23–27. According to GRCh37/hg19 (<http://genome.ucsc.edu/>), the genomic segment was 210,050 bp long.

We also performed array CGH and qPCR for the fusion point in 15 patients other than the probands and 47 clinically normal relatives from the 27 families (Figures 1 and 2C). The duplications/triplications were identified in all the 15 patients. Thus, in a total of 42 patients, duplications/triplications were found in 29 SHFM patients, 11 SHFLD patients, and two GWC patients. Furthermore, the duplications/triplications were also present in 22 of the 47 clinically normal relatives. In particular, they were invariably identified in either of the clinically normal parents when both of them were examined; they were also present in other clinically normal relatives in families 7, 12, 24, and 25.

Since the above data indicated the presence of duplications/triplications in clinically normal subjects, we performed qPCR for the fusion point in 1,000 Japanese controls. The fusion point was detected in a single copy in two subjects (Subjects 1 and 2 in Figure 2C). We also performed array CGH in 200 of the 1,000 controls including the two subjects, confirming the duplications in the two subjects and lack of other copy number variations, including deletions involving *BHLHA9*, which were not registered in the Database of Genomic Variants in the 200 control subjects. The frequency of duplications/triplications was significantly higher in the probands than in the control subjects (27/51 vs. 2/1,000, $P = 3.5 \times 10^{-37}$).

Various haplotype patterns on the duplicated/triplicated segments

We carried out genotyping for rs3951819 (A/G SNP on *BHLHA9*) and *D17S1174* (CA repeat microsatellite locus) on the genomic segment subjected to duplications/triplications (Figure 2A), and determined rs3951819-*D17S1174* haplotype patterns. Representative results are shown in Figure 2D, and all the data are available on request. Various haplotype patterns were identified on the single, the duplicated, and the triplicated segments, and the [A-14] haplotype was most prevalent on the duplicated/triplicated segments (Table 1). While the distribution of CA repeat lengths on the single segments was discontinuous, similar discontinuous distribution was

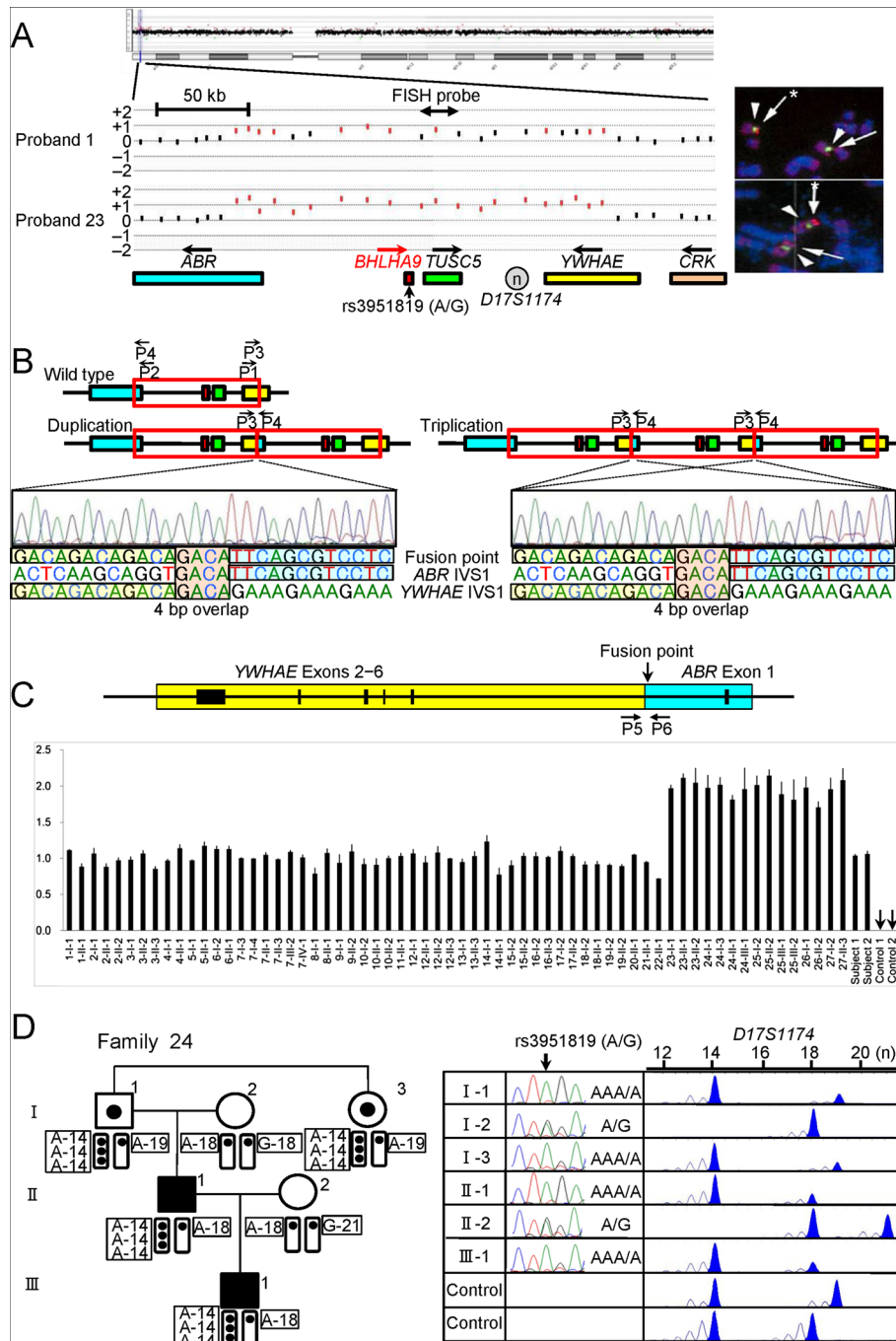


Figure 2 (See legend on next page.)

(See figure on previous page.)

Figure 2 Identification and characterization of the duplications/triplications involving *BHLHA9* at chromosome 17p13.3. **A.** Array CGH and FISH analyses in proband 1 and proband 23 with GWC. In array CGH analysis, the black and the red dots denote the normal and the increased copy numbers, respectively. Since the log₂ signal ratios for a ~200 kb region encompassing *BHLHA9* are around +0.5 in the proband 1 and around +1.0 in the proband 23, this indicates the presence of three and four copies of this region in the two probands, respectively. In FISH analysis, two red signals with an apparently different density are detected by the 8,289 bp PCR probe (the stronger signals are indicated with asterisks). The green signals derive from an internal control probe (CEP17). The arrows on the genes show transcriptional directions. Rs3951819 (A/G) resides within *BHLHA9*. **B.** Determination of the fusion point. The fusion has occurred between intron 1 of *ABR* and intron 1 of *YWHAE*, and is associated with a 4 bp (GACA) microhomology. P1–P4 show the position of primers. **C.** Quantitative real-time PCR analysis. The upper part denotes the fusion point. P5 & P6 show the position of primers. The lower part shows the copy number of the fusion point in patients/subjects with duplications/triplications (indicated by a family-generation-individual style corresponding to that in Figure 1 and Additional file 5). Subject-1 and subject-2 denote the two control subjects with the duplication, and control-1 and control-2 represent normal subjects without the duplication/triplication. **D.** The rs3951819 (A/G SNP)–*D17S1174* (CA repeat number) haplotype patterns in family 24. Assuming no recombination between rs3951819 and *D17S1174*, the haplotype patterns of the family members are determined as shown here. The haplotype patterns of the remaining families have been interpreted similarly.

also observed in the Japanese general population (see Additional file 3).

Genomic environments around the breakpoints

The breakpoint on *YWHAE* intron 1 resided on a simple *Alu* repeat sequence, and that on *ABR* intron 1 was present on a non-repetitive sequence. There was no low copy repeat around the breakpoints. Comparison of the frequencies of known rearrangement-inducing DNA features between 600 bp sequences around the breakpoints and those of 48 regions selected at an interval of 1.5 Mb from chromosome 17 revealed that palindromes, several types of non-B DNA structures, and a rearrangement-associated sequence motif were abundant around the breakpoint on *YWHAE* intron 1 (see Additional file 4).

Clinical findings of families 1–27

Clinical assessment revealed several notable findings. First, duplications/triplications were associated with SHFM, SHFLD, GWC, or normal phenotype, with inter- and intra-familial clinical variability (Figure 1A). Second, in the 42 patients, split hand (SH) was more prevalent than split foot (SF) (41/42 vs. 17/42, $P = 6.2 \times 10^{-9}$), and long bone defect (LBD) was confined to lower extremities (0/42 vs. 13/42, $P = 4.1 \times 10^{-5}$) (Table 2 and Additional file 5). Third, there was no significant sex difference in the ratio between patients with limb malformations and patients/carriers with duplications/triplications (26/38 in males vs. 16/26 in females, $P = 0.60$) (Table 2 and Additional file 5). Fourth, the ratio of LBD positive families was significantly higher in triplications than in duplications (4/5 vs. 16/22, $P = 0.047$) (Figure 1A and Table 2). Fifth, while the duplications/triplications were transmitted from patients to patients, from carriers to patients, and from a carrier to a carrier (from I-1 to II-2 in family 12), transmission from a patient to a carrier was not identified (Figure 1A); it should be pointed out, however, that molecular analysis in a clinically normal child born to an affected parent was possible only in a single adult subject (II-1 in family 27), and that molecular analysis in clinically

Table 1 The rs3951819 (A/G SNP) – *D17S1174* (CA repeat number) haplotype

Patterns of the 210,050 bp segment subjected to copy number gains

Haplotype pattern	Family
<Single segment>	
[A-14]	1, 5, 9, 15, 17, 19, 23, 26
[A-16]	12
[A-18]	3, 14, 15, 24, 25, 26
[A-19]	2, 6, 13, 19, 20, 24, 25, 27
[A-21]	5, 23
[G-12]	17
[G-14]	2, 3, 6, 12, 13, 19, 26
[G-18]	3, 5, 17, 18, 24, 25
[G-19]	9, 12, 18, 20, 25
[G-21]	1, 9, 19, 24, 27
[A-14] or [G-14]	16
[A-18] or [G-18]	4
[A-19] or [G-19]	4
[A-21] or [G-21]	16
<Duplicated segments>	
[A-14] + [A-14]	5, 12, 13, 14, 15, 20
[A-14] + [A-18]	1
[A-14] + [G-18] or [G-14] + [A-18]	2, 3, 4, 6, 9, 16, 17
[A-14] + [G-18] or [A-14] + [G-19]	18
[A-14] + [G-14] or [G-14] + [G-14]	19
<Tripllicated segments>	
[A-14] + [A-14] + [A-14]	23, 24
[A-14] + [A-14] + [G-14]	25
[A-14] + [A-19] + [A-19]	26
[A-14] + [G-18] + [G-18] or [G-14] + [A-18] + [G-18]	27

The haplotype patterns written in the left column have been detected in at least one patient/subject in the families described in the right column. Genotyping could not be performed in several patients/subjects who had been repeatedly examined previously, because of the extremely small amount of DNA samples that were virtually used up in the sequencing and array CGH analyses.

Table 2 Summary of clinical findings in patients/carriers with duplications/triplications involving *BHLHA9*

	SHFM (+) patients			LBD (+) patients			Patient ratio*			LBD (+) families		
	SH	SF	P-value	U-LBD	L-LBD	P-value	Male	Female	P-value	Trip	Dup	P-value
This study	41/42	17/42	6.2×10^{-9}	0/42	13/42	4.1×10^{-5}	26/38	16/26	0.60	4/5	16/22	0.047
Previous studies	63/84	23/84	8.6×10^{-10}	11/91	42/91	5.7×10^{-7}	68/114	31/79	5.7×10^{-3}
Sum	104/126	40/126	1.1×10^{-16}	11/133	55/133	3.0×10^{-10}	94/152	47/105	7.6×10^{-3}

SHFM: split-hand/foot malformation; SH: split hand; SF: split foot; LBD: long bone deficiency; U: upper; L: lower; Trip: triplication; and Dup: duplication. In the previous studies, patients without detailed phenotypic description and those of unknown sex have been excluded (3–9).

*The ratio between patients with limb malformations and patients/carriers with duplications/triplications, i.e. the number of patients over the number of patients plus carriers.

normal children <20 years old was possible only in two subjects (II-2 in family 12 and II-1 in family 15). Lastly, limb malformation was inherited in an apparently autosomal dominant manner (from patients to patients), or took place as an apparently *de novo* event or as an apparently autosomal recessive trait (from clinically normal parents to a single or two affected children) (Figure 1A).

Attempts to identify a possible modifier(s)

The variable expressivity and incomplete penetrance in families 1–27 suggest the presence of a possible modifier (s) for the development of limb malformations. Thus, we performed further molecular studies in patients/subjects in whom DNA samples were still available, and compared the molecular data between patients with SHFM and those with SHFLD for the assessment of variable expressivity and between SHFM, SHFLD, or total patients and carriers for the evaluation of incomplete penetrance.

We first examined the possibility that the modifier(s) resides within or around *BHLHA9* (see Additional file 6). There was no *BHLHA9* mutation in all the 21 examined probands with SHFM, SHFLD, or GWC, as described in the section of “Sequence analysis of the known causative/candidate genes”. The rs3951819 A/G SNP pattern on the duplicated/triplicated segments was apparently identical between patients and carriers (e.g. Figure 2D), and the frequency of A/G allele on the normal chromosome 17 was similar between SHFM and SHFLD patients and between SHFM, SHFLD, or total patients and carriers (see Additional file 7). The results of other known SNPs on *BHLHA9* (rs185242872, rs18936498, and rs140504068) were not informative, because of absence or extreme rarity of minor alleles. Furthermore, in SHFM families 7, 12, and 18, sequencing of a 7,406 bp region encompassing *BHLHA9* and Southern blot analysis using five probes and *MfeI*-, *SspI*-, and *SacI*-digested genomic DNA revealed no variation specific to the patients, and methylation analysis for a CpG rich region at the upstream of *BHLHA9* delineated massive hypomethylation in all the patients/carriers examined.

Next, we examined the possibility that a variant(s) of known causative genes constitutes the modifier(s). Since rs34201045 in *TP63* was identified in the mutation

analysis, we compared rs34201045 genotyping data between the 27 probands and the 15 carriers. The allele and genotype frequencies were similar between SHFM and SHFLD patients and between SHFM, SHFLD, or total patients and carriers (see Additional file 8).

We finally performed exome sequencing in SHFM families 13 and 17–19. However, there was no variation specific to the patients. In addition, re-examination of the genomewide array CGH data showed no discernible copy number variation specific to the patients.

Discussion

BHLHA9 overdosage and clinical characteristics

We identified duplications/triplications of a ~200 kb genomic segment involving *BHLHA9* at 17p13.3 in 27 of 51 families with SHFM, SHFLD, or GWC. To our knowledge, this is the first study revealing the underlying genetic factor for the development of GWC, and demonstrating the presence of triplications involving *BHLHA9* that were suggested but not confirmed in the previous studies [5,9]. Furthermore, this study indicates that *BHLHA9*-containing duplications/triplications are the most frequent underlying factor for the development of limb malformations at least in Japan. Notably, SHFLD and GWC with LBD were significantly more frequent in patients with triplications than in those with duplications, and the duplications/triplications were identified in clinically normal familial members and in the general population. These findings imply that increased *BHLHA9* copy number constitutes a strong susceptibility, rather than a causative, factor with a dosage effect for the development of a range of limb malformations. Since *Bhlha9* is expressed in the developing ectoderm adjacent to the AER rather than the AER itself in mouse embryos [6], *BHLHA9* appears to play a critical role in the limb development by interacting with the AER. While the duplications/triplications identified in this study included *TUSC5* and generated an *ABR-YWHAE* chimeric gene (Figure 2C), *TUSC5* duplication and the chimeric gene formation are not common findings in the previously reported patients with duplications at 17p13.3 and SHFM and/or SHFLD [5–9]. In addition, none of *Tusc5*, *Abr*, and *Ywhae* is specifically expressed in the developing mouse limb buds [22] (A Transcriptome Atlas Database

for Mouse Embryo of Eurexpress Project, <http://www.eurexpress.org/ee/project/>).

Several clinical findings are noteworthy in patients/subjects with duplications/triplications. First, SH was more frequent than SF in this study as well as in the previous studies, and LBD was confined to lower extremities in this study and was more frequent in lower extremities than in upper extremities in the previous studies (Table 2) [4-10]. This implies that *BHLHA9* overdosage exerts differential effects on the different parts of limbs. Second, while limb malformations were similarly identified between males and females in this study, they were more frequently observed in males than in females in the previous studies (Table 2) [4-10]. In this regard, it has been reported that testosterone influences the digital growth pattern as indicated by the lower second to fourth digit length ratio in males than in females [23-25], and that Caucasian males have higher serum testosterone values and lower second to fourth digit length ratios than Oriental males [26,27]. Such testosterone effects on the digital growth pattern with ethnic difference may explain why male dominant manifestation was observed in the previous studies primarily from Caucasian countries and was not found in this study. Lastly, LBD was more prevalent in patients with triplications than in those with duplications. This suggests that LBD primarily occurs when the effects of *BHLHA9* overdosage are considerably elevated.

Genomic basis of the Japanese founder copy number gains

The duplications/triplications were associated with the same fusion point and variable haplotype patterns. Since there was no sequence homology or low-copy repeats around the breakpoints, it is unlikely that such duplications/triplications were recurrently produced in different individuals by non-allelic homologous recombination (NAHR) [17,20]. Instead, it is assumed that a Japanese founder duplication took place in a single ancestor, and was spread with subsequent triplication and modification of the haplotype patterns.

The most likely genomic basis of the Japanese duplications/triplications is illustrated in Additional file 9. Notably, a 4 bp (GACA) microhomology was identified at the duplication fusion point (Figure 2B). A microhomology refers to two to five nucleotides common to the sequences of the two breakpoints, and is found as an overlapping sequence at the join point [16,19,20]. This suggests that the Japanese founder duplication was generated by replication-based mechanisms such as fork stalling and template switching (FoSTeS) and microhomology-mediated break-induced replication (MMBIR), because the presence of such a microhomology is characteristic of FoSTeS/MMBIR [17-20]. Indeed, such a simple tandem duplication with a microhomology can be produced by one time FoSTeS/

MMBIR [17-20], although it could also be generated by non-homologous end-joining (NHEJ) [17]. Since the [A-14] haplotype was most prevalent on the duplicated/triplicated segments, it is inferred that a genomic rearrangement occurred in an ancestor with the [A-14] haplotype, yielding the founder duplication with the [A-14] + [A-14] haplotype. Furthermore, the presence of multiple stimulants for genomic rearrangements around the breakpoint on *YWHAE* intron 1 would have facilitated the generation of the founder duplication. In particular, non-B structures are known to stimulate the occurrence of both replication-based FoSTeS/MMBIR and double-strand breaks and resultant NHEJ [17,28,29], although the relative importance of each non-B DNA structure is largely unknown.

Subsequent triplication and haplotype modification can develop from the Japanese founder duplication through unequal interchromatid and interchromosomal recombinations [17,20]. Indeed, a tandem triplication with the [A-14] + [A-14] + [A-14] haplotype can be generated by unequal exchange between sister chromatids with the [A-14] + [A-14] haplotype, and various haplotype patterns are yielded by unequal interchromosomal exchanges involving the duplicated or triplicated segments. Furthermore, the haplotype variation would be facilitated by unequal exchanges between sister chromatids harboring duplications/triplications with various haplotype patterns and by the further unequal interchromosomal exchanges.

Underlying factors for the phenotypic variability

The duplications/triplications were accompanied by limb malformations with variable expressivity and incomplete penetrance. Although this may suggest the presence of a possible modifier(s) for the development of limb malformations, such a modifier(s) was not detected. In particular, while patient-to-carrier transmission of duplications/triplications was not identified in this study, even patient-to-carrier-to-patient transmission has been reported in three pedigrees [5,6,10]. Such transmission pattern with incomplete penetrance characterized by skipping of a generation is apparently inexplicable by assuming a modifier (s) interacting with *BHLHA9* or independent of *BHLHA9* on the duplication/triplication positive chromosome 17, on the normal chromosome 17, or on other chromosomes (Figure 3, Models A, B, and C, see also the legends in Figure 3).

In this regard, it is noteworthy that the development of limb malformations is obviously dependent on the size of genomic segment subjected to copy number gains. Actually, limb malformation has occurred in only one of 21 large duplications encompassing *BHLHA9* (average 1.55 Mb, mean 1.12 Mb) and in 29 of 80 small duplications encompassing *BHLHA9* (average 244 kb, mean 263 kb) ($P = 5.9 \times 10^{-3}$) [8]. Consistent with this, the patients with large and

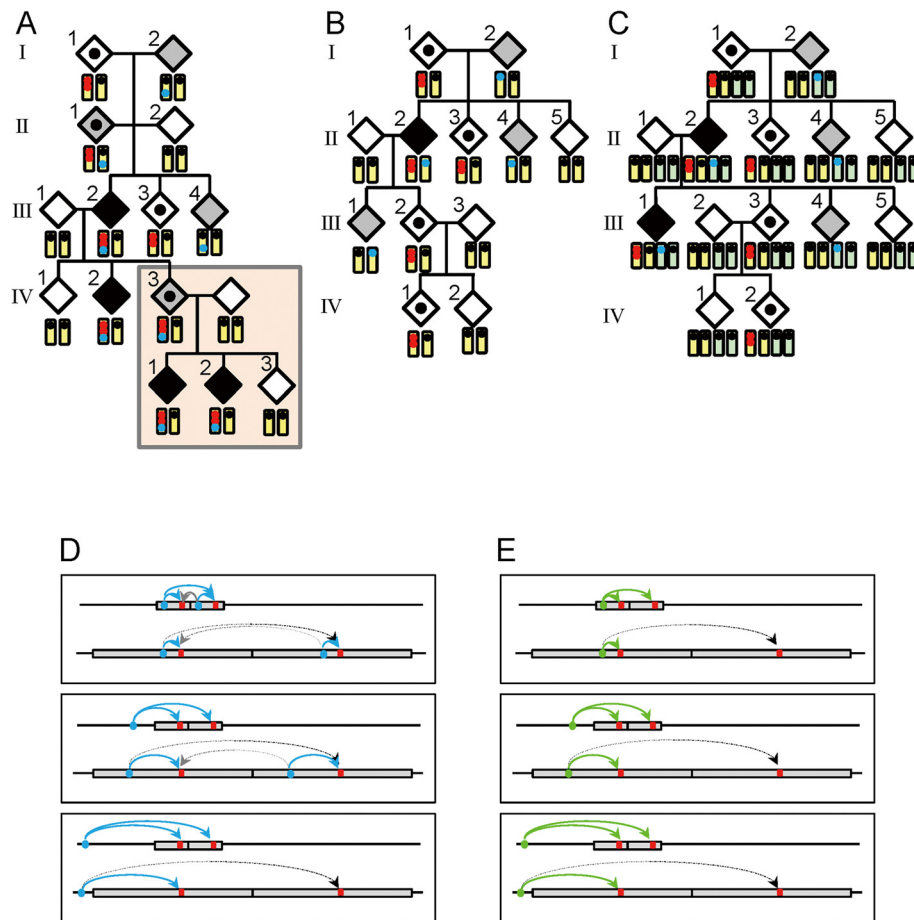


Figure 3 Models for a modifier(s) and effects of the duplication size. In models **A–C**, the yellow bars show chromosome 17, and the light green bars indicate other chromosomes. The two red dots represent the duplication at 17p13.3, and the blue dots indicate a putative modifier(s). Black painted diamonds represent limb malformation positive patients, dot-associated and gray painted diamonds indicate clinically normal carriers with the duplications and the modifier(s) respectively, and white painted diamonds denote clinically normal subjects without both the duplications and the modifier(s). **A**. This model assumes that co-existence of the duplication and a *cis*-acting modifier(s) causes limb malformation. If co-existence of the duplication and the *cis*-acting modifier(s) is associated with incomplete penetrance, this can explain all the transmission patterns observed to date, including the patient-to-carrier transmission and the presence of ≥ 2 affected children. **B**. This model postulates that the presence of a *cis*-acting modifier(s) on the normal chromosome 17 leads to limb malformation by enhancing the expression of the single *BHLHA9*, together with duplicated *BHLHA9* on the homologous chromosome. **C**. This model postulates that co-existence of the duplication at 17p13.3 and a modifier(s) on other chromosome causes limb malformation. In models **D–E**, the red bars represent *BHLHA9*, the blue circles indicate a physiological *cis*-regulatory element for *BHLHA9*, and the green circles indicate a non-physiological modifier(s) for *BHLHA9*. **D**. The physiological *cis*-regulatory element may be duplicated or non-duplicated, depending on its position relative to the size of the duplications. *BHLHA9* expression can be higher in small duplications than large duplications. **E**. The non-physiological modifier(s) can be transferred to various positions of the duplication positive chromosome 17, depending on the recombination places (see Model A). *BHLHA9* expression can be higher in small duplications than large duplications irrespective of the position of the modifier(s).

small duplications were ascertained primarily due to developmental retardation and limb malformation, respectively [8]. It is likely that a physiological *cis*-regulatory element for *BHLHA9* (e.g., an enhancer) can frequently but not invariably work on both of the duplicated *BHLHA9* when the duplication size is small but is usually incapable of working on duplicated *BHLHA9* when the duplication size is large, probably because of the difference in the chromatin structure (see Model D in Figure 3). Similar findings have also been reported in other genes. For example, small

(~150 kb) and relatively small (600–800 kb) duplications involving a putative testis-specific enhancer(s) for *SOX9* have caused 46,XX testicular and ovotesticular disorders of sex development respectively, whereas large duplications (~2 Mb) involving the enhancer(s) have permitted normal ovarian development in 46,XX individuals [30].

Thus, a plausible explanation may be that a range of limb malformations emerge when the effects of *BHLHA9* overdosage exceed the threshold for the development of SHFM, SHFLD, or GWC, depending on the conditions of

other genetic and environmental factors including the size of duplications/triplications as an important but not definitive factor. One may argue that this notion is inconsistent with the apparent anticipation phenomenon that is suggested by the rare patient-to-carrier transmission and the frequent carrier-to-patient transmission of the duplications/triplications, because no specific factor(s) exaggerating the development of limb malformations is postulated in the next generation. However, the skewed transmission pattern would primarily be ascribed to ascertainment bias rather than anticipation [31]. Indeed, while clinically normal parents of disease positive children would frequently be examined for the underlying genetic factor(s) of the children, clinically normal children born to disease positive parents would not usually be studied for such factor(s), as exemplified in this study. Similarly, the frequent patient-to-patient transmission of the duplications/triplications would also be ascribed to ascertainment bias, because molecular studies would preferentially be performed in such families. Nevertheless, the apparently autosomal dominant inheritance pattern of limb malformations in several families may still suggest the relevance of a non-physiological *cis*-acting modifier(s) (see Models A and E in Figure 3). It is possible that such a modifier(s), once transferred onto the duplication/triplication positive chromosome 17, is usually co-transmitted with the duplications/triplications, leading to a specific condition in which the effects of *BHLHA9* overdosage frequently but not invariably exceed the threshold for the development of limb malformations in offsprings with the duplications/triplications.

Remarks

Several matters should be pointed out in the present study. First, in contrast to diverse duplication sizes in non-Japanese populations [5-9], the size of the genomic segment subjected to duplications/triplications was identical in this study. Since families 1–27 were derived from various places of Japan, there is no selection bias in terms of a geographic distribution. Rather, since the small duplications/triplications identified in this study were not associated with developmental retardation, it is likely that they spread throughout Japan primarily via carriers with normal fitness and were found via patients with limb malformations. Obviously, this notion does not exclude the possible presence of other types of duplications/triplications at 17p13.3 in Japan. Second, except for the duplications/triplications at 17p13.3, we could reveal a homozygous *WNT10B* mutation (SHFM6) only in a single SHFM family and chromosome 10q24 duplications (SHFM3) only in three SHFM families. Thus, underlying factors are still unknown in the remaining 20 families, although tiny deletions and/or duplications affecting the known SHFM loci might have

been overlooked because of the low resolution of the array. In addition, although all the probands had a normal karyotype, there might be cryptic translocations and/or inversions involving the known SHFM loci. Third, no deletion of *BHLHA9* was identified in the 51 probands and in the 200 control subjects. This argues against the relevance of *BHLHA9* haploinsufficiency to limb malformations, and coincides with the Japanese founder duplication being produced by a replication-mediated mechanism rather than an interchromatid/interchromosomal (but not an intrachromatid) NAHR that can lead to both deletions and duplications as a mirror image [17]. Furthermore, it remains to be determined (i) whether gain-of-function mutations (and possibly loss-of-function mutations as well) of *BHLHA9* are identified in patients with limb malformations, (ii) whether duplications/triplications involving *BHLHA9* underlie limb malformations other than SHFM, SHFLD, and GWC, and (iii) whether *BHLHA9*-containing duplications/triplications are also the most frequent underlying factors for limb malformations in non-Japanese populations.

Conclusions

The results imply that (i) duplications/triplications involving *BHLHA9* at chromosome 17p13.3 constitute a strong susceptibility factor for the development of a range of limb malformations including SHFM, SHFLD, and GWC; (ii) the Japanese founder duplication was generated by a replication-based mechanism and spread with subsequent triplication and haplotype modification through recombination-based mechanisms; and (iii) clinical variability appears to be due to multiple factors including the size of duplications/triplications. Thus, the present study provides useful information on the development of limb malformations.

Additional files

Additional file 1: Table S1. Primers utilized in this study.

Additional file 2: Figure S1. Real-time PCR analysis.

Additional file 3: Figure S2. *D17S1174* analysis in 200 Japanese control subjects, showing discontinuous distribution of the CA repeat numbers, as observed in the Japanese families with limb malformations.

Additional file 4: Table S2. *In silico* analysis for specific structures around the breakpoint-flanking regions and control regions.

Additional file 5: Table S3. Phenotypes in patients/subjects with increased copy number of *BHLHA9*.

Additional file 6: Figure S3. Genomic region encompassing *BHLHA9* examined in this study.

Additional file 7: Table S4. Polymorphism analysis of rs3951819 (A/G SNP) in *BHLHA9*.

Additional file 8: Table S5. Polymorphism analysis of rs34201045 (4 bp insertion) in *TP63*.

Additional file 9: Figure S4. Genomic basis of the Japanese founder copy number gain.

Abbreviations

AER: Apical ectodermal ridge; CEP17: Centromere of chromosome 17; CGH: Comparative genomic hybridization; Dup: Duplication; FoSTeS: Fork stalling and template switching; GWC: Gollop-Wolfgang complex; L: Lower; LBD: Long bone defect; MMBIR: Microhomology-mediated break-induced replication; NAHR: Non-allelic homologous recombination; N.E.: Not examined; NHEJ: Non-homologous end-joining; qPCR: Quantitative real-time PCR; SF: Split foot; SH: Split hand; SHFLD: SHFM with long bone deficiency; SHFM: Split-hand/foot malformation; Trip: Triplication; U: Upper.

Competing interests

The authors have nothing to declare.

Authors' contributions

Molecular analysis using human samples was performed by EN, HK, FK, RY, SN, SW, KY, TT, SS, MF, and TT, ST, and SY; clinical assessment and blood sampling by RK, HT, SM, TK, TH, MK, AS, KS, HO, NH, HN, EH, TN, HY, GN, and TO; design of this study and interpretations of the data by HA, SI, and TO; and paper writing by TO. All authors read and approved the final manuscript.

Acknowledgements

This work was supported in part by Grants-in-Aid for Scientific Research on Innovative Areas [22132004-A01] from the Ministry of Education, Culture, Sports, Science and Technology, by Grant for Research on Intractable Diseases from the Ministry of Health, Labor and Welfare [H24-048], and by Grants from National Center for Child Health and Development [23A-1, 24-7]. The funders had no role in study design, data collection and analysis, decision to publish, or preparation of the manuscript.

Author details

¹Department of Pediatrics, Hamamatsu University School of Medicine, Hamamatsu 431-3192, Japan. ²Laboratory of Bone and Joint Diseases, Center for Integrative Medical Sciences, RIKEN, Tokyo, Japan. ³Department of Orthopedic Surgery, Tokyo, Japan. ⁴Division of Medical Genetics, National Center for Child Health and Development, Tokyo, Japan. ⁵Section of Clinical Genetics, Department of Pediatrics, Tenshi Hospital, Sapporo, Japan. ⁶Department of Pediatrics, Central Hospital, Aichi Human Service Center, Kasugai, Japan. ⁷Department of Human Genetics, Nagasaki University Graduate School of Biomedical Sciences, Nagasaki, Japan. ⁸Department of Medical Genetics, Shinshu University School of Medicine, Matsumoto, Japan. ⁹Department of Pediatrics, Keio University School of Medicine, Tokyo, Japan. ¹⁰Department of Orthopedics, National Rehabilitation Center for Disabled Children, Tokyo, Japan. ¹¹Division of Medical Genetics, Saitama Children's Medical Center, Saitama, Japan. ¹²Department of Rehabilitation Medicine, University of Tokyo, Tokyo, Japan. ¹³Department of Genetic Counseling, Graduate School of Humanities and Sciences, Ochanomizu University, Tokyo, Japan. ¹⁴Department of Orthopedic Surgery, Japanese Red Cross Nagoya Daiichi Hospital, Nagoya, Japan. ¹⁵Department of Pediatrics, Dokkyo Medical University Koshigaya Hospital, Koshigaya, Japan. ¹⁶Division of Medical Genetics, Tokyo, Japan. ¹⁷Department of Pediatric Imaging, Tokyo Metropolitan Children's Medical Center, Tokyo, Japan. ¹⁸Division of Neurology/Molecular Brain Science, Kobe University Graduate School of Medicine, Kobe, Japan. ¹⁹Department of Systems Biomedicine, National Research Institute for Child Health and Development, Tokyo, Japan. ²⁰Department of Systems Biomedicine, Graduate School of Medical and Dental Sciences, Tokyo Medical and Dental University, Tokyo, Japan. ²¹Department of Molecular Endocrinology, National Research Institute for Child Health and Development, Tokyo, Japan. ²²Present address: Laboratory of Metabolism Center for Cancer Research, National Cancer Institute, Bethesda, MD, USA.

Received: 15 April 2014 Accepted: 22 July 2014

Published online: 21 October 2014

References

1. Duijff PH, van Bokhoven H, Brunner HG: **Pathogenesis of split-hand/split-foot malformation.** *Hum Mol Genet* 2003, **12**:R51-60.
2. Gurrieri F, Everman DB: **Clinical, genetic, and molecular aspects of split-hand/foot malformation: an update.** *Am J Med Genet A* 2013, **161A**:2860-2672.
3. Lango Allen H, Caswell R, Xie W, Xu X, Wragg C, Turnpenny PD, Turner CL, Weedon MN, Ellard S: **Next generation sequencing of chromosomal rearrangements in patients with split-hand/split-foot malformation provides evidence for DYNC11/1 exonic enhancers of DLX5/6 expression in humans.** *J Med Genet* 2014, **51**:264-267.
4. Leziovitz K, Maestrelli SR, Cotrim NH, Otto PA, Pearson PL, Mingroni-Netto RC: **A novel locus for split-hand/foot malformation associated with tibial hemimelia (SHFLD syndrome) maps to chromosome region 17p13.1-17p13.3.** *Hum Genet* 2008, **123**:625-631.
5. Armour CM, Bulman DE, Jarinova O, Rogers RC, Clarkson KB, DuPont BR, Dwivedi A, Bartel FO, McDonnell L, Schwartz CE, Boycott KM, Everman DB, Graham GE: **17p13.3 microduplications are associated with split-hand/foot malformation and long-bone deficiency (SHFLD).** *Eur J Hum Genet* 2011, **19**:1144-1151.
6. Klopocki E, Lohan S, Doelken SC, Stricker S, Ockeloen CW, Soares Thiele de Aguiar R, Leziovitz K, Mingroni Netto RC, Jamsheer A, Shah H, Kurth I, Habenicht R, Warman M, Devriendt K, Kortass U, Hempel M, Rajab A, Mäkitie O, Naveed M, Radhakrishna U, Antonarakis SE, Horn D, Mundlos S: **Duplications of BHLHA9 are associated with ectrodactyly and tibia hemimelia inherited in non-Mendelian fashion.** *J Med Genet* 2012, **49**:119-125.
7. Petit F, Andrieux J, Demeer B, Collet LM, Copin H, Boudry-Labis E, Escande F, Manouvrier-Hanu S, Mathieu-Dramard M: **Split-hand/foot malformation with long-bone deficiency and BHLHA9 duplication: two cases and expansion of the phenotype to radial agenesis.** *Eur J Med Genet* 2013, **56**:88-92.
8. Curry CJ, Rosenfeld JA, Grant E, Gripp KW, Anderson C, Aylsworth AS, Saad TB, Chizhikov VV, Dybose G, Fagerberg C, Falco M, Fels C, Fichera M, Graakjaer J, Greco D, Hair J, Hopkins E, Huggins M, Ladda R, Li C, Moeschler J, Nowaczyk MJ, Ozmore JR, Reitano S, Romano C, Roos L, Schnur RE, Sell S, Suwannarat P, Svaneby D, et al: **The duplication 17p13.3 phenotype: analysis of 21 families delineates developmental, behavioral and brain abnormalities, and rare variant phenotypes.** *Am J Med Genet A* 2013, **161A**:1833-1852.
9. Luk HM, Wong VC, Lo IF, Chan KY, Lau ET, Kan AS, Tang MH, Tang WF, She WM, Chu YW, Sin WK, Chung BH: **A prenatal case of split-hand malformation associated with 17p13.3 triplication - a dilemma in genetic counseling.** *Eur J Med Genet* 2014, **57**:81-84.
10. Petit F, Jourdain AS, Andrieux J, Baujat G, Baumann C, Beneteau C, David A, Fairve L, Gaillard D, Gilbert-Dussardier B, Jouk PS, Le Caignec C, Loget P, Pasquier L, Porchet N, Holder-Espinasse M, Manouvrier-Hanu S, Escande F: **Split hand/foot malformation with long-bone deficiency and BHLHA9 duplication: report of 13 new families.** *Clin Genet* 2014, **85**:464-469.
11. Kano H, Kurosawa K, Horii E, Ikegawa S, Yoshikawa H, Kurahashi H, Toda T: **Genomic rearrangement at 10q24 in non-syndromic split-hand/split-foot malformation.** *Hum Genet* 2005, **118**:477-483.
12. Matsuyama J, Mabuchi A, Zhang J, Iida A, Ikeda T, Kimizuka M, Ikegawa S: **A pair of sibs with tibial hemimelia born to phenotypically normal parents.** *J Hum Genet* 2003, **48**:173-176.
13. Kagami M, Sekita Y, Nishimura G, Irie M, Kato F, Okada M, Yamamori S, Kishimoto H, Nakayama M, Tanaka Y, Matsuoka K, Takahashi T, Noguchi M, Tanaka Y, Masumoto K, Utsunomiya T, Kouzan H, Komatsu Y, Ohashi H, Kurosawa K, Kosaki K, Ferguson-Smith AC, Ishino F, Ogata T: **Deletions and epimutations affecting the human 14q32.2 imprinted region in individuals with paternal and maternal upd(14)-like phenotypes.** *Nat Genet* 2008, **40**:237-242.
14. Iida A, Okamoto N, Miyake N, Nishimura G, Minami S, Sugimoto T, Nakashima M, Tsurusaki Y, Saitsu H, Shiina M, Ogata K, Watanabe S, Ohashi H, Matsumoto N, Ikegawa S: **Exome sequencing identifies a novel INPPL1 mutation in opsismodysplasia.** *J Hum Genet* 2013, **58**:391-394.
15. Cer RZ, Donohue DE, Mudunuri US, Temiz NA, Loss MA, Stamer NJ, Halusa GN, Volfovsky N, Yi M, Luke BT, Bacolla A, Collins JR, Stephens RM: **Non-B DB v2.0: a database of predicted non-B DNA-forming motifs and its associated tools.** *Nucl Acids Res* 2013, **41**:D94-D100.
16. Kornreich R, Bishop DF, Desnick RJ: **α -Galactosidase A gene rearrangements causing Fabry disease: identification of short direct repeats at breakpoints in an Alu-rich gene.** *J Biol Chem* 1990, **265**:9319-9326.
17. Gu W, Zhang F, Lupski JR: **(2008) Mechanisms for human genomic rearrangements.** *Pathogenetics* 2008, **1**:4.
18. Vissers LE, Bhatt SS, Janssen IM, Xia Z, Lalani SR, Pfundt R, Derwinska K, de Vries BB, Gilissen C, Hoischen A, Nesteruk M, Wisniewicka-Kowalnik B, Smyk

- M, Brunner HG, Cheung SW, van Kessel AG, Veltman JA, Stankiewicz P: **Rare pathogenic microdeletions and tandem duplications are microhomology-mediated and stimulated by local genomic architecture.** *Hum Mol Genet* 2009, **18**:3579–3593.
19. Hastings PJ, Ira G, Lupski JR: **A microhomology-mediated break-induced replication model for the origin of human copy number variation.** *PLoS Genet* 2009, **5**:e1000327.
 20. Colnaghi R, Carpenter G, Volker M, O'Driscoll M: **The consequences of structural genomic alterations in humans: genomic disorders, genomic instability and cancer.** *Semin Cell Dev Biol* 2011, **2011**(22):875–885.
 21. Ugur SA, Tolun A: **Homozygous WNT10b mutation and complex inheritance in Split-Hand/Foot Malformation.** *Hum Mol Genet* 2008, **17**:2644–2653.
 22. Oort PJ, Warden CH, Baumann TK, Knotts TA, Adams SH: **Characterization of Tusc5, an adipocyte gene co-expressed in peripheral neurons.** *Mol Cell Endocrinol* 2007, **276**:24–35.
 23. Manning JT, Scutt D, Wilson J, Lewis-Jones DI: **The ratio of 2nd to 4th digit length: a predictor of sperm numbers and concentrations of testosterone, luteinizing hormone and oestrogen.** *Hum Reprod* 1998, **13**:3000–3004.
 24. Manning JT, Trivers RL, Singh D, Thornhill R: **The mystery of female beauty.** *Nature* 1999, **399**:214–215.
 25. Williams TJ, Pepitone ME, Christensen SE, Cooke BM, Huberman AD, Breedlove NJ, Breedlove TJ, Jordan CL, Breedlove SM: **Finger-length ratios and sexual orientation.** *Nature* 2000, **404**:455–456.
 26. Heald AH, Ivison F, Anderson SG, Cruickshank K, Laing I, Gibson JM: **Significant ethnic variation in total and free testosterone concentration.** *Clin Endocrinol* 2003, **58**:262–266.
 27. Manning JT, Stewart A, Bundred PE, Trivers RL: **Sex and ethnic differences in 2nd to 4th digit ratio of children.** *Early Hum Dev* 2004, **80**:161–168.
 28. Wang G, Vasquez KM: **Non-B DNA structure-induced genetic instability.** *Mutat Res* 2006, **598**:103–119.
 29. Zhao J, Bacolla A, Wang G, Vasquez KM: **Non-B DNA structure-induced genetic instability and evolution.** *Cell Mol Life Sci* 2010, **67**:43–62.
 30. Benko S, Gordon CT, Mallet D, Sreenivasan R, Thauvin-Robinet C, Brendehaug A, Thomas S, Bruland O, David M, Nicolino M, Labalme A, Sanlaville D, Callier P, Malan V, Huet F, Molven A, Dijoud F, Munnich A, Faivre L, Amiel J, Harley V, Houge G, Morel Y, Lyonnet S: **Disruption of a long distance regulatory region upstream of SOX9 in isolated disorders of sex development.** *J Med Genet* 2011, **48**:825–830.
 31. Fraser FC: **Trinucleotide repeats not the only cause of anticipation.** *Lancet* 1997, **350**:459–460.

doi:10.1186/s13023-014-0125-5

Cite this article as: Nagata *et al.*: Japanese founder duplications/triplications involving *BHLHA9* are associated with split-hand/foot malformation with or without long bone deficiency and Gollop-Wolfgang complex. *Orphanet Journal of Rare Diseases* 2014 **9**:125.

Submit your next manuscript to BioMed Central and take full advantage of:

- Convenient online submission
- Thorough peer review
- No space constraints or color figure charges
- Immediate publication on acceptance
- Inclusion in PubMed, CAS, Scopus and Google Scholar
- Research which is freely available for redistribution

Submit your manuscript at
www.biomedcentral.com/submit



Modeling type II collagenopathy skeletal dysplasia by directed conversion and induced pluripotent stem cells

Minoru Okada¹, Shiro Ikegawa², Miho Morioka¹, Akihiro Yamashita¹, Atsushi Saito³, Hideaki Sawai⁴, Jun Murotsuki⁵, Hirofumi Ohashi⁶, Toshio Okamoto⁷, Gen Nishimura⁸, Kazunori Imaizumi³ and Noriyuki Tsumaki^{1,9,*}

¹Cell Induction and Regulation Field, Department of Cell Growth and Differentiation, Center for iPS Cell Research and Application, Kyoto University, Japan, ²Laboratory of Bone and Joint Diseases, Center for Integrated Medicinal Sciences, RIKEN, Japan, ³Department of Biochemistry, Graduate School of Biomedical & Health Sciences, University of Hiroshima, Japan, ⁴Department of Obstetrics and Gynecology, Hyogo College of Medicine, Japan, ⁵Maternal and Fetal Medicine, Miyagi Children's Hospital, Tohoku University School of Medicine, Japan, ⁶Division of Medical Genetics, Saitama Children's Medical Center, Japan, ⁷Department of Pediatrics, Asahikawa Medical University, Japan, ⁸Department of Pediatric Imaging, Tokyo Metropolitan Children's Medical Center, Japan and ⁹Japan Science and Technology Agency, CREST, Tokyo, Japan

Received January 10, 2014; Revised and Accepted August 26, 2014

Type II collagen is a major component of cartilage. Heterozygous mutations in the type II collagen gene (*COL2A1*) result in a group of skeletal dysplasias known as Type II collagenopathy (COL2pathy). The understanding of COL2pathy is limited by difficulties in obtaining live chondrocytes. In the present study, we converted COL2pathy patients' fibroblasts directly into induced chondrogenic (iChon) cells. The COL2pathy-iChon cells showed suppressed expression of *COL2A1* and significant apoptosis. A distended endoplasmic reticulum (ER) was detected, thus suggesting the adaptation of gene expression and cell death caused by excess ER stress. Chondrogenic supplementation adversely affected the chondrogenesis due to forced elevation of *COL2A1* expression, suggesting that the application of chondrogenic drugs would worsen the disease condition. The application of a chemical chaperone increased the secretion of type II collagen, and partially rescued COL2pathy-iChon cells from apoptosis, suggesting that molecular chaperons serve as therapeutic drug candidates. We next generated induced pluripotent stem cells from COL2pathy fibroblasts. Chondrogenically differentiated COL2pathy-iPS cells showed apoptosis and increased expression of ER stress-markers. Finally, we generated teratomas by transplanting COL2pathy iPS cells into immunodeficient mice. The cartilage in the teratomas showed accumulation of type II collagen within cells, a distended ER, and sparse matrix, recapitulating the patient's cartilage. These COL2pathy models will be useful for pathophysiological studies and drug screening.

INTRODUCTION

The type II collagen produced by chondrocytes is the major component of the cartilage extracellular matrix (1). The *COL2A1* gene encodes the type II collagen $\alpha 1$ chain. Supramolecular assembly of three $\alpha 1$ chains to form trimer molecules occurs in the endoplasmic reticulum (ER) lumen (2). The helical collagen

molecules are trafficked via the Golgi network to the plasma membrane, and are then secreted into the extracellular space (3). There, the collagen proteins are assembled into dense fibrils.

Heterozygous mutations of *COL2A1* give rise to a spectrum of phenotypes predominantly affecting cartilage, collectively termed type II collagenopathies (COL2pathy) (4,5). Among them, achondrogenesis type II (ACGII) and hypochondrogenesis (HCG)

*To whom correspondence should be addressed at: Center for iPS Cell Research and Application, Kyoto University, 53 Kawahara-cho, Shogoin, Sakyo-ku, Kyoto 606-8507, Japan. Tel: +81 753667045; Fax: +81 753667047; Email: ntsunami@cira.kyoto-u.ac.jp

are lethal due to respiratory insufficiency, which is secondary to an abnormal chest wall skeleton. Individuals with HCG show a less severe phenotype compared with those with ACGII. Patients with spondyloperipheral dysplasia (SPD) live into adulthood and show a combination of platyspondyly and brachydactyly and early onset osteoarthritis (6).

Recent studies suggest that misfolded mutant collagens induce significant ER stress and trigger the ER stress signaling (7,8). Increased expression of ER stress markers, *Grp94* and *Chop*, is observed in mice with an ENU-induced missense mutation in *Col2a1* (9). Apoptosis was detected in the chondrocytes of mice harboring a *Col2a1* mutation (10). Mouse models have enormously contributed to the understanding of COL2pathy. However, the clinical translation of the findings may be diminished by the differences in size and locomotion between mice and humans. For example, the thickness of articular cartilage in the distal femur is 2.2 mm in humans, whereas it is 0.030 mm in mice (11). The volume density of chondrocytes in articular cartilage (chondrocytes + matrix) is about 2% in humans, whereas it is 15–40% in mice. The growth plate cartilage of humans and mice may also differ.

The emerging importance of the ER stress signaling in the pathology of COL2pathy offers the possibility of a new treatment strategy. If the misfolded protein load in the ER can be reduced to levels that can be managed by the cell, then the serious deleterious outcomes of an unresolved ER stress signaling, such as apoptosis, could be ameliorated (7). One promising approach uses small chemical chaperones, which can stabilize proteins in their native conformation and rescue mutant protein folding and/or trafficking defects, but such agents have never been tested for COL2pathy.

With the development of induced pluripotent stem (iPS) cells, cardiomyocytes, neurons and hepatocytes can be obtained by the differentiation of iPS cells derived from patients with various diseases (12–14). These cells, generated through iPS cells, may serve as a useful platform for exploring disease mechanisms and for drug screening. On the other hand, cells generated by directed conversion can also serve as a useful platform for exploring disease mechanisms, as neurons directly converted from skin fibroblasts from Alzheimer's disease patients recapitulated the pathophysiology of the disease (15). We previously developed a method to convert mouse dermal fibroblasts (MDFs) (16) and human dermal fibroblasts (HDFs) (17) directly into chondrogenic cells named induced chondrogenic (iChon) cells by transducing fibroblasts with two reprogramming factors (c-Myc and Klf4) and one chondrogenic factor (Sox9). Cells do not undergo a pluripotent state during direct induction of iChon cells from fibroblast culture by transduction of c-Myc, Klf4 and SOX9 (18). Human and mouse iChon cells express marker genes for chondrocytes but not fibroblasts and can form cartilage when transplanted into the subcutaneous spaces of immunodeficiency mice.

In order to provide live chondrocytes which recapitulate the features of COL2pathy, we generated chondrocytes from the HDFs of patients with COL2pathy using three different approaches: the induction of COL2pathy-iChon cells; the generation of COL2pathy-iPS cells, followed by chondrogenic differentiation and the generation of teratoma-containing cartilage from COL2pathy-iPS cells. These chondrocytes obtained through cellular reprogramming technologies suffered from

abnormalities caused by excess ER stress and showed specific responses to reagents. The findings of our study may contribute to understanding the pathophysiology of the disease and to drug discovery for COL2pathy.

RESULTS

HDFs from patients with COL2pathy are normal

HDFs were obtained from two ACGII patients (ACGII-1 and ACGII-2), one HCG patient (HCG-1) and one SPD patient (SPD-1) (Supplementary Material, Table S1). The ACGII-2 patient showed an intermediate phenotype between ACGII and platyspondylic lethal skeletal dysplasia (PLSD)-Torrance type. Control HDFs from two different neonates were purchased (WT-1 and WT-2). A sequencing analysis of genomic DNA extracted from the patients' HDFs revealed heterozygous mutations in *COL2A1* in all patients (Supplementary Material, Fig. S1A). The ACGII-1 patient had a substitution mutation located at the acceptor site of exon 41. RT-PCR (Supplementary Material, Fig. S1B) and a sequencing analysis revealed the existence of multiple lengths of short mRNAs lacking various combinations of exons, thus resulting in inframe deletion by exon skipping. HDFs from patients with COL2pathy (COL2pathy-HDFs) showed morphologies and proliferation rates similar to those of control HDFs (WT-HDFs) (Supplementary Material, Fig. S1C and D). These results are consistent with the fact that neither WT-HDFs nor COL2pathy-HDFs express *COL2A1* (Supplementary Material, Fig. S1E). Accordingly, the transduction efficiencies did not differ between COL2pathy-HDFs and WT-HDFs (Supplementary Material, Fig. S1F).

Disturbed chondrocytic maturation of COL2-pathy iChon cells

We converted COL2pathy-HDFs into iChon cells and investigated whether COL2pathy-iChon cells can be used for disease modeling. Transduction of COL2pathy-HDFs with c-MYC, KLF4 and SOX9 produced a few Alcian blue-positive nodules, whereas the transduction of WT-HDFs produced substantial numbers of Alcian blue-positive nodules 21 days after transduction (Day 21) (Fig. 1A and Supplementary Material, Fig. S2A). The number of Alcian blue-positive nodules appeared to correlate with the severity of the diseases: ACGII-iChon cell culture showed a lower number of nodules than SPD-iChon cell culture. We next examined the iChon cells at earlier stages after transduction. By Day 7, WT-iChon cell colonies composed of polygonal-shaped cells had appeared (Fig. 1B, top panels; Supplementary Material, Movie S1). A polygonal shape is a characteristic of chondrocyte morphology, whereas HDFs are spindle-shaped. More than 90% of these polygonal cell colonies became condensed and subsequently multilayered, forming nodules by Day 13 (Fig. 1B, top panels; Supplementary Material, Fig. S2B and C). Approximately 95% of the nodules showed positive Alcian blue staining (Supplementary Material, Fig. S2B and C). The transduction of COL2pathy-HDFs also produced COL2pathy-iChon cell colonies composed of polygonal-shaped cells (Fig. 1B, bottom panels) with a comparable efficiency as the transduction of WT-HDFs (Supplementary Material, Fig. S2B, black bars). However, 80% of these

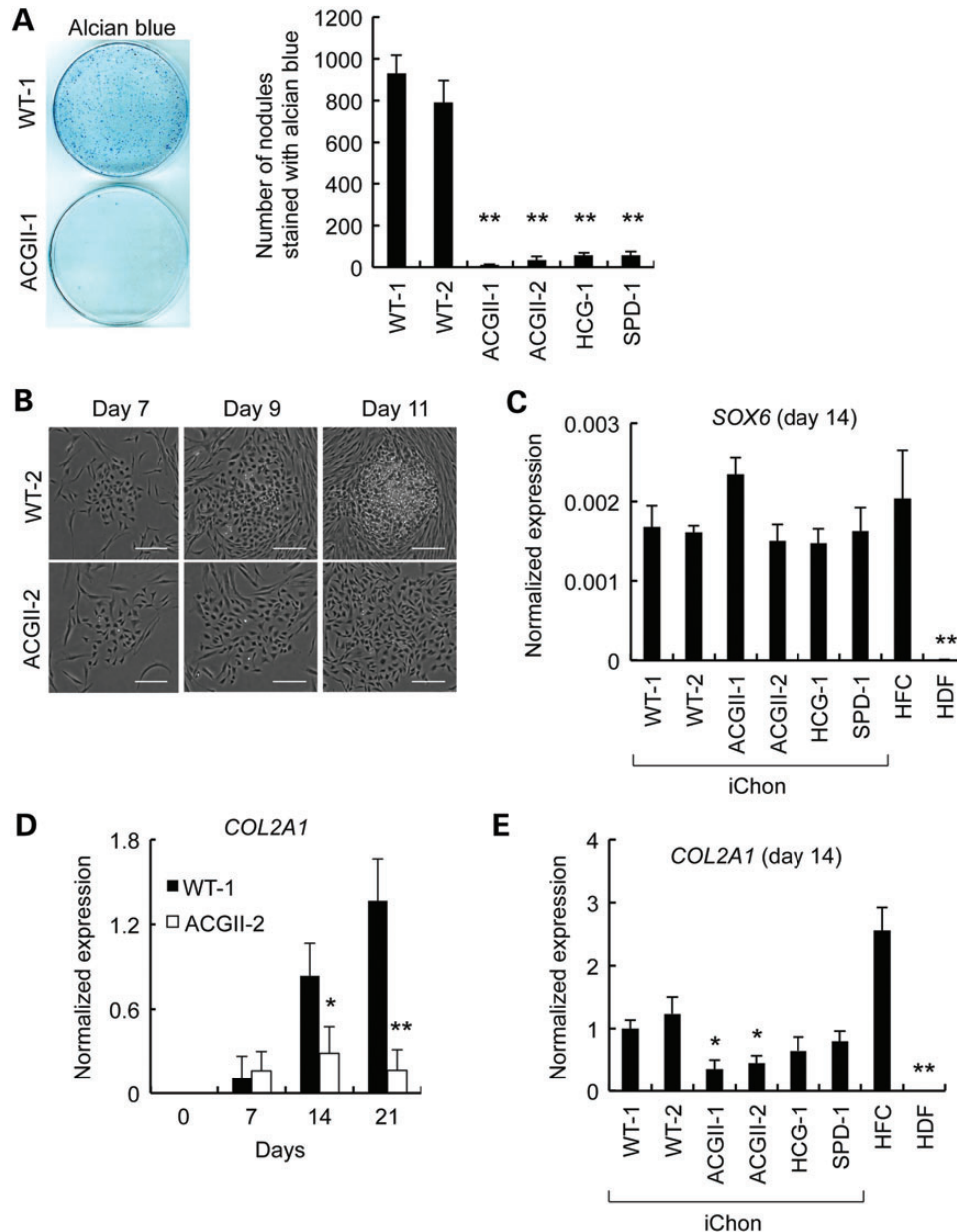


Figure 1. Disturbed chondrocytic maturation of COL2pathy-iChon cells. (A) After the transduction of HDFs with three factors (*c-MYC*, *KLF4* and *SOX9*), 1×10^5 cells were re-seeded into 100 mm dishes (Day 1). The dishes were stained with Alcian blue on Day 21. (Left) Representative images of the Alcian blue staining of iChon culture dishes from control WT-1-HDFs and patient ACGII-1-HDFs. (Right) The number of nodules positively stained with Alcian blue. $**P < 0.01$ compared with WT-1 and WT-2 ($n = 3$). (B) Images of iChon cell colonies induced from WT-2-HDFs and ACGII-2-HDFs seven, nine and 11 days after transduction. Bars, 200 μ m. (C) The iChon cell colonies were picked up on Day 14 and were subjected to a real-time RT-PCR expression analysis of *SOX6*. $**P < 0.01$ compared with WT- and COL2pathy-iChon cells ($n = 3$). HFC, redifferentiated human fetal chondrocytes. (D) The iChon cell colonies were picked up at various intervals after transduction and were subjected to a real-time RT-PCR expression analysis for *COL2A1*. $*P < 0.05$, $**P < 0.01$ compared with WT-1 ($n = 3$). (E) The iChon cell colonies were picked up on Day 14 and were subjected to a real-time RT-PCR expression analysis for *COL2A1*. $*P < 0.05$, $**P < 0.01$ compared with WT-1 and WT-2 ($n = 3$).

COL2pathy-iChon cell colonies became neither condensed nor multilayered (Fig. 1B bottom panels; Supplementary Material, Fig. S2B), and were not stained with Alcian blue (Supplementary Material, Fig. S2B and C).

We picked up iChon cell colonies and subjected them to a real-time RT-PCR expression analysis. The expression levels of *SOX5* and *SOX6*, whose expression levels are induced by *SOX9* (19), were similarly activated in WT-iChon cells and COL2pathy-iChon cells on Day 14 compared with those of

HDFs (Fig. 1C and Supplementary Material, Fig. S2D). The expression levels of *SOX5* and *SOX6* in WT-iChon cells and COL2pathy-iChon cells were comparable to those of redifferentiated fetal chondrocytes (HFC), thus suggesting that chondrogenic commitment occurs in COL2pathy-iChon cells, as well as in WT-iChon cells. *COL2A1* transcription was initially activated similarly in WT-iChon cells and ACGII-2-iChon cells on Day 7 (Fig. 1D). The expression levels of *COL2A1* increased in WT-1-iChon cells as the time passed after transduction,

suggesting that WT-1-iChon cells undergo chondrocytic maturation. On the other hand, the *COL2A1* expression in ACGII-2-iChon cells was suppressed as time passed on Days 14 and 21 (Fig. 1D and E). Furthermore, the expression levels of other cartilage matrix genes, such as *ACAN* and *COMP*, were also lower in COL2pathy-iChon cells than in control iChon cells on Day 14 (Supplementary Material, Fig. S2E). These results indicate that the chondrocytic maturation was disturbed in COL2pathy-iChon cells despite the activation of expression of *SOX5* and *SOX6*, which activate cartilage matrix gene expression in cooperation with *SOX9* (20,21). These results suggest that an unknown mechanism(s) represses the expression of cartilage matrix genes in COL2pathy-iChon cells after the initial activation of type II collagen gene expression.

Decreased cell viabilities and increased ER stress in COL2pathy-iChon cells

We noticed that some COL2pathy-iChon cell colonies disappeared during culture (Supplementary Material, Fig. S3A and Supplementary Material, Movie S1). Approximately 20–30% of COL2pathy-iChon cell colonies disappeared by Day 18 (Supplementary Material, Fig. S3B). A growth curve analysis showed that the WT-1-iChon cells kept growing, whereas the numbers of ACGII-1- and HCG-1-iChon cells did not change or gradually decreased (Supplementary Material, Fig. S3C). The TUNEL assay revealed that more cells in COL2pathy-iChon cell colonies were TUNEL-positive than were the WT-iChon cell colonies around Day 15 (Fig. 2A). A transmission electron microscopic analysis revealed that the ER was distended in ACGII-2-iChon cells (Fig. 2B) on Day 14. The expression levels of *BIP* and *CHOP* were increased in COL2pathy-iChon cells on Day 18 (Fig. 2C), suggesting that there were increased ER stress signaling. The degree of increase was correlated with the severity of the patients' diseases. There are several pathways which transmit ER stress signals. *XBPI* splicing was detected in COL2pathy-iChon cells but not in WT-iChon cells on Day 17 (Fig. 2D), suggesting that the IRE1 pathway is involved in transmitting the ER stress. eIF2 α was highly phosphorylated in the COL2pathy iChon cells compared with that in WT-iChon cells on Day 17 (Fig. 2E), suggesting that the PERK pathway is also involved in transmitting the ER stress. The expression levels of *GRP94* were increased in COL2pathy-iChon cells compared with those in WT-iChon cells on Day 18 (Fig. 2C), and cleaved ATF6 was detected in COL2pathy-iChon cells, but not in WT-iChon cells on Day 17 (Fig. 2F), suggesting that the ATF6 pathway is also involved in the transmission of ER stress. These results collectively suggest that COL2pathy-iChon cells have elevated ER stress and undergo apoptosis.

Ascorbic acid is a co-factor for prolyl hydroxylase and facilitates collagen triple helix formation, but the iChon cells were induced using DMEM culture medium with 10% FBS without ascorbic acid. To confirm that type II collagen trimers were formed in the iChon cells, we performed a western blot analysis using anti-type II collagen antibodies under the non-reducing condition (without dithiothreitol and 2-mercaptoethanol) using samples obtained from the iChon cells on Day 19. We detected type II collagen molecules with a size between 268 and 460 kDa in the lysates from COL2pathy-iChon cells, but not in the lysates from WT-iChon cells (Fig. 2G, left top panel). On

the other hand, we detected type II collagen molecules with a size between 268 and 460 kDa in the supernatant from WT-iChon cell cultures, but it was minimally present in the supernatant from COL2pathy-iChon cell cultures (Fig. 2G, right panel). These results suggest that type II collagens were folded correctly in both WT- and COL2pathy-iChon cells, even when they were cultured in the absence of ascorbic acid. The folded type II collagen molecules were immediately secreted from WT-iChon cells, whereas misfolded type II collagen trimers were probably retained in the COL2pathy-iChon cells. These results collectively suggest that the excess ER stress in the COL2pathy-iChon cells is likely associated with the misfolding of type II collagen.

To confirm that the misfolding of mutant proteins is responsible for the abnormalities of the COL2pathy-iChon cells, we induced WT- and COL2pathy-iChon cells in the presence of ascorbic acid. We added ascorbic acid to the medium from Day 6 to Day 17 during the induction of WT- and COL2pathy-iChon cells, and subjected them to an analysis on Day 17. The application of ascorbic acid did not significantly change the number of Alcian blue-positive nodules in the WT-iChon cell culture, but did significantly decrease the numbers of Alcian blue-positive nodules in the ACGII-1- and HCG-1-iChon cell cultures (Fig. 3A). The addition of ascorbic acid increased the expression levels of ER stress markers; *BIP*, *GFP94* and *CHOP*, in the COL2pathy-iChon cells (Fig. 3B). The presence of ascorbic acid in the culture did not affect the *XBPI* splicing in either WT- or COL2pathy-iChon cells (Fig. 3C). The administration of ascorbic acid increased the amount of phosphorylated eIF2 α (Fig. 3D) and cleaved ATF6 (Fig. 3E) in the COL2pathy-iChon cells. Therefore, the presence of ascorbic acid enhanced the abnormalities and increased the activation of ER stress pathways, including the PERK pathway and the ATF6 pathway, in COL2pathy iChon cells, supporting the idea that the misfolding of mutant proteins is responsible for the abnormalities of COL2pathy-iChon cells.

To examine how type II collagen molecules became degraded in the ACGII-iChon cells, we generated iChon cells in the presence of ascorbic acid, treated them with MG132 (a proteasome inhibitor) or bafilomycin A1 (a lysosome inhibitor), collected cell lysates and subjected them to a western blot analysis using an anti-type II collagen antibody (Fig. 3F). The addition of bafilomycin A1 increased the amount of type II collagen, whereas the addition of MG132 did not, suggesting that there is lysosomal degradation of type II collagen.

Chondrogenic supplementation adversely affects COL2pathy-iChon cells

We analyzed how chondrogenic stimulation with BMP2 and TGF β 1 (B + T) affects COL2pathy-iChon cells (Fig. 4A). The addition of B + T to WT-iChon cell culture slightly increased the numbers of Alcian blue-positive nodules due to the chondrogenic effects of B + T (Fig. 4A and Supplementary Material, Fig. S4A). On the other hand, the addition of B + T to COL2pathy-iChon cell culture decreased the numbers of Alcian blue-positive nodules. The degree of decrease correlated with the severity of the original patient diseases.

We picked up and reseeded iChon colonies, and continued their cultivation in the presence or absence of B + T, for the

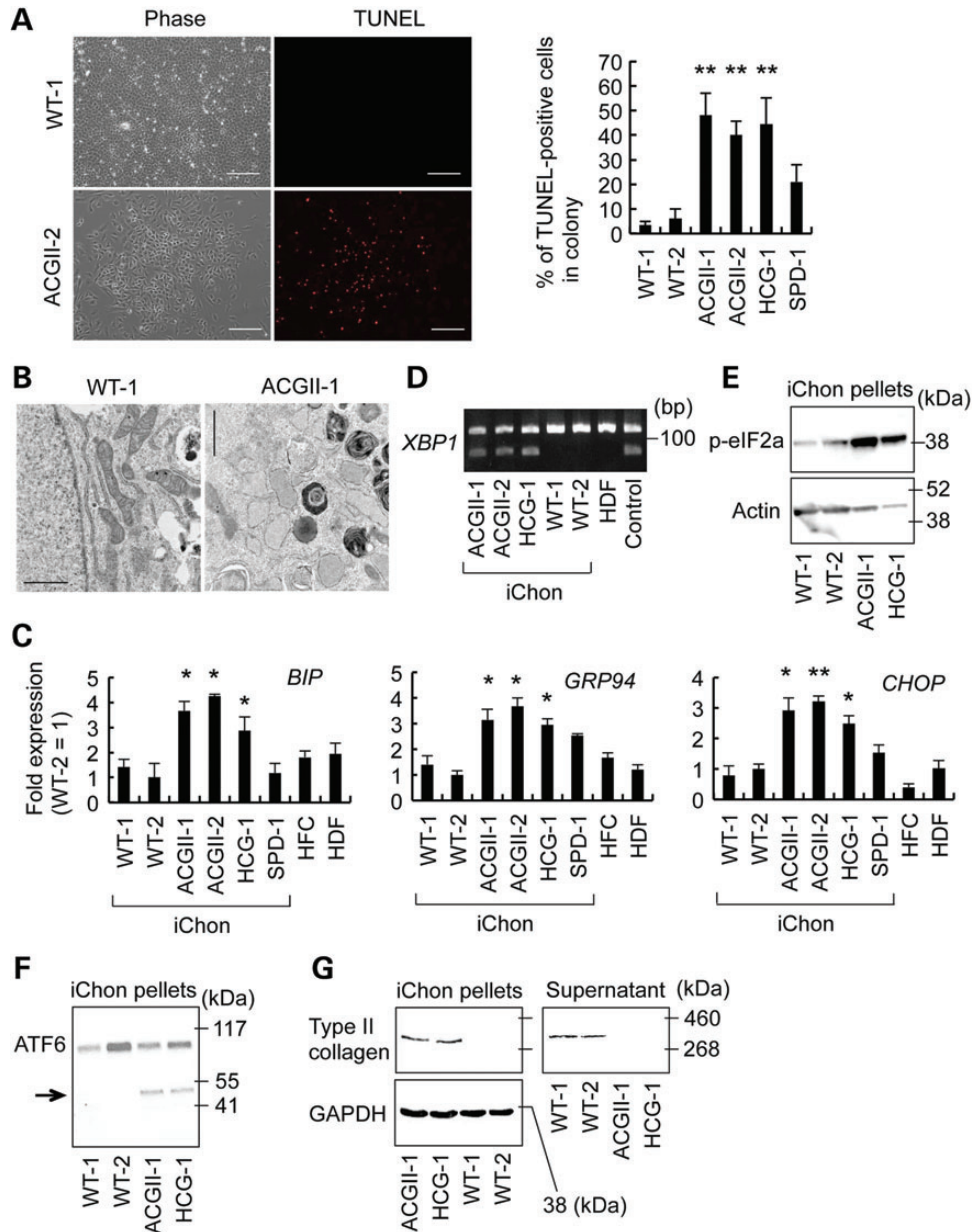


Figure 2. An analysis of the apoptosis and ER stress in COL2pathy-iChon cells. (A) (Top) TUNEL assay of iChon cell colonies on Day 14. Bars, 200 μ m. (Bottom) The ratio of the number of TUNEL-positive cells to the total number of cells within each iChon cell colony was calculated around Day 15. * $P < 0.05$, ** $P < 0.01$ compared with WT-1 and WT-2 ($n = 5$). (B) A transmission electron microscopic analysis of WT-1- and ACGII-2-iChon cells on Day 14. Bars, 1 μ m. (C) The iChon cell colonies were picked up on Day 18 and were subjected to a real-time RT-PCR expression analysis of ER stress markers, *BIP*, *GRP94* and *CHOP*. HFC, redifferentiated human fetal chondrocytes. * $P < 0.05$, ** $P < 0.01$ compared with WT-1 and WT-2 ($n = 3$). (D) The iChon cell colonies were picked up on Day 17 and were subjected to a RT-PCR analysis of the splice variants of *XBP1*. As a control, HDFs treated with 10 μ g/ml tunicamycin for 4 h were used. (E) The iChon cell colonies were picked up on Day 17 and were subjected to a western blot analysis of the phospho-eIF2a expression in iChon cells. (F) The iChon cell colonies were picked up on Day 17 and were subjected to a western blot analysis of the ATF6 expression in iChon cells. The arrow shows cleaved ATF6. (G) The iChon cell colonies were picked up on Day 17 and transferred to a well of a six-well plate. The medium was changed on Day 18. The supernatants and cells were collected on Day 19 and subjected to a western blot analysis of the type II collagen expression under the non-reducing condition.

expression analysis (Fig. 4B). The WT-iChon cell colonies stayed alive, regardless of the presence or absence of B + T (Supplementary Material, Fig. S4B). On the other hand, 10% of ACGII-2 iChon cell colonies died in the absence of B + T (Fig. 4C). The addition of B + T caused the death of half of ACGII-2-iChon cell colonies (Fig. 4C). A real-time RT-PCR analysis revealed that the addition of B + T increased the

expression of *COL2A1* in both WT-1- and ACGII-2-iChon cell colonies (Supplementary Material, Fig. S4C and Fig. 4D). The addition of ascorbic acid did not affect the viability of WT-iChon cells, but did decrease the viabilities of ACGII-iChon cells both in the presence and absence of B + T (Supplementary Material, Fig. S4D). Together, these findings suggest that the addition of B + T forced COL2pathy-iChon cells to express

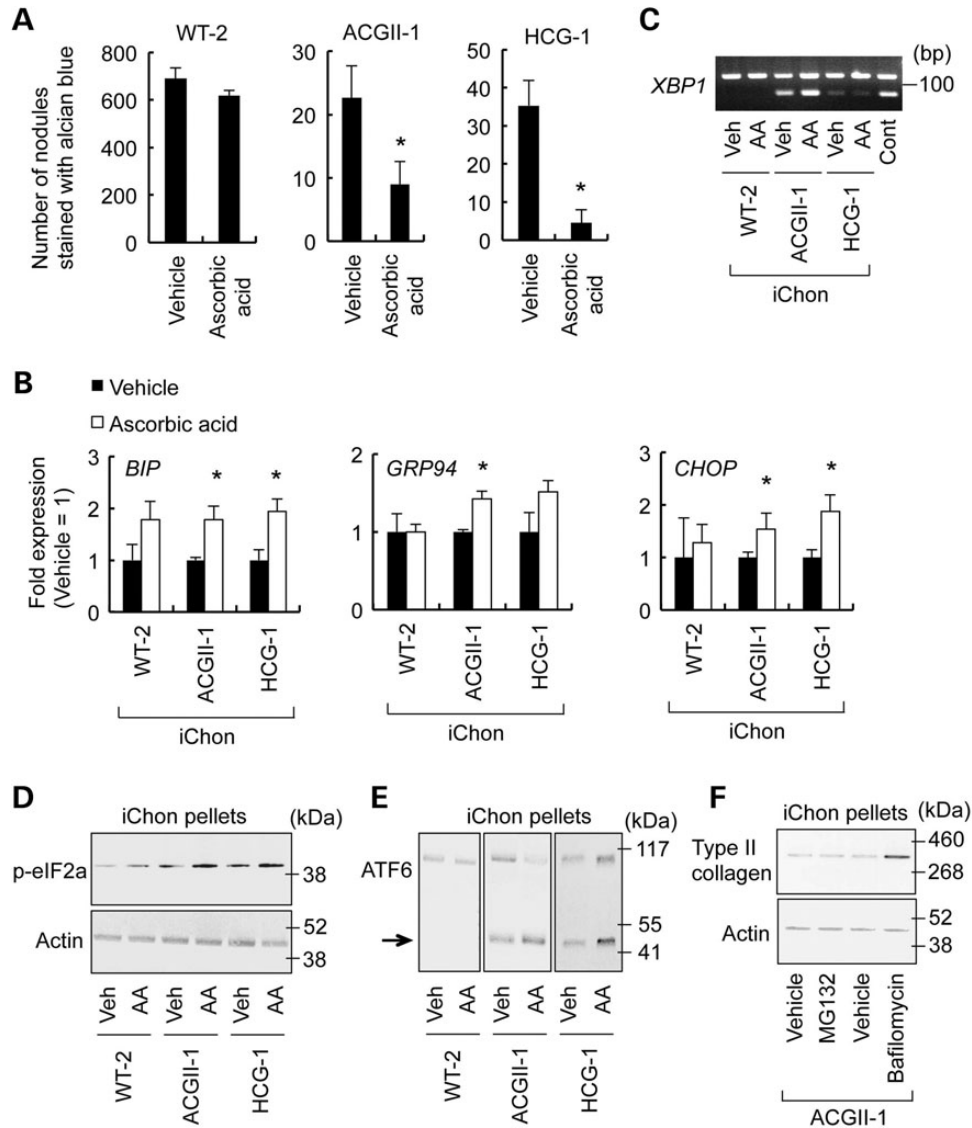


Figure 3. The effects of ascorbic acid on the abnormalities in COL2pathy-iChon cells. WT- and COL2pathy-iChon cells were induced in the presence and absence of ascorbic acid from Day 6 to Day 17. The iChon cell cultures were stained with Alcian blue on Day 17 (A). The iChon cell colonies were picked up for the RT-PCR and Western blot analyses on Day 17 (B–F). (A) After the transduction of HDFs with three factors (*c-MYC*, *KLF4* and *SOX9*), 1×10^5 cells were re-seeded onto 100 mm dishes (Day 1) and cultured in the presence or absence of ascorbic acid. The dishes were stained with Alcian blue on Day 17. The number of nodules positively stained with Alcian blue was counted. * $P < 0.05$, ** $P < 0.01$ ($n = 3$). (B) The results of the real-time RT-PCR expression analysis of ER stress markers; *BIP*, *GRP94* and *CHOP*. HFC, redifferentiated human fetal chondrocytes. * $P < 0.05$, ** $P < 0.01$ compared with WT-1 and WT-2 ($n = 3$). (C) The results of the RT-PCR analysis of the splice variants of *XBP1* on Day 17. HDFs treated with 10 $\mu\text{g/ml}$ tunicamycin for 4 h were used as a control. (D) The results of the western blot analysis of the phospho-eIF2a expression in iChon cells. (E) The results of the western blot analysis of the ATF6 expression in iChon cells. The arrow show cleaved ATF6. (F) The results of the western blot analysis of type II collagen in iChon cells in the presence of a proteasome inhibitor (MG132) or lysosome inhibitor (bafilomycin A1).

COL2A1, including mutant *COL2A1*, thus resulting in an increased amount of misfolded protein and ER stress, which eventually led to the death of iChon cells and reduced the numbers of Alcian blue-positive nodules.

TMAO, a chemical chaperone, improved secretion of type II collagen and partially reduced apoptosis in COL2pathy-iChon cells

We then examined whether a chemical chaperone known to regulate protein folding could rescue the COL2pathy-iChon cells from abnormalities. The addition of trimethylamine

N-oxide (TMAO) partially, but significantly, decreased the degree of apoptosis in COL2pathy-iChon cells (Fig. 4E). The addition of TMAO increased the amount of extracellularly secreted type II collagen (Fig. 4F), increased the Alcian blue staining (Supplementary Material, Fig. S4E) and reduced the expression levels of ER stress-related markers, *BIP*, *CHOP*, *GRP94*, *p58IPK* and *ERdj4* (Fig. 4G and Supplementary Material, Fig. S4F), in COL2-pathy iChon cell culture. These results suggest that TMAO may stabilize the misfolded type II collagen molecules, leading to the improved secretion and accumulation of the extracellular molecules and rescuing cells from apoptosis in COL2pathy-iChon cell culture.

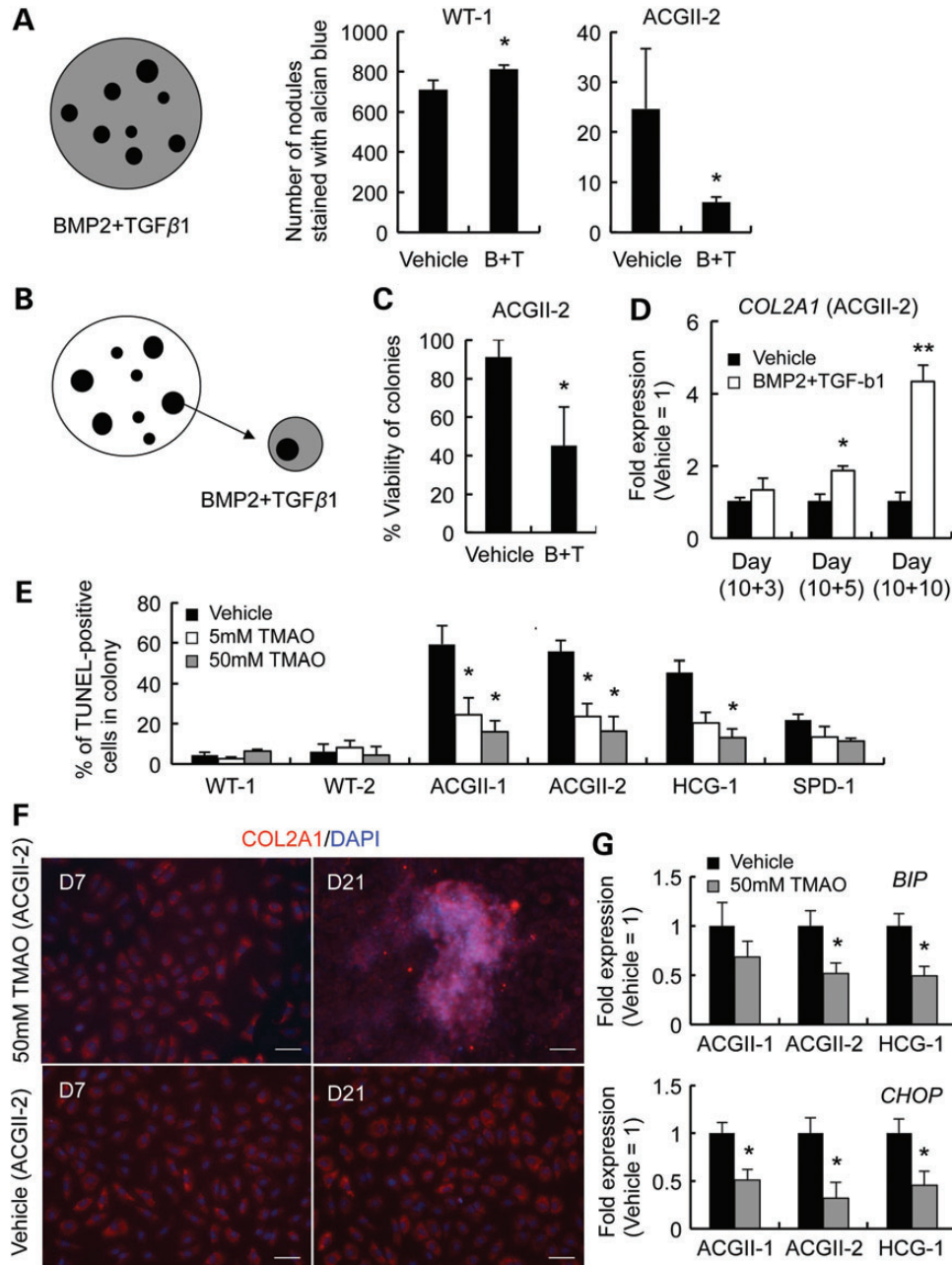


Figure 4. Effects of BMP2/TGFβ1 and chemical chaperones on COL2pathy-iChon cells. In (A) and (B), the black dots indicate iChon colonies and grey areas represent medium containing BMP2 and TGFβ1. B + T, presence of BMP2 and TGFβ1. (A) After the transduction of HDFs with three factors (*c-MYC*, *KLF4* and *SOX9*), 1×10^5 cells were re-seeded into 100 mm dishes (Day 1). BMP2 and TGFβ1 were added to the medium from Day 10 to Day 18, and dishes were subjected to Alcian blue staining on Day 18. The numbers of Alcian-blue positive nodules were counted. $*P < 0.05$ compared with dishes in the absence of BMP2 and TGFβ1 (Vehicle) ($n = 3$). (B) A schematic representation of the experiments in (C) and (D). We picked up iChon cell colonies on Day 10, replated them into individual wells and cultured them in the presence or absence of BMP2 and TGFβ1. (C) The ratio of the number of wells in which iChon cells survived for 15 days to the number of wells that initially had ACGII-2-iChon cell colonies. A total of 10–12 ACGII-2-iChon cell colonies were picked up and individually replated into new wells for each experiment. $*P < 0.05$ compared with the ratio in the absence of BMP2 and TGFβ1 (Vehicle) ($n = 3$). (D) The results of a real-time RT-PCR expression analysis of *COL2A1* in ACGII-2-iChon cells cultured in the presence or absence of BMP2 and TGFβ1 for 3, 5 and 10 days. $*P < 0.05$, $**P < 0.01$ compared with iChon colonies in the absence of BMP2 and TGFβ1 (Vehicle) ($n = 3$). (E) The effects of TMAO on the COL2pathy-iChon cells. TMAO was added to the cultures at a final concentration of 5 or 50 mM from Day 7 to Day 18. The iChon cell colonies were subjected to a TUNEL staining analysis on Day 18. The ratios of the number of TUNEL-positive cells to the number of total cells in each iChon colony are shown. $*P < 0.05$ compared with iChon colonies cultured in the absence of TMAO (Vehicle) ($n = 5$). (F) Immunocytochemical staining of ACGII-iChon cell nodules for type II collagen in the presence or absence of TMAO on Days 7, 14 and 21. Bars, 100 μm. (G) The COL2pathy-iChon cells were cultured in the presence or absence of TMAO. iChon colonies were picked up on Day 18 and were subjected to a real-time RT-PCR expression analysis of ER stress markers, *BIP* and *CHOP*. $*P < 0.05$ compared with WT-1 and WT-2 ($n = 3$).

Generation of ACGII- and HCG-specific iPS cells

Another approach to modeling COL2pathy is the generation of iPS cells, followed by differentiation of these cells toward chondrocytes. This approach takes time, but has an advantage in that it can provide an almost unlimited supply of materials, because once iPS cells are established, they can be expanded indefinitely.

We next generated iPS cells from the HDFs from two controls (WT-1 and WT-2), two ACGII patients (ACGII-1 and ACGII-2) and one HCG patient (HCG-1). We established three independent iPS cell lines (#) for each individual (Supplementary Material, Table S2). There were no obvious differences in the induction efficiency, cell morphologies (Fig. 5A), expression levels of pluripotent markers (Fig. 5B and C) or pluripotency as indicated by teratoma formation (Fig. 5D), between the WT-iPS cells, ACGII-iPS and HCG-iPS cells (Supplementary Material, Table S2). The karyotypes of the WT-iPS and ACGII-iPS cells examined were normal (Fig. 5E and Supplementary Material, Table S2). The ACGII-iPS and HCG-iPS cells were indistinguishable from control iPS cells, which was consistent with the fact that type II collagen is expressed by neither HDFs (Supplementary Material, Fig. S1E) nor the resulting iPS cells (Fig. 5F), and is unlikely to be expressed during the process of inducing the iPS cells.

In vitro differentiation of ACGII-iPS and HCG-iPS cells toward chondrocytes

We generated chondrocytes from iPS cells by following the previously described method (23), with some modifications. The targeted differentiation of iPS cells toward prochondrogenic cells was performed by serially adding combinations of growth factors for 14 days (Supplementary Material, Fig. S5A). The expression of pluripotency markers (*OCT3/4* and *NANOG*) decreased, and the expression of mesoendodermal markers (*T* and *KDR*) transiently increased, in the WT-iPS, ACGII-iPS and HCG-iPS cells that underwent differentiation (Supplementary Material, Fig. S5B). On Day 14, differentiated WT-iPS cells, ACGII-iPS and HCG-iPS cells were multilayered (Fig. 6A). We then scraped the cells and subjected them to pellet culture for chondrogenic maturation. The expression levels of chondrocytic markers increased gradually in the differentiated WT-iPS cells, whereas the level increased slightly on Days 14 and 28 and decreased on Day 42 in the differentiated ACGII-iPS and HCG-iPS cells (Fig. 6B). We then analyzed the pellets histologically. Cells were embedded in matrix, which was positively stained with safranin O, in the pellets generated from differentiated WT-iPS cells, whereas the pellets of differentiated ACGII-iPS cells were not stained with safranin O (Fig. 6C and Supplementary Material, Fig. S6). The cells in the pellets of differentiated ACGII-iPS cells underwent apoptosis, as indicated by their expression of cleaved caspase-3 and positive TUNEL staining (Fig. 6C). The expression of ER stress markers in differentiated ACGII-iPS and HCG-iPS cells was significantly elevated compared with that in differentiated WT-iPS cells on Day 42 (Fig. 6D and Supplementary Material, Fig. S5C). Furthermore, TMAO reduced the expression of ER stress markers (Supplementary Material, Fig. S5D). These results indicate that the chondrogenic differentiation of ACGII-iPS and HCG-iPS cells causes ER stress and apoptosis.

To determine which types of chondrocytic cells were generated by these two methods (induction of iChon cells and chondrogenic differentiation of iPS cells), we analyzed the expression of marker genes for growth plate cartilage and articular cartilage (Supplementary Material, Fig. S7). The WT-iChon cells and chondrogenically differentiated WT-iPS cells expressed markers for articular cartilage (*PRG4* and *CILP*), but not markers for hypertrophic chondrocytes in the growth plate (*COL10A1* and *MMP13*). These results suggest that the iChon cells and chondrogenically differentiated iPS cells may have the characteristics of articular chondrocytes or epiphyseal proliferative chondrocytes in primordial cartilage.

Modeling of ACGII-cartilage in teratomas in immunodeficient mice

We next examined the cartilage in teratomas formed by the transplantation of iPS cells into immunodeficient mice. A histological analysis of the teratomas revealed that cartilage tended to be smaller, and that the extracellular matrix was thinner and more weakly stained with safranin O in the teratomas formed by ACGII-iPS cells compared with the cartilage in teratomas formed by WT-iPS cells (Fig. 7A). The chondrocytes were large in the teratomas formed by ACGII-iPS cells. These histological findings recapitulate the findings of cartilage obtained from ACGII patients at the time of autopsy (24,25).

An immunohistochemical analysis showed that type II collagen existed abundantly in the extracellular matrix, but not inside of cells, in the cartilage in the teratomas formed by WT-iPS cells (Fig. 7B, top panels). On the other hand, type II collagen existed in a thin matrix in a reduced amount, and existed within the cells, in the cartilage in the teratomas formed by ACGII-iPS cells (Fig. 7B, bottom panels). The type II collagen detected within these cells may correspond to the accumulation of misfolded type II collagen in the rER. Cartilage containing such chondrocytes bearing type II collagen within the cells were absent in the immunohistological sections of teratomas formed by control iPS cells (Fig. 7C).

An electron microscopic analysis revealed a distended rER in the chondrocytes in the teratomas formed by ACGII-iPS cells (Fig. 7D). The extracellular matrix showed reduced densities of collagen fibrils (Fig. 7E). These results collectively demonstrate that COL2pathy-specific teratomas contain cartilage which recapitulates the cartilage tissue in patients with COL2pathy.

DISCUSSION

We herein performed disease modeling for type II collagenopathies using three approaches: (i) directed conversion from patient-specific HDFs to iChon cells; (ii) the generation of iPS cells from patient-specific HDFs, followed by the differentiation of these cells toward chondrocytes *in vitro* and (iii) the generation of iPS cells, followed by the formation of teratomas containing cartilage in mice. Using these approaches, the expected pathological features, such as elevated expression of ER stress markers, apoptosis, the retention of type II collagen within cells and abnormal ultrastructure of the extracellular matrix, were recapitulated. In addition, the severity of diseases tended to correlate with degrees of abnormalities in the COL2pathy-

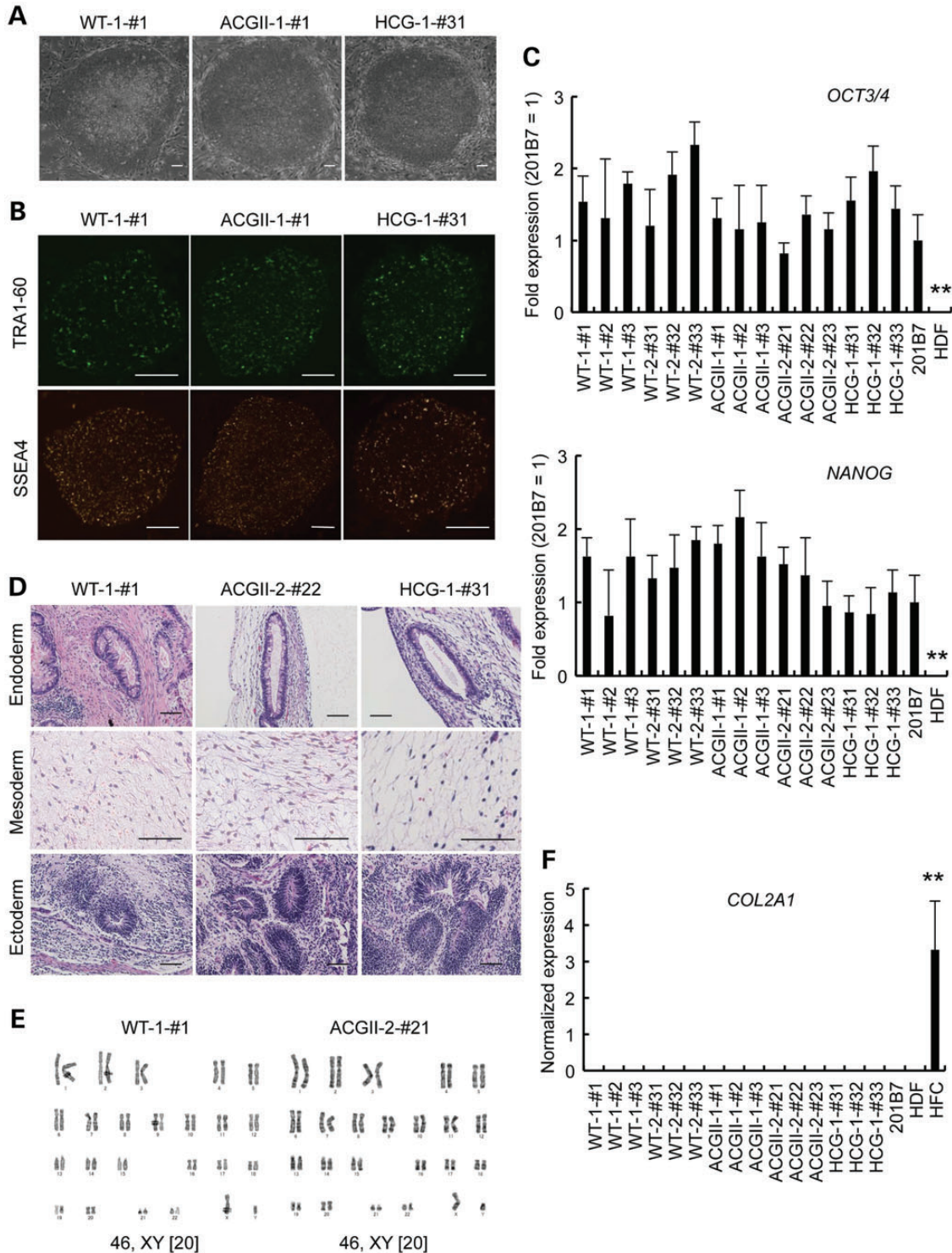


Figure 5. Generation of iPS cells from HDFs from two control neonates (WT-1 and WT-2), HDFs from two ACGII patients (ACGII-1 and ACGII-2) and HDFs from one HCG patient (HCG-1). Three independent iPS cell lines (#) were established for each individual. **(A)** The morphology of iPS cells generated from WT-1-HDFs, ACGII-1-HDFs and HCG-1-HDFs. There were not obvious differences in the cell morphologies between WT-iPS cells and ACGII-iPS cells. Bars, 50 μ m. **(B)** The immunocytochemical analysis. WT-1-#1-iPS cells, ACGII-1-#1-iPS cells and HCG-1-#31-iPS cells expressed TRA1-60 and SSEA4. Bars, 100 μ m. **(C)** The results of a real-time RT-PCR expression analysis of *OCT3/4* and *NANOG* in iPS cell lines. The previously reported iPS cell clone, 201B7 (22), was used as a positive control. There were no significant differences in the expression levels among the WT-iPS cells, ACGII-iPS cells and HCG-iPS cells. ($n = 3$). $**P < 0.01$ compared with iPS cell lines. **(D)** The results of the teratoma formation assay. iPS cells were injected into testicular capsules. The masses formed at the injected sites were recovered 6–8 weeks after injection, and were subjected to a histological analysis. Teratomas containing tissues from all three germ layers were formed by the injection of WT-1-#1 iPS cells, ACGII-2-#22 iPS cells and HCG-#31-iPS cells. Hematoxylin and eosin staining. Bars, 100 μ m. **(E)** The results of a karyotype analysis of iPS cell lines (WT-1-#1 and ACGII-2-#21). A total of 20 cells for each cell line was examined. The numbers in brackets indicate the number of cells showing the karyotype presented. All 20 cells in both cell lines showed a normal 46XY karyotype. **(F)** The results of a real-time RT-PCR expression analysis of *COL2A1* expression in iPS cell lines. HFC, redifferentiated human fetal chondrocytes. ($n = 3$). $**P < 0.01$ compared with iPS cell lines.

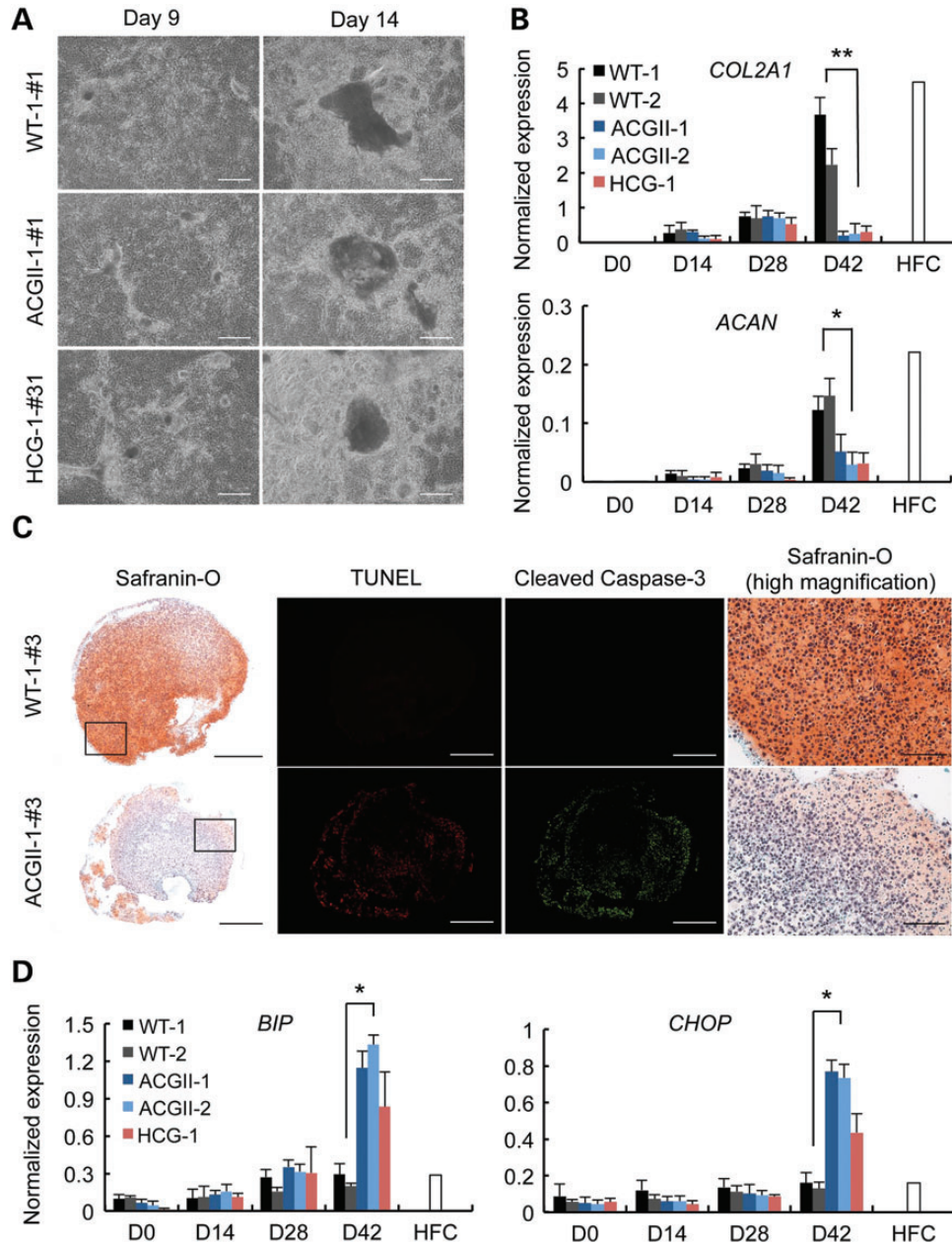


Figure 6. Chondrogenic differentiation of COL2pathy-iPS cells. (A) iPS cells were differentiated toward chondrocytes following the protocol shown in Supplementary Material, Figure S5A. A phase contrast image of the cultures on Days 9 and 14. Bars, 200 μm . (B) The results of the expression analysis for chondrogenic markers. Cells or pellets were harvested on Days 0, 14, 28 and 42, and were subjected to a real-time RT-PCR expression analysis. * $P < 0.05$, ** $P < 0.01$ compared with WT-1 and WT-2 ($n = 3$). HFC, redifferentiated human fetal chondrocytes. (C) The histological analysis of the pellet culture of chondrogenically differentiated ACGII-iPS cells. Pellets were subjected to an analysis on Day 42. Sections were stained with safranin O, immunostained with anti-cleaved caspase-3 and subjected to the TUNEL assay. Magnified images of the boxed region in the left panels are shown in the right panels. The bars in the left and center panels, 500 μm ; bars in the right panels, 50 μm . (D) The results of the expression analysis for ER stress markers. Cells or pellets were harvested on Days 0, 14, 28 and 42, and were subjected to a real-time RT-PCR expression analysis. ** $P < 0.01$ compared with WT-1 and WT-2 ($n = 3$). HFC, redifferentiated human fetal chondrocytes.

iChon cells. These results suggest that the models presented in this study can provide a useful platform for investigating the pathomechanisms of and drug screening for COL2pathy. In fact, we investigated the cellular response of the model to reagents which increase ER stress (BMP and TGF β) or reduce ER stress (TMAO), which provided insights into the pathomechanisms underlying COL2pathy and some information for drug discovery.

The cellular consequences of ER stress signaling are context-dependent, and range from adaptation to cell death, depending on the levels of ER stress signaling (8). By analyzing iChon cell models of COL2pathy, we discovered several findings that may contribute to understanding the pathomechanisms of COL2pathy. The COL2pathy-iChon cells are chondrogenically committed, because the levels of *SOX5* and *SOX6* expression in the COL2pathy-iChon cells were similar to those in control iChon

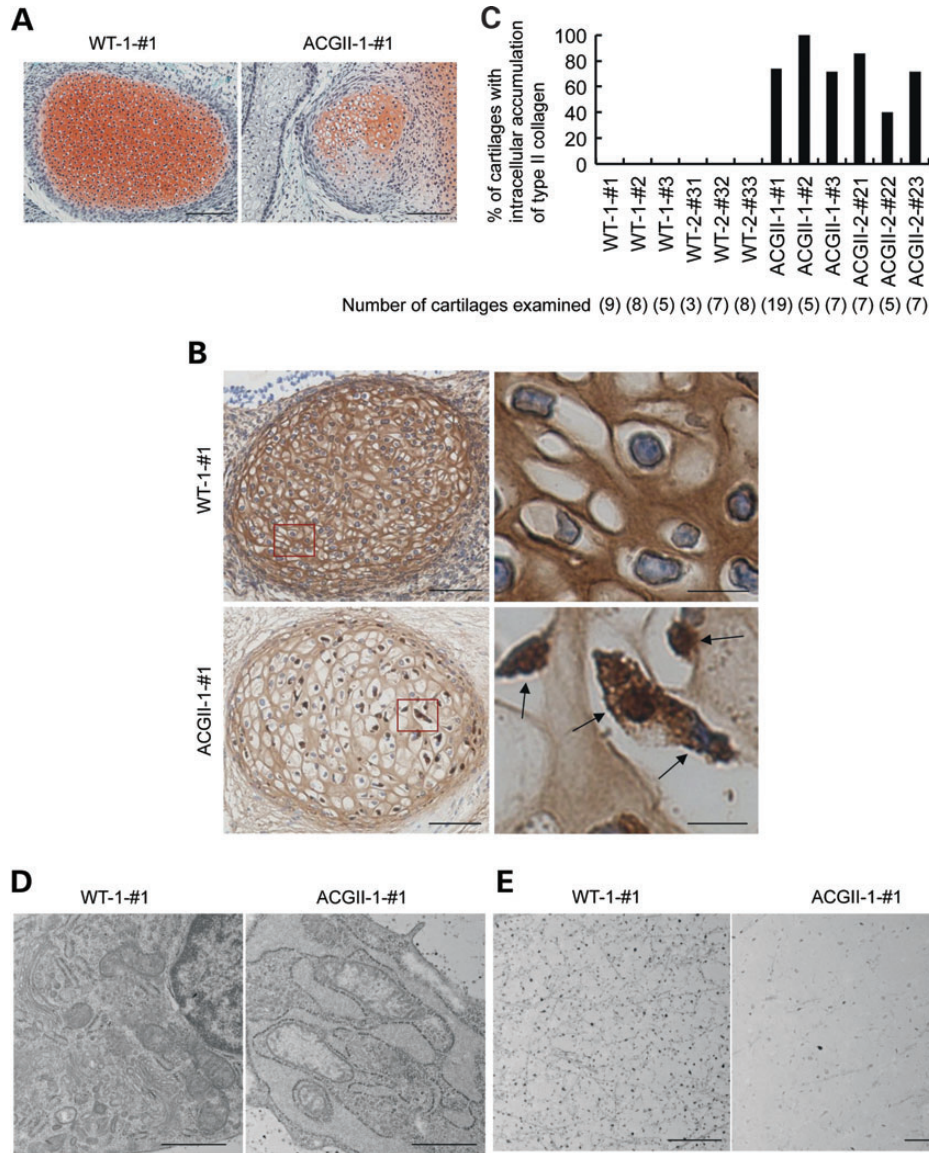


Figure 7. Examination of the cartilage formed in teratomas. (A) Safranin O-fast green-iron hematoxylin staining. The extracellular matrix was intensely stained with safranin O in the cartilage in teratomas generated by the injection of WT-1-#1-iPS cells. The extracellular matrix was weakly stained with safranin O in the cartilage in teratomas generated by injection of ACGII-1-#1-iPS cells. Bars, 200 μ m. (B) Immunohistochemistry for type II collagen in the cartilage in teratomas generated by injection of WT-1-#1-iPS cells and ACGII-1-#1-iPS cells. The boxed regions in the left panels are magnified and shown on the right. Note the intense signal (arrows) within the chondrocytes in the bottom right panel. Bars, 100 μ m (left), 20 μ m (right). (C) The number of cartilage tissues which contained chondrocytes bearing type II collagen within cells was divided by the total number of cartilage tissues on the immunohistological sections of teratomas. The total number of cartilage tissues is indicated at the bottom. (D) The results of a transmission electron microscopic analysis of chondrocytes. Note the distended rER in chondrocytes in the cartilage in teratomas generated by injection of ACGII-1-#1-iPS cells. Bars, 1 μ m. (E) The results of a transmission electron microscopic analysis of the extracellular matrix. Note the sparse collagen fibrils in the extracellular matrix in the cartilage in teratomas generated by injection of ACGII-1-#1-iPS cells. Bars, 1 μ m.

cells and were comparable to those in HFCs on Day 14 (Fig. 1C and Supplementary Material, Fig. S2D). The expression levels of *COL2A1* gradually increased during the maturation of iChon cells (Fig. 1D), probably resulting in an accumulation of mutant *COL2A1* and unfolded protein in the rER in COL2pathy-iChon cells (Fig. 2B). This caused ER stress signaling (Fig. 2C–F). When the ER stress is moderate, ER stress signaling may result in adaptations to reduce the expression of *COL2A1* (Fig. 1D and E) and other cartilage matrix genes (Supplementary Material, Fig. S2E) to decrease the amount of misfolded protein. When ER stress is further increased due to the

maturation of iChon cells, the increased ER stress signaling may induce cell death (Fig. 2A and Supplementary Material, Movie S1).

Controlling *COL2A1* expression is important in the development of the disease phenotype

We found that the treatment of COL2pathy-iChon cells with BMP2 and TGF β 1 inhibited the formation of chondrogenic nodules and caused cell loss (Fig. 4A and C). The treatment increased the expression of *COL2A1* (Fig. 4D) and probably

mutant *COL2A1*, which likely resulted in increased ER stress. This finding could explain the abnormalities observed in tissue morphogenesis during development and growth in the individuals with COL2pathy, because prochondrogenesis factors, including BMPs and TGF β s, necessarily presage the emergence of a specific developmental phenotype. During the development and growth of COL2pathy patients, prechondrogenic cells may initially adapt to the ER stress. However, when the chondrogenic cells mature in response to exposure to growth factors, including BMPs and TGF β s, the expression of *COL2A1* increases, increasing the ER stress beyond the limit of adaptation, triggering apoptotic signaling and the development of the disease phenotype. Thus, the ability of a cell to adapt to ER stress, and the nature of its adaptation strategies, can determine the disease phenotype.

Molecular chaperones can be a candidate therapeutic drug for COL2pathy

The adverse effects of BMP2 and TGF β 1 on the survival of COL2pathy-iChon cells suggest that the application of chondrogenic drugs will likely worsen the symptoms in patients with COL2pathy. However, we also discovered that chemical chaperones may be a promising treatment, because TMAO decreased the apoptosis of COL2pathy-iChon cells (Fig. 4E). TMAO is a natural chemical chaperone that directly acts on proteins in the unfolded state, thereby increasing the folding rate and stability of various mutant, otherwise labile, proteins (26). This function of TMAO led to improved secretion of type II collagen (Fig. 4F), decreasing ER stress in COL2pathy iChon cells (Fig. 4G and Supplementary Material, Fig. S4F) and differentiated COL2pathy iPS cells (Supplementary Material, Fig. S5D). It remains to be analyzed whether TMAO can rescue the folding of type II collagen in COL2pathy iChon cells. Additional studies will be needed to screen for more effective chemical chaperones that substantially rescue these cells from apoptosis that may be clinically applicable.

COL2pathy-iChon cells, chondrogenically differentiated COL2pathy-iPS cells and cartilage in teratomas from COL2pathy-iPS cells can be used complementarily

We detected abnormalities in COL2pathy-iChon cells as early as Day 14. This is a relatively short-term culture, and given them an advantage compared with iPS cells, which take several months to generate and subsequently redifferentiate into chondrocytes. Another advantage of this model is that a lot of iChon cell colonies can be obtained in each experiment. Time-lapse observations over the course of iChon cell induction showed that each iChon cell colony appears to be clonal (17, 18), although it is possible that more than one cell may give rise to an iChon cell colony. Multiple colonies can be examined in iChon cell models, contributing to the reproducibility of the results. On the other hand, the abnormalities are exaggerated in iChon cell models. The formation of chondrogenic nodules from COL2pathy-iChon cells was severely reduced, whereas cartilage is still formed in COL2pathy patients, although to a lesser extent than healthy subjects. An advantage of using iPS cells is their ability to be expanded almost indefinitely, making it possible to use them for high-throughput drug screening.

We herein demonstrated that the cartilage in the teratomas generated from ACGII-iPS cells recapitulates the phenotypes seen in the cartilage of patients. The effects of candidate drug can be tested on human cartilage, by applying them to the mice harboring teratoma.

While useful for exploring pathologies that result from impaired protein trafficking, these cell-based models may have more limited utility when exploring pathologies that result from altered signaling between cells or between cells and matrix components. Matricellular signaling defects are emerging as an important pathogenic mechanism in skeletal diseases, and such defects are not well modeled in culture systems, because they do not yet recapitulate the complex structure of the mammalian growth plate and articular cartilages.

High-throughput screening, which requires a large number of cells may be performed using chondrogenically differentiated COL2Pathy-iPS cells. When the optimal category of therapeutic drug is determined (for example, molecular chaperone) and the numbers of compounds for screening are limited, the COL2pathy-iChon cells from fibroblasts can be used for the screening of these limited compounds. Such disease modeling by directed conversion of cells and iPS cells would also be useful for other skeletal dysplasias and cartilage diseases, and may have other applications for difficult to obtain tissues.

MATERIALS AND METHODS

Cell culture

COL2-pathy HDFs derived from four different patients (Supplementary Material, Table S1) were obtained from the cell banks of the Coriell Institute and Saitama Children's Medical Center. Control HDFs from two different neonates were purchased from KURABO (Strain #1439 and #789013). HDFs were cultured in DMEM (Sigma) with 10% FBS (Invitrogen), 50 U/ml penicillin and 50 μ g/ml streptomycin. Human iChon cells were induced and maintained in DMEM (Sigma) with 10% FBS (Invitrogen), 50 U/ml penicillin and 50 μ g/ml streptomycin. Human iPS cells were maintained in DMEM/F12 (Sigma) with 20% Knockout Serum Replacement (Invitrogen), 2 mM L-glutamine, 100 μ M non-essential amino acids, 100 μ M β -mercaptoethanol, 4 ng/ml bFGF (Wako), 50 U/ml penicillin and 50 μ g/ml streptomycin on mitomycin-C-treated mouse embryonic fibroblasts.

Generation of iChon cells

Retroviral transduction was performed as described (17). Briefly, after nucleofection of the mouse *slc7a1* gene (Takahashi *et al.*, 2007), human fibroblasts were infected with retroviruses encoding c-MYC, KLF4 and SOX9 using Plat-E cells and the pMX system (Day 0). The next day, the infected fibroblasts (1×10^5 cells) were re-seeded into 100 mm dishes (Day 1), unless otherwise specified. In the case of iChon cell colony expansion, the infected fibroblasts (2×10^4 cells) were re-seeded into 100 mm dishes, and iChon cell colonies were picked up using 200 μ l pipettes under a microscope, and were then re-seeded into the wells of a 24-well plate. The iChon cells were generated and maintained in DMEM supplemented with 10% FBS, unless otherwise specified. In the experiments shown in Figure 3, 50 μ g/ml of ascorbic acid (Nacalai) or

vehicle (water) was added to the medium from Day 6 to Day 17, and cells were subjected to an analysis on Day 17.

Alcian blue and toluidine blue staining

Cells were fixed in 100% methanol (Nacalai Tesque, Japan) for 2 min at -20°C , stained with pH 2.5 Alcian blue (Merck) or pH 4.1 toluidine blue (Wako) for 2 h at 25°C , and washed three times with distilled water. The Alcian blue- or toluidine blue-positive colony numbers were counted using the NIS Element software program (Nikon). We defined a colony as a cell cluster that was more than 0.5 mm in diameter.

Immunofluorescence

iChon cells were cultured on slides, fixed in 4% paraformaldehyde for 15 min at 25°C , washed three times with PBS and blocked for 18 h in PBS containing 0.3% BSA (Sigma) and 0.1% Triton X-100 (Nacalai) at 4°C . Primary antibodies against COL2A1 (Collagen II Ab-2, Thermo scientific), SSEA4 (ab16287, abcam) and TRA-1-60 (ab16288, abcam) in PBS containing 0.3% BSA and 0.1% Triton X-100 were applied for 1 h at 25°C . After washing the samples three times with PBS, secondary antibodies were applied for 1 h at 25°C .

RT-PCR and real-time RT-PCR analyses

The total RNA was extracted using RNeasy Mini Kits (Qiagen) or TRIzol (Invitrogen). The total RNAs prepared from the redifferentiated human primary fetal chondrocytes (HFC) were purchased from Cell Applications, Inc. (402RD-R10f). RT-PCR and real-time quantitative RT-PCR were performed as described previously (16). Briefly, 100 ng of total RNA was used to synthesize the first-strand cDNA (20 μl scale) that was used as a template (2 μl after 1:5 dilution) for RT-PCR and real-time RT-PCR. Real-time RT-PCR was performed in 384-well plates using the Step-One-Plus real-time PCR system (Applied Biosystem). Normalized expression levels were calculated using the comparative CT method, with the *GAPDH* mRNA expression level used as internal control. The primers used for real-time RT-PCR are listed in Supplementary Material, Table S3. Real-time RT-PCR was carried out with 'n' samples (each sample consisted of 10–20 iChon colonies) in Figures 1–4 and Supplementary Material, Figures S1, S2 and S4, or with one iPS clone tested in triplicate in Figures 5, 6 and Supplementary Material, Figures S5 and S7.

The primers used for the RT-PCR amplification of *COL2A1* cDNA fragments from ACGII-1 iChon cells (the experiment shown in Supplementary Material, Fig. S1B) are: forward, GAGAAGGGAGAAGTTGGACCTC and reverse, AGCCTC TCCTTTGTCACCTCTG. The primers used for the RT-PCR amplification of *XBPI* cDNA fragments from iChon cells (the experiments shown in Figs 2D and 3C) were: forward, AATG AAGTGAGGCCAGTGGCC and reverse, AATACCGCCAG AATCCATGGG.

TUNEL assay

iChon cell colonies were fixed in freshly prepared 4% paraformaldehyde for 1 h at 25°C . An *in situ* cell death detection kit

(TMR red; Roche) was used according to the manufacturer's instructions. The ratio of TUNEL positive cells to the total cells in one iChon colony was calculated in this study. The numbers of colonies examined are indicated in the figure legends.

Antibodies and inhibitors

The primary antibodies against COL2A1 (Santa Cruz), phospho-eIF2a (Cell Signaling), ATF6 (abcam), GAPDH (Santa Cruz), and b-Actin (Cell Signaling) were applied for the western blot analyses using total cell extracts and supernatants prepared from iChon cell cultures. Alkaline phosphatase-conjugated secondary antibodies were purchased from Invitrogen. MG132 (Abcam) and bafilomycin A1 (Abcam) were used as the proteasome and lysosome inhibitors, respectively, as described in a previous report (27). We treated iChon cells with final concentration of 4 μM MG132 or 200 nM bafilomycin A1 for 18 h.

Western blot

Samples were subjected to electrophoresis in 3–8% Tris–Acetate gels (Invitrogen) in the absence of dithiothreitol and 2-mercaptoethanol (under non-reducing condition) to detect type II collagen, and in gradient 4–12% Bis–Tris gels (Invitrogen) in the presence of 200 mM dithiothreitol after boiling for 5 min at 95°C to detect phospho-eIF2a and ATF6. The separated proteins were transferred to nitrocellulose membranes and incubated for 1 h at 25°C in 5% skim milk. The indicated primary antibodies (COL2A1 at a dilution of 1:200, phospho-eIF2a at 1:1000, ATF6 at 1:500, and GAPDH and β -Actin at 1:2000) were applied for 18 h at 4°C . After washing the samples three times with PBS, alkaline phosphatase-conjugated secondary antibodies (1:2000) were applied for 1 h at 25°C . After washing the membranes, the proteins were detected by the 4-nitro-blue-tetrazolium-chloride and 5-bromo-4-chloro-3-indolyl-phosphate reactions.

Preparation of TMAO

The stock TMAO (Tokyo chemical industry, Japan) solution was prepared by dissolving TMAO in distilled water at a concentration of 5 M. Aliquots of stock TMAO/water solutions were added to the culture medium. As a control, an equal amount of water was added to the medium. A total of 50 $\mu\text{g}/\text{ml}$ ascorbic acid was added in addition to the medium in the experiment of Supplementary Material, Figure S4D.

Preparation of chondrogenic supplements

Chondrogenic supplementation was performed using 50 ng/ml BMP2 and 10 ng/ml TGF β 1 as a working concentration. Stock solutions of the chondrogenic supplements were prepared at $\times 1000$ concentration in PBS containing 0.1% BSA, and were added to the culture medium. As a control, an equal volume of PBS containing 0.1% BSA was added to the medium.

Generation of human iPS cells and teratomas

Episomal plasmid vectors (Mixture Y4: *OCT3/4*, *SOX2*, *KLF4*, *L-MYC*, *LIN28*, and *p53* shRNA) were electroporated into

human fibroblasts (28) with the Neon transfection system (Invitrogen). A week after transduction, 1×10^5 cells were re-seeded into 100 mm dishes with feeders. The cells were subsequently cultured in hiPS medium. To form teratomas, we injected 1×10^6 hiPS cells into the testicular capsules of BALB/c AJcl-*nu/nu* male mice. Then, 6–8 weeks later, tumors were cut into 5 mm pieces and fixed in 10% formalin. The tissue was embedded in paraffin and stained with hematoxylin and eosin.

In vitro chondrogenic differentiation of human iPS cells

Chondrogenic differentiation was performed following a previous report (23), with some modifications. To remove feeder cells, iPS cells were seeded and cultured in ReproFF2 (ReproCELL) medium on matrigel-coated dishes for two or three passages. After removing feeders (Day 0), the iPS cells were cultured in RPMI 1640 (Days 1–3) or DMEM (Days 4–14) supplemented with 1% FBS and human recombinant proteins (25 ng/ml WNT3A (R&D), 25 ng/ml Activin-A (R&D), 20 ng/ml FGF2 (R&D), 10 ng/ml TGF β 1 (Peprotech), 40 ng/ml BMP2 (Astellas, Japan) and 100 ng/ml GDF5 (PTT) (Supplementary Material, Fig. S5A). Differentiated cells were scraped on Day 14, and 5×10^5 cells were centrifuged at 500 g for 10 min in a 15 ml tube. Pellets were cultured in DMEM with 10% FBS, 50 μ g/ml ascorbic acid, 10 ng/ml TGF β 1, 10^{-7} M dexamethasone, 100 μ g/ml sodium pyruvate and ITS (10 μ g/ml insulin, 5.5 μ g/ml transferrin and 6.7 ng/ml sodium selenite) for 4 weeks (Days 14–42).

Immunohistochemical staining

Teratoma formation was induced using six control iPS and six ACGII iPS cell lines. Semi-serial histological sections generated from formalin-fixed teratomas were immunostained with the primary and secondary antibodies. For a positive control, sections obtained from the joint capsule of a knee from a rat were used to test the anti-type II antibodies (SBA-1320-01, BIOZOL).

Electron microscopy

Teratomas or iChon cells were fixed with 4% paraformaldehyde and 2% glutaraldehyde. Post-fixation was performed with 2% osmium tetroxide. In the case of the teratoma analysis, cartilage tissues were found according to the morphology of cells and toluidine blue staining. After dehydration, embedding and polymerization, ultrathin sections were stained with 2% uranyl acetate. They were observed with a HITACHI 7650 electron microscope at an acceleration voltage of 80 kV.

Statistical analysis

The data are shown as averages and standard deviations. In this study, we used two-tailed Student's *t*-tests or one-way ANOVA (analysis of variance) with a Tukey–Kramer *post-hoc* test for multiple comparisons. *P*-values <0.05 were considered to be statistically significant.

All experiments were approved by the institutional review board of Kyoto University and the institutional biosafety committee of Kyoto University.

SUPPLEMENTARY MATERIAL

Supplementary Material is available at HMG online.

ACKNOWLEDGEMENTS

We thank Nobuhiko Kan for providing samples. We thank Kaori Fujita and Hiromi Kishi for assistance.

FUNDING

This study was supported in part by the Japan Science Technology Agency (JST) (CREST to N.T.); Scientific Research Grants (24791541 and 26861187 to M.O., 24390354 to N.T.) from MEXT; the Research Center Network for Realization of Regenerative Medicine (to N.T.); and the Scientific Research from the Ministry of Health, Labor and Welfare of Japan (to H.S. and N.T.).

REFERENCES

- Olsen, B.R., Reginato, A.M. and Wang, W. (2000) Bone development. *Annu. Rev. Cell Dev. Biol.*, **16**, 191–220.
- Khoshnoodi, J., Cartailier, J.-P., Alvares, K., Veis, A. and Hudson, B.G. (2006) Molecular recognition in the assembly of collagens: terminal noncollagenous domains are key recognition modules in the formation of triple helical protomers. *J. Biol. Chem.*, **281**, 38117–38121.
- Kielty, C.M., Hopkinson, I. and Grant, M.E. (1993) In Royce, P.M. and Steinmann, B. (eds), *Connective Tissue and its Heritable Disorders: Molecular, Genetic, and Medical Aspects*. Wiley-Liss, Inc., New York, pp. 103–147.
- Warman, M.L., Cormier-Daire, V., Hall, C., Krakow, D., Lachman, R., LeMerrer, M., Mortier, G., Mundlos, S., Nishimura, G., Rimoin, D.L. *et al.* (2011) Nosology and classification of genetic skeletal disorders: 2010 revision. *Am. J. Med. Genet. Part A*, **155A**, 943–968.
- Ala-Kokko, L., Baldwin, C.T., Moskowitz, R.W. and Prockop, D.J. (1990) Single base mutation in the type II procollagen gene (COL2A1) as a cause of primary osteoarthritis associated with a mild chondrodysplasia. *Proc. Natl Acad. Sci. USA*, **87**, 6565–6568.
- Zankl, A., Zabel, B., Hilbert, K., Wildhardt, G., Cuenot, S., Xavier, B., Ha-Vinh, R., Bonafè, L., Spranger, J. and Superti-Furga, A. (2004) Spondyloperipheral dysplasia is caused by truncating mutations in the C-propeptide of COL2A1. *Am. J. Med. Genet. Part A*, **129A**, 144–148.
- Bateman, J.F., Boot-Handford, R.P. and Lalandé, S.R. (2009) Genetic diseases of connective tissues: cellular and extracellular effects of ECM mutations. *Nat. Rev. Genet.*, **10**, 173–183.
- Tsang, K.Y., Chan, D., Bateman, J.F. and Cheah, K.S.E. (2010) In vivo cellular adaptation to ER stress: survival strategies with double-edged consequences. *J. Cell Sci.*, **123**, 2145–2154.
- Furuichi, T., Masuya, H., Murakami, T., Nishida, K., Nishimura, G., Suzuki, T., Imaizumi, K., Kudo, T., Ohkawa, K., Wakana, S. *et al.* (2011) ENU-induced missense mutation in the C-propeptide coding region of Col2a1 creates a mouse model of platyspondylic lethal skeletal dysplasia, Torrance type. *Mammalian Genome: Official Journal of the International Mammalian Genome Society*, **22**, 318–328.
- Hintze, V., Steplewski, A., Ito, H., Jensen, D.a., Rodeck, U. and Fertala, A. (2008) Cells expressing partially unfolded R789C/p.R989C type II procollagen mutant associated with spondyloepiphyseal dysplasia undergo apoptosis. *Hum. Mutat.*, **29**, 841–851.
- Aigner, T., Cook, J.L., Gerwin, N., Glasson, S.S., Laverty, S., Little, C.B., McIlwraith, W. and Kraus, V.B. (2010) Histopathology atlas of animal model systems - overview of guiding principles. *Osteoarth. Cartil.*, **18**(Suppl. 3), S2–S6.
- Sun, N., Yazawa, M., Liu, J., Han, L., Sanchez-Freire, V., Abilez, O.J., Navarrete, E.G., Hu, S., Wang, L., Lee, A. *et al.* (2012) Patient-specific induced pluripotent stem cells as a model for familial dilated cardiomyopathy. *Sci. Translat. Med.*, **4**, 130ra147.

13. Israel, M.a., Yuan, S.H., Bardy, C., Reyna, S.M., Mu, Y., Herrera, C., Hefferan, M.P., Van Gorp, S., Nazor, K.L., Boscolo, F.S. *et al.* (2012) Probing sporadic and familial Alzheimer's disease using induced pluripotent stem cells. *Nature*, **482**, 216–220.
14. Egawa, N., Kitaoka, S., Tsukita, K., Naitoh, M., Takahashi, K., Yamamoto, T., Adachi, F., Kondo, T., Okita, K., Asaka, I. *et al.* (2012) Drug screening for ALS using patient-specific induced pluripotent stem cells. *Sci. Translat. Med.*, **4**, 145ra104–145ra104.
15. Qiang, L., Fujita, R., Yamashita, T., Angulo, S., Rhinn, H., Rhee, D., Doege, C., Chau, L., Aubry, L., Vanti, W.B. *et al.* (2011) Directed conversion of Alzheimer's disease patient skin fibroblasts into functional neurons. *Cell*, **146**, 359–371.
16. Hiramatsu, K., Sasagawa, S., Outani, H., Nakagawa, K., Yoshikawa, H. and Tsumaki, N. (2011) Generation of hyaline cartilaginous tissue from mouse adult dermal fibroblast culture by defined factors. *J. Clin. Invest.*, **121**, 640–657.
17. Outani, H., Okada, M., Yamashita, A., Nakagawa, K., Yoshikawa, H. and Tsumaki, N. (2013) Direct induction of chondrogenic cells from human dermal fibroblast culture by defined factors. *PLoS ONE*, **8**, e77365.
18. Outani, H., Okada, M., Hiramatsu, K., Yoshikawa, H. and Tsumaki, N. (2011) Induction of chondrogenic cells from dermal fibroblast culture by defined factors does not involve a pluripotent state. *Biochem. Biophys. Res. Commun.*, **411**, 607–612.
19. Akiyama, H., Chaboissier, M.C., Martin, J.F., Schedl, A. and de Crombrughe, B. (2002) The transcription factor Sox9 has essential roles in successive steps of the chondrocyte differentiation pathway and is required for expression of Sox5 and Sox6. *Genes Dev.*, **16**, 2813–2828.
20. Lefebvre, V., Li, P. and de Crombrughe, B. (1998) A new long form of Sox5 (L-Sox5), Sox6 and Sox9 are coexpressed in chondrogenesis and cooperatively activate the type II collagen gene. *EMBO J.*, **17**, 5718–5733.
21. Smits, P., Li, P., Mandel, J., Zhang, Z., Deng, J.M., Behringer, R.R., de Crombrughe, B. and Lefebvre, V. (2001) The transcription factors L-Sox5 and Sox6 are essential for cartilage formation. *Dev Cell*, **1**, 277–290.
22. Takahashi, K., Tanabe, K., Ohnuki, M., Narita, M., Ichisaka, T., Tomoda, K. and Yamanaka, S. (2007) Induction of pluripotent stem cells from adult human fibroblasts by defined factors. *Cell*, **131**, 861–872.
23. Oldershaw, R.A., Baxter, M.A., Lowe, E.T., Bates, N., Grady, L.M., Soncin, F., Brison, D.R., Hardingham, T.E. and Kimber, S.J. (2010) Directed differentiation of human embryonic stem cells toward chondrocytes. *Nat. Biotechnol.*, **28**, 1187–1194.
24. Lee, H.S., Doh, J.W., Kim, C.J. and Chi, J.G. (2000) Achondrogenesis type II (Langer-Saldino achondrogenesis): a case report. *J. Korean Med. Sci.*, **15**, 604–608.
25. Chan, D., Cole, W.G., Chow, C.W., Mundlos, S. and Bateman, J.F. (1995) A COL2A1 mutation in achondrogenesis type II results in the replacement of type II collagen by type I and III collagens in cartilage. *J. Biol. Chem.*, **270**, 1747–1753.
26. Bandyopadhyay, A., Saxena, K., Kasturia, N., Dalal, V., Bhatt, N., Rajkumar, A., Maity, S., Sengupta, S. and Chakraborty, K. (2012) Chemical chaperones assist intracellular folding to buffer mutational variations. *Nat. Chem. Biol.*, **8**, 238–245.
27. Ishida, Y., Yamamoto, A., Kitamura, A., Lamande, S.R., Yoshimori, T., Bateman, J.F., Kubota, H. and Nagata, K. (2009) Autophagic elimination of misfolded procollagen aggregates in the endoplasmic reticulum as a means of cell protection. *Mol. Biol. Cell*, **20**, 2744–2754.
28. Okita, K., Matsumura, Y., Sato, Y., Okada, A., Morizane, A., Okamoto, S., Hong, H., Nakagawa, M., Tanabe, K., Tezuka, K. *et al.* (2011) A more efficient method to generate integration-free human iPS cells. *Nat. Methods*, **8**, 409–412.

Two Japanese familial cases of Caffey disease with and without the common *COL1A1* mutation and normal bone density, and review of the literature

Taichi Kitaoka · Yoko Miyoshi · Noriyuki Namba · Kohji Miura · Takuo Kubota · Yasuhisa Ohata · Makoto Fujiwara · Masaki Takagi · Tomonobu Hasegawa · Harald Jüppner · Keiichi Ozono

Received: 26 August 2013 / Revised: 8 December 2013 / Accepted: 11 December 2013 / Published online: 4 January 2014
© Springer-Verlag Berlin Heidelberg 2014

Abstract Caffey disease, also known as infantile cortical hyperostosis, is a rare bone disease characterized by acute inflammation with swelling of soft tissues and hyperostosis of the outer cortical surface in early infancy. The common heterozygous mutation of the *COL1A1* gene, p.Arg1014Cys, has been reported in patients with Caffey disease. However, its pathogenesis remains to be elucidated, and the reason for the incomplete penetrance and transient course of the disease is still unclear. In the present study, we performed mutation analysis of the *COL1A1* and *COL1A2* genes and measured bone mineral density in two Japanese familial cases of Caffey disease. The index case and two clinically healthy members of one family carry the common heterozygous mutation; in contrast, no mutation in *COL1A1* or *COL1A2* was identified in the affected members of the second family. In addition, we found normal bone mineral density in adult patients of both families who have had an episode of cortical hyperostosis regardless of the presence or absence of the common p.Arg1014Cys mutation. **Conclusion:** The results reveal that Caffey disease is genetically heterogeneous and that affected and unaffected

adult patients with or without the common *COL1A1* mutation have normal bone mineral density.

Keywords Cortical bone · Hyperostosis · Type 1 collagen · Mutation · Bone mineral density · Bone formation

Abbreviations

MRI Magnetic resonance imaging
NSAIDs Non-steroidal anti-inflammatory drugs

Introduction

Caffey disease (OMIM 114000), also known as infantile cortical hyperostosis, is a rare bone disease characterized by acute inflammation with swelling of soft tissues and hyperostoses of the outer cortical surface in early infancy [7, 11, 13]. Radiographs of long bones, mandible, clavicles, ribs, and scapulae indicate massive periosteal bone formation and consequently increased cortical thickness. In a separate clinical situation, cortical hyperostosis is sometimes observed after long-term administration of prostaglandin E for ductus-dependent cyanotic congenital heart disease, suggesting inflammatory events in Caffey disease [8, 15, 22]. Magnetic resonance imaging (MRI) of bone can also detect characteristic diaphyseal thickening and inflammatory signals in adjacent muscle, connective tissue, and in the bone marrow of patients with Caffey disease [14, 17, 18]; hence, the disease seems not to be confined to bone. Caffey disease resolves spontaneously, but sometimes recurs in childhood. Non-steroidal anti-inflammatory drugs (NSAIDs) or corticosteroids are sometimes used to improve inflammation and pain [4, 21].

T. Kitaoka · Y. Miyoshi · N. Namba · K. Miura · T. Kubota · Y. Ohata · M. Fujiwara · K. Ozono (✉)
Department of Pediatrics, Osaka University Graduate School of Medicine, 2-2 Yamada-oka, Suita, Osaka 565-0871, Japan
e-mail: keioz@ped.med.osaka-u.ac.jp

M. Takagi · T. Hasegawa
Department of Pediatrics, Keio University School of Medicine, 35 Shinano-cho, Shinjuku-ku, Tokyo 160-8582, Japan

H. Jüppner
Endocrine Unit and Pediatric Nephrology Unit, Departments of Medicine and Pediatrics, Massachusetts General Hospital and Harvard Medical School, 55 Fruit Street, Boston, MA 02114-2696, USA

The common heterozygous mutation of the *COL1A1* gene, p.Arg1014Cys (counted from the initiator methionine or p.Arg836Cys with respect to the first glycine of the triple helical domain of the alpha 1 chain of type I collagen [$\alpha 1(I)$]), has been reported in patients with Caffey disease in Canada, Australia [10], Thailand [20], Korea [3], India [16], and Italy [2]. This heterozygous mutation is also found in patients with severe prenatal cortical hyperostosis [12]. On the other hand, parents who had no features of Caffey disease were reported to carry the mutation [3]. The reason for the incomplete penetrance of the disease has not been elucidated [19], and how the mutated collagen leads to hyperostotic bone lesion is still unknown [10, 11]. In addition, the mutation is not identified in some cases of Caffey disease. Thus, analysis of familial cases of Caffey disease may contribute to the understanding of the pathogenesis of the disease and bone biology.

It is well known that *COL1A1* mutations are responsible for osteogenesis imperfecta, a disorder characterized by bone fragility, ligamentous laxity, blue sclerae, dentinogenesis imperfecta, and low bone mineral density [5]. In contrast, the patients with the *COL1A1* p.Arg1014Cys mutation in Caffey disease have cortical bone thickening, but no bone fragility. However, fractures possibly due to bone fragility were reported in two members of a Thai family with Caffey disease [20]. These two patients harbor the common mutation, but the correlation between the p.Arg1014Cys mutation, bone mineral density, and fractures has not been evaluated in this family [20].

Here, we report two Japanese familial cases of Caffey disease, one of which has the common mutation whereas the other has no mutation in the *COL1A1* or *COL1A2* genes. In addition, we examined bone mineral density in these patients.

Patients and methods

Patients

Family A (COL1A1 mutation positive)

The proband (II-1), a 6-month-old female infant, was referred for evaluation of swelling and deformity in both legs and forearms noted since the age of 3 months. The antenatal, perinatal, and neonatal periods had been uneventful, and all developmental milestones had been attained normally. Her parents stated that they had no history of leg swelling during infancy or childhood. Radiographs of the bones revealed cortical bone thickening of both femora, tibiae, radii, ulnae, and swelling of the surrounding soft tissues (Table 1, Fig. 1). The diagnosis of Caffey disease was made on the basis of symptoms, signs, and radiographic findings; periodic

examination was continued without medication. The swelling resolved spontaneously at the age of 1 year and 6 months. Serial radiographs revealed periosteal thickening and widening of the long bones over 3 years (Fig. 1). She developed recurrence at the age of 11 years, which resolved again spontaneously. She is now 12 years old with no medical problems except for mild deformity of her legs. She has had no features of osteogenesis imperfecta such as bone fracture, ligamentous and joint laxity, blue sclerae, deafness, and dentinogenesis imperfecta. The growth parameters were appropriate for her age; height 148 cm (−0.3 SD) and body weight 39.2 kg (−0.4 SD). Her brother (II-3) had a normal antenatal and perinatal history. Right lower leg swelling and deformity and left thigh swelling manifested at the age of 11 months. Radiographs demonstrated deformity and subperiosteal resorption of the right tibia and left femur, thus confirming cortical hyperostosis (Fig. 1). At the age of 2 years and 2 months, the right lower leg and left thigh remained swollen. In contrast, the mother (I-2) had no abnormal radiographic findings of the lower legs at the age of 36 years. According to her memory, she had no symptoms and signs of cortical hyperostosis during infancy or childhood. She could not recall any clinical history suggesting either joint laxity or skin hyperelasticity.

Family B (COL1A1 mutation negative)

The proband (III-1) had swelling of the left thigh and the right lower leg and irritability since the age of 1 month. Radiographs of the bones at the age of 2 months (Fig. 2) revealed cortical bone thickness of the right tibia and swelling of the surrounding soft tissues. MRI showed large lesions with increased T2-weighted signal intensity in the surrounding soft tissue and the bone marrow of the lower legs. She had difficulty walking due to the length difference of her legs and was referred to our hospital at the age of 2 years and 8 months. Physical examination revealed tender, diffuse, immobile swellings over the anterior aspects of both legs, which were hard in consistency. The neighboring knee and ankle joints appeared to be normal. There were no swellings over the jaw, clavicles, ribs, or elsewhere in the body (Table 1). She has had no evidence of joint laxity or skin hyperextensibility. Developmental milestones were not delayed. The patient is now 11 years old, her height and weight are within the normal range but the leg deformity persists, and her leg length discrepancy is 1.2 cm. The mother (II-2) had a history of bone swelling in childhood. Her brother (III-2) was born uneventfully at 39 weeks of gestation and had left lower leg swelling and deformity at the age of 3 months (Fig. 2). The maternal granduncle (I-1) had a history of swelling of legs, although no medical history or radiographs were available. The parents were not consanguineous and did not come from the same community.

Table 1 Radiological features in individuals evaluated for the *COL1A1* p.Arg1014Cys mutation

Family no.	Pedigree no.	p.Arg1014Cys	Sex	Onset	Hyperostosis									
					Femur	Tibia	Fibula	Humerus	Radius	Ulna	Clavicle	Mandible	Ribs	
A ^a	II-1	+	F	3 months	R/L	R	R	–	R	R	–	–	–	
	II-2	+	F	–	–	–	–	–	–	–	–	–	–	
	II-3	+	M	2 years	L	R	–	–	–	–	–	–	–	
	I-2	+	F	–	–	–	–	–	–	–	–	–	–	
B ^a	III-1	–	F	1 month	+	+	+	–	–	–	–	–	–	
	III-2	–	M	months	+	+	+	–	–	–	–	–	–	
	III-3	–	F	–	–	–	–	–	–	–	–	–	–	
	II-2	–	F	3 years	+	+	+	–	–	–	–	–	–	
Australia [4, 9]	II-1	+	F	3 weeks	+	R/L	+	+	+	+	+	+	–	
	II-2	+	F	2 weeks	+	+	+	+	R/L	R/L	+	+	–	
Thai [19]	I-3	+	M	/	–	R/L	–	–	R/L	–	–	–	+	
	II-2	+	M	0 month	–	R/L	/	–	R/L	/	–	–	–	
	II-7	+	M	/	–	–	–	–	–	–	–	–	+	
	II-11	+	F	S	–	R	/	–	–	–	–	–	–	
	III-15	+	F	11 days	–	R/L	–	–	–	–	–	–	–	
	III-3	–	F	/	–	–	–	–	+	/	–	–	–	
Korea A [3]	II-1	+	M	2 months	R	R/L	–	–	R/L	R	–	+	–	
Korea B [3]	II-1	+	M	9 months	–	R/L	–	–	–	–	–	+	–	
	II-2	+	F	4 months	R	R/L	–	–	R/L	R/L	–	+	–	
Korea C [3]	II-1	+	F	1 month	–	–	L	–	R/L	–	–	+	–	
Korea D [3]	II-1	+	F	2 months	–	R/L	–	–	R	–	–	+	–	
	I-1	–	M	–	–	–	–	–	–	–	–	–	–	
	I-2	+	F	–	–	–	–	–	–	–	–	–	–	
	Korea E [3]	II-2	+	M	0 month	–	R/L	–	–	–	–	–	–	–
		I-1	+	M	–	–	–	–	–	–	–	–	–	–
I-2	–	F	–	–	–	–	–	–	–	–	–	–		
France [11]	Pt	+	M	0 day	+	+	+	+	–	–	–	+	+	
India [15]	Pt	+	M	3 months	R/L	R/L	–	–	–	–	–	–	–	
Italy [2]	VI-1	+	F	14 days	+	+	–	–	+	+	–	/	/	
	VII-2	+	M	2 months	–	+	+	–	+	+	–	/	/	
	V-2	+	M	15 days	–	+	+	–	–	–	–	/	/	
	VI-4	+	F	2 months	–	+	+	+	+	+	–	/	/	
	VII-3	+	M	10 days	–	+	+	–	+	+	–	/	/	
	V-5	+	M	20 days	+	+	–	+	+	+	+	/	/	
	IV-11	+	M	/	/	/	/	/	/	/	/	/	/	
	VI-11	+	M	–	–	–	–	–	–	–	–	–	–	
V-3	+	M	/	/	/	/	/	/	/	/	/	/		

F female, M male, /no data available, R right, L left, + presence of the common mutation or clinical signs, – absence of the common mutation or clinical signs, S soon after birth

^a Families presented on this paper

Mutational analysis of *COL1A1* and *COL2A2*

The mutation analysis was approved by the ethics committees of Osaka University Graduate School of Medicine and Keio University School of Medicine, and informed consent was obtained from the proband and family members for the

analysis of the *COL1A1* and *COL2A2* genes. Genomic DNA was extracted from peripheral blood by using the QuickGene-810 and QuickGene DNA whole blood kit (FUJIFILM Corporation, Tokyo, Japan) according to the manufacturer's instructions. We analyzed the previously reported mutation in *COL1A1* by digestion of the purified polymerase chain

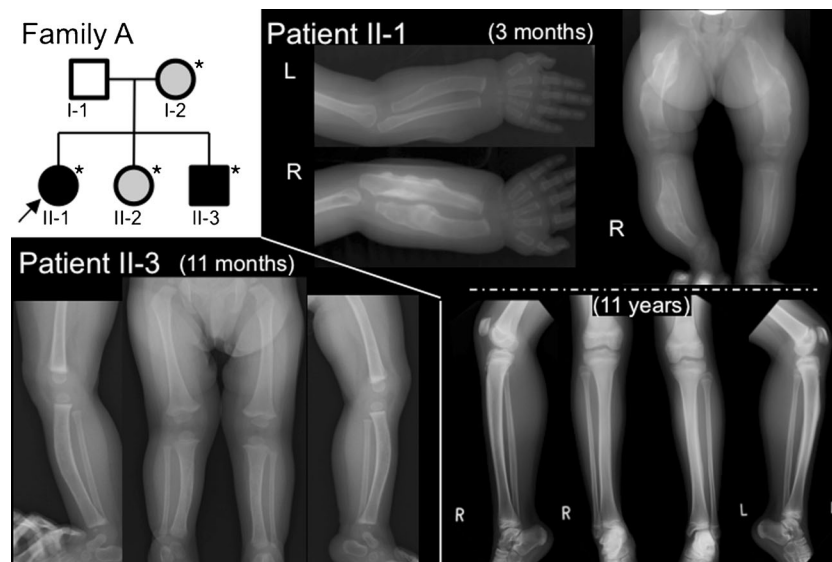


Fig. 1 *Left upper panel* shows the pedigree of family A (*COL1A1* mutation positive). *Black symbol*, affected individual; *white symbols*, no symptoms according to history; *gray symbols*, mutation-positive, but healthy family members; *asterisk*, mutation-positive individual. The *arrow* indicates proband of family A. *Right upper panel* (II-1 at the age

of 3 months): cortical bone thickness of the right radius, right ulna, both femora, and the right tibia. *Right lower panel* (II-1 at the age of 11 years): mild deformity of the legs. *Left lower panel* (II-3 at the age of 11 months): mild deformity of both tibiae

reaction (PCR) product with HypCH4IV [10]. In family B, we analyzed all coding exons and flanking introns of *COL1A1* and *COL1A2* by PCR and direct sequencing.

Dual-energy X-ray absorptiometry analysis

The bone mineral density (BMD) Z score or T score of the lumbar spine for L₂₋₄ was determined by dual-energy X-ray absorptiometry (DXA; Discovery A, Hologic).

Results

Mutation

The proband of family A had the common heterozygous p.Arg1014Cys mutation in *COL1A1*, as did her affected younger brother. In addition, her mother and younger sister also carry the same mutation, but they have had no history of soft tissue swelling and bone deformity. They also have no

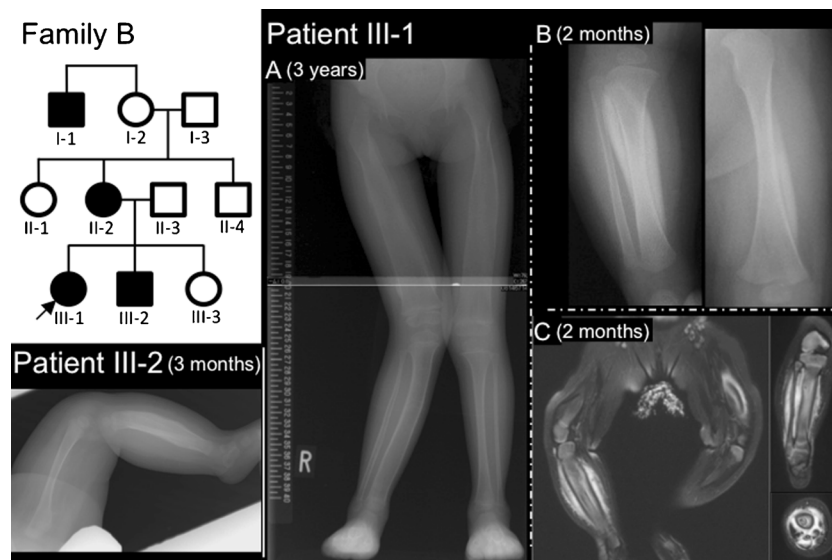


Fig. 2 *Left upper panel* shows the pedigree of family B (mutation negative). *Black symbol*, affected individual; *white symbols*, no symptoms according to history. The *arrow* indicates the proband of family B. *Right panel: a* (III-1 at the age of 3 years) bone deformity of both femora and the right tibia, *b* (III-1 at the age of 2 months) cortical bone thickness of the

right tibia and swelling of the surrounding soft tissues, and *c* (III-1 at the age of 2 months) MRIs (fat-saturated T2-weighted images) revealing large lesions in the surrounding soft tissues and bone marrow with increased signal intensity on lower legs. *Left lower panel* (III-2 at the age of 3 months): cortical bone thickness of left lower leg

evidence of either joint laxity or soft skin. Her healthy father could not be examined.

The three patients in family B had no detectable mutation in either *COL1A1* or *COL2A2*. Exome sequencing was not feasible in this family.

BMD

The proband of family A showed a BMD of 0.852 g/cm² of L2–L4 (Z score +0.3) at the age of 12 years. Her mother, who has regular menstrual cycles, had a L2–L4 and total hip BMD of 1.096 g/cm² (T score +0.8) and 0.990 g/cm² (T score +1.2), respectively, at the age of 36 years.

The mother (II-2) of family B, who also has regular menstrual cycles, had L2–L4 BMD of 1.138 g/cm² (T score +1.1) at the age of 40 years.

Discussion

We found the common *COL1A1* mutation, p.Arg1014Cys, in the proband of family A (II-1) and the younger brother (II-3) who both presented with clinical and radiographic findings consistent with Caffey disease, whereas the same mutation was detected in her mother (I-2) who was asymptomatic and with normal radiological findings. Furthermore, her sister (II-2) who had no signs or symptoms suggesting this disease had also the same mutation. This family indicates rather low penetrance of Caffey disease as has been reported previously [3, 9, 10]. Gensure et al. reported that only 79 % of the family members with this mutation had signs or symptoms of Caffey disease [10]. Although the precise mechanism has yet to be elucidated, it is likely that an additional genetic or environmental condition is required for the manifestation of the disease. Likewise, the factor(s) contributing to the recurrence of the disease is unknown [1]. However, it is most likely that the p.Arg1014Cys substitution in *COL1A1* is linked to Caffey disease because several familial cases have been reported to have this mutation (Table 1). In the “osteogenesis imperfecta & Ehlers-Danlos syndrome variant databases” [6], this mutation was not found in patients with osteogenesis imperfecta or healthy subjects.

No mutations in *COL1A1* or *COL1A2* were identified in the patients of family B. However, bone lesions consistent with the diagnosis of familial Caffey disease were found in the femora, tibiae, and fibulae of the affected individuals in family B (Table 1). Thus, there can be considerable overlap between familial cases with and without the *COL1A1* mutation (Table 1). Since we could not identify a novel mutation in *COL1A1* or *COL1A2*, it appears likely that another heterozygous mutation in an as-of-yet unknown gene is responsible for the affected members of family B and possibly other cases of Caffey disease, too, either infantile or prenatal forms. This is strong

evidence that similar phenotypic findings can be caused by different mutations. Exome analysis may be necessary to identify the responsible gene, although relatively low penetrance and few family members may prevent identification.

Increased T2-weighted images in patient II-1 of family B reflected increased water content consistent with edema surrounding the hyperostotic cortical bone and bone marrow [17, 18]. Although the pathogenesis of Caffey disease remains unclear, this edema suggested inflammatory events in the soft connective tissues surrounding the affected bone and bone marrow [11]. Inflammatory cytokines including prostaglandin E may stimulate periosteal reaction, although we did not examine inflammatory cytokines in our patients.

Bone mineral density of patients with Caffey disease has been reported in only one patient [20]; however, the relation between bone mineral density and the p.Arg1014Cys mutation has not been investigated. The patients in family A, the girls and their asymptomatic mother, had normal bone mineral density. In addition, the mother of family B who was symptomatic during childhood and does not carry the common mutation also had normal bone mineral density. These results suggest that Caffey disease, regardless of the p.Arg1014Cys mutation, is not associated with alterations in bone strength.

In conclusion, we obtained further evidence for genetic heterogeneity of Caffey disease and demonstrated normal bone mineral density in adult patients with this disease.

Acknowledgments This study was supported in part by grants-in-aid from the Ministry of Health, Labour, and Welfare (KH20Q007a-1) of Japan.

Conflict of interest All the authors do not have anything to declare.

References

- Borochowitz Z, Gozal D, Misselevitch I, Aunallah J, Boss JH (1991) Familial Caffey's disease and late recurrence in a child. *Clin Genet* 40:329–335. doi:10.1111/j.1399-0004.1991.tb03104.x
- Cerruti-Mainardi P, Venturi G, Spunton M, Favaron E, Zignani M, Provera S, Dallapiccola B (2007) Infantile cortical hyperostosis and *COL1A1* mutation in four generations. *Eur J Pediatr* 170:1385–1390. doi:10.1007/s00431-011-1463-0
- Cho TJ, Moon HJ, Cho DY, Park MS, Lee DY, Yoo WJ, Chung CY, Choi IH (2008) The c.3040C>T mutation in *COL1A1* is recurrent in Korean patients with infantile cortical hyperostosis (Caffey disease). *J Hum Genet* 53:947–949. doi:10.1007/s10038-008-0328-5
- Couper RT, McPhee A, Morris L (2001) Indomethacin treatment of infantile cortical periostosis in twins. *J Paediatr Child Health* 37:305–308. doi:10.1046/j.1440-1754.2001.00633.x
- Cundy T (2012) Recent advances in osteogenesis imperfecta. *Calcif Tissue Int* 90:439–449. doi:10.1007/s00223-012-9588-3
- Dalgleish R (1997) The human type I collagen mutation database. *Nucleic Acids Research* 25:181–187. <http://www.le.ac.uk/genetics/collagen/index.html>
- Dutta S, Jain N, Bhattacharya A et al (2005) Infantile cortical hyperostosis. *Indian Pediatr* 42:64–66

8. Estes K, Nowicki M, Bishop P (2007) Cortical hyperostosis secondary to prostaglandin E1 therapy. *J Pediatr* 151:441. doi:[10.1016/j.jpeds.2007.02.066](https://doi.org/10.1016/j.jpeds.2007.02.066)
9. Fried K, Manor A, Pajewski M, Starinsky R, Vure E (1981) Autosomal dominant inheritance with incomplete penetrance of Caffey disease (infantile cortical hyperostosis). *Clin Genet* 19:271–274. doi:[10.1111/j.1399-0004.1981.tb00708.x](https://doi.org/10.1111/j.1399-0004.1981.tb00708.x)
10. Gensure RC, Mäkitie O, Barclay C, Chan C, Depalma SR, Bastepe M, Abuzahra H, Couper R, Mundlos S, Silencio D (2005) A novel *COL1A1* mutation in infantile cortical hyperostosis (Caffey disease) expands the spectrum of collagen-related disorders. *J Clin Invest* 115:1250–1257. doi:[10.1172/JCI200522760](https://doi.org/10.1172/JCI200522760)
11. Glorieux FH (2005) Caffey disease: an unlikely collagenopathy. *J Clin Invest* 115:1142–1144. doi:[10.1172/JCI25148](https://doi.org/10.1172/JCI25148)
12. Kamoun-Goldrat A, Martinovic J, Saada J, Sonigo-Cohen P, Razavi F, Munnich A, Merrer ML (2008) Prenatal cortical hyperostosis with *COL1A1* gene mutation. *Am J Med Genet A* 146A:1920–1824. doi:[10.1002/ajmg.a.32351](https://doi.org/10.1002/ajmg.a.32351)
13. Kamoun-Goldrat A, le Merrer M (2008) Infantile cortical hyperostosis (Caffey disease): a review. *J Oral Maxillofac Surg* 66:2145–2150. doi:[10.1016/j.joms.2007.09.007](https://doi.org/10.1016/j.joms.2007.09.007)
14. Katz DS, Eller DJ, Bergman G, Blankenberg FG (1997) Caffey's disease of the scapula: CT and MR findings. *AJR Am J Roentgenol* 168:286–287. doi:[10.2214/ajr.168.1.8976971](https://doi.org/10.2214/ajr.168.1.8976971)
15. Letts M, Pang E, Simons J (1994) Prostaglandin-induced neonatal periostitis. *J Pediatr Orthop* 14:809–813
16. Ranganath P, Laine CM, Gupta D, Mäkitie O, Phadke SR (2011) *COL1A1* mutation in an Indian child with Caffey disease. *Indian J Pediatr* 78:877–879. doi:[10.1007/s12098-010-0339-z](https://doi.org/10.1007/s12098-010-0339-z)
17. Saatci I, Brown JJ, McAlister WH (1996) MR findings in a patient with Caffey's disease. *Pediatr Radiol* 26:68–70. doi:[10.1007/BF01403711](https://doi.org/10.1007/BF01403711)
18. Sanders DG, Weijers RE (1994) MRI findings in Caffey's disease. *Pediatr Radiol* 24:325–327. doi:[10.1007/BF02012117](https://doi.org/10.1007/BF02012117)
19. Saul RA, Lee WH, Stevenson RE (1982) Caffey's disease revisited. Further evidence for autosomal dominant inheritance with incomplete penetrance. *Am J Dis Child* 136:55–60. doi:[10.1001/archpedi.1982.0390370058014](https://doi.org/10.1001/archpedi.1982.0390370058014)
20. Suphapeetiporn K, Tongkobpetch S, Mahayosnond A, Shotelersuk V (2007) Expanding the phenotypic spectrum of Caffey disease. *Clin Genet* 71:280–284. doi:[10.1111/j.1399-0004.2007.00768.x](https://doi.org/10.1111/j.1399-0004.2007.00768.x)
21. Thometz JG, DiRaimondo CA (1996) A case of recurrent Caffey's disease treated with naproxen. *Clin Orthop Relat Res* 323:304–309
22. Ueda K, Saito A, Nakano H et al (1980) Cortical hyperostosis following long-term administration of prostaglandin E1 in infants with cyanotic congenital heart disease. *J Pediatr* 97:834–836

Presentation Brief 1

骨格徴候を伴う，過成長症候群

大園 恵一

大阪大学大学院医学系研究科 小児科学

成長障害は，臨床的には低身長が問題となることが多いが，過成長も同様に重要な疾患が原因となるので注目すべきである。過成長をきたす疾患の鑑別診断としては，胎児期からの過成長であるかどうか，骨格徴候を伴うかどうか，キーポイントとなる。講演では骨格徴候を伴う過成長症候群を対象とし，以下の疾患についてオリジナルデータを含めて解説した。

Sotos 症候群は，過成長，大頭，発達障害を 3 主徴とし，心臓や尿路系の奇形を伴うこともある。過成長は乳幼児期に明らかであるが，次第に成長速度は減速して，成人身長は正常であることも多い。NSDI (nuclear receptor-binding SET domain-containing protein 1) が責任遺伝子である。

Weaver 症候群は出生時からの過成長，特徴的顔貌，骨年齢促進，発達遅滞などを特徴とし，成人期も高身長であることが多い。EZH2 (enhancer of zeste, drosophila, homolog 2) が原因遺伝子であることが明らかにされている。EZH2 は SET 領域を含むヒストンメチルトランスフェラーゼをコードし，NSDI はヒストンメチルトランスフェラーゼの複合体形成分子をコードするが，メチル化を行うリジン残基の位置は異なる。

Loeys-Dietz 症候群は Marfan syndrome type II とも呼ばれ，Marfan 様体型は呈するが，水晶体の亜脱臼は示さず，動脈瘤を発症するなどの特徴を有する。一般的には，クモ状指は呈するが，高身長を呈しないとされる。本症候群の責任分子は，TGF- β 受容体 1 あるいは 2，TGF- β ，SMAD3 である。われわれは，高身長を呈し，動脈瘤がない本症候群の 1 例を経験しており，高身長をきたす疾患の一つとしても考慮すべきと考えている。

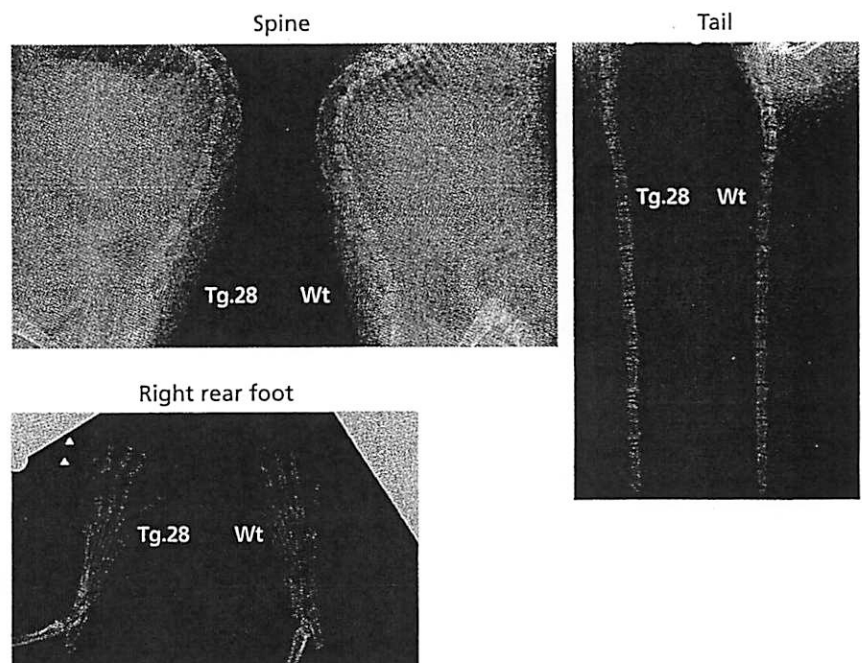
CNP 受容体機能獲得型異常症

C 型ナトリウム利尿ペプチド (CNP) はナトリウム利尿ペプチドファミリーに属し，内軟骨性骨化のための重要な因子である。CNP

はナトリウム利尿ペプチド受容体 B (NPR-B) と結合し，グアニル酸シクラーゼ領域が活性化され cGMP を産生し，cGMP 依存性プロテインキナーゼ (PKG II) を介して FGF 受容体 3 シグナル系の MAP キナーゼ伝達を抑制することにより軟骨の分化・増殖を調整している。CNP 過剰産生トランスジェニック (Tg) マウスは過成長をきたし，CNP あるいは NPR-B ノックアウトマウスは矮小化することも報告されている。Acromesomelic dysplasia, type Maroteaux として報告した低身長を呈する骨系統疾患が，NPR-B の機能喪失型変異である。さらにわれわれは，NPR-B の機能獲得型変異による高身長家系を 2012 年に報告した。本変異受容体を軟骨において発現する Tg マウスは，椎体や趾骨の延長を示した (図)。その後，NPR-B の機能獲得型変異による高身長家系は，韓国，欧州でも認められ，疾患単位として確立した。近年では，軟骨無形成症に対する身長促進治療薬として CNP アナログの開発も進んでおり，低身長を主症状とする骨系統疾患などに対する臨床応用が期待されている。

図 機能獲得型変異 NPR-B を軟骨において発現するトランスジェニックマウスの骨 X 線画像

本トランスジェニックマウス (Tg.28) は，椎体，尾骨，趾骨などが野生型に比べて伸長していた。



10. 内分泌

軟骨無形成症

大阪大学大学院医学系研究科小児科学 おお その けい いち 大園 恵一

本疾患は四肢短縮型低身長をきたす代表的疾患で、3型線維芽細胞増殖因子受容体(FGFR3)異常ファミリーに分類される。骨単純X線像では、腰椎椎弓根間距離の狭小化などが特徴的である。合併症として水頭症、大孔狭窄、睡眠時無呼吸などがある。-3SD以下の低身長に対し、成長ホルモン治療が行われる。

診断のポイント

軟骨無形成症(achondroplasia)は、四肢短縮型低身長をきたす代表的疾患である。軟骨無形成症およびより軽症の軟骨低形成症(hypochondroplasia)は、3型線維芽細胞増殖因子受容体(fibroblast growth factor receptor 3: FGFR3)異常ファミリーに分類される¹⁾²⁾。軟骨無形成症では、低身長、四肢短縮、顔貌異常、頭囲拡大、三尖手などがみられる。

骨単純X線像としては、太く短い管状骨、骨幹端のcupping、弾丸様椎体、腓骨が脛骨より長いこと、腰椎椎弓根間距離の狭小化などが特徴的である(図)。その他、頭蓋冠は大きいものに対して顔面骨および頭蓋底は小さいこと、小さな坐骨切痕小骨盤腔などの所見がみられる。新生児期には扁平椎を認めることがある。症状と骨X線像とあわせて診断を行う。

遺伝子診断として、軟骨無形成症におけるFGFR3遺伝子の検討では、98%以上の症例で380番目のグリシンがアルギニン酸に変換される(p.G380R)変異が認められる¹⁾²⁾。軟骨低形成症においても同じFGFR3遺伝子に変異が認められるが、全例ではない。もっとも多い変異はp.N540Kである。軟骨低形成症は軽症で、診断に苦慮する場合もあり、遺伝子検査も参考にする。

重症度評価

軟骨無形成症および軟骨低形成症は、タナトフォ



図 軟骨無形成症患児の腰椎正面像

椎弓根間距離が腰椎L1からL5にかけて正常では広がるのに対して、むしろ狭くなっている。座骨切痕が短縮しているのも特徴である

リック骨異形成症(thanatophoric dysplasia), SADDAN (severe achondroplasia with developmental delay and acanthosis nigricans) とともに、FGFR3異常ファミリーに分類される。タナトフォリック骨異形成症はもっとも重症で致死性とされていたが、新生児医療の進歩により生存例も増えてきたので、病名を致死性からタナトフォリック骨異形成症に変更している。軟骨低形成症はもっとも軽症で正常との境界例もあると考えられるが、もっとも多いp.N540K変異を伴う例では、低身長は明らかであることが多い。

基本病態

本疾患をひきおこす変異FGFR3は恒常的に活性化された状態にあり、細胞内シグナル伝達分子のmitogen-activated protein kinase (MAPK) およびStat1の活性化により軟骨細胞の分化を促進する一方で、細胞増殖を抑制する結果、長管骨の伸長が不良となり、四肢短縮性低身長を呈する骨系統疾患がひきおこされる。また、思春期の成長スパートがみられず、この間にも相対的に低身長の程度が悪化する。低身長は年齢とともに正常からの差が顕著となり、最終身長は男性130cm程度、女性125cm程度である。

正確な発症頻度は不明であるが、軟骨無形成症では出生15,000~20,000人に1人程度とされている。FGFR3異常ファミリーに属する疾患では新規突然変異による例が多いが、次世代へは常染色体優性遺伝する。

私の治療方針

軟骨無形成症に関し、早期に正確な病気の説明を行い、両親の受け入れを促す。見た目の問題を重視されることもあるが、通常の社会生活を営む成人患者も多いことを述べる。何よりも患者自身が前向きであることが多く、医療関係者や両親はサポートにまわる姿勢で接するとよい。少なくとも3歳までは、定期的な診察と頭部MRI検査により大孔狭窄、水頭症の進行に注意する。頸部に負担がかかるような運動や、激しい運動を避けるように指導している。入学時には、机や椅子、トイレ、手洗いなどに関し、著しい低身長であることがハンディとならないように配慮を求める。

軟骨異栄養症（軟骨無形成症および軟骨低形成症）の低身長に対する内科的治療としては、成長ホルモン（growth hormone: GH）治療が選択される。GH量は0.35 mg/kg/週と多いので、糖尿病などの副作用の有無を確実に検討していく必要がある。神経学的な問題を避けるために、3歳以降でのGH治療開始が望ましいと考えている。当科の経験では、軟骨低形成症では身長のカッチアップがみられ、軟骨無形成症でも半数程度は身長増加効果がみられる。脚延長術に関しては、整形外科医から親のみならず本人にもていねいに説明をしたうえで、同意をとる必要がある。

管理の実際

現在のところ本症を完治させる治療法はないが、低身長や睡眠時無呼吸症候群（sleep apnea syndrome: SAS）などの合併症に対する治療が行われるようになり、QOLは改善されてきている。知的にも問題となることはほとんどない（時に分娩時障害に伴う後遺症が問題となる）が、頸定や独歩などの身体運動的指標は遅れる。軟骨低形成症には神経発達上の問題がみられる場合があるので、注意する。

合併症として、交通性水頭症、大孔狭窄、SAS、中耳炎、脊柱管狭窄症、不整咬合などが問題となる。また、腰椎部の前彎が増強して殿部が後方に突出し、肘関節では伸展障害がみられる。脳神経外科、整形外科、耳鼻科などとの連携が大切である。

骨端線閉鎖を伴わない-3 SD以下の低身長の本疾患患者において成長ホルモン治療が適応となっているが、手術的治療を考慮するほどの大孔狭窄、脊柱管狭窄、水頭症、脊髄・馬尾圧迫などがMRI/CT上で認められる場合、および神経症状が認められる場合には適応とならない。低身長に対して脚延長術も行われる。

軟骨無形成症の重要な合併症の一つとしては、前述したようにSASがある³⁾。軟骨無形成症にSASが合併する原因としては、中枢性の原因の他に、顔面骨や胸郭の低形成に基づく気道の解剖学的異常や気管・気管支の脆弱性などがあると考えられる。SAS

の確定診断のためには睡眠ポリソムノグラフィ検査（polysomnography: PSG）が行われる。SASの原因および程度に応じて、扁桃腺・アデノイド摘出術や持続陽圧呼吸（continuous positive airway pressure: CPAP）療法が行われる。

最新ガイドライン

わが国のガイドラインはないが、GRJ（Gene Reviews Japan）ホームページの軟骨無形成症サイト（<http://grj.umin.jp/grj/achondroplasia.htm>）の記載は参考となる。海外では、Health Supervisionとして論文文化されており、軟骨無形成症患者のフォローアップに役立つ^{3)~5)}。しかしながら、エビデンスレベルの高いデータには乏しく、論文報告やアンケート調査結果に基づいた内容となっている。

近年のトピックス

Na利尿ペプチドファミリーに属するC型Na利尿ペプチド（C-type natriuretic peptide: CNP）が、内軟骨性骨形成に重要な因子であることが明らかとなった。CNPはNa利尿ペプチド受容体B（natriuretic peptide receptor B: NPRB）と結合し、細胞内にてcGMPを産生し、cGMP依存性蛋白キナーゼGII（cGMP-dependent protein kinase GII: PKGII）を介してFGFR3シグナル系のMAPK伝達を抑制することにより、軟骨の分化・増殖を調整している⁶⁾。CNP過剰産生トランスジェニック（Tg）マウスは過成長をきたし、CNPあるいはNPRBノックアウトマウス

は矮小化することも報告されている。また、軟骨無形成症モデルマウスに対し、CNPの持続静脈投与により成長促進作用があることが報告された。近年では、軟骨無形成症に対する身長促進治療薬としてCNPアナログの開発も進んでおり⁷⁾、低身長を主症状とする骨系統疾患などに対する臨床応用が期待されている。

ピットフォールと対策

本症に伴う水頭症は交通性であることが一般的で、すぐにシャント術の適応とはならない。しかし、水頭症が進行する場合や神経学的合併症がある場合は脳外科医に相談し、シャント術を行うかどうかを決定する。

大孔狭窄も合併率は高く、その存在のみで手術適応とはならないが、腱反射の亢進や下肢の麻痺があり、脊髄空洞症への進展が懸念される場合には適応となる。

小児科医はSASの合併率が高いことに注意する

必要がある。小児のPSGが行える施設は多くはないが、夜間の血中酸素濃度、心拍数のモニターを行い、低酸素血症と心拍数の増加がある場合はSASの合併を疑い、PSGを施行する。

中耳炎の合併率も高く、本症の全体的な管理は小児科医が中心となって行い、必要に応じて他科に相談していくシステムの構築が必要である。

文献

- 1) Vajo Z et al.: *Endocr Rev* 21:23-39, 2000
- 2) Foldynova-Trantirkova S et al.: *Hum Mutat* 33:29-41, 2012
- 3) Mogayzel PJ Jr et al.: *J Pediatr* 132:667-671, 1998
- 4) Trotter TL et al.: *Pediatrics* 116:771-783, 2005
- 5) Ireland PJ et al.: *J Paediatr Child Health* 48:443-449, 2012
- 6) Yasoda A et al.: *Nat Med* 10:80-86, 2004
- 7) Lorget F et al.: *Am J Hum Genet* 91:1108-1114, 2012

著者連絡先

〒565-0871 大阪府吹田市山田丘2-2
大阪大学大学院医学系研究科小児科学
大藪恵一

タナトフォリック骨異形成症 1 型・2 型の診断基準と重症度分類（案）

厚生労働科学研究

胎児・新生児骨系統疾患の診断と予後に関する研究班

致死性骨異形成症の診断と予後に関する研究班

第 2 版：平成 27 年 2 月 10 日

<診断基準>

本診断基準によりタナトフォリック骨異形成症 1 型または 2 型の診断を確定する。それぞれの項目については下の解説を参照すること。

A. 症状

- 1) 著明な四肢の短縮
- 2) 著明な胸郭低形成による呼吸障害
- 3) 巨大頭蓋（または相対的的巨大頭蓋）

B. 出生時の単純エックス線画像所見（正面・側面）

- 1) 四肢（特に大腿骨と上腕骨）長管骨の著明な短縮と特有の骨幹端変形
- 2) 肋骨の短縮による胸郭低形成
- 3) 巨大頭蓋（または相対的的巨大頭蓋）と頭蓋底短縮
- 4) 著明な椎体の扁平化
- 5) 方形骨盤（腸骨の低形成）

C. 遺伝子検査

線維芽細胞増殖因子受容体 3（fibroblast growth factor receptor 3：FGFR3）遺伝子のアミノ酸変異を生じる点突然変異

D. 診断の確定

次の 1) と 2) の両方を満たせば診断が確定する。また 1) は満たすが、2) は満たさないまたは明確ではない場合は、1) と 3) の両方を満たせば診断が確定する。

- 1) 「A. 症状」の項目 1) ～ 3) のすべてを満たすこと。
- 2) 「B. 出生時の単純エックス線画像所見」の項目 1) ～ 5) のすべてを満たすこと。
- 3) 「C. 遺伝子検査」でいずれかの変異が同定されること。

<解説>

A. 症状

- 1) 著明な四肢の短縮は、特に近位肢節（大腿骨や上腕骨）にみられ、低身長となるが、体幹の短縮は軽度またはほぼ正常である。骨の短縮に対して、軟部組織は正常に発育するため、四肢で長軸と直角方向に皮膚の皺襞が生じる。
- 2) 著明な胸郭低形成により呼吸障害や腹部膨隆を示す。胎児期には嚥下困難による羊水過多がほぼ必発で、しばしば胎児水腫を呈する。多くは出生直後から呼吸管理が必要で、呼吸管理を行わない場合は、呼吸不全により新生児死亡に至ることが多い。
- 3) 巨大頭蓋は頭蓋冠の巨大化によるもので、顔面中央部は比較的低位形成となり、前頭部突出や鼻根部陥凹（鞍鼻）と中央部の平坦な顔貌を示す。なお、相対的的巨大頭蓋(relative macrocephaly)とは実際には頭蓋の大きさは標準値と変わらないか軽度の拡大であるが、胸郭低形成、四肢の長管骨の著明な短縮と椎体の扁平化により生じた低身長など、四肢体幹が小さくなるため、頭蓋が相対的に大きく見えることを意味する。
- 4) その他の症状としては筋緊張の低下、大泉門開大、眼球突出などがある。短管骨も短縮するので短指趾症となり、三尖手(trident hand)を示すこともある。また、加齢により皮膚の黒色表皮腫が出現することが多い。

B. 出生時の単純エックス線画像所見（正面・側面）

エックス線画像では骨格異常の全体パターンの認識が重要であり、上記の個々の所見の同定にあたっては、診断経験の豊富な医師の読影意見や成書の図譜等を参照し、異常所見を診断することが必須である。なお、これらのエックス線画像所見の診断は出生時（出生後満 28 日未満の新生児期）に撮影された画像を対象とする。

- 1) 四肢（特に大腿骨と上腕骨）長管骨は著明な短縮を示す。しかし四肢長管骨の短縮の程度を客観的に評価するための出生後の身体計測やエックス線的計測値は報告されていない。ひとつの指標としては出生前の超音波検査の胎児大腿骨長(femur length: FL)計測値で、少なくとも妊娠 22 週以降 28 週未満では 4SD 以上、妊娠 28 週以降は 6SD 以上の短縮がみられる。出生後の身体計測やエックス線的計測においてもこれらの値を指標としうる。

また、特有の骨幹端変形があり、長管骨の骨幹端は軽度不整と骨幹方向への杯状陥凹(cupping)、軽度拡大（flaring または splaying）を示し、骨幹端縁は角状突起様(spur)となる。これらの所見により近位端骨幹端には骨透亮像を認める。1 型では大腿骨の彎曲が著明で電話受話器様変形(French telephone receiver femur)を示す。2 型では大腿骨は直状で短縮の程度は 1 型よりやや軽度のことが多く、彎曲は認めないかきわめて軽度である。

- 2) 肋骨の短縮により胸郭は低位形成となりベル状胸郭となる。
- 3) 巨大頭蓋と頭蓋底短縮のために、前頭部が突出し、顔面中央部は比較的低位形成である。2 型では側頭部の膨隆により頭蓋骨のクローバー葉様変形(cloverleaf skull)を認めることが多いが、これは 1 型でも認めることがあり、また 2 型でも認めないことがあるので、1 型と 2 型の確定には大腿骨の所見が優先される。また、大後頭孔の狭窄による脳幹圧迫症状を呈することが多い。

- 4) 著明な椎体の扁平化により椎間腔は拡大し、椎体は正面像ではH字またはU字型を示し、側面像では前縁がやや丸みを帯びる。正面像での腰椎椎弓根間距離の狭小化は診断のための客観的な指標であるが、在胎週の早い例では目立たないこともある。
- 5) 方形骨盤（腸骨の低形成）は骨盤骨の所見として重要である。腸骨は低形成で垂直方向に短縮し、横径は相対的に拡大する。腸骨翼は正常の扇型を示さず方型である。坐骨切痕は狭く短縮し、臼蓋は水平化している。Y軟骨部分の陥凹骨突起と組み合わせは三尖臼蓋として観察される。

C. 遺伝子検査

遺伝子検査は確定診断としての意義が大きい。

- 1) 1型：線維芽細胞増殖因子受容体3（fibroblast growth factor receptor 3：FGFR3）遺伝子の点突然変異によりアミノ酸の置換や終止コドンへの置換が生じることが原因である。アミノ酸の置換（c.742C>T ⇒ Arg248Cys、c.746C>G ⇒ Ser249Cys、c.1108G>T ⇒ Gly370Cys、c.1111A>T ⇒ Ser371Cys、c.1118A>G ⇒ Tyr373Cys、c.1949A>T ⇒ Lys650Met）や、終止コドンのアミノ酸への置換（c.2419T>G ⇒ stop807Gly、c.2419T>Cまたはc.2419T>A ⇒ stop807Arg、c.2421A>Tまたはc.2421A>C ⇒ stop807Cys、c.2420G>T ⇒ stop807Leu、c.2421A>G ⇒ stop807Trp）などが報告されている。日本人では Arg248Cys が1型の約60～70%にみられ最も多く、次いで Tyr373Cys が20～30%に見られる。それ以外の変異や既知の変異が検出されないものが、～10%程度存在する。
- 2) 2型：全例で FGFR3 遺伝子の c.1948A>G ⇒ Lys650Glu 変異が報告されている。
- 3) 遺伝子変異については新たな変異が報告される可能性があるため、必ずしも前項の変異に限定されるものではないが、アミノ酸変異を伴わない遺伝子変異では疾患原因とはならない。こうした遺伝子変異の情報についてはウェブ上の GeneReviews®（米国 NCBI のサイト <http://www.ncbi.nlm.nih.gov/> の中のデータベース）などの記載を参考にする。
- 4) 理論上は常染色体優性遺伝形式をとるが、出生後の新生児期から乳幼児期に死亡することが多く、ほとんどは妊孕性のある年齢に至らないことや、その年齢に至ったとしても妊孕性は期待できないことから、実際の発症は全例が新生突然変異である。従って発症頻度は出生児（死産を含む）の 1/20,000～1/50,000 程度と稀である。

<重症度分類>

診断基準自体を重症度分類等とし、診断基準を満たすものをすべて対象（重症）とする。